UNIVERSITÀ DI PARMA

UNIVERSITÀ DEGLI STUDI DI PARMA

DOTTORATO DI RICERCA IN
"Scienze Chimiche"

CICLO XXXV

Guest Encapsulation in Calixarenes: Properties and Reactivity of Caged Ions and Molecules

Coordinatore:
Chiar.mo Prof. Alessia Bacchi

Tutori:
Chiar.mi Prof. Andrea Secchi, Prof. Gianpiero Cera

Dottoranda: Federica Cester Bonati

Anni Accademici 2019/2020-2022/2023

Table of Contents

Abstract

The development of modern nanotechnologies is more challenging than ever. Understanding and controlling the properties at molecular level is at the base for creating new materials endowed with specific chemical and physical features. This work proposes new synthetic strategies in different fields of supramolecular chemistry, such as molecular receptors, photoresponsive materials, and catalysis. It can be summarised as follows.

Chapter 1 describes the synthesis of upper-to-upper oriented calix[6]arene-based [3]rotaxane, as prototypes for the synthesis of molecular cages, as new containers for *host-guest* systems. The synthetic strategy adopted consists of a threading and capping approach applied to a two-station bis-viologen salt. The correct orientation of the components is obtained thanks to the unidirectional threading process of the templating axle. The effect of the distance between the two-station axle is also evaluated.

The supramolecular-assisted synthesis of a series of head-to-head bis-calix[6]arene cages is reported in Chapter 2. This method involves the formation of oriented [3]pseudorotaxane complexes between the templating axle and two functionalized macrocycles. The clipping reaction with a proper linker leads to the formation of the cage. Preliminary studies on the complexation properties are also presented.

The ability of a heteroditopic calix[6]arene macrocycle to form pseudorotaxane complexes with stilbazolium dyes is described in Chapter 3. This study evaluates the effect of the solvent polarity and the length of the alkyl chain inserted into the stilbazolium salt on the threading process. The non-palindrome nature of the calix[6]arene receptor cavity allows the formation of two orientational isomers with this asymmetric guest. The orientation adopted by the encapsulated guest inside the host cavity affects the optical properties of the former.

The synthesis and characterization of stilbazolium-based [2]rotaxanes are presented in Chapter 4. The separation of the two orientational isomers is now possible as the complexes are interlocked species. This allows the straightforward study of the encapsulation and orientation effects on the spectroscopic properties of the isomers both in solution and in the solid state, which are remarkably enhanced with respect to the unencapsulated dye.

Chapter 5 includes the synthesis of a series of new achiral and chiral digold(I) resorcin[4]arene-based cavitand complexes and their application in the cycloisomerization and alkoxycyclization reactions of 1,6-dienynes. The constrained environment and non-covalent interactions between the macrocycle and the substrate modify the outcome of the transformations.

Glossary of Terms

Axle: an acyclic (thread-shaped) molecule, or molecular unit, that can be surrounded by a macrocyclic host to yield rotaxane-type structures.

Calixarene Annulus: the fictitious ring passing through the methylene bridges of calixarenes.

Calixtube: A polycyclic structure with at least two calixarenes covalently connected in a coaxial manner.

Catenane: A species composed of two or more interlocked macrocyclic components that are not covalently connected to each other. The interlocked rings cannot be separated without breaking the covalent bonds of the macrocycles. The term catenane is derived from the Latin catena meaning "chain".

CH- π: Weak non-covalent interaction occurring between a positively polarised H atom of a CH group and the π cloud of an organic moiety.

Lower rim: The region of a calixarene where the phenolic OH groups are located. The terms narrow rim is also used.

Molecular device: an assembly of a discrete number of molecular components de-signed to achieve a specific function. Each molecular component performs a single act, while the entire supramolecular assembly performs a more complex function, which results from the cooperation of the various components.

Molecular machine: a particular type of molecular device in which the relative position of the component parts can change as a result of some external stimulus.

Pseudorotaxane: a supramolecular architecture consisting in a macrocycle ("rota") threaded with a linear axle ("axis") and held together by non-covalent interactions. The pseudorotaxane is in equilibrium with its separated components.

Rotaxane: a molecular architecture consisting of a macrocycle ("rota") and an axle ("axis") mechanically interlocked and kinetically trapped with one another due to

the presence of large moieties ("stoppers") at the ends of the axial component which prevent disassociation (dethreading) of the components.

Stopper: a bulky molecular unit incorporated in the components of rotaxanes and catenanes that limits the amplitude of intercomponent movements. Typically, stoppers are the terminal units of the axle component in a rotaxane.

Upper rim: The region of the calixarene at the para position of the phenolic OH. The term wider rim is also used.

Wheel: a macrocyclic (ring-shaped) molecule that can surround an acyclic guest to yield rotaxane-type structures.

Viologen: a 4,4'-bipyridinium moiety.

Abbreviations and Acronyms

CT: Charge-transfer

DCC: N,N'-Dicyclohexylcarbodiimide

DMP: Dess-Martin Periodinane

DMSO: Dimethyl sulfoxide

ee: Enantiomeric excess

er: Enantiomeric ratio

EDC: 1-Ethyl-3-(3-dimethylaminopropyl)carbodiimide

ESI: Electrospray Ionization

HR-MS: High Resolution Mass Spectrometry

JohnPhos: (2-Biphenyl)di-tert-butylphosphine

L: Ligand

MALDI: Matrix Assisted Laser Desorption Ionization

NMR: Nuclear magnetic resonance

TsO: Tosylate

UV: Ultraviolet

General introduction

Since the beginning of the industrial age, the progress of technology has been related to the manufacturing of intelligent materials and devices. The development of this technology goes hand in hand with the progressive miniaturisation of the components used to construct these devices and machines. Thus, it becomes important to control the assembly and functions of nanometre-sized artificial structures with high precision. Therefore, the miniaturisation of components and the availability of responsive devices are critical issues for the development of modern nanotechnology.

The traditional path to achieve the miniaturisation of components for designing new nanodevices is performed using the so-called "top-down" approach. Such an approach manipulates progressively smaller pieces of matter using modern techniques. [1,2] However, it is now evident that this methodology is subject to severe limitations for sub-100 nm objects. For example, modern computer technology has approached the limits of its physical capabilities. However, as Richard P. Feynman stated in his renowned address to the American Physical Society in 1959, entitled "there is plenty of room at the bottom,[3] to move towards further miniaturisation, science and technology must tread new paths. An alternative strategy to manufacturing nanodevices is the "bottom-up approach", which starts from nano- or sub-nanoscale objects (i.e. atoms or molecules) to build nanostructures endowed with specific functions.[4]

Supramolecular chemistry focuses on systems composed of several spontaneously assembled subunits, which are held together through non-covalent interactions.[5,6] Unlike traditional chemistry, which is based on the manipulation of covalent bonds, supramolecular chemistry exploits the reversible non-covalent interactions (i.e. Coulomb interactions, hydrogen bonding, halogen bonding, van der Waals interactions, and metallic coordination) to hold the

components of a system together. These interactions are weak, but they can afford stable supramolecular complexes operating cooperatively. Therefore, they are a powerful tool for organising chemical species in space to endow aggregates with specific functions. For all these reasons, it is easily foreseen that supramolecular chemistry may assume a fundamental role in the bottom-up approach to intelligent nanomaterials.[7]

In supramolecular chemistry, a *Host* is defined as a molecular entity with convergent binding sites (Lewis basis donor atoms, hydrogen bond donors, etc.). Conversely, a *Guest* is a specie (neutral or charged) presenting divergent and complementary binding sites. The host-guest binding is a thermodynamic process. The constant governing the relative equilibrium between the interacting species is called the binding or association constant (K_{bind}). It describes the degree of supramolecular association.[8] For a 1:1 host-guest system, K_{bind} is determined using the concentration of species present at equilibrium from equation (1).

$$H + G \underset{}{\overset{K_{bind}}{\rightleftharpoons}} HG$$

$$K_{bind} = \frac{[H]\,[G]}{[HG]} \qquad (1)$$

The K_{bind} is usually calculated using NMR, UV-Vis, fluorescence spectroscopy or calorimetric titrations. These investigation tools provide information on the formation of the host-guest adduct.[9] The binding constants are related to the free energy of complexation in agreement with the Gibbs equation: $\Delta G° = -RT \ln K_{bind}$.

The supramolecular hosts are usually designed to interact with their guests through multiple binding contacts. When several host binding sites cooperate in guest binding, such a phenomenon is called *cooperativity*.[10–12] If the overall stability of the complex is greater than the sum of the energies of the host interactions with the individual binding sites, the result is positive cooperativity.

The concept of cooperativity invoked in supramolecular chemistry is the *chelate effect* described in classical coordination chemistry textbooks. Cooperative/chelating effects alone, however, do not always account for the remarkable stability of several host-guest complexes. The hosts in these complexes are usually macrocycles with convergent binding sites. The additional stability of these systems with respect to their acyclic analogues is usually defined as *macrocyclic effect*.[13,14] This effect is also related to the host's *preorganisation*.[15] As a straightforward example, bicyclic receptors like *cryptands* are more effective than monocyclic receptors such as *coronands* (Figure 1). Host preorganisation is crucial as it represents a significant advantage for the overall free energy complexation.

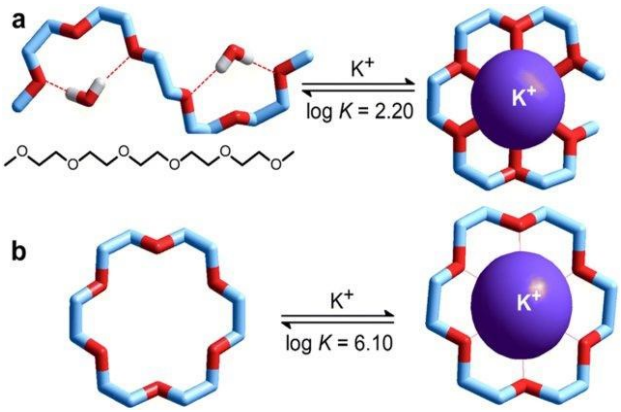

Figure 1 Schematical representation of macrocyclic effect in polyether complexes of alkali metal ions (potassium). Reprinted from Ref.15. Copyright © 2020 Springer Nature Switzerland.

In addition to preorganisation, the host-guest affinity is also determined by another critical parameter called *complementarity*.[16] An efficient host should have binding sites correctly arranged in space to bind a complementary guest.

Concepts such as macrocyclic effect, preorganisation and complementarity are the basis on which supramolecular chemistry has developed and grown. In the last thirty years, countless examples of working devices and prototypes of

molecular machines based on the principles of supramolecular chemistry have been described.[17] Indeed, nowadays, supramolecular chemistry has found a primary role in materials chemistry and nanoscience.[18]

Mechanically interlocked molecules (MIMs) and their synthesis

A *pseudorotaxane* (see Figure 2a) is a supramolecular complex consisting of a linearly symmetric molecular species that intertwines a macrocycle,[19,20]which are held together by non-covalent interactions. The nature and magnitude of the components' intermolecular forces determine the complex's thermodynamic stability.[19,20] When bulky substituents, whose steric hindrance is larger than the macrocycle internal diameter, are attached to the termini of the axial component, a new chemical compound, defined as *rotaxane,* is formed (see Figure 2b).[21] The bulky substituents thus mechanically confine the axial component within the macrocycle. If the threaded part has a cyclic shape, the resulting interlocked specie is called *catenane* (see Figure 2c). In MIMs chemistry, the term "wheel" is often used to describe the cyclic component, while "axle" indicates the linear component. Instead, the term "stoppers" is employed to represent the bulky groups at the axle endings in rotaxane structures. The number of components in pseudorotaxanes and rotaxanes is given in square brackets before the name (see figure 2).

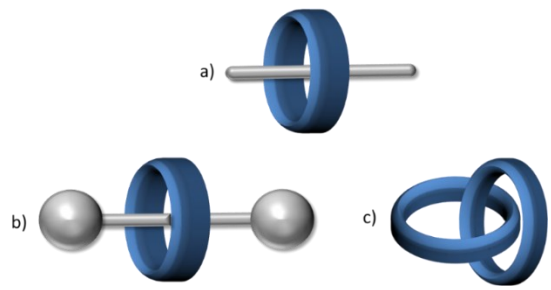

Figure 2 Cartoons illustrating the shape of (a) [2]pseudorotaxane, (b) [2]rotaxane, and (c) [2]catenane structures.

Many different architectures can be built by connecting a variable number of elements. As an example, cartoons of daisy chains, polyrotaxanes, polycatenanes and knots structures have been illustrated in Figure 3.

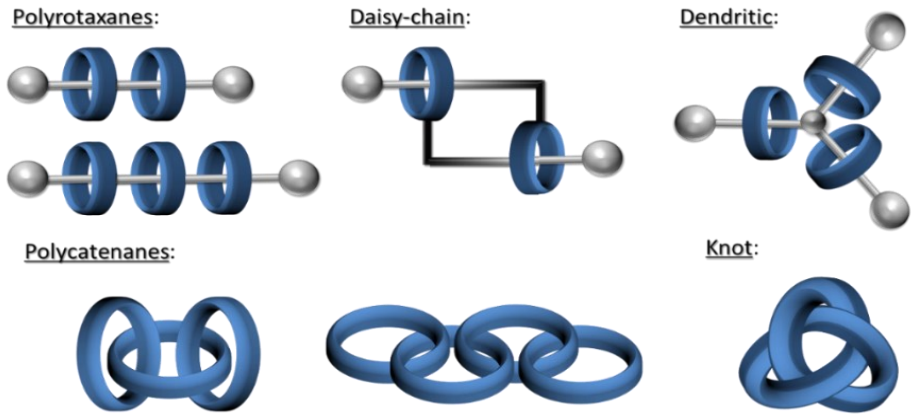

Figure 3 Cartoons of several MIMs architectures.

MIMs are synthetically challenging targets since arranging two or more independent molecules in space is difficult. This represents an essential requirement when many desired mechanical bonds must be formed predictably. Methods for MIMs synthesis have greatly upgraded since the first low-yield synthesis based on statistical trials. The most reliable synthetic methodology so far developed is based on the formation of a [n]pseudorotaxane precursor. In this supramolecular complex, the axle (possibly in the shape of a semi-dumbbell) and the wheel are previously organised in a correct arrangement by the intermolecular forces holding the components together.[22] These methods, collectively called *passive template approaches*, have been extended to the synthesis of rather intricated MIMs, often with excellent outcomes.[23]

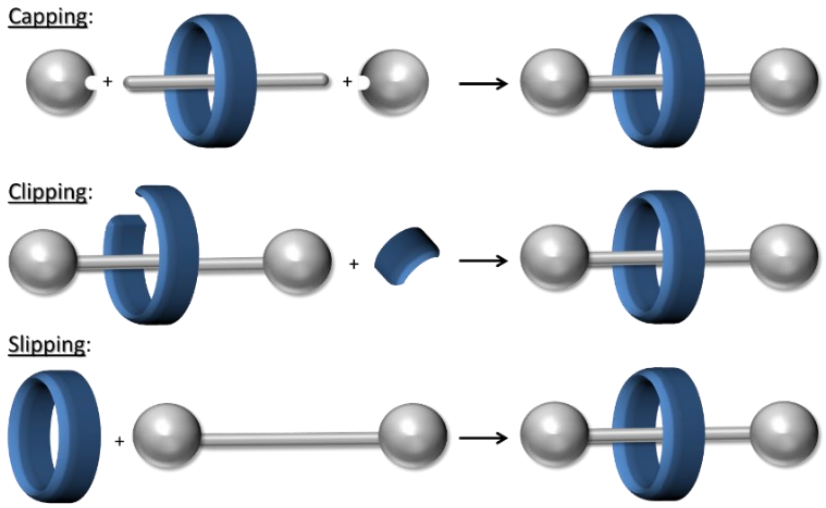

Figure 4 Synthetic strategies for rotaxanes synthesis.

The most used approach for rotaxane synthesis is called the *capping* strategy, or more precisely, *threading* and *capping* (Figure 4 above). As previously described, this strategy is based on the covalent introduction of bulky stoppers on ending reactive groups in the threaded axle. A partially formed macrocycle is instead used in the *clipping* strategy (Figure 4 centre). This component is wrapped around an axial component and held in place by supramolecular interactions. Afterwards, it undergoes a clipping reaction to complete its macrocyclic structure. Another rotaxane synthesis strategy is *slipping*[24] (Figure 4 below). It is established on the preparation of the singular rotaxane parts (i.e. the wheel and the capped thread or dumbbell) that are heated in solution to promote the "sliding" of the now enlarged macrocycle over the axle stopper. This transition affords the interlocked compound, which is more thermodynamically stable than the separate species. The size complementarity between macrocycles and stoppers strongly influences the rate constants for these processes. Regarding the *catenanes* preparation, the most straightforward strategies employed are based on: a) the clipping of a reactive threaded axle having adequately long arms (Figure 5, top) or b) the

introduction of a complementary linker to an already complexed axle (Figure 5, bottom).[25,26]

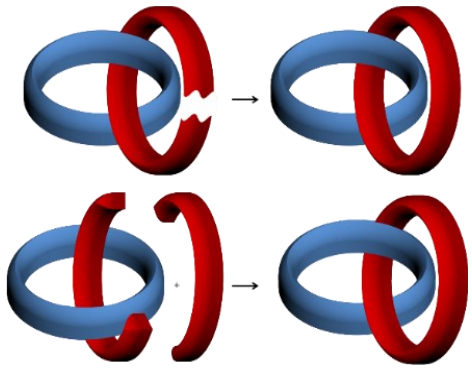

Figure 5 Synthetic approaches for catenanes synthesis.

The *active template* method is an elegant and complementary strategy introduced by Leigh and co-workers for synthesising interlocked species (Figure 6). This innovative strategy relies on using a reactive unit, typically a metal ion, incorporated into the wheel component. Through coordination, the metal ion guides the position of the components that must react and favour the bond(s) formation.[27] Many different metal-catalysed reactions have been exploited to realise rotaxanes and catenanes.[28-31] An interesting feature of this approach is that it allows synthesising MIMs that are otherwise inaccessible using the strategies described before. Furthermore, these syntheses require only a sub-stoichiometric amount of metal catalyst.

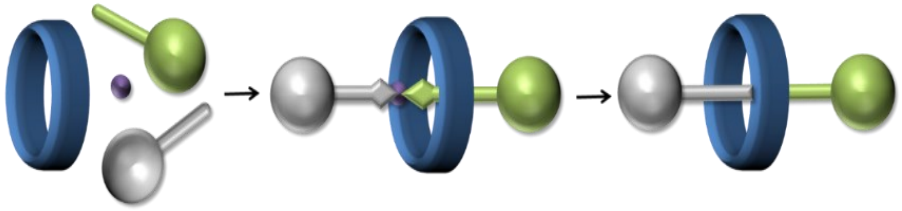

Figure 6 Cartoons illustrating the MIMs synthesis through the active metal template strategy: the ''half-dumbbell''precursors are depicted in grey and green, the macrocycle in blue and the metal ion catalyst in purple.

MIM synthesis under kinetic and thermodynamic control

The synthetic strategies to MIMs so far described require precise orientation of the molecular components before the final reaction step, in which the covalent bonds permanently fix the shape of the entangled molecule. The reaction proceeds under kinetic control if the stabilising operating forces are kept in the transition state, and irreversible stoppering reactions are employed (see Figure 7, left). Unfortunately, such an approach can also yield unwanted by-products, such as uncomplexed dumbbells or unlinked rings, which lower the processes' efficiency with the loss of starting material. It should be noted that the resulting interlocked compounds are usually more stable than their free counterparts. This suggests that MIM's synthesis might be performed under thermodynamic control[32] when it is based on the formation of reversible bonds (see Figure 7, right). This approach has already been used to prepare several complex architectures[33] and new materials.[34]

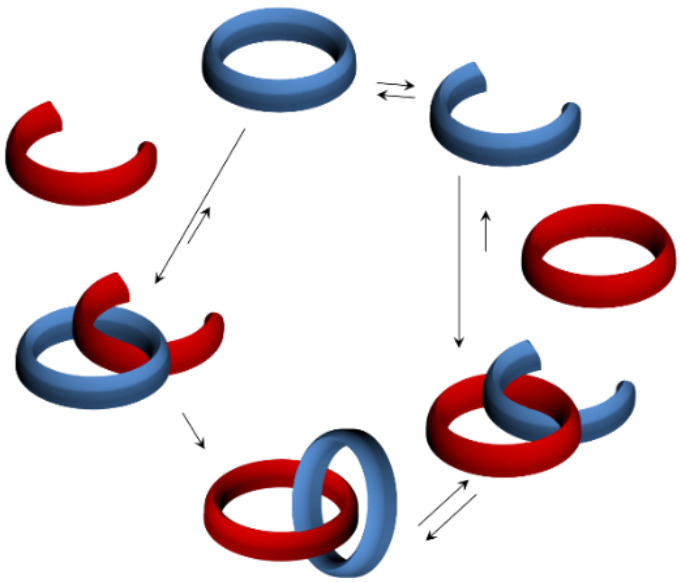

Figure 7 Schematic representation of kinetically controlled (left) and thermodynamically regulated (right) reactions for catenanes synthesis.

Pseudorotaxanes and oriented rotaxanes

The possibility that supramolecular architectures can perform programmed tasks is strictly related to their physicochemical properties and the geometrical arrangement of their components. In this context, the construction of interlocked structures capable of carrying out a unidirectional movement of their components upon the application of proper stimuli represents a topic of growing interest. The macrocycles used for manufacturing MIMs can be subdivided into two categories: those having a planar shape (i.e. crown ethers) and those endowed with a hollow 3D structure. In the latter category are enclosed calixarenes, cucurbiturils, and cyclodextrins. Planar macrocycles and symmetric hollow receptors like cucurbiturils have a palindrome structure. In simpler words, especially in the case of hollow macrocycles, they present the same face on both sides of their cavities. Hence, an axial guest (symmetric or non-symmetric) can thread their cavity from both the access yielding the same product (Figures 8a and c). Conversely, when using non-symmetric hollowed 3D hosts, in which the cavity accesses are different for size and/or for chemical properties, threading from non-symmetric axles results in the formation of a pair of orientational pseudorotaxane isomers. If bulky stoppers are attached to the termini of the threaded non-symmetric axial component, two constitutionally isomeric rotaxanes are obtained, eventually (Figure 8b). Analogously, it becomes possible to realise oriented catenanes by exploiting macrocycles endowed with a "facial" asymmetry (Figure 8d). It should be observed that these orientational isomers can only be interconverted by breaking and reforming their covalent bonds.

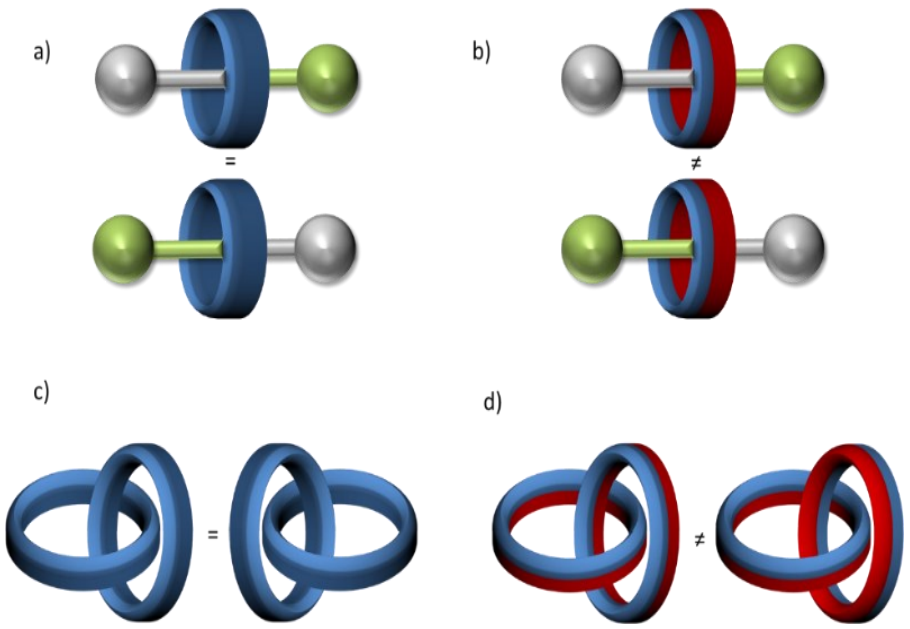

Figure 8 Cartoons representing MIMs architectures composed of palindromic wheels. Orientational isomers are obtained when a non-symmetrical axial component is used before the locking reactions.

Examples of their selective synthesis have been reported [35] mainly by exploiting cyclodextrins as wheels (see Figure 9).[36,37]

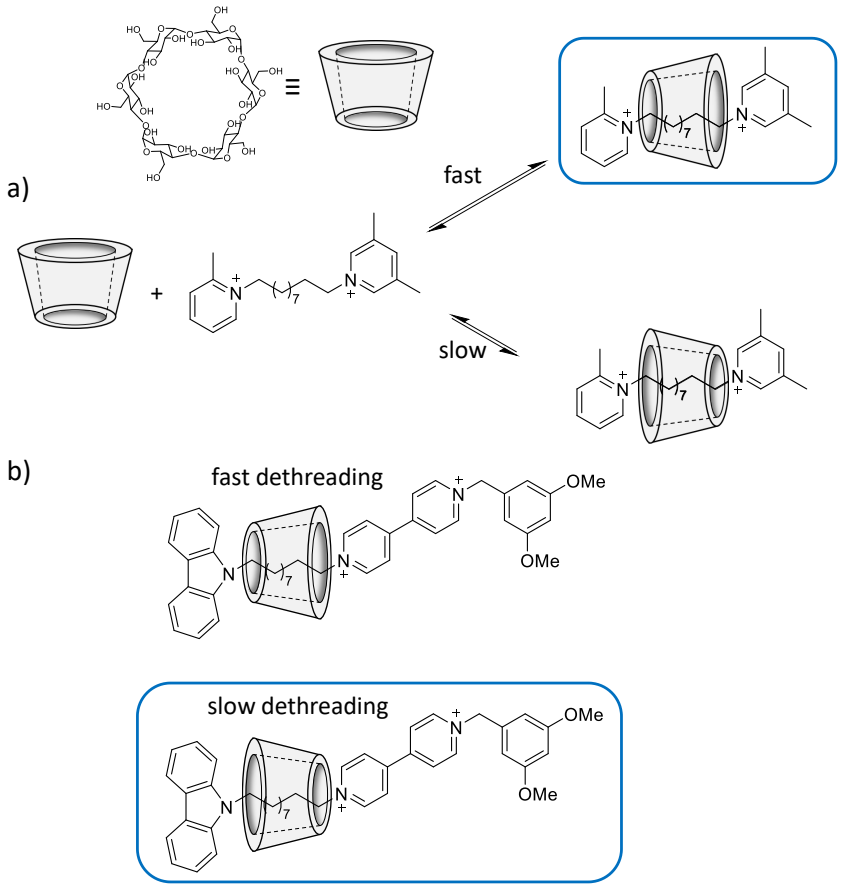

Figure 9 a) The steric hindrance of the stoppers of pyridinium-based axle control the orientation of the resulting pseudorotaxane isomers (see ref. 36); b) the conformation adopted by oriented rotaxanes is responsible for the different threading and unthreading velocities (see ref. 37).

It is also possible to exploit the different functionalisation of the cavity accesses of a hollow host to pivot the geometrical arrangement (orientation) of an included guest.[38] For example, Methyl Orange (MO) dye is oriented in a β-cyclodextrin host with its dimethylamino group located towards the wider gate of the macrocycle (see Figure 10, left). This orientation is wholly reversed when the anionic sodium heptakis[6-deoxy-6- (3-thiopropionate)]-β-CD is used because of the repulsive interaction between the MO sulphonate group with the host carboxylate appended on the macrocycle narrow rim (see Figure 10, right). [39]

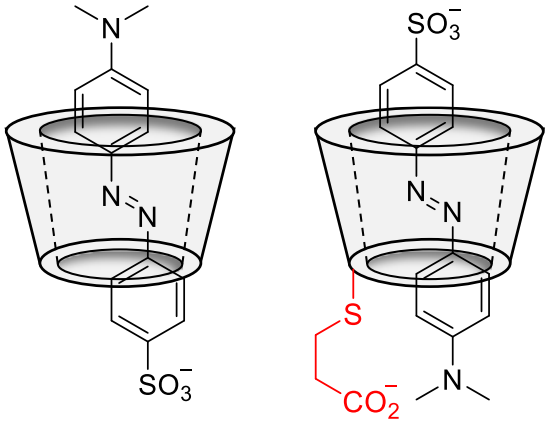

Figure 10 Oriented pseudorotaxane isomers generated by the complexation of Methyl Orange (MO) dye by cyclodextrins (CDs).

Heteroditopic Calix[6]arene-based Pseudorotaxanes and Rotaxanes

Calix[n]arenes are a class of synthetic macrocycles extensively employed as versatile platforms for preparing receptors capable of complexing neutral and ionic species.[40] They are synthesised in very high yields through condensation of p-*tert*-butylphenol and formaldehyde in basic conditions.[41] Most importantly, the resulting macrocycle's size, i.e. the number of phenolic units, can be adjusted by suitably modifying the base employed and the nature of the solvent. Calix[4]arene derivatives have been the most studied in this class. Indeed, thanks to the facile and regioselective functionalisation of their phenolic oxygens, the conformation mobility of calix[4]arene can be restricted at will, and different geometry can be obtained: *cone*, *partial cone*, 1,2-*alternate* and 1,3-*alternate*. The calixarenes chemistry is gradually changed in the last thirty years. From the pioneering works on their selective and stereocontrolled functionalisation, we now advocate transferring their remarkable binding properties to the development of sensors, smart devices and active surface coatings among the several applications found.[40,42–44] Although the impressive achievements got with calix[4]arene derivatives, the larger members of this class, i.e. calix[6] or calix[8]arenes, have been relatively less explored. If adequately modified on their

phenolic and aromatic portions, these artificial receptors exhibit unique properties compared to the palindrome receptors previously introduced.[45] In stark contrast to other non-palindrome water-soluble receptors such as cyclodextrins, which can form inclusion complexes by exploiting the hydrophobic effect, their π-rich hydrophobic cavity allows calix[6]arenes to function smoothly in weakly polar organic media.

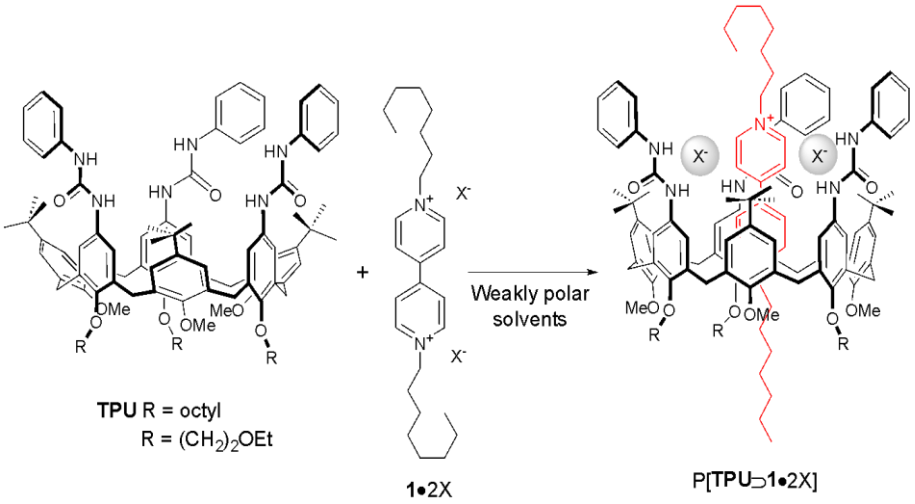

Figure 11 Formation of [2]pseudorotaxane complex between a calix[6]arene-based wheel (**TPU**) and a viologen-based axle (**1**•2X) in weakly polar solvents (toluene, benzene, dichloromethane, chloroform).

The possibility of exploiting the large cavity of calix[6]arenes to produce a new family of devices and molecular machine prototypes based on pseudorotaxanes, rotaxanes and catenanes is relatively recent.[46] In that seminal paper, a calix[6]arene (**TPU**) having its phenolic groups functionalised with methyl and octyl groups in alternate positions, and bearing three phenylureas opposite the octyloxy groups, was shown to be able to include a dioctylviologen salt as diiodide (**1**•2I) in weakly polar media, forming the pseudorotaxane (P) complex P[**TPU**⊃**1**]2I (Figure 11). The structure of this supramolecular adduct was deduced in solution via a plethora of NMR experiments. Then it was clearly demonstrated in the solid state by X-ray diffraction. The resolved X-ray structure showed that

the dicationic portion of the viologen-salt is intertwined into the calix[6]arene annulus with its two counteranions (green spheres in Figure 12) that are hydrogen bonded to the phenylureas NH groups present onto the macrocycle larger rim (Figure 12).

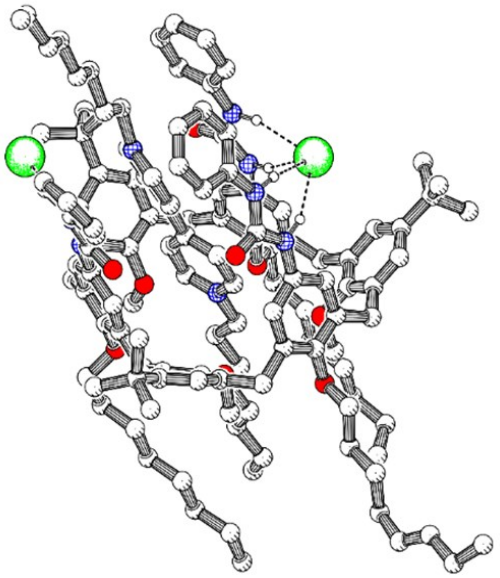

Figure 12 Pluton view of the X-ray crystal structure of P[**TPU**⊃**1**]2I; the hydrogen atoms have been omitted for clarity except those involved in the H bonds.

The inclusion of the viologen salt in the π-rich aromatic cavity of **TPU** was always witnessed by the formation of a red-coloured chloroform or toluene solution. This colour arises from a weak and broad absorption band in the corresponding optical spectrum at λ = 460 nm. It has been assigned to a charge transfer (CT) interaction which arises from the proximity of the calixarene aromatic rings and the aromatic portion of the dialkyl viologen unit. Spectrophotometric titrations in dichloromethane solution with dioctylviologen axles endowed with counteranions of different coordination strengths (TsO, PF_6) were then employed to obtain more details on the formation of these pseudorotaxanes.[47] These studies revealed that the stability constant (K_{bind}) for the complexation of the tosylate salt is quasi an order of magnitude (6.0 vs 0.8×10^6 M^{-1}) larger than that

calculated for PF_6. This significant difference indicated that ion coupling to the axle is essential in the threading process since the coordination of the two counteranions is crucial for loosening and breaking the tight ion pairs before threading the viologen axle. The same wheel **TPU** was also used for the synthesis of rotaxane R[**TPU**⊃**2**]2Br by stoppering with two bulky diphenylacetyl units the hydroxyl endings of a bis-ω-hydroxydodecylviologen thread (Figure 13).[46]

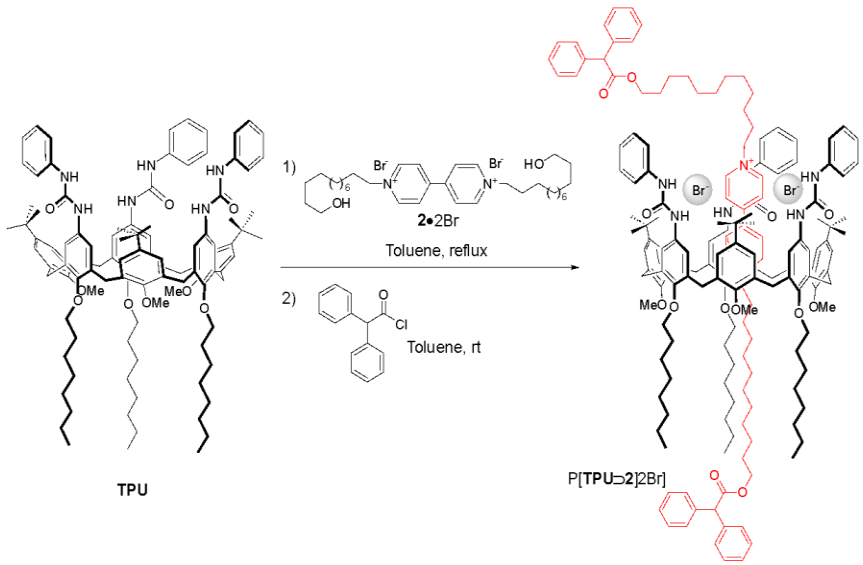

Figure 13 Synthesis of rotaxane R[**TPU**⊃**2**]2Br using the *threading and capping* approach.

These findings soon led to questions about the mechanism of the threading process. In particular, the factors concerning the directionality of axle threading that, in principle, may occur through the wider (with phenylureas) or narrower rim (with methoxy and octyloxy groups) of the calix[6]arenic wheel. To solve the puzzle, asymmetrical axles bearing a pre-installed diphenylacetyl stopper, such as **3**•2OTs and **4**•2OTs (Figure 14), were employed and reacted with a **TPU** wheel having three ethylethoxy chains in place of the octyloxy ones.[48,49] The ^{1}H NMR analysis showed the selective formation of only one of the two possible pseudorotaxane orientational isomers with both **3**•2OTs and **4**•2OTs. Furthermore, the only formed isomer was always that presenting the

diphenylacetic stopper positioned at the macrocycle wider rim indicated as P[**TPU**⊃**3**$_{up}$]2OTs and P[**TPU**⊃**4**$_{up}$]2OTs (Figure 14). These findings supported the hypothesis that the threading of the axle proceeded selectively through the calix[6]arene rim bearing the phenyl urea units.

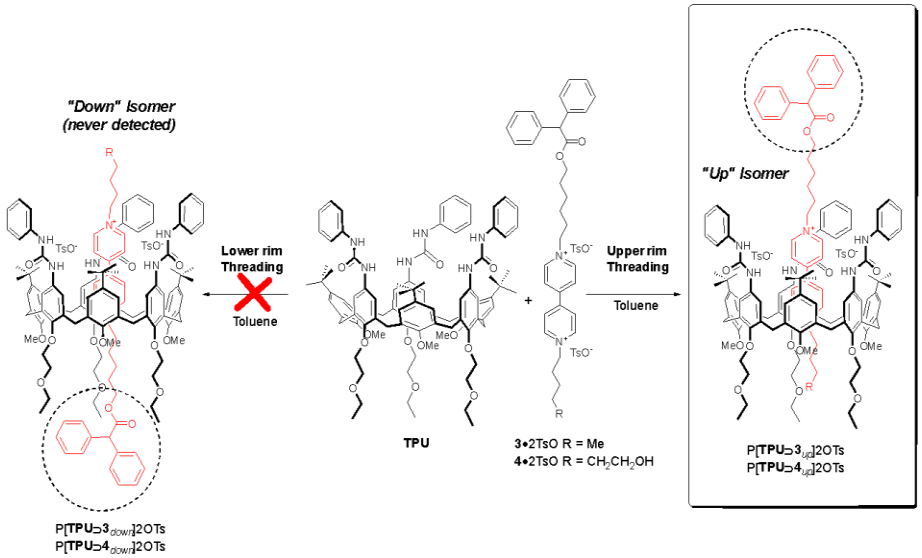

Figure 14 Selective formation of the *Up* orientational isomer in the self-assembly reaction of **TPU** with axles **3**•2TsO and **4**•2TsO.

The unidirectionality of axle threading was explained by considering that a) in low polarity solvents, the inward orientation of the **TPU** three methoxy groups inside the calixarene cavity disfavours this access for steric reasons; b) in the solvents used (benzene, toluene, dichloromethane or chloroform), viologen salts **3**•2TsO and **4**•2TsO behave as tight ion pairs. Hence, it is reasonable to assume that a partial separation of the ion pair must occur before axle threading; and c) this ion-pair separation occurs thanks to the hydrogen-bonding abilities of the phenylureas placed onto the macrocycle larger rim (see Figure 15).

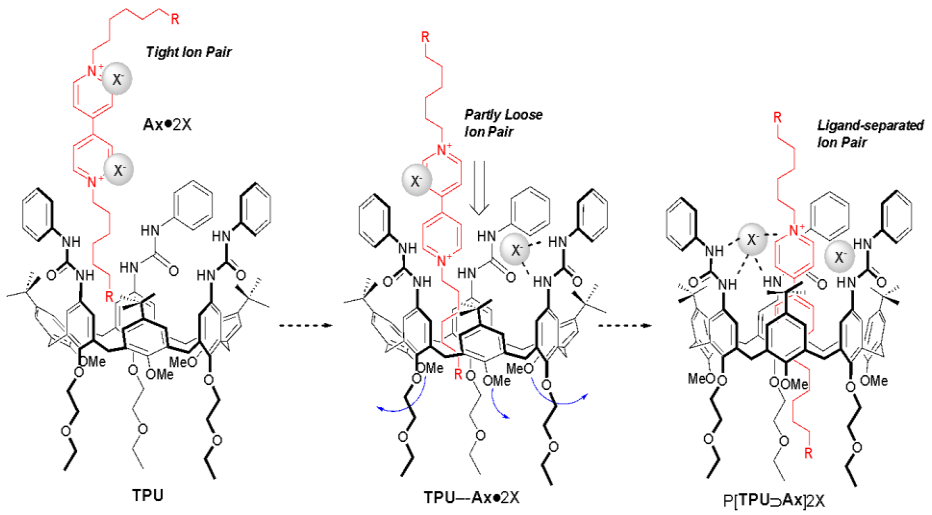

Figure 15 Hypothesised mechanism of threading of a generic viologen axle **Ax•**2X in **TPU**: the phenylureas coordinate, by hydrogen bonding, the axle counteranions and guide the axle threading from the wheel larger rim (see text).

In a scenario dominated by hydrogen bonding interactions, other important parameters, such as solvent polarity and temperature, should play a primary role in dictating the axle threading. To investigate these factors, pseudorotaxane P[**TPU**⊃**4**$_{up}$]2OTs was self-assembled in a polar solvent such as CH_3CN (Figure 16).[50] The enhanced polarity of the solvent influences the binding capacity of the calixarene macrocycle, modifying the extent of the ion coupling with the axle. A decrease in the pivotal role of the macrocycle phenylurea units was thus observed. Yet, in this solvent, the wheel methoxy groups result expulsed from the cavity, and the steric hindrance of this access is thus significantly reduced. Hence, axle **4** can thread **TPU** from both its gates yielding the two orientational isomers P[**TPU**⊃**4**$_{up}$]2OTs and P[**TRPU**⊃**4**$_{down}$]2OTs in a 1:2 ratio (Figure 16). This result again demonstrated that the process's directionality does not rely on the size of the cavity accesses but mainly on the guest ion-pairing.

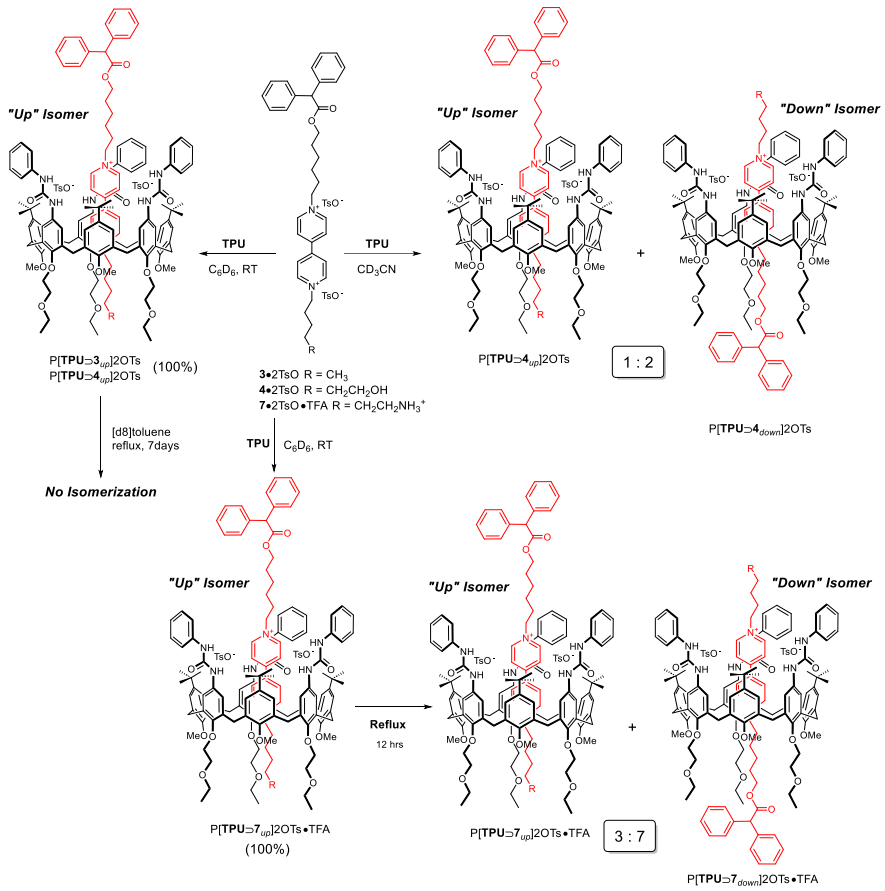

Figure 16 Effect of solvent polarity on the directionality of pseudorotaxane formation between **TPU** and several bis-viologen axles (see also text).

The thermodynamic and kinetic aspects of the threading process were examined in a study,[51] in which a series of mono-stoppered viologen axles (**3**•2TsO, **4**•2TsO and **7**•2TsO, Figure 16) were involved in a threading process with **TPU** at different temperatures, using benzene-d_6 as a solvent. All tested axles thread the wheel from the upper rim at room temperature for kinetic reasons. On the other hand, at higher temperatures, the wheel threading is still kinetically controlled with the exclusive formation of the *up* isomer when the viologen axle bears a neutral alkyl terminus (i.e. **3**•2TsO and **4**•2TsO). Conversely, the thermodynamic *down* product is formed at 340 K with axle **7**•2TsO•TFA carrying an ammonium terminus on its unstoppered alkyl chain (Figure 16).

Template-assisted synthesis of calix[6]arene-based MIMs

Based on what was observed in the previous seminal studies, the threading of dialkylviologen axles in low polarity solvents is always selectively occurring across the upper rim of the calix[6]arene wheel primarily because the phenylureido groups engage hydrogen bonding interactions with tosylate counter-ions promoting ion pair dissociation. On these premises, the effort of our research group was then shifted to disclosing the factors affecting the formation of calix[6]arene-based MIMs. As stated in the first part of this introductory chapter, most of the synthetic approaches to MIMs rely on the employment of metal ions, which can provide the correct spatial rearrangement of the precursors and ultimately play an active role in promoting the formation of the covalent bonds leading to the interlocked structure.[27] In a diverse but complementary approach, our group verified as a "semi-axle" derivative such as the *N*-octadecyl pyridylpyridinium salt **9**•OTs can be recognised by the **TPU** wheel in toluene giving rise to the formation of a 1:1 mixture of semi-pseudorotaxane orientational isomers P[**TPU**⊃**9**$_{up}$]OTs and P[**TPU**⊃**9**$_{down}$]OTs (Figure 17). This mixture was treated with *n*-pentyl tosylate **8** to yield pseudorotaxanes P[T**PU**⊃**10**$_{down}$]2OTs and P[**TPU**⊃**10**$_{up}$]2OTs in a 7:3 abundance thus suggesting that the reaction takes place preferentially on the isomeric complex P[**TPU**⊃**9**$_{down}$]OTs, which presents a more reactive nucleophilic site. Kinetic analysis of the alkylation process fitted with an S_N2 type mechanism with a rate constant of 1.4×10^{-4} s^{-1} for the reaction conducted with the calixarene wheel and 8.6×10^{-6} s^{-1} for the "unassisted" one. These results highlighted that, under present reaction conditions, the alkylation is 16 times faster when the calixarene is employed.[52]

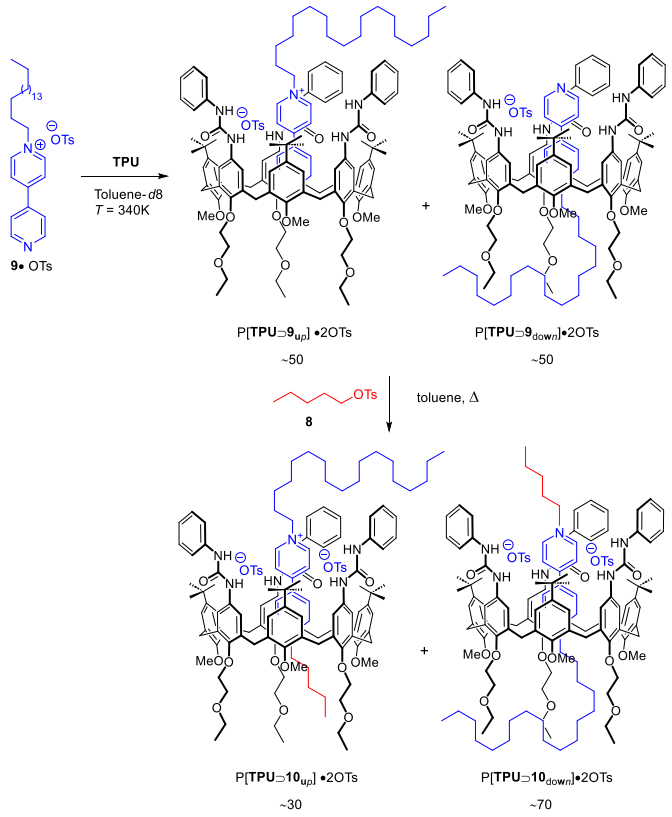

Figure 17 Template-assisted approach for pseudorotaxane synthesis.

This result paved the way for the study of an unprecedented "metal-free template-directed" synthesis of oriented rotaxanes.[53] As previously described, the synthesis of calix[6]arene-based [2]rotaxanes is traditionally achieved by the directional insertion of a 1,1-dialkyl-4,4-bipyridinium axis (possibly with a capped end) into the calix[6]arene, followed by a capping (acylation) reaction. The rate-determining step of this approach is the alkylation of the bipyridine or pyridylpyridinium ion, which takes 7 days at reflux (Figure 18a). Thus, a more sustainable approach was realised by a supramolecular-assisted strategy exploiting the different reactivities of the oriented semi-pseudorotaxanes (Figure 18b).

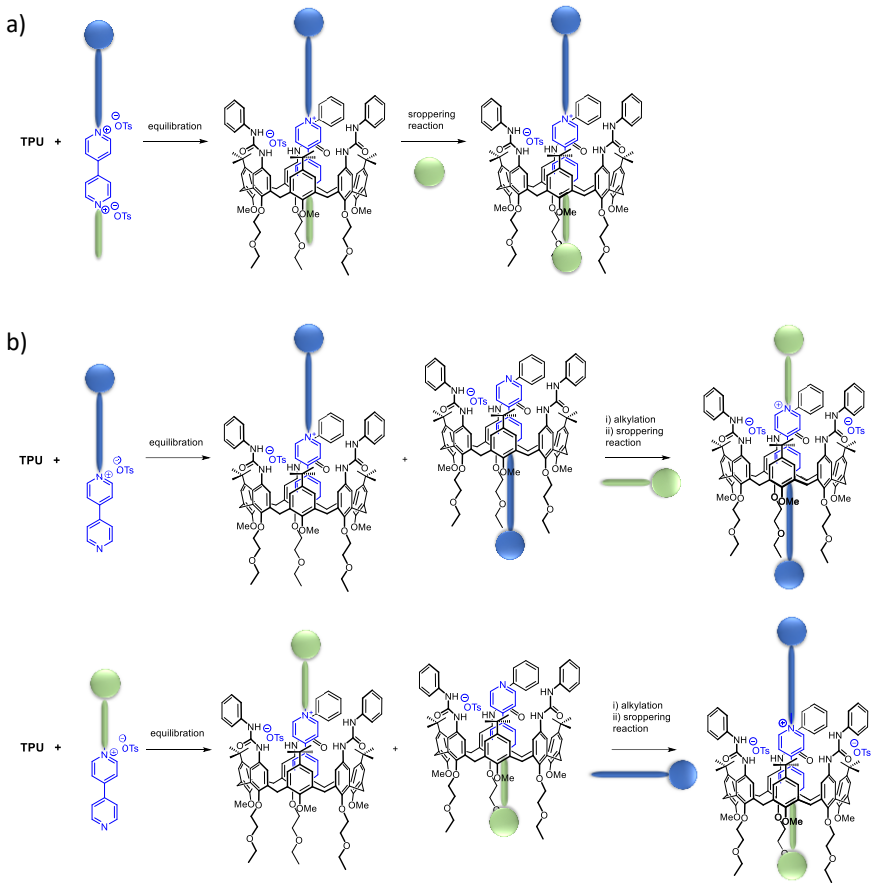

Figure 18 Different approaches for the synthesis of rotaxane: a) traditional threading and capping strategy; b) template-assisted synthesis.

It is essential to highlight that the new strategy allowed for a more sustainable synthesis of the two possible rotaxanes oriented with the longer chain facing the lower and upper rim, respectively. This would otherwise be impossible to accomplish using the traditional approach. In particular, as before, the equilibrium of a pyridylpyridinium salt **10**•OTs (whose synthesis takes only 24 h) with **TPU** wheel led to a 1:1 mixture of semi-pseudorotaxanes P[**TPU**⊃**11**$_{up}$]OTs and P[**TPU**⊃**11**$_{down}$]OTs. Furthermore, this mixture could be treated with 12-hydroxy-n-dodecyl tosylate in refluxing toluene for 4 days, followed by the usual stoppering reaction with diphenylacetyl chloride (Figure 19) to produce rotaxane R[**TPU**⊃**12**$_{down}$]2OTs in 63% of the total yield exclusively. This result unequivocally

indicated that only the semi-pseudorotaxane P[**TPU**⊃**11**$_{down}$]OTs has undergone an accelerated alkylation reaction.

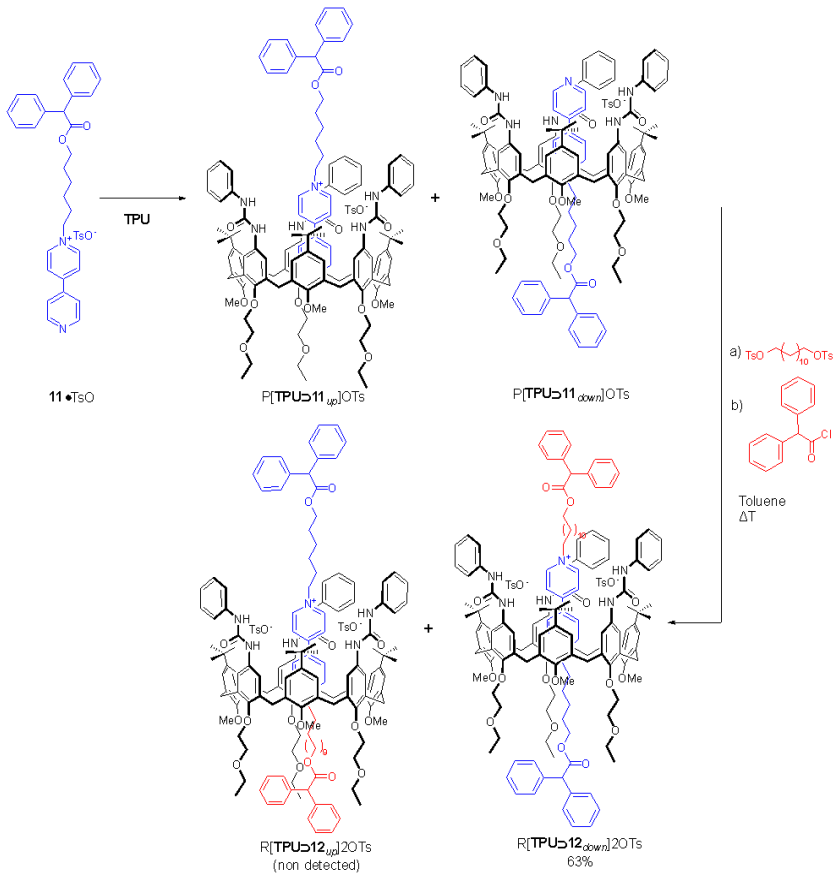

Figure 19 Synthesis of calix[6]arene-based rotaxanes using a "template-assisted" approach.

All of this evidence led to the conclusion that the deep encapsulation of the pyridyl pyridinium unit of **11** in the cavity of **TPU** results in i) a more exposed nucleophilic nitrogen at the macrocycle upper rim, ii) a drastic change of the axle electron density that improved the nucleophilicity of the exposed nitrogen itself. Together with the ability of urea moieties to stabilise the transition state by performing hydrogen bonding interactions, the above results suggest the "innate" selectivity of the calixarene wheel in promoting a template-assisted synthesis of rotaxanes.

References

[1] I. Amato, *Science* **1998**, *282*, 402–405.

[2] J. W. Judy, *Smart Mater. Struct.* **2001**, *10*, 1115.

[3] R. P. Feynman, *Eng. Sci.* **1960**, *23*, 22–36.

[4] H.-D. Yu, M. D. Regulacio, E. Ye, M.-Y. Han, *Chem. Soc. Rev.* **2013**, *42*, 6006–6018.

[5] J. W. Steed, D. R. Turner, K. Wallace, *Core Concepts in Supramolecular Chemistry and Nanochemistry*, John Wiley & Sons, **2007**.

[6] H.-J. Schneider, A. Yatsimirsky, *Principles and Methods in Supramolecular Chemistry*, Wiley, **2000**.

[7] J. W. Steed, J. L. Atwood, *Supramolecular Chemistry*, John Wiley & Sons, Ltd, Chichester, **2009**.

[8] K. A. Connors, *Binding Constants: The Measurement of Molecular Complex Stability*, Wiley, **1987**.

[9] C. A. Schalley, *Analytical Methods in Supramolecular Chemistry*, Wiley-VCH Verlag GmbH & Co. KGaA, Weinheim, Germany, **2012**.

[10] J. D. Badjić, A. Nelson, S. J. Cantrill, W. B. Turnbull, J. F. Stoddart, *Acc. Chem. Res.* **2005**, *38*, 723–732.

[11] C. A. Hunter, H. L. Anderson, *Angew. Chem. Int. Ed.* **2009**, *48*, 7488–7499.

[12] G. Ercolani, L. Schiaffino, *Angew. Chem. Int. Ed.* **2011**, *50*, 1762–1768.

[13] G. Melson, *Coordination Chemistry of Macrocyclic Compounds*, Springer US, **2012**.

[14] K. Goto, in *Compr. Supramol. Chem. II* (Eds.: J.L. Atwood, G.W. Gokel, L. Barbour), Elsevier Science, **2017**.

[15] L. Fabbrizzi, *ChemTexts* **2020**, *6*, 10.

[16] J. B. Wittenberg, L. Isaacs, in *Supramol. Chem.*, John Wiley & Sons, Ltd, **2012**.

[17] J. L. Atwood, J. W. Steed, *Encyclopedia of Supramolecular Chemistry*, CRC Press, **2004**.

[18] V. Balzani, *Pure Appl. Chem.* **2008**, *80*, 1631–1650.

[19] J.-P. Sauvage, C. Dietrich-Buchecker, Eds. , *Molecular Catenanes, Rotaxanes and Knots: A Journey Through the World of Molecular Topology*, Wiley-VCH, Weinheim, **1999**.

[20] R. S. Forgan, J.-P. Sauvage, J. F. Stoddart, *Chem. Rev.* **2011**, *111*, 5434–5464.

[21] D. H. Rouvray, R. B. King, *Topology in Chemistry: Discrete Mathematics of Molecules*, **2002**.

[22] D. Philp, J. F. Stoddart, *Synlett* **1991**, *1991*, 445–458.

[23] T. J. Hubin, D. H. Busch, *Coord. Chem. Rev.* **2000**, *200–202*, 5–52.

[24] M. Asakawa, P. R. Ashton, R. Ballardini, V. Balzani, M. Bělohradský, M. T. Gandolfi, O. Kocian, L. Prodi, F. M. Raymo, J. F. Stoddart, M. Venturi, *J. Am. Chem. Soc.* **1997**, *119*, 302–310.

[25] J. G. Hansen, N. Feeder, D. G. Hamilton, M. J. Gunter, J. Becher, J. K. M. Sanders, *Org. Lett.* **2000**, *2*, 449–452.

[26] M. Weck, B. Mohr, J.-P. Sauvage, R. H. Grubbs, *J. Org. Chem.* **1999**, *64*, 5463–5471.

[27] J. D. Crowley, S. M. Goldup, A.-L. Lee, D. A. Leigh, R. T. Mc Burney, *Chem. Soc. Rev.* **2009**, *38*, 1530–1541.

[28] S. M. Goldup, D. A. Leigh, T. Long, P. R. McGonigal, M. D. Symes, J. Wu, *J. Am. Chem. Soc.* **2009**, *131*, 15924–15929.

[29] Y. Sato, R. Yamasaki, S. Saito, *Angew. Chem. Int. Ed.* **2009**, *48*, 504–507.

[30] V. Aucagne, K. D. Hänni, D. A. Leigh, P. J. Lusby, D. B. Walker, *J. Am. Chem. Soc.* **2006**, *128*, 2186–2187.

[31] J. D. Crowley, K. D. Hänni, A.-L. Lee, D. A. Leigh, *J. Am. Chem. Soc.* **2007**, *129*, 12092–12093.

[32] W. R. Dichtel, O. Š. Miljanić, W. Zhang, J. M. Spruell, K. Patel, I. Aprahamian, J. R. Heath, J. F. Stoddart, *Acc. Chem. Res.* **2008**, *41*, 1750–1761.

[33] F. Aricó, T. Chang, S. J. Cantrill, S. I. Khan, J. F. Stoddart, *Chem. – Eur. J.* **2005**, *11*, 4655–4666.

[34] D. W. Steuerman, H.-R. Tseng, A. J. Peters, A. H. Flood, J. O. Jeppesen, K. A. Nielsen, J. F. Stoddart, J. R. Heath, *Angew. Chem. Int. Ed.* **2004**, *43*, 6486–6491.

[35] Q.-C. Wang, X. Ma, D.-H. Qu, H. Tian, *Chem. – Eur. J.* **2006**, *12*, 1088–1096.

[36] T. Oshikiri, Y. Takashima, H. Yamaguchi, A. Harada, *J. Am. Chem. Soc.* **2005**, *127*, 12186–12187.

[37] J. W. Park, H. J. Song, *Org. Lett.* **2004**, *6*, 4869–4872.

[38] M. M. Safont-Sempere, G. Fernández, F. Würthner, *Chem. Rev.* **2011**, *111*, 5784–5814.

[39] N. Mourtzis, K. Eliadou, K. Yannakopoulou, *Supramol. Chem.* **2004**, *16*, 587–593.

[40] C. D. Gutsche, *Calixarenes: An Introduction*, Royal Society Of Chemistry, **2008**.

[41] C. D. Gutsche, *Calixarenes Revisited*, **1998**.

[42] P. Neri, J. L. Sessler, M.-X. Wang, P. Neri, J. L. Sessler, M.-X. Wang, Eds. , *Calixarenes and Beyond*, Springer International Publishing, **2016**.

[43] M.-Z. Asfari, V. Böhmer, J. Harrowfield, J. Vicens, *Calixarenes 2001*, Springer Science & Business Media, **2007**.

[44] J. Vicens, J. Harrowfield, Eds., *Calixarenes in the Nanoworld*, Springer Science & Business Media, **2006**.

[45] M. Xue, Y. Yang, X. Chi, X. Yan, F. Huang, *Chem. Rev.* **2015**, *115*, 7398–7501.

[46] A. Arduini, R. Ferdani, A. Pochini, A. Secchi, F. Ugozzoli, *Angew. Chem. Int. Ed.* **2000**, *39*, 3453–3456.

[47] A. Credi, S. Dumas, S. Silvi, M. Venturi, A. Arduini, A. Pochini, A. Secchi, *J. Org. Chem.* **2004**, *69*, 5881–5887.

[48] M. Semeraro, A. Arduini, M. Baroncini, R. Battelli, A. Credi, M. Venturis, A. Pochini, A. Secchi, S. Silvi, M. Venturi, A. Pochini, A. Secchi, S. Silvi, *Chem. - Eur. J.* **2010**, *16*, 3467–3475.

[49] A. Arduini, F. Calzavacca, A. Pochini, A. Secchi, *Chem. - Eur. J.* **2003**, *9*, 793–799.

[50] A. Arduini, F. Ciesa, M. Fragassi, A. Pochini, A. Secchi, *Angew. Chem. Int. Ed.* **2005**, *44*, 278–281.

[51] A. Arduini, R. Bussolati, A. Credi, G. Faimani, S. Garaudée, A. Pochini, A. Secchi, M. Semeraro, S. Silvi, M. Venturi, *Chem. - Eur. J.* **2009**, *15*, 3230–3242.

[52] G. Orlandini, G. Ragazzon, V. Zanichelli, A. Secchi, S. Silvi, M. Venturi, A. Arduini, A. Credi, *Chem. Commun.* **2017**, *53*, 6172–6174.

[53] V. Zanichelli, G. Ragazzon, G. Orlandini, M. Venturi, A. Credi, S. Silvi, A. Arduini, A. Secchi, *Org. Biomol. Chem.* **2017**, *15*, 6753–6763.

Chapter 1. Oriented calix[6]arene-based [3]rotaxanes towards the synthesis of molecular cages

Introduction

One of the ultimate goals for contemporary chemists is to control the assembly and the functions of artificial nano-sized structures, achieving the highest possible precision. The miniaturisation of the components and the availability of responsive devices are, in fact, critical issues for the development of modern nanotechnologies. The bottom-up approach provides the most promising strategy for controlling the aggregation at the nanometre level, which starts from nanoscale objects, namely atoms, ions, or molecules, to build up ordered nanostructures endowed with specific functions. Molecular capsules or cages are molecular scaffolds endowed with a nano-sized cavity isolated from the bulk phase, which can host a complementary guest molecule by various noncovalent interactions with the cage structure.[1–8] These assemblies are of particular interest in the development of containers that can provide stability to highly reactive guests,[9,10] such as phosphonium cations,[11] cyclobutadiene,[12] or even reactive elemental white phosphorus.[13] Capsular assemblies create a cavity in which the guest molecules frequently exhibit modifications as consequences of the confinement and, therefore, might be exploited as nanoscale “flasks” or reactors able to manipulate the physical and chemical properties of the trapped species.[14,15]

A peculiar class of molecular capsules is one in which the hollow cavity is composed of two hemispherical or curved molecules. Rebek and co-workers synthesised several cavitand-based containers held together by a network of reversible interactions or covalent bridges (Figure 1.1). They explored their behaviour as hosts, supramolecular containers, and reactors.[16,17] Because of its

preorganisation, calix[4]arene macrocycle has been an exploited building block for the synthesis of capsules in which the components are held together by noncovalent interactions,[18–20] or they are covalently bound through the insertion of molecular bridges.[21]

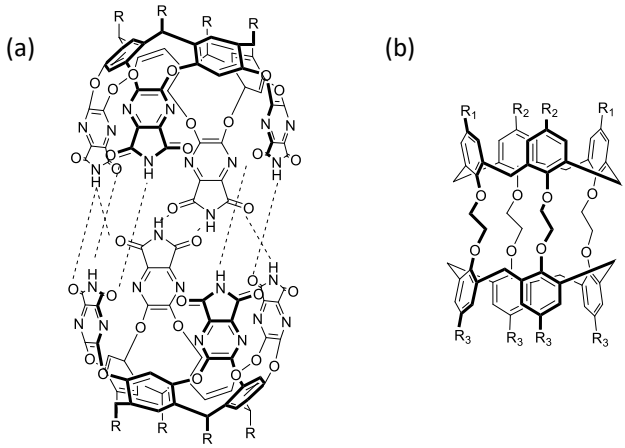

Figure 1.1 Examples of calix[4]arene capsules from (a) Rebek,[16] and (b) Kovalev.[21]

For the larger calix[6]arene macrocycle, the control of its large conformational flexibility remains a significant concern. Examples of noncovalent and covalent calix[6]arene-based capsules have been reported by the group of Jabin, who reported the synthesis of several calix[6]arene tubes for the encapsulation of organic ions.[22–24] Our research group tackled the synthesis of molecular capsules via hydrogen bond-guided self-assembly of tricarboxy[25] and triureido[26] calix[6]arene-based derivatives. These latter capsules displayed ability in encapsulating *N*-substituted pyridinium guests but also solvent molecules. We also reported on the formation and complexation properties of covalently linked double calix[6]arenes with imino and 1,4-phenylendiimino bridges[27] and the ability of a head-to-tail biscalix[6]arene to form pseudorotaxane complex with viologen salts was demonstrated.[28]

Synthesising covalently bound molecular capsules is often difficult because of the necessity of preorganising the capsule subcomponents in space before the final

linking event. These challenging syntheses may thus benefit from a templating effect exerted by “ad hoc” complexed species capable of interacting with both molecular capsule subcomponents, as found, for example, in pseudorotaxanes and rotaxanes.[29–31] In these supramolecular complexes, the axial component and the macrocycles (wheels) are organised with the correct mutual geometrical arrangement because of the intermolecular recognition between the axle with the wheels.

In the last two decades, we have exploited a series of tris-(*N*-phenylureido) calix[6]arenes, such as **TPU** (see Scheme 1.1), as hosts to synthesise Molecular Interlocked Molecules (MIMs).[32] It was discovered that electron-poor guests such as *N*,*N*′-dialkylviologen salts could thread the calix[6]arene annulus to give pseudorotaxanes complexes that, after thread capping or linking, led to the synthesis of [*1*]- and [*2*]rotaxanes.[33,34] More enticing were the findings that, in low polarity solvents, the threading process is governed by the functionality on the different rims of the calix[6]arene macrocycle. In particular, it occurs only from the macrocycle upper rim where the H-bond donating urea groups pivot the entrance of this ion-pair into the aromatic cavity of the host.[32]

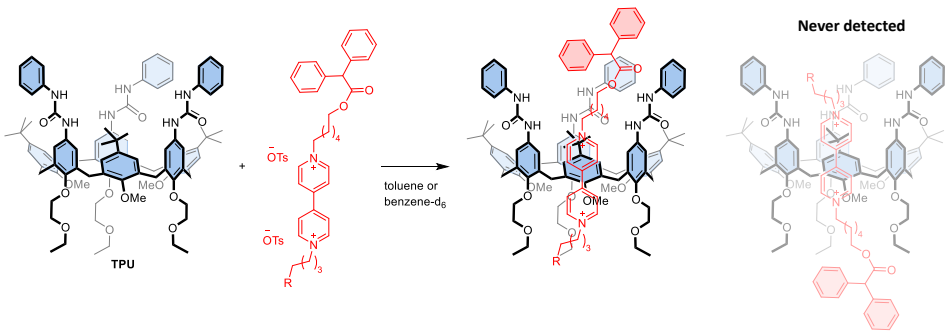

Scheme 1.1 Unidirectional threading of bis-viologen salts for the synthesis of oriented calix[6]arene-based [2]pseudorotaxanes.

Furthermore, because of the inherent asymmetry of the **TPU** cavity, introducing additional asymmetry elements in the thread, either as different stoppers or

length of the alkyl spacers, yields oriented [*2*]catenanes[35] and [*2*]rotaxanes.[36] On these premises, it is foreseen that the formation of the upper-to-upper bridged calix[6]arene capsules can benefit from the complexation of a bis-viologen axle capable of spatially orienting two suitably functionalised calix[6]arene wheels before their bridging.

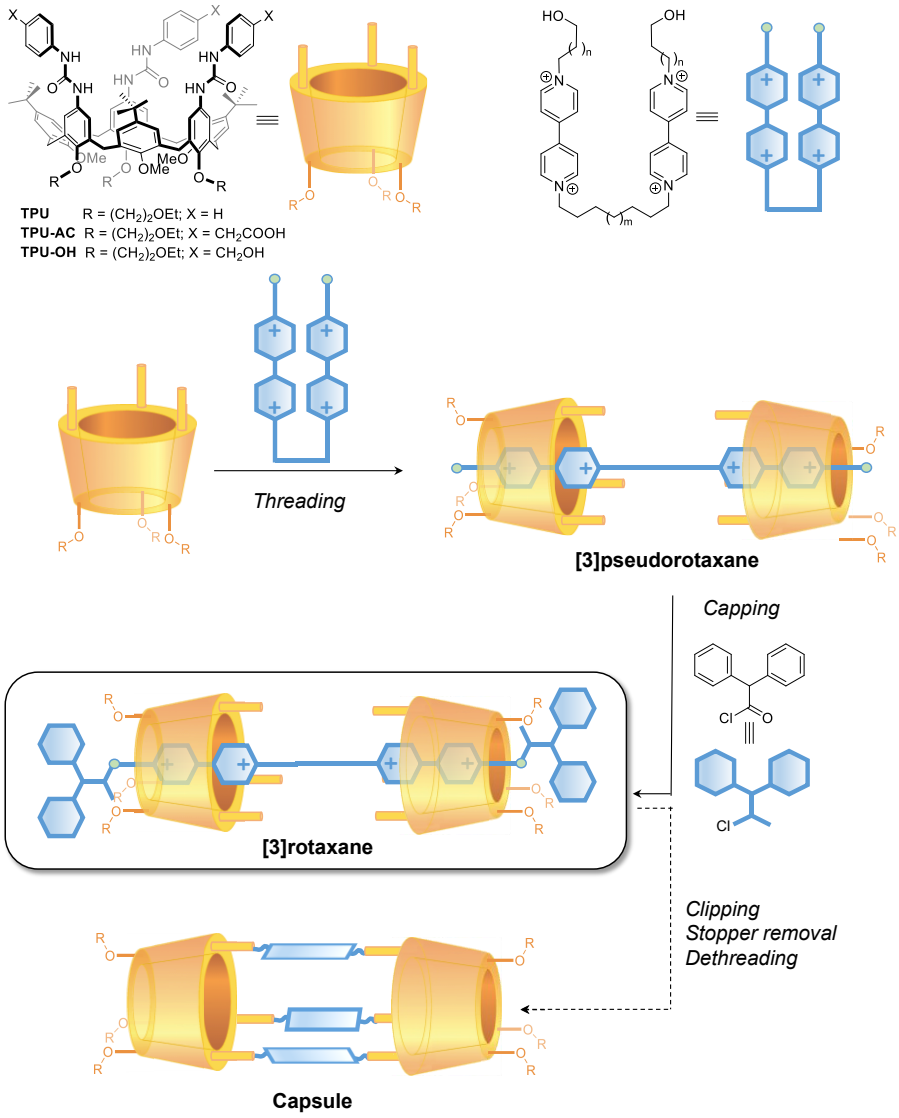

Figure 1.2 Template-assisted strategy for the synthesis of upper-to-upper calix[6]arene [*3*]rotaxanes.

In the present study, we aim to evaluate the templating effect[37,38] of a series of bis-viologen axles in promoting the formation of a series of upper-to-upper orientational [*3*]pseudorotaxanes (Figure 1.2). In addition, the effect of the length of the alkyl chain separating two calix[6]arene wheels and the space between the stoppers and the macrocycles in the resulting [*3*]rotaxanes will also be tackled (Figure 1.2). The method's optimisation finally aims to synthesise new [*3*]rotaxanes in which the facing calix[6]arene upper rims are decorated with either carboxy or hydroxymethyl groups. The latter could potentially be employed as grafting points for the formation of covalent bridges between the two macrocycles to create upper-to-upper bridged capsules through a stepwise threading/capping/clipping/stopper removal/axle dethreading procedure.

Results and Discussion

A series of axles of the type $\mathbf{4}_m$ (m = 12) and $\mathbf{5}_m$ (m = 6 and 12), where m indicates the length of the alkyl spacer between the viologen units, were prepared in good yields by reaction of the known pyridylpyridinium tosylates **1**-**2** with the corresponding ditosylates $\mathbf{3}_m$ in refluxing acetonitrile for four days (Scheme 1.2). Apart from the variable length of the internal spacer, these axles were also characterised by two external ω-hydroxyalkyl chains of different sizes: C6 for $\mathbf{4}_{12}$ and C12 for $\mathbf{5}_{6,12}$.

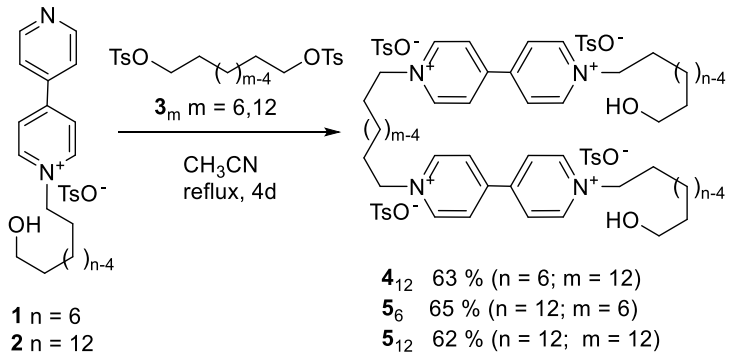

Scheme 1.2 Synthesis of bis-viologen axles.

A hydroxy group was present at the endings of these chains for the capping reaction, eventually leading to the oriented [*3*]rotaxane formation. The variable length of the external chains was chosen to explore whether the formation of the [*3*]rotaxanes could be affected by steric hindrance between the axle stoppers and the macrocycle.

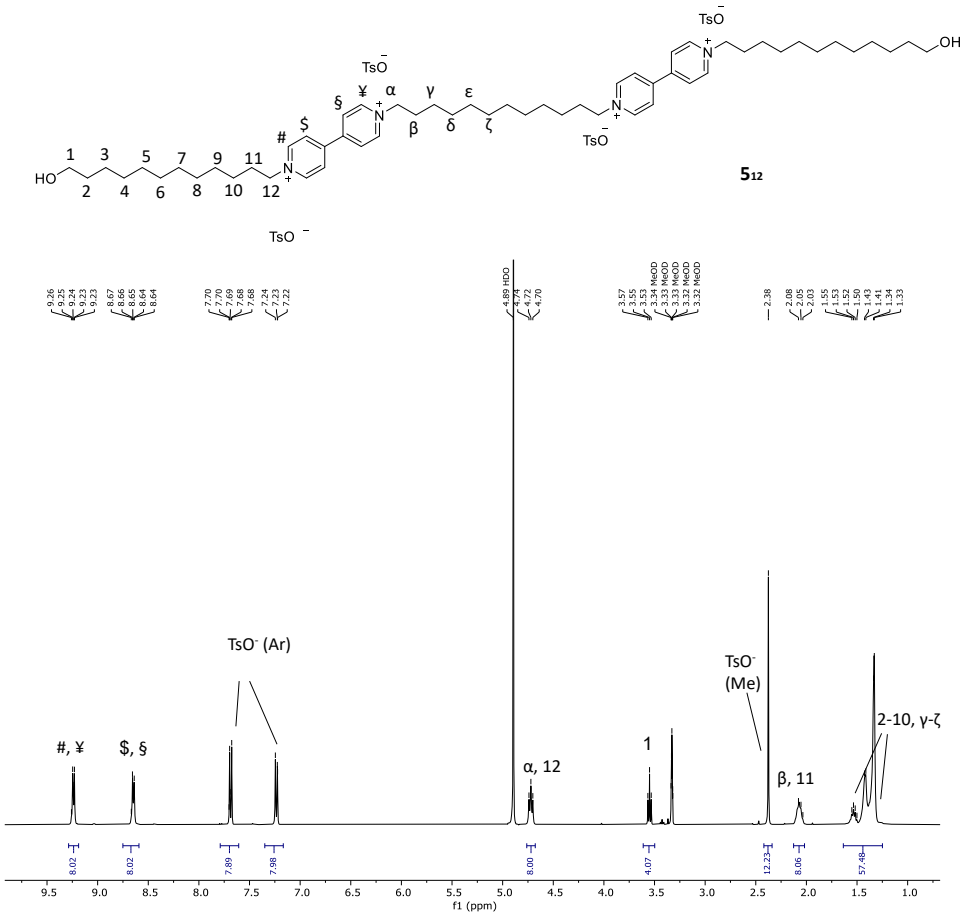

Figure 1.3 ^{1}H NMR spectrum (400 MHz, CD_3OD) of compound **5**$_{12}$.

The identity of the synthesised bis-viologen axles **4**$_{12}$ and **5**$_{6,12}$ was confirmed through a plethora of ^{1}H NMR and ESI-MS measurements. As an example, the ^{1}H NMR spectrum of **5**$_{12}$, taken in CD_3OD (Figure 1.3), shows several diagnostic resonances, such as the multiplet centred at 4.70 ppm corresponding to the eight protons of the four methylene groups α and *12* linked to the pyridinium moieties,

and a triplet at 3.53 ppm for the four protons of the two hydroxymethyl groups *1*. On the other hand, the two bipyridinium units resonate as two doublets, each integrating for eight protons, at 9.22 (protons ¥, #) and 8.63 ppm ($,§).

To evaluate the effect of the length of the axle components on the [*3*]pseudorotaxane formation, **TPU** was used as a wheel prototype (Scheme1.3). Indeed, it is known that the threading of **TPU** with an asymmetric *N,N'*-dialkyl viologen axle in weakly polar solvents is unidirectional and occurs with the axle's shortest alkyl chain through the macrocycle wider rim.[39] Therefore, the complexation reaction between **TPU** and any of the axles $\mathbf{4}_{12}$ and $\mathbf{5}_{6,12}$ would always lead to upper-to-upper [*3*]pseudorotaxane orientational isomers in which the two calix[6]arene upper rims are facing each other (Scheme 1.3).

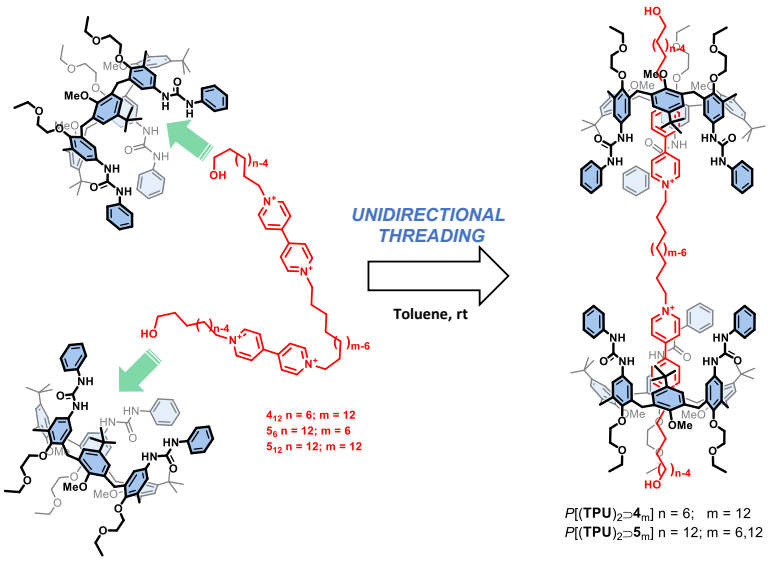

Scheme 1.3 Formation of [3]pseudorotaxanes *P*[(**TPU**)$_2$⊃**4**$_m$] and *P*[(**TPU**)$_2$⊃**5**$_m$].

To verify this hypothesis, an NMR experiment was performed: $\mathbf{5}_6$ (1 equiv.) was suspended in a solution of **TPU** (2 equiv.) in deuterated benzene. After stirring at room temperature for 24 h, the mixture appeared still heterogeneous and pale orangish-coloured. The solid suspension was filtered off, and the resulting homogeneous solution was submitted to NMR measurements. The

corresponding ^{1}H NMR spectrum (Figure 1.4b) shows that the axle-wheel interaction restricts the fluxionality of **TPU** in C_6D_6 (Figure 1.4a). A more significant proof of the wheels' threading was given by the downfield shift, with sharpening, experienced by the signal of the methoxy groups of **TPU** ($\Delta\delta$ ~1.4 ppm) and by the downfield shift of its NH signals ($\Delta\delta$ ~2 ppm), which are engaged in H-bonding with the tosylates (cf. Figure 1.4a and 1.4b, pale blue continuous lines).

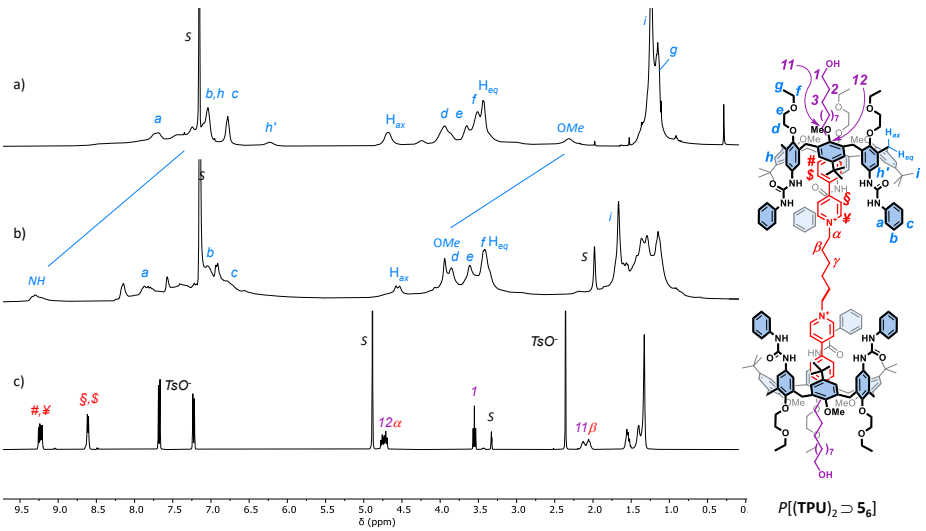

Figure 1.4 ^{1}H NMR stack plot (400 MHz, C_6D_6) of a) **TPU**; b) mixture of $\mathbf{5}_6$ with **TPU** (2 eq.); c) $\mathbf{5}_6$ (taken in CD_3OD for solubility reasons).

More interesting results came from the threading experiments with the axles having the longer internal C12 spacer $\mathbf{4}_{12}$ and $\mathbf{5}_{12}$. In both cases, the suspensions in benzene turned homogeneous and deeply red coloured after a few hours of stirring. This colour is usually a naked-eye sign of the pseudorotaxane formation since it derives from a charge transfer (CT) interaction between the π-rich cavity of **TPU** and the π-poor bipyridinium moiety of the axle. The formation of a [*3*]pseudorotaxane complex, labelled as *P*[(**TPU**)$_2$⊃$\mathbf{5}_{12}$] in Scheme 1.3, was confirmed by the correct 1:2 ratio between the proton NMR signals assigned, based on our previous studies on similar systems,[32] to the threaded axle and the

wheel (Figure 1.5). Among these signals, it is worth noting an AX system (geminal coupling) of two doublets at 4.57 and 3.38 ppm, the latter partially overlapped by other intense resonances, for the bridging methylene protons of the macrocycle. Such a system confirms that the threaded wheels are adopting a *cone* conformation around the axle. The splitting of the resonances of the axle bis-pyridinium units instead witnessed the upper-to-upper orientation of the wheels. In the free $\mathbf{5}_{12}$, the two pairs of pyridinium protons labelled ¥, #, and *$*, *§* resonate as two undistinguishable doublets at 9.24 and 8.65 ppm, respectively.

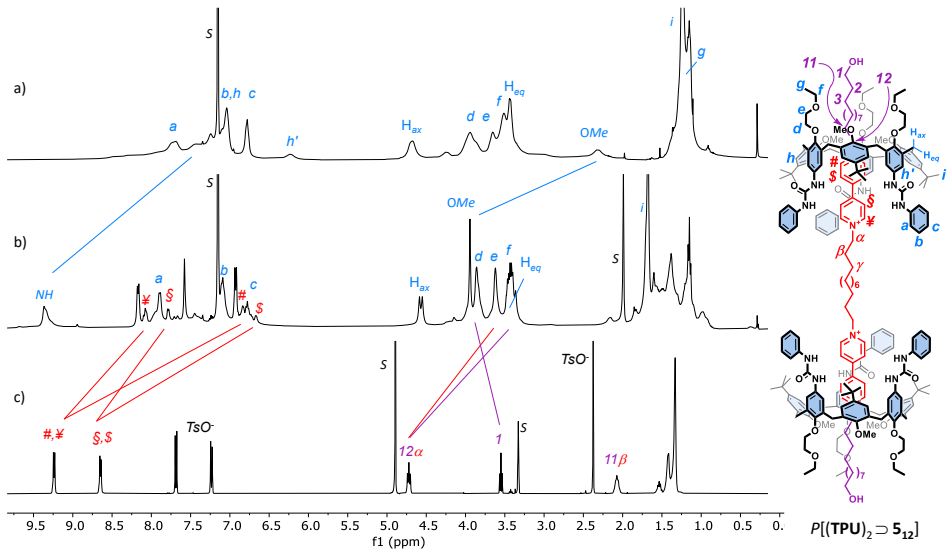

Figure 1.5 ^{1}H NMR stack plot (400 MHz, C_6D_6) of a) **TPU**; b) mixture of $\mathbf{5}_{12}$ with **TPU** (2 eq.); c) $\mathbf{5}_{12}$ (taken in CD_3OD for solubility reasons).

Upon inclusion, because of the asymmetry of the calix[6]arene cavity, they give rise to four upfield-shifted broad resonances at 8.1, 7.8, 6.8 and 6.7 ppm, which were identified thanks to an HSQC experiment (Figure 1.6). The extent of each upfield shift is, however, different: the *ortho* (#) and *meta* (*$*) protons of the two pyridinium rings deeply engulfed in the cavities are more upfield-shifted [$-\Delta\delta \sim$ 2.1 (#) and 1.6 (*$*) ppm] than those of the "facing" pyridinium rings [$-\Delta\delta \sim$ 1.2 (¥) and 0.75 (*§*) ppm]. Compared, the resonances of the methylene groups directly

linked to these pyridinium rings (α and *12*) underwent a minor upfield shift ($-\Delta\delta$ ~ 1 ppm), and their splitting was less significant (red and purple lines).

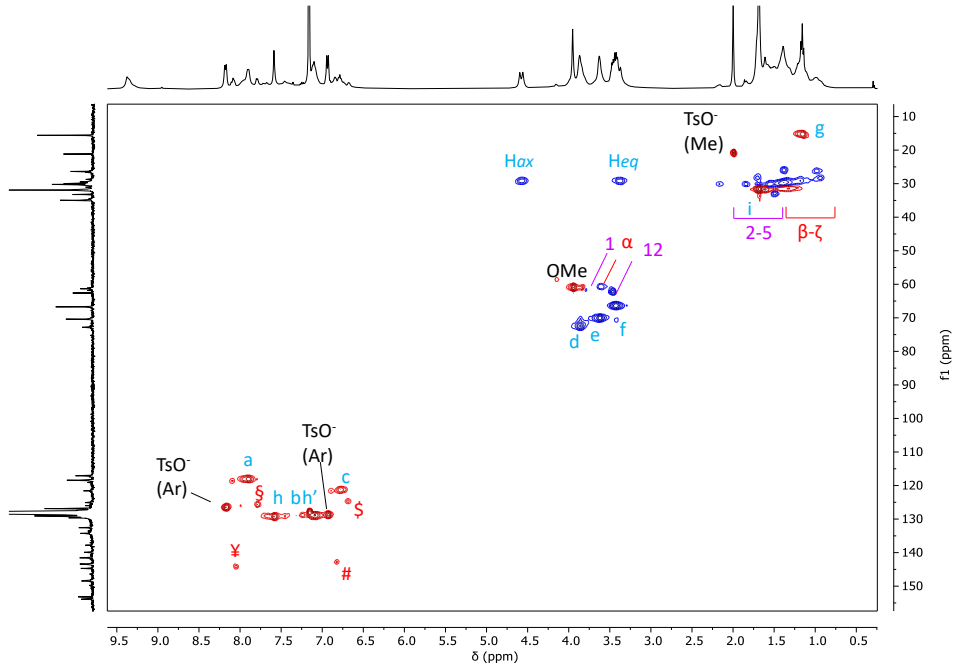

Figure 1.6 Edited HSQC NMR spectrum (400 MHz, benzene-d_6) of [*3*]pseudorotaxane *P*[(**TPU**)$_2$⊃**5$_{12}$**].

It is important to observe that the ^{1}H NMR spectrum of the threading experiment having **5**$_{12}$ as the axle shows narrower resonances than **5**$_6$. This reduced fluxionality could be thus ascribed to a better geometrical fit of the two calix[6]arene wheels around the axle endowed with the longer C12 alkyl spacer. Taken together, these complexation experiments suggest that: *i*) the C6 internal spacer of **5**$_6$ is too short for correct placement of the wheels around the two viologen units, and *ii*) threading of **4**$_{12}$ and **5**$_{12}$ occurs selectively leading to *upper*-to-*upper* [*3*]pseudorotaxane orientational isomers.

The synthesis of the interlocked species was then accomplished by capping the protruding hydroxymethyl endings of the encapsulated axles **4**$_{12}$ and **5**$_{12}$ with bulky diphenylacetyl (DPA) stoppers in toluene, as previously reported.[33,34] After

chromatographic separation, [*3*]rotaxanes *R*[(**TPU**)$_2$⊃**6**$_{12}$] and *R*[(**TPU**)$_2$⊃**7**$_{12}$] were isolated in 15% and 21% of yield, respectively.

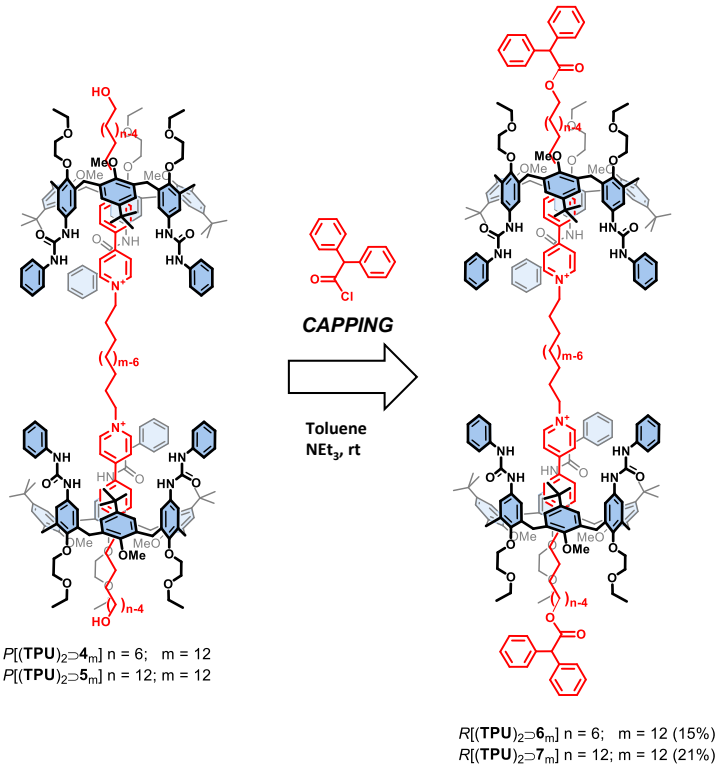

Scheme 1.4 Synthesis of [3]rotaxanes *R*[(**TPU**)$_2$⊃**6**$_{12}$] and *R*[(**TPU**)$_2$⊃**7**$_{12}$].

As expected, the shorter C6 external alkyl spacer of **4**$_{12}$ slightly reduces the success of the stoppering reaction for steric reasons. The successful formation of the interlocked compounds was initially verified through HR-MS measurements. *R*[(**TPU**)$_2$⊃**6**$_{12}$] displays a doubly charged molecular ion at m/z 2172.64861 (z = 2), whose isotopic pattern agrees with that of the target interlocked structure that has lost two tosylates (see Figure 1.7). *R*[(**TPU**)$_2$⊃**7**$_{12}$] gives rise instead to a triply charged molecular ion (base peak at m/z = 1446.48779 with z = 3) after losing one tosylate group, and a doubly charged molecular ion at m/z = 2256.74536 (z = 2) from the structure without two tosylates (see Figure 1.8).

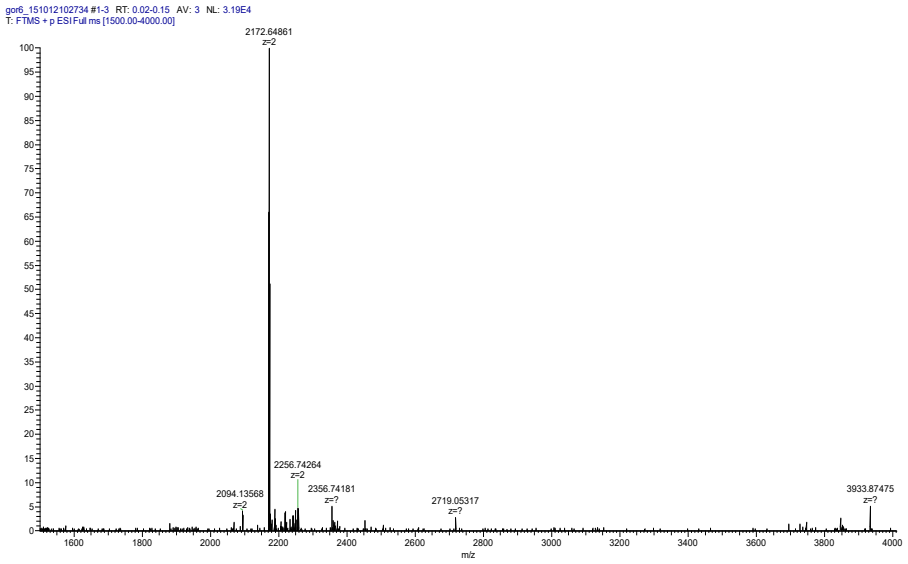

Figure 1.7 HR-MS (ESI, Orbitrap LQ) spectrum of [*3*]rotaxane *R*[(**TPU**)$_2$⊃**6$_{12}$**].

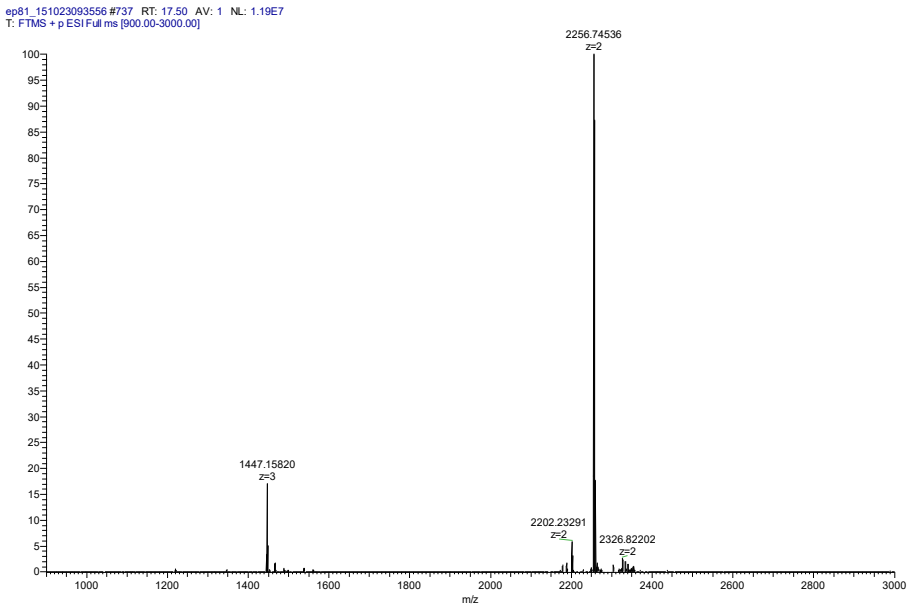

Figure 1.8 HR-MS (ESI, Orbitrap LQ) spectrum of [3]rotaxane *R*[(**TPU**)$_2$⊃**7$_{12}$**].

The synthesised [3]rotaxanes species were then fully characterised through a series of 1D and 2D NMR experiments.

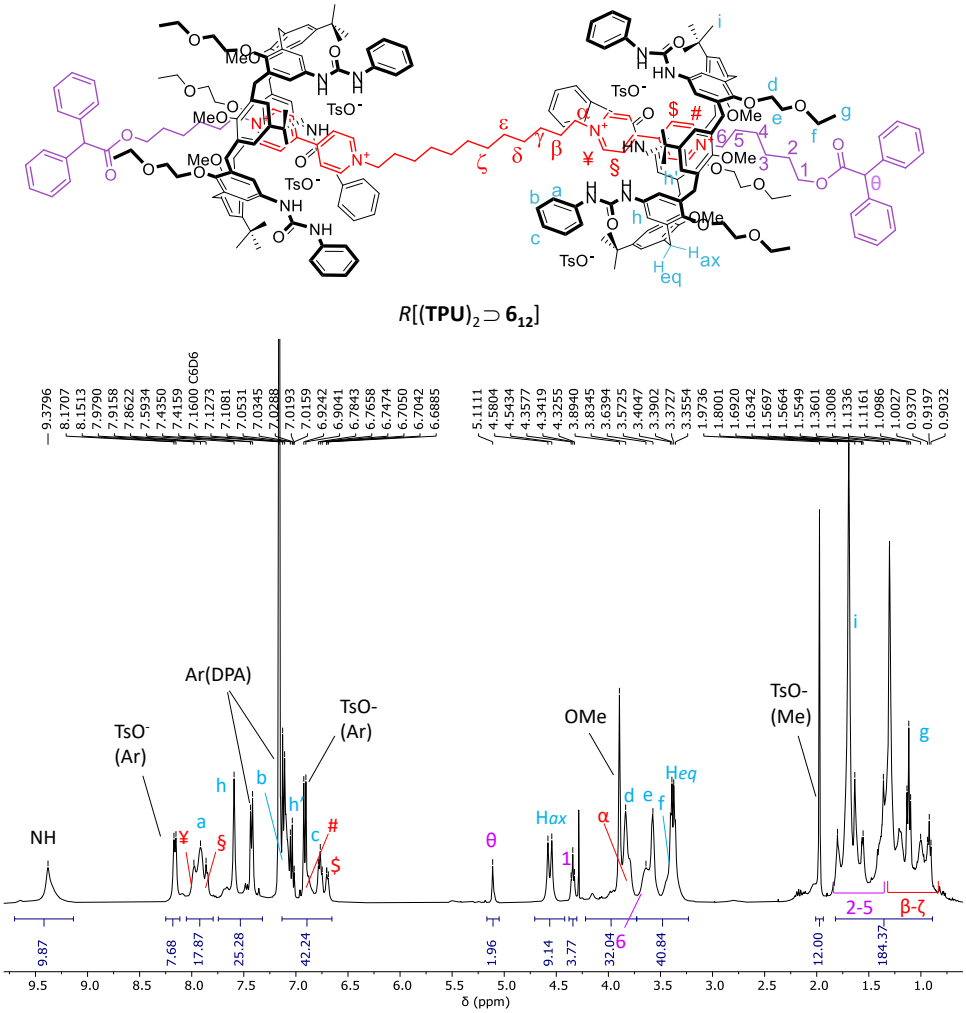

Figure 1.9 ^{1}H NMR spectrum (400 MHz, benzene-d$_6$) of [*3*]rotaxane *R*[(**TPU**)$_2$⊃**6$_{12}$**].

By observing the ^{1}H NMR spectrum of *R*[(**TPU**)$_2$⊃**6**$_{12}$] depicted in Figure 1.9, several different features can be noticed with respect to the ^{1}H NMR spectrum of its [*3*]pseudorotaxane precursor: *i*) a general improvement of the signals' resolution, *ii*) a crowding of signals in the aromatic region, and *iii*) the presence of a sharp signal at 5.1 ppm labelled as *θ* in Figure 1.9. Based on our previous studies on similar rotaxane systems,[40] this signal was assigned to the methine proton of the stoppers introduced on the axle endings. The capping reaction also affects the resonance of the nearby methylene group (*1*). In fact, in its

pseudorotaxane precursor, this group gives rise to an overlapped hidden triplet at 3.85 ppm, while in the [*3*]rotaxane is visible, downfield shifted ($\Delta\delta \sim 0.5$ ppm), at 4.35 ppm. Once again, the bis-pyridinium resonances of the capped thread (i.e. the dumbbell) in *R*[(**TPU**)$_2$⊃**6**$_{12}$] result largely upfield-shifted compared to those of the free **4**$_{12}$.

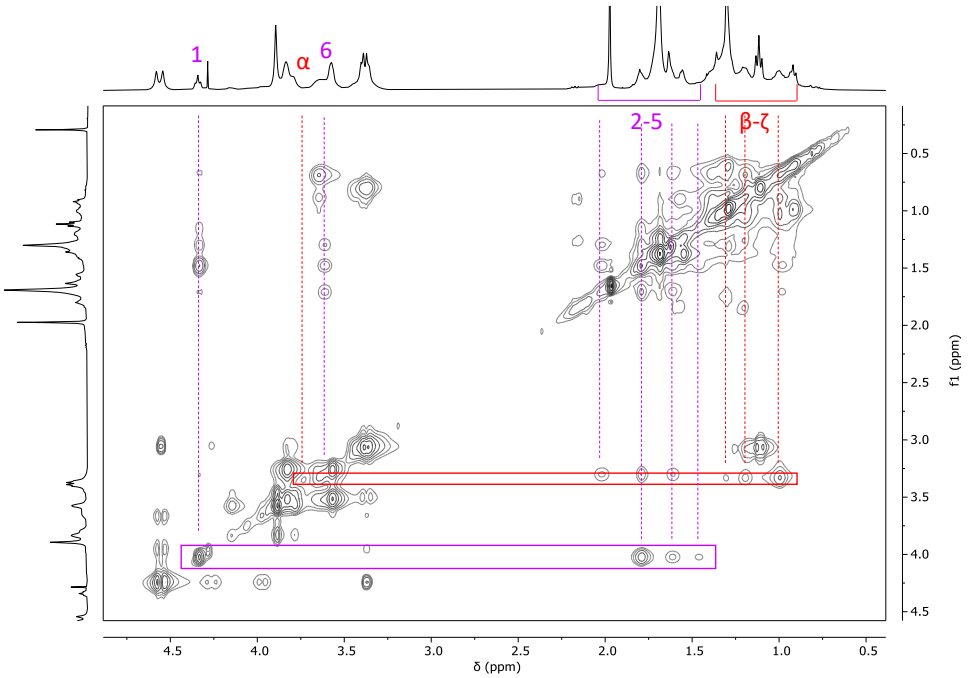

Figure 1.10 2D TOCSY NMR spectrum (400 MHz, benzene-d$_6$, MT = 0.06 s) of [*3*]rotaxane *R*[(**TPU**)$_2$⊃**6**$_{12}$] (zoom between 0.5-5 ppm).

Thanks to a series of TOCSY experiments, the identification of the outer and internal alkyl spacers was achieved starting from those of the methylene groups labelled as α and *6*. By considering the symmetric upper-to-upper arrangement of the calix[6]arene wheels of this interlocked structure, the resonances of the internal spacer, highlighted in the spectrum of Figure 1.10 in purple (protons 2-5), experience a higher shielding effect than those of the external arms, highlighted in red (protons β-ζ). Similar NMR features were observed for *R*[(**TPU**)$_2$⊃**7**$_{12}$].

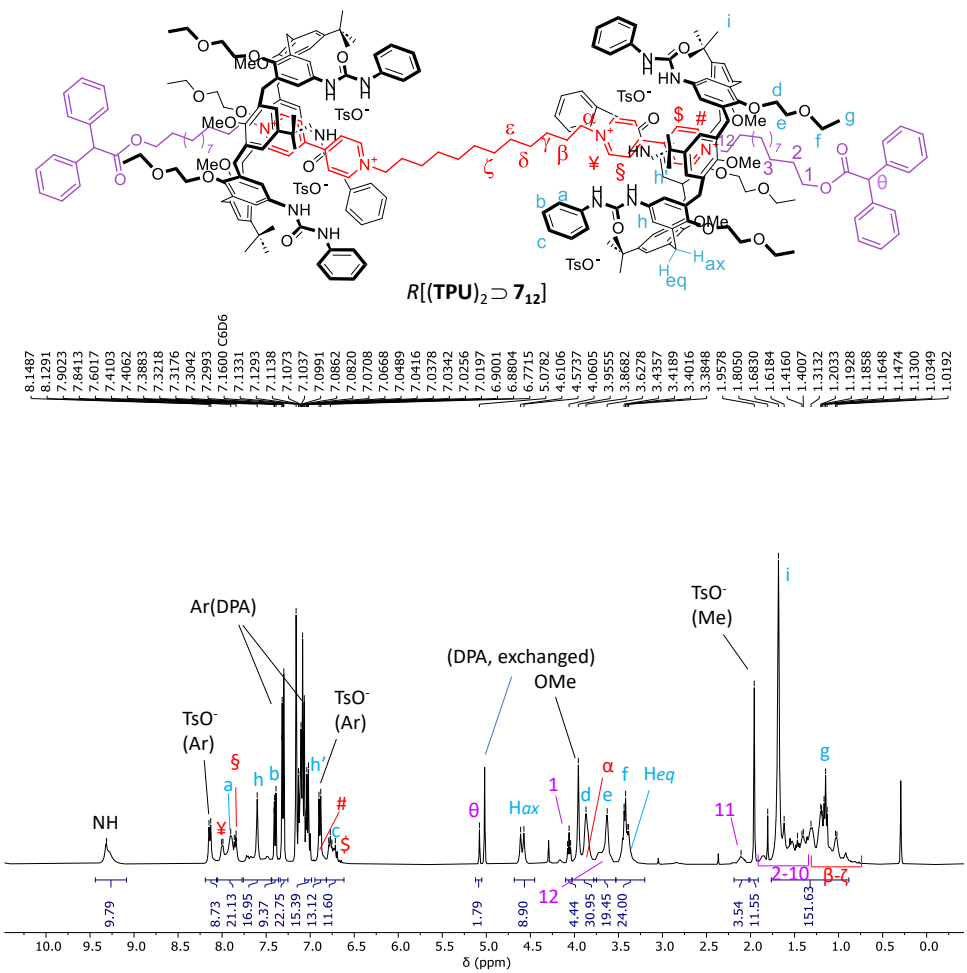

Figure 1.11 ^{1}H NMR spectrum (400 MHz, benzene-d_6) of [*3*]rotaxane *R*[(**TPU**)$_2$⊃**7$_{12}$**]. The resonance with the DPA label at 5.02 ppm is associated with the signal of the diphenylacetate methine proton that exchanged the tosylates upon axle stoppering.

The aromatic protons from the stoppering diphenyl acetate group can be identified in the aromatic region; the sharp signal corresponding to the methine proton θ resonates at 5.01 ppm. As observed before, the methylene group *1* experiences a downfield shift from 3.45 ppm in the pseudorotaxane to 4.05 ppm when in the [*3*]rotaxane ($\Delta\delta \sim 0.5$ ppm); in *R*[(**TPU**)$_2$⊃**7**$_{12}$], the bis-pyridinium protons appear considerably upfield-shifted than those of the free **5**$_{12}$. Complete signals' assignment was obtained through a series of 2D NMR measurements

(COSY, TOCSY, HSQC). As an example, the HSQC spectrum of *R*[(**TPU**)$_2$⊃**7**$_{12}$] is reported (Figure 1.12).

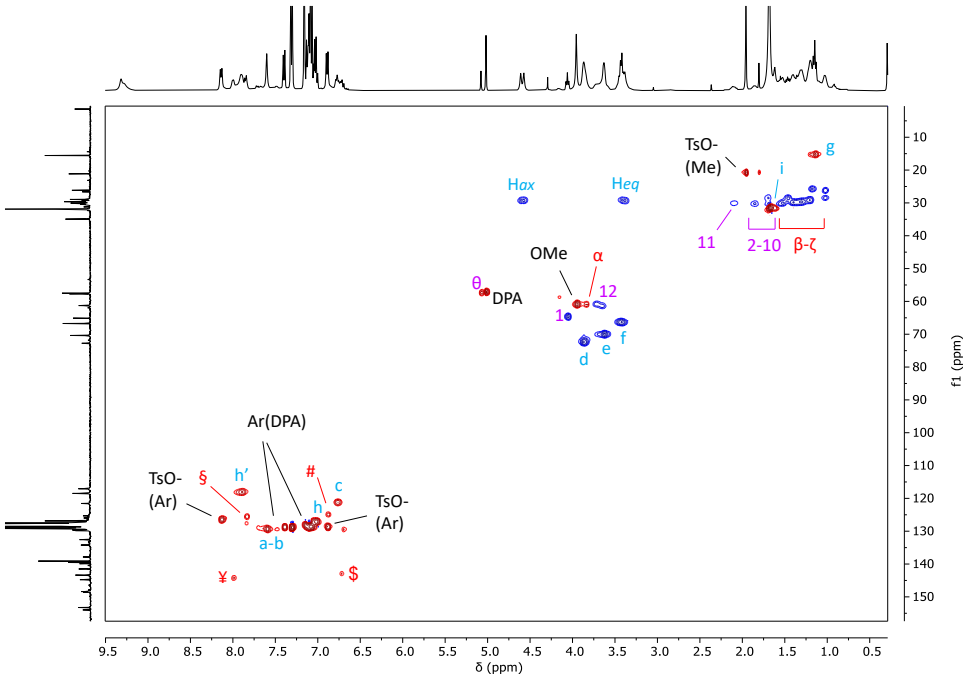

Figure 1.12 Edited HSQC NMR spectrum (400 MHz, benzene-d$_6$) of [*3*]rotaxane *R*[(**TPU**)$_2$⊃**7**$_{12}$].

Prompted by these results, we eventually explored the possibility of employing complementary axle stoppering units. To this aim, we opted for a triphenylsilyl (TPS) moiety since the bulkiness of this protecting group also allows its employment as a stopper for rotaxane synthesis. Moreover, the TPS stoppering group should be easier to take off than the diphenyl acetate moiety in the eventual stopper removal step. To pursue this possibility, [3]pseudorotaxane *P*[(**TPU**)$_2$⊃**5**$_{12}$] was reacted with chlorotriphenylsilane in the presence of imidazole as the base. This strategy was discreetly successful since the corresponding [*3*]rotaxane *R*[(**TPU**)$_2$⊃**8**$_{12}$] was isolated in 14% of yield after chromatographic separation. The ^{1}H NMR spectrum of [3]rotaxane *R*[(**TPU**)$_2$⊃**8**$_{12}$] (see Figure 1.13) exhibits a pattern of signals that reproduces the features of *R*[(**TPU**)$_2$⊃**7**$_{12}$], except for the peaks corresponding to the stoppering groups. In

particular, it is possible to distinguish the signals of the aromatic protons of the TPS stoppering group at 7.8 and 7.2 ppm. In this case, bis-pyridinium protons resonate at 7.9 (¥), 7.8 (§) and 6.75 (#, $). Moreover, differently from *R*[(**TPU**)$_2$⊃**7**$_{12}$], the signal of protons *1* appears hidden under those of protons *d*. Indeed, the corresponding 2D HSQC spectrum (Figure 1.14) shows that the signal of *1* resonates at 3.8 ppm.

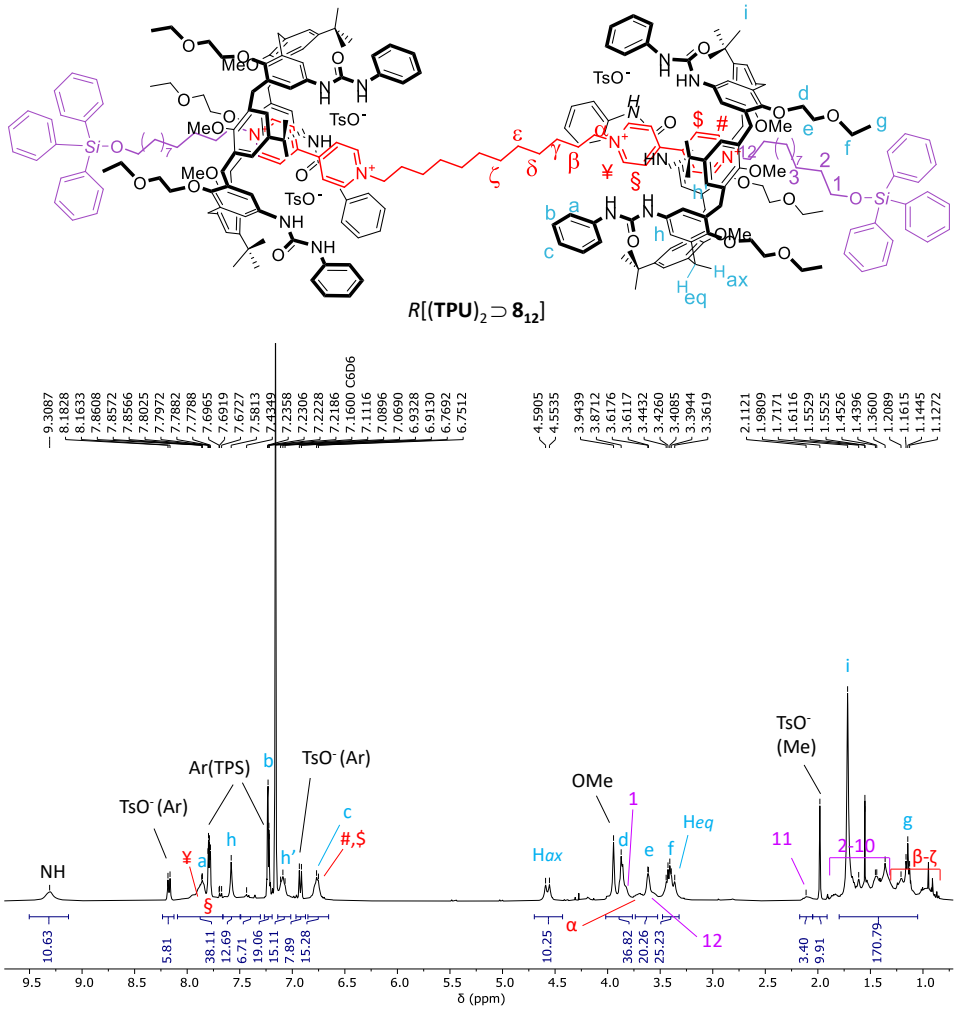

Figure 1.13 ^{1}H NMR spectrum (400 MHz, benzene-d$_6$) of [*3*]rotaxane *R*[(**TPU**)$_2$⊃**8$_{12}$**].

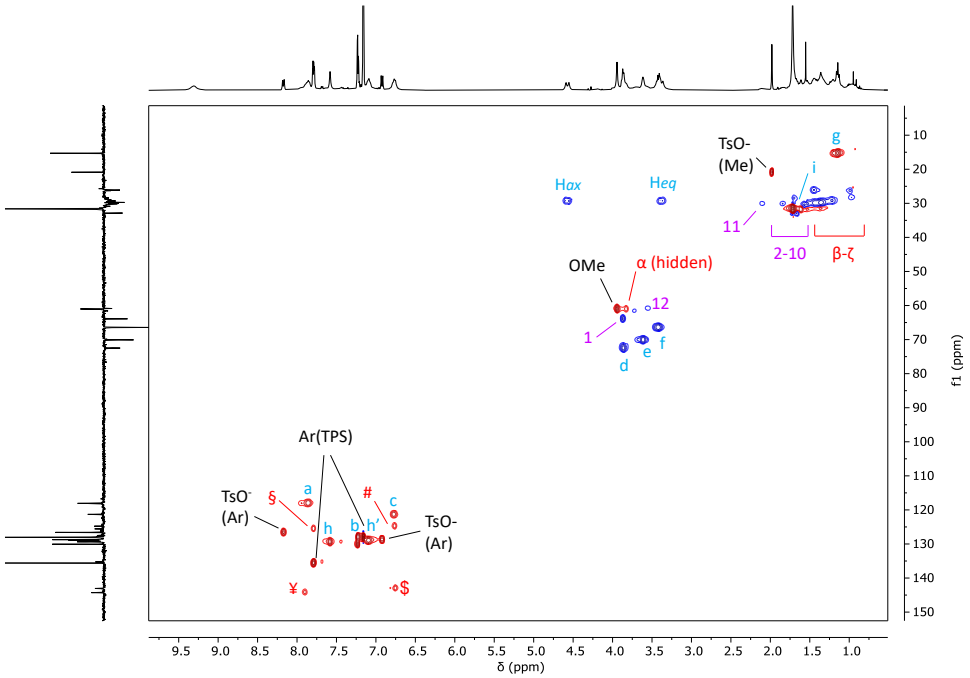

Figure 1.14 Edited HSQC NMR spectrum (400 MHz, benzene-d_6) of [*3*]rotaxane *R*[(**TPU**)$_2$⊃**8$_{12}$**].

Finally, the [*3*]rotaxane formation was confirmed by high-resolution mass spectrometry measurements (ORBITRAP LQ). In the corresponding spectrum, the peaks of three molecular ions can be recognised: one at m/z= 1074.87341 with z = 4 in which *R*[(**TPU**)$_2$⊃**8**$_{12}$] has lost its four tosylates, one at m/z= 1490.16818 with z = 3, which is attributed to the rotaxane without three tosylates, and finally one at m/z= 2320.75902 (z = 2) resulting from the loss of two tosylates. The m/z values and the experimental isotopic distributions fully match the corresponding simulated spectra (see Figure 1.15).

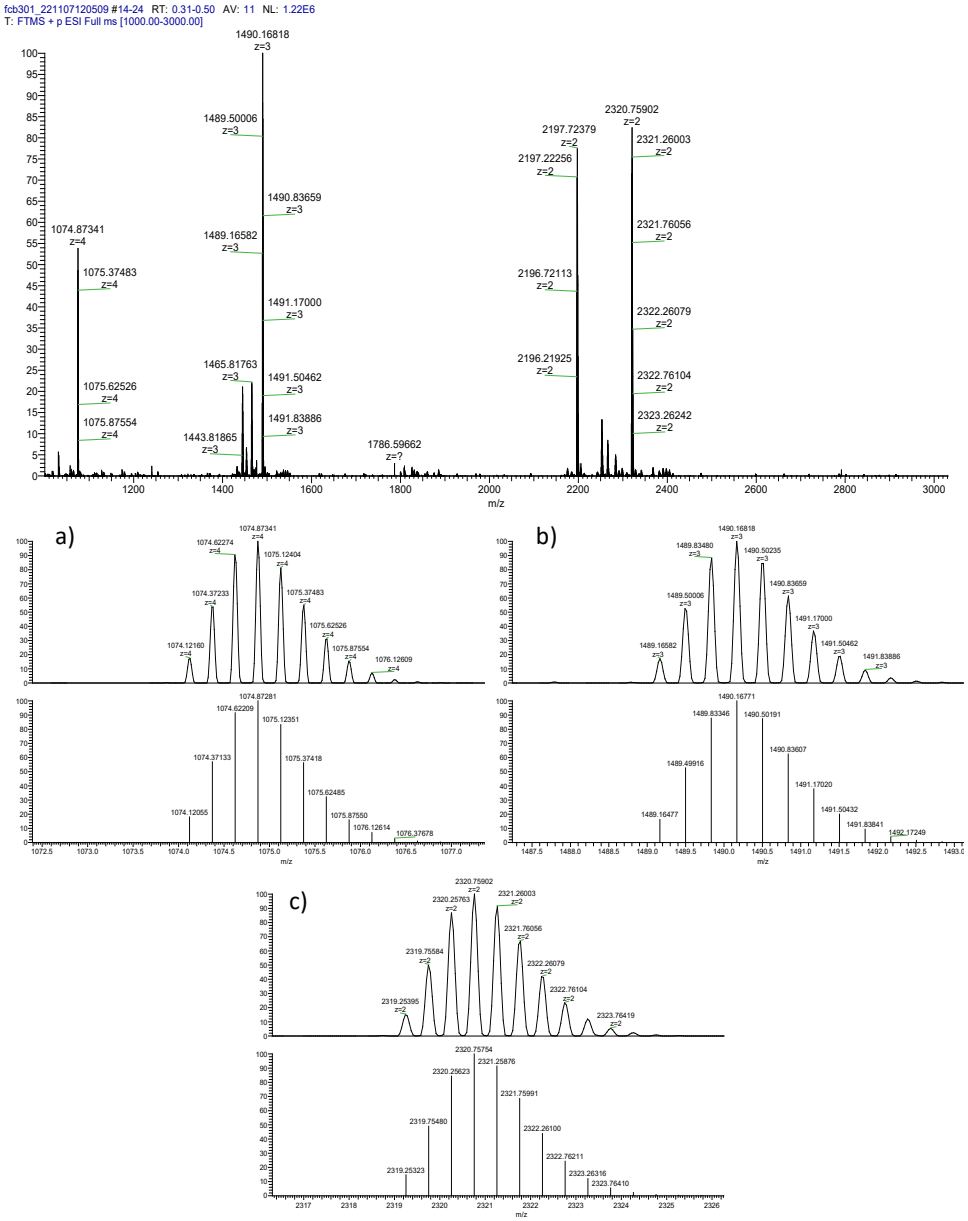

Figure 1.15 HR-MS (ESI, Orbitrap LQ) spectrum of [*3*]rotaxane R[$(TPU)_2$⊃**8**$_{12}$] showing the quadruple, triply and doubly charged molecular ions (top). Experimental and calculated isotopic distribution for the quadruple (a), triply (b) and doubly (c) charged molecular ion.

Motivated by the successful preparation of these interlocked structures, we planned to exploit the bis-viologen axles' templating effect for the synthesis of upper-to-upper bridged calix[6]arene-based capsules, as schematised in Figure

1.2. First, however, it becomes mandatory to decorate the phenylurea units of **TPU** with functional groups that allow the linking of the macrocyclic subunits with bridges of proper length and rigidity. To this aim, we designed calix[6]arene wheels that present the carboxylic and hydroxymethyl groups onto their phenylureas protected respectively as a *tert*-butyl ester (**TPU-ES**) and silyl ether (**TPU-OTBS**) (Figure 1.2). In principle, these protecting groups can be removed by using conditions that do not affect the ester group of the DPA stoppers and the macrocycle urea moieties. Consequently, after successful deprotection and activation, the resulting carboxyl (**TPU-ES**) and hydroxymethyl (**TPU-OTBS**) groups can be reacted with appropriate (nucleophilic or electrophilic) bifunctional linkers to yield the desired cages. Both wheels were prepared using the convergent synthesis depicted in Scheme 1.5. First, the two amino derivatives **13** and **14**, bearing the carboxylic and hydroxymethyl-protected functionalities, were synthesised from the nitro derivatives **9** and **10**. 2-(4-nitrophenyl)acetic acid **9** was protected using *tert*-butanol and DCC in the presence of a base in dichloromethane at room temperature to achieve **11** in 70 % yield. Instead, (4-nitrophenyl)methanol **10** was reacted with *tert*-butyldimethylsilyl chloride and triethylamine in dichloromethane affording **12** in 90 % yield. The nitro derivatives **11** and **12** were then reduced to desired amines **13** and **14** with H_2 and Pd/C in ethyl acetate, obtaining the conversion in 95 % yield.

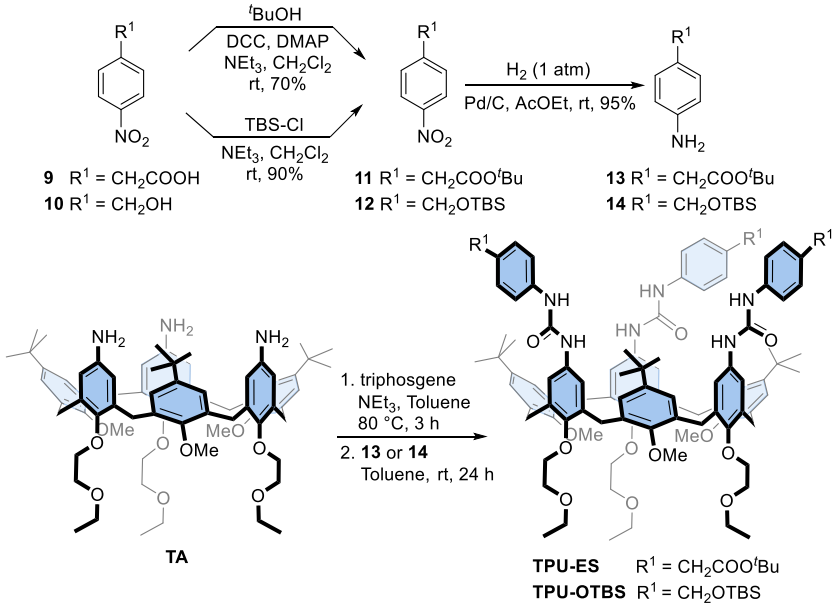

Scheme 1.5 Synthesis of triphenylureido *p*-substituted calix[6]arene macrocycles **TPU-ES** and **TPU-OTBS**.

Then, the known triamino calix[6]arene **TA**[26] was activated with triphosgene in toluene at 80 °C for three hours in order to generate three isocyanate moieties at its upper rim. After that, it was directly reacted with either **13** or **14** at room temperature to afford the target calix[6]arene derivatives **TPU-ES** and **TPU-OTBS** in 78% and 72% yields, respectively. Like **TPU**, the ^{1}H NMR spectra of these calix[6]arene derivatives present several broad resonances. Nonetheless, those associated with the inserted functionalities are easily recognisable. For instance, in the spectrum of **TPU-ES** (Figure 1.16), the methylene protons *c* can be observed as a singlet that resonates at 3.40 ppm, and the protons corresponding to the *tert*-butyl group (protons *j*) are detectable at 1.44 ppm.

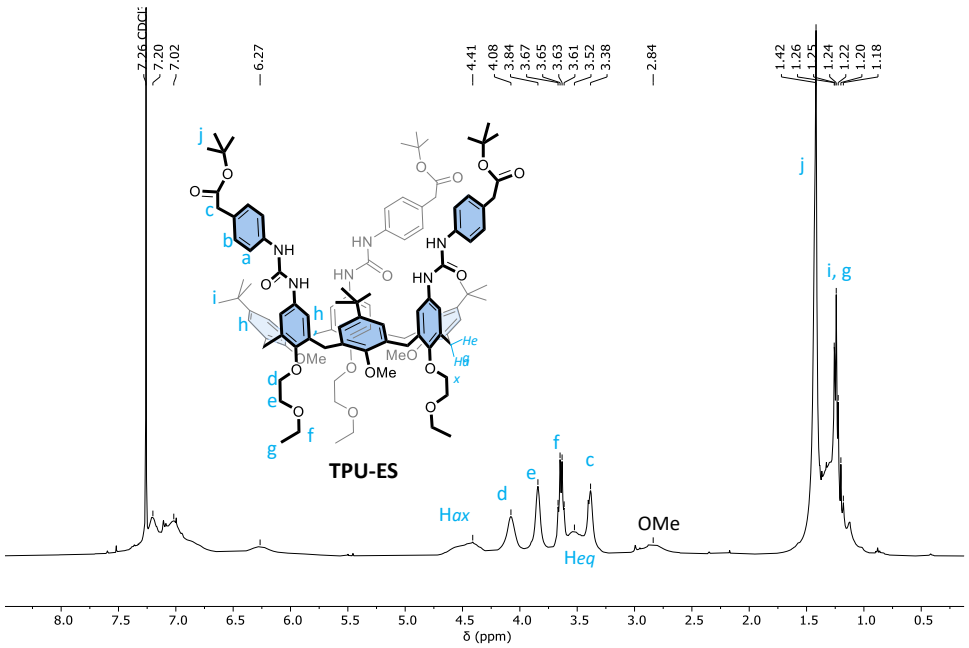

Figure 1.16 ^{1}H NMR spectrum (400 MHz, $CDCl_3$) of compound **TPU-ES**.

Likewise, diagnostic signals can be assigned for **TPU-OTBS**. In this case, methylene protons (*c*) resonate at 4.57 ppm, while the *tert*-butyl and methyl protons of the protecting group, labelled as *j* and *k*, are identified at 0.91 and 0.05 ppm, respectively (see Figure 1.17). High-resolution mass spectroscopy measurements (ORBITRAP LQ) finally confirmed the identity of the two novel macrocycles.

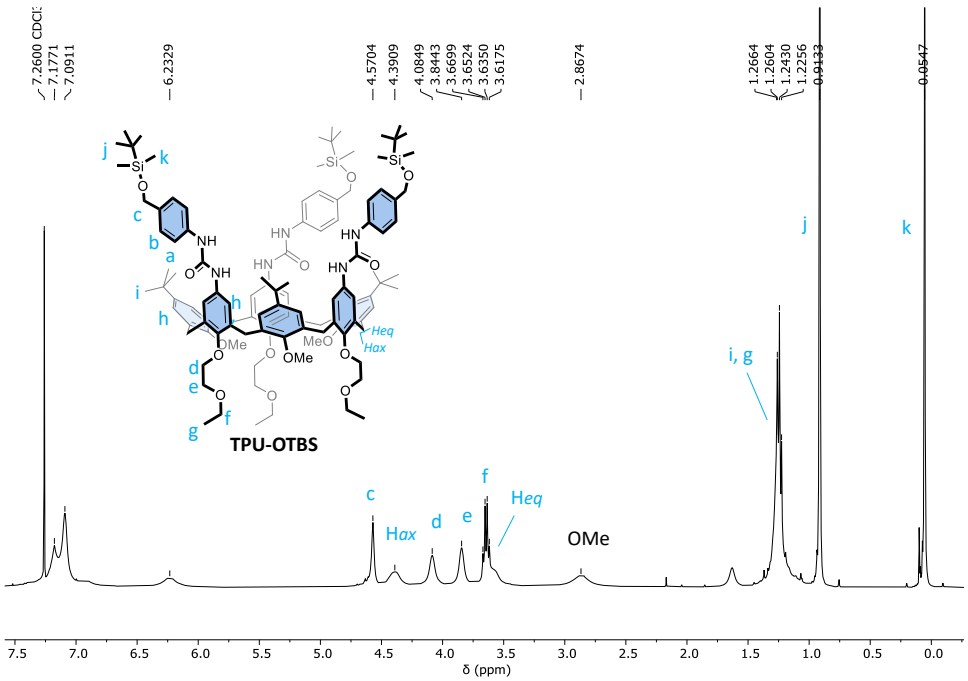

Figure 1.17 ^{1}H NMR spectrum (400 MHz, $CDCl_3$) of compound **TPU-OTBS**.

The synthesis of the [*3*]rotaxanes was thus performed by suspending axle $\mathbf{5}_{12}$ in a toluene solution containing a two-fold amount of the corresponding macrocycle (**TPU-ES** or **TPU-OTBS**). The resulting mixtures were stirred at room temperature for 24 hours. However, the mixture containing **TPU-OTBS** remained heterogeneous, even after stirring with heating (80 °C) for 24 hours. This unexpected result suggests that the bulkiness of the TBS protecting group prevents the threading of the bis-viologen axle inside the cavity of this calix[6]arene derivative. Fortunately for us, the mixture with **TPU-ES** turned homogeneous and red-coloured. A portion of this solution was thus evaporated to dryness, taken up with benzene-d_6, and submitted to a series of 1D and 2D NMR measurements to verify the formation of the [*3*]pseudorotaxane *P*[(**TPU-ES**)$_2$⊃$\mathbf{5}_{12}$] with the desired upper-to-upper orientation of the calix[6]arene wheels.

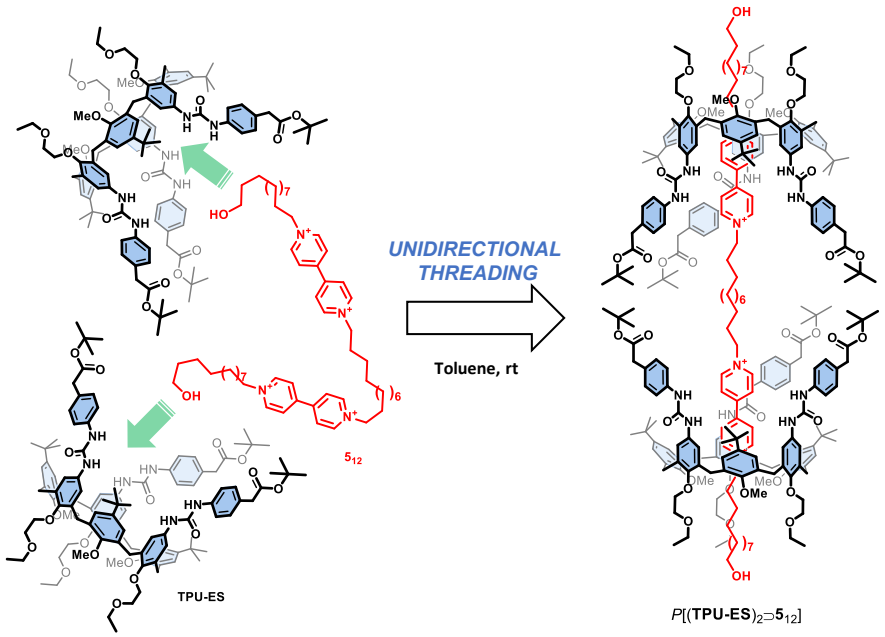

Scheme 1.6 Formation of [3]pseudorotaxanes *P*[(**TPU-ES**)$_2$⊃**5**$_{12}$].

Its ^{1}H NMR spectrum (Figure 1.18b) shows a signals pattern similar to *P*[(**TPU**)$_2$⊃**5**$_{12}$] (Figure 1.5b) except for the expected presence of the resonances relative to the methylene (*c*) and *tert*-butyl (*j*) groups at 3.45 and 1.70 ppm, respectively. As in the other cases, in the spectrum of [*3*]pseudorotaxane *P*[(**TPU-ES**)$_2$⊃**5**$_{12}$] we can observe the up-field shift of the bis-pyridinium protons (¥, #, and *$*, *§*) and the splitting of signals *12-α* and *11-β*, when axle **5**$_{12}$ is complexed by two macromolecules. Additionally, protons *1* give rise to a signal down-field shifted from 3.55 to 3.95 ppm. Finally, the six *OMe* groups of **TPU-ES** are detectable as a very sharp signal at 3.95 ppm in the [3]pseudorotaxane, thus witnessing the threading of the calix[6]arene cavities by the axle.

After the successful formation of the oriented [*3*]pseudorotaxane, the ω-hydroxymethyl endings of **5**$_{12}$ were stoppered as usual with two equivalents of DPA-Cl to yield the novel [*3*]rotaxane *R*[(**TPU-ES**)$_2$⊃**7**$_{12}$] in 24% of yield, after chromatographic separation (Scheme 1.7). MS-ESI and NMR measurements confirmed the success of these stoppering reactions.

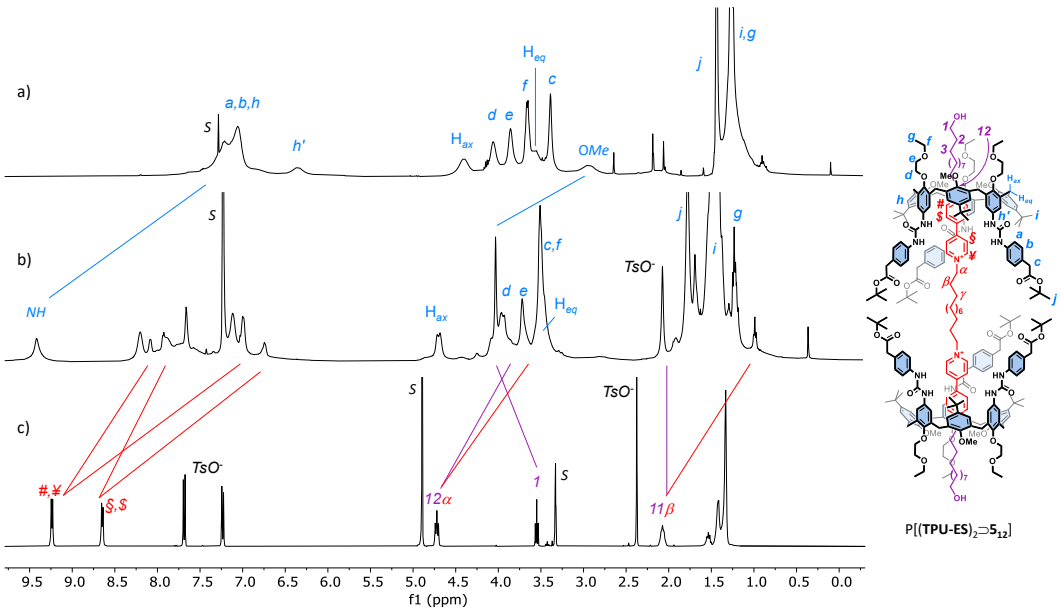

Figure 1.18 ^{1}H NMR spectra (400 MHz) of a) **TPU-ES**, b) [*3*]pseudorotaxane *P*[(**TPU-ES**)$_2$⊃**5**$_{12}$] in C_6D_6 and c) **5**$_{12}$ (taken in CD_3OD for solubility reasons).

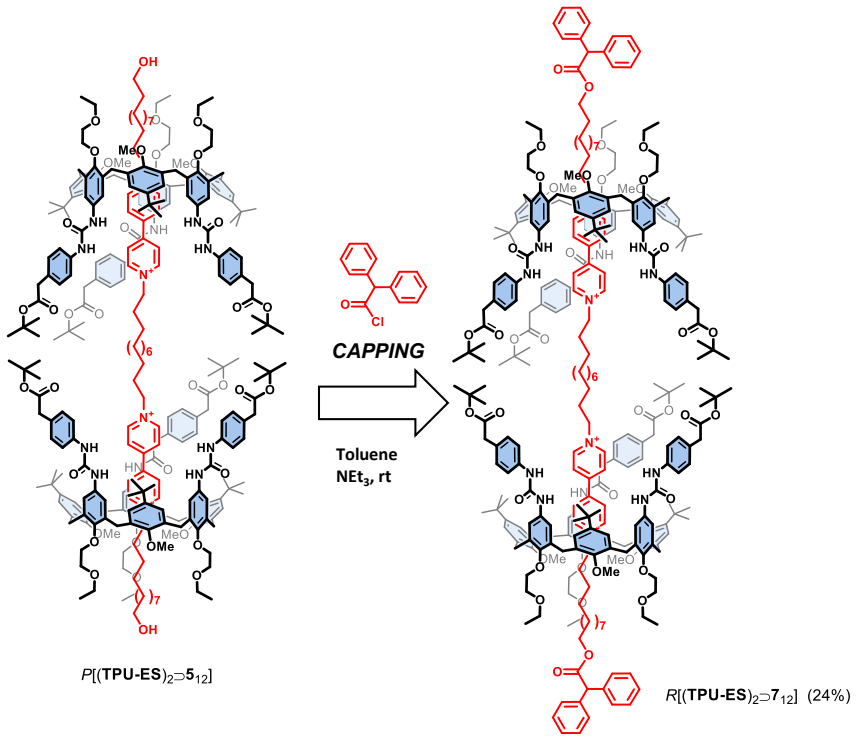

Scheme 1.7 Synthesis of [3]rotaxanes *R*[(**TPU-ES**)$_2$⊃**7**$_{12}$].

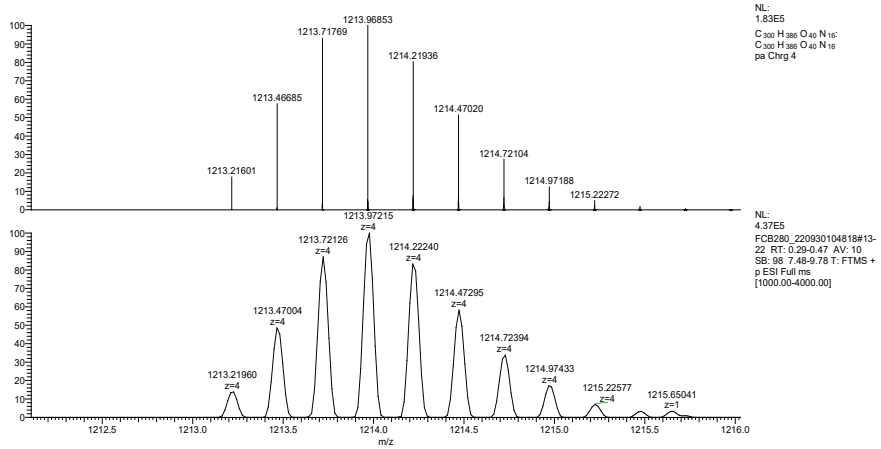

Figure 1.19 calculated (top) and experimental (down) isotopic distribution of peak found in high resolution mass spectrum of *R*[(**TPU-ES**)$_2$⊃**7**$_{12}$] for the quadruple charged molecular ion.

The HR-MS spectrum of the isolated compound shows a quadruple charged molecular ion (base peak at m/z = 1213.96853 with z =4), whose isotopic pattern agrees with that of the target interlocked structure that has lost four tosylates (Figure 1.19). The ^{1}H NMR spectrum (Figure 1.20) shows a unique singlet at 5.08 ppm for the methine proton θ of the DPA stoppers. This signal accounts for the symmetric upper-to-upper arrangement of the two **TPU-ES** wheels around the dumbbell **7**$_{12}$. Another evidence of the successful stoppering reaction is an aromatic spectrum region crowded with signals, for which the DPA aromatic protons are responsible. The complete signal assignment was achieved with 2D NMR measurements such as HSQC, COSY, TOSCY and ROESY experiments. The 2D HSQC spectrum has been reported in Figure 1.21 to show the identification of all the diagnostic signals.

The same strategy was employed for the synthesis of [*3*]rotaxane *R*[(**TPU-ES**)$_2$⊃**8**$_{12}$] using triphenylsilyl moiety as the stoppering group. [*3*]pseudorotaxane *P*[(**TPU-ES**)$_2$⊃**5**$_{12}$] was reacted with two equivalents of chlorotriphenylsilane and imidazole as the base, in toluene. The corresponding [*3*]rotaxane *R*[(**TPU-ES**)$_2$⊃**8**$_{12}$] was isolated in 17% of yield after chromatographic separation.

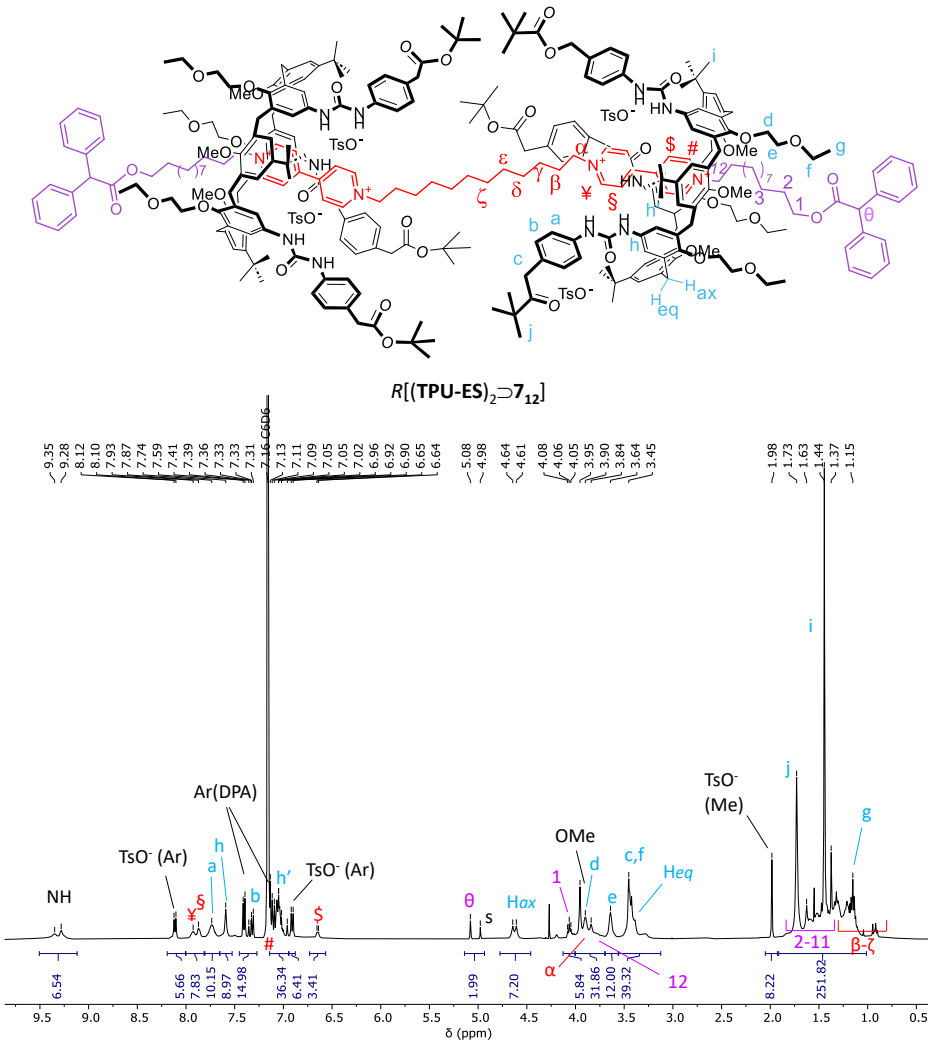

Figure 1.20 ^{1}H NMR spectrum (400 MHz, benzene-d$_6$) of [*3*]rotaxane *R*[(**TPU-ES**)$_2$⊃**7**$_{12}$]. The resonance with the S label at 5.02 ppm is associated with the signal of the diphenylacetate methine proton that exchanged the tosylates upon axle stoppering.

Then, the interlocked structure *R*[(**TPU-ES**)$_2$⊃**8**$_{12}$] was characterised through MS and NMR analyses. Unlike DPA, the TPS stoppers do not yield any diagnostic proton NMR resonance that can be exploited to assess which orientational isomer forms upon axle stoppering. However, the spectra of the two interlocked structures are almost perfectly overlapping (cf. Figure 1.20 and 1.23) except for the presence in the spectrum of *R*[(**TPU-ES**)$_2$⊃**8**$_{12}$] of supplementary aromatic

resonances, in the 7.8 – 7.2 ppm range, and the shift at higher fields (3.92 ppm, overlapped) of the previously visible resonance assigned to axle methylene group (*1*) (Figure 1.23). An upfield shift, the latter, originated by the replacement of an electron-withdrawing group (DPA) with a donating one (TPS) onto the thread hydroxyl endings. Most importantly, like *R*[(**TPU-ES**)$_2$⊃**7**$_{12}$], also the spectrum of *R*[(**TPU-ES**)$_2$⊃**8**$_{12}$] shows a single sharp signal at 3.95 ppm for the three methoxy groups at the macrocycle lower rim. This would indicate that the two calix[6]arene macrocycles are experiencing an identical magnetic environment. In other words, they are adopting the expected upper-to-upper symmetric arrangement of the macrocycles around the dumbbell.

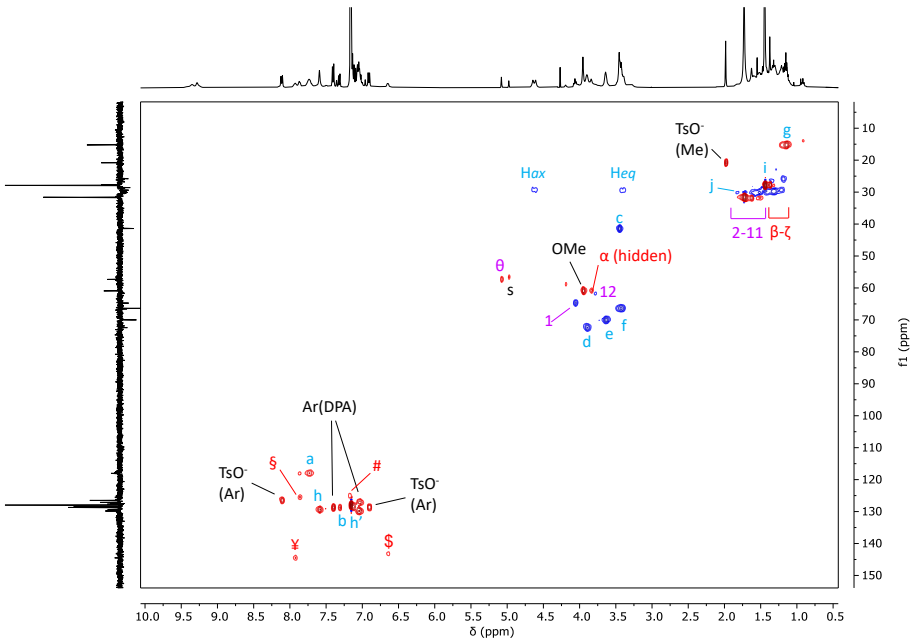

Figure 1.21 Edited HSQC NMR spectrum (400 MHz, benzene-d$_6$) of [*3*]rotaxane *R*[(**TPU-ES**)$_2$⊃**7**$_{12}$].

The HR-MS spectrum (Figure 1.22) shows a quadruple charged molecular ion with m/z = 1245.97588 (z = 4) and a triply charged molecular ion with m/z = 1718.29895 (z = 3). The experimental isotopic distributions perfectly match the calculated one.

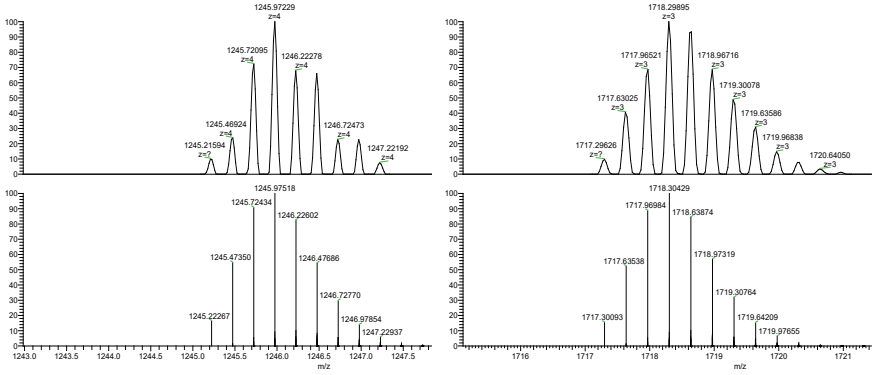

Figure 1.22 experimental (top) and calculated (down) isotopic distributions of peaks found in high resolution mass spectrum of *R*[(**TPU-ES**)$_2$⊃**8$_{12}$**] for the quadruple and triply charged molecular ion.

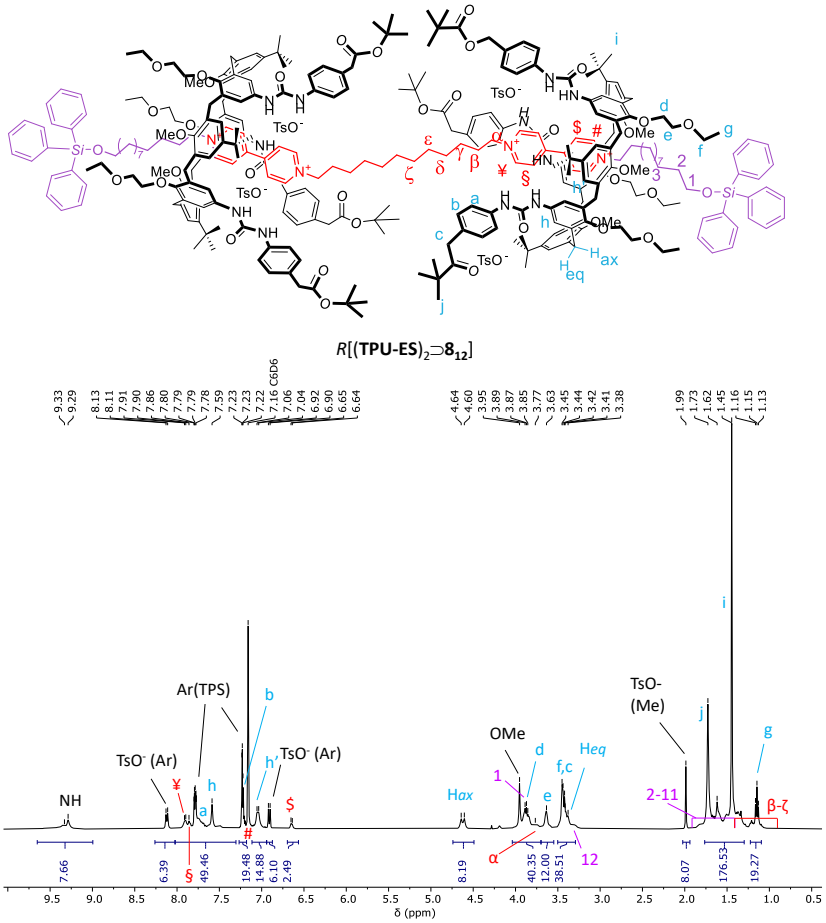

Figure 1.23 ^{1}H NMR spectrum (400 MHz, benzene-d$_6$) of [*3*]rotaxane *R*[(**TPU-ES**)$_2$⊃**8**$_{12}$].

Finally, the deprotection of the carboxyl groups of *R*[(**TPU-ES**)$_2$⊃**7**$_{12}$] and *R*[(**TPU-ES**)$_2$⊃**8**$_{12}$] was attempted by using *p*-toluenesulfonic acid monohydrate (TsOH·H$_2$O) in refluxing dichloromethane. Unfortunately, the reaction carried out with *R*[(**TPU-ES**)$_2$⊃**8**$_{12}$] led to a degradation of the rotaxane, likely due to a partial or complete axle de-stoppering reaction. Instead, the target [*3*]rotaxane *R*[(**TPU-AC**)$_2$⊃**7**$_{12}$] was isolated in good yield (60%) after chromatographic separation.

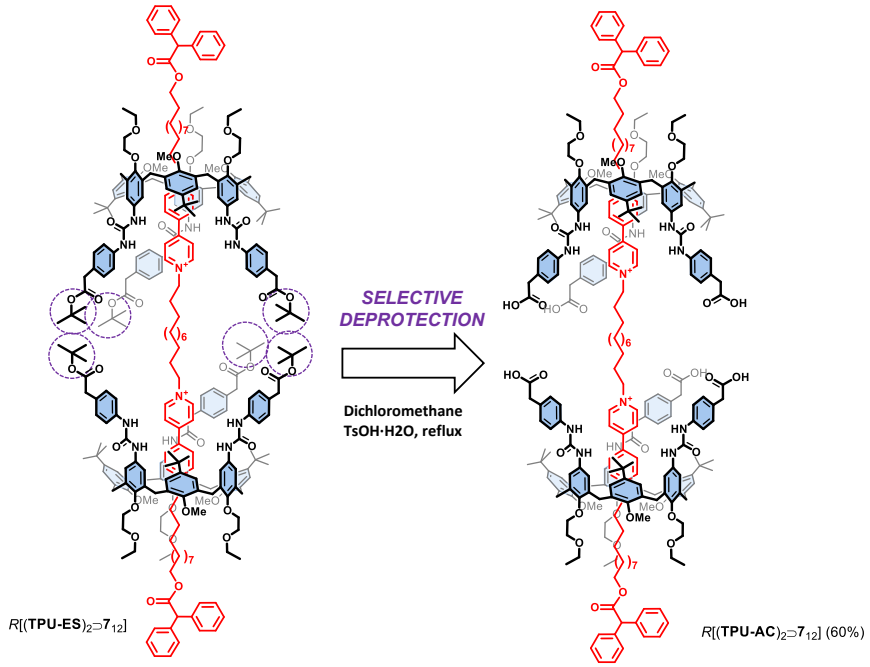

Scheme 1.8 Synthesis of [3]rotaxanes *R*[(**TPU-AC**)$_2$⊃**7**$_{12}$].

The formation of *R*[(**TPU-AC**)$_2$⊃**7**$_{12}$] was first verified by high-resolution mass analysis (see Figure 1.24): the spectrum exhibits the quadruple charged molecular ion at m/z = 1129.87418 (z = 4), which is attributed to the target structure that has lost four tosylates; the triply charged peak at m/z = 1563.50269 (z = 3) corresponds to the structure without three tosylates; lastly, the peak at m/z = 2430.76027 (z = 2) is assigned to the molecular ion without two tosylates.

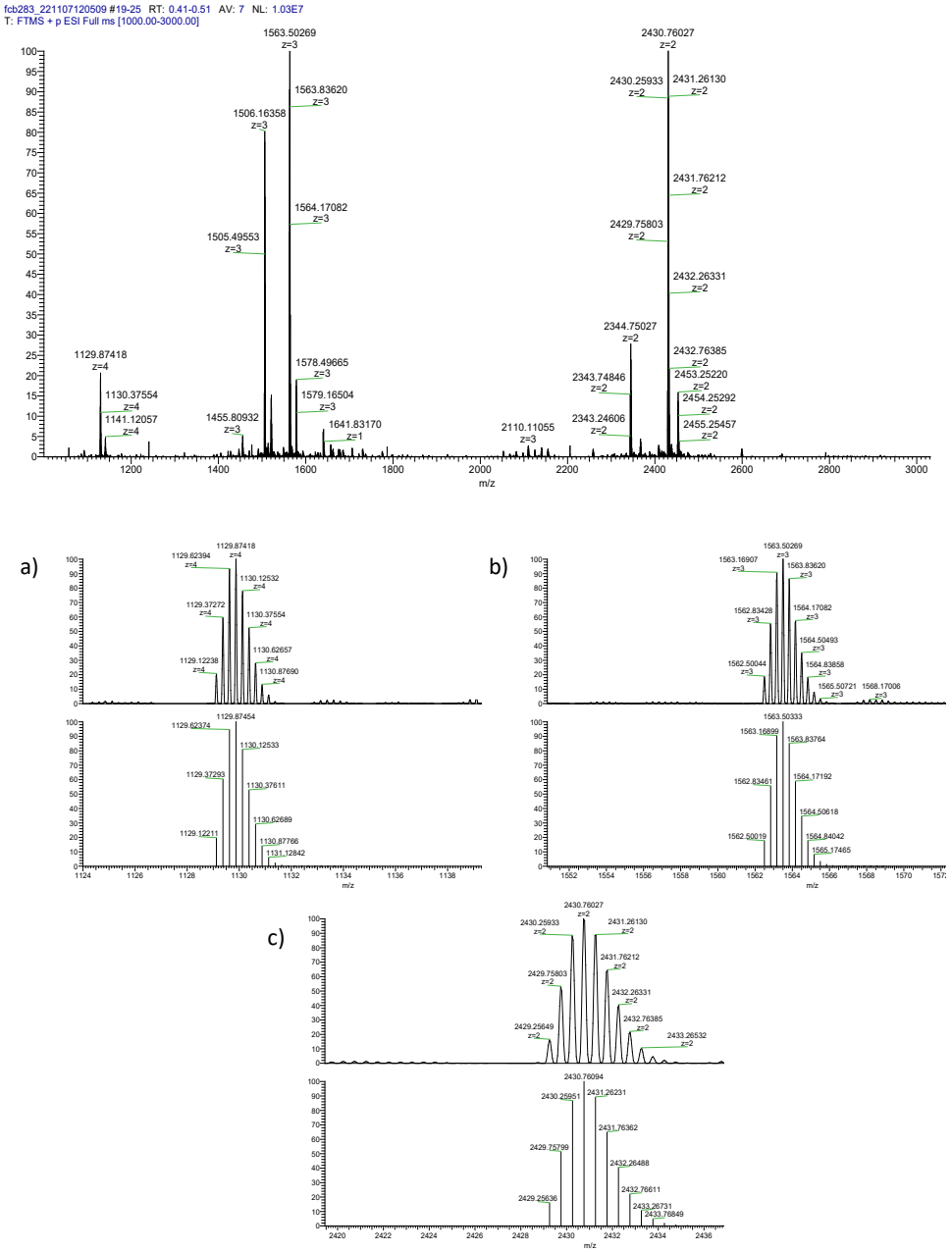

Figure 1.24 HR-MS (ESI, Orbitrap LQ) spectrum of [*3*]rotaxane *R*[(**TPU-AC**)$_2$⊃**7**$_{12}$] showing the quadruple, triply and doubly charged molecular ions (top). Experimental and calculated isotopic distribution for the quadruple (a), triply (b) and doubly (c) charged molecular ions (bottom).

Albeit HR-MS measurements confirmed the identity of *R*[(**TPU-AC**)$_2$⊃**7**$_{12}$], the interpretation of its ^{1}H NMR spectrum, taken in deuterated dichloromethane for

solubility reasons, was anything but straightforward. Broad resonances characterised the entire spectrum except for the diagnostic methine signal (θ) of the DPA stoppers (Figure 1.25b). The signals' broadness could be explained by considering a marked fluxionality of this structure on the NMR timescale. Still, the reasons for such mobility were less clear if the structures of *R*[(**TPU-ES**)$_2$⊃**7$_{12}$**] and *R*[(**TPU-AC**)$_2$⊃**7$_{12}$**] were compared. However, a perusal of the spectrum revealed the total absence of the three tosylate counterion resonances, which are usually sharp and easily identified, thus suggesting that a neutral (zwitterionic) form of this [*3*]rotaxane, in which four out of six carboxyl groups are ionised, was present in the dichloromethane solution.

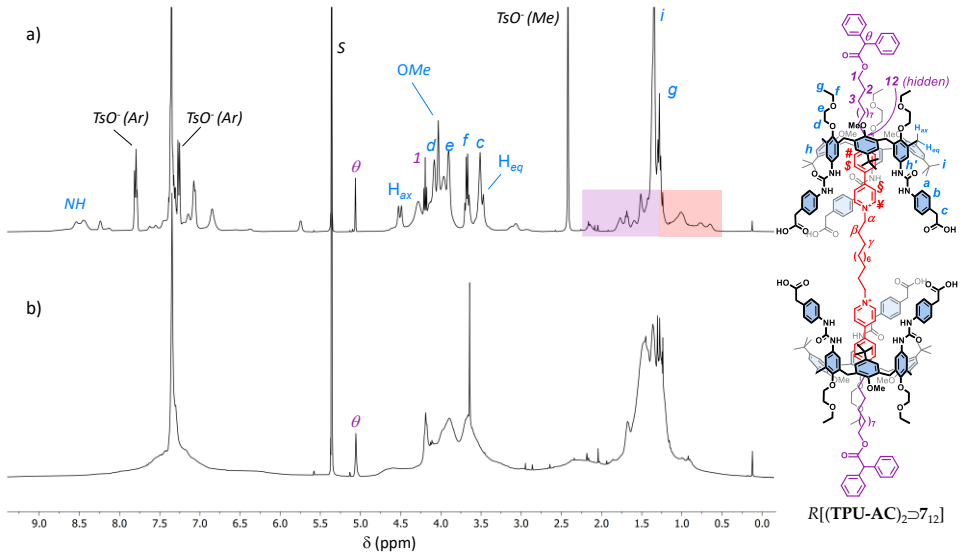

Figure 1.25 ^{1}H NMR spectra (400 MHz) of *R*[(**TPU-AC**)$_2$⊃**7$_{12}$**] in CD_2Cl_2 before (a) and after (b) the treatment of the solution with 4 eq. of TsOH·H_2O. The purple and orange boxes in (a) highlight the upfield-shifted resonances of the external and internal alkyl chains of the complexed dumbbell (**7**$_{12}$).

As a result, a reasonable hypothesis for such mobility was that the lack of anions coordination could significantly reduce the preorganisation of the macrocycles. To verify our hypothesis, four equivalents of TsOH·H_2O were added to the dichloromethane solution of *R*[(**TPU-AC**)$_2$⊃**7$_{12}$**]. The new ^{1}H NMR spectrum

obtained (Figure 1.25a) shows that the interlocked structure fully recovered its preorganisation, giving rise to sharper resonances assigned to the structure thanks to a series of 2D NMR measurements. Importantly, these findings confirmed the critical role played by the H-bonding donor ability of the phenylurea groups in the preorganisation and complexation abilities of this type of calix[6]arene macrocycle. 2D HSQC is thus reported to show the complete signal assignment.

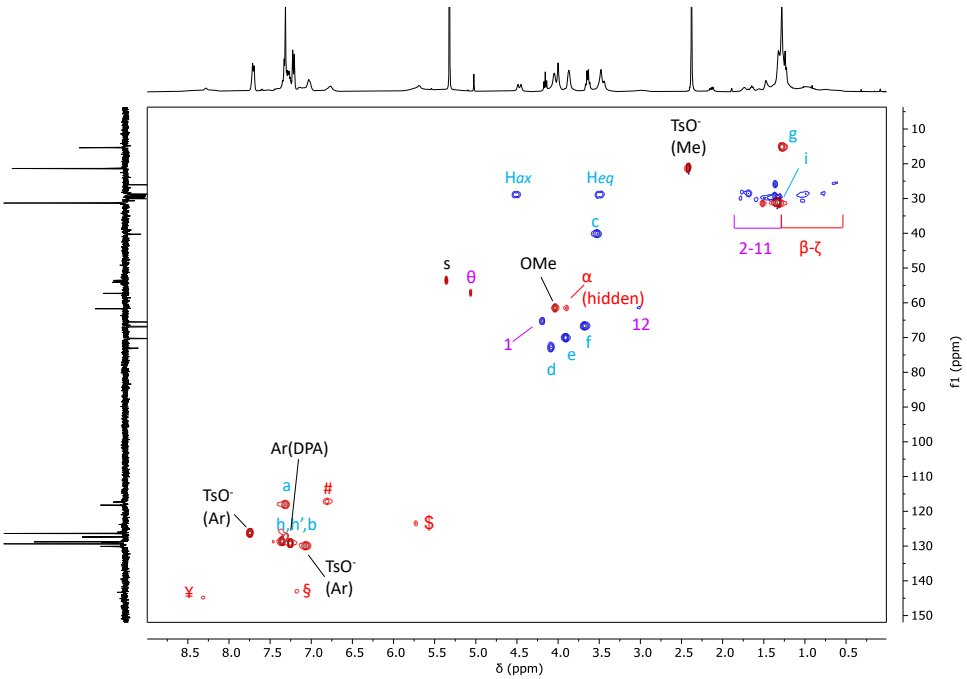

Figure 1.26 Edited HSQC NMR spectrum (400 MHz, CD_2Cl_2) of [*3*]rotaxane *R*[(**TPU-AC**)$_2$⊃**8**$_{12}$].

Conclusions

In summary, in this study, we have reported the preparation, using a threading and capping approach, of a series of calix[6]arene-based upper-to-upper oriented [*3*]rotaxane isomers bearing diphenylacetyl or triphenylsilyl stoppers. The success in synthesising these rather complicated interlocked structures has been possible thanks to the template effect exerted by a bis-viologen thread functionalised at

its ending with hydroxymethyl groups. Furthermore, the correct distance between the bis-pyridinium units of the axle in promoting the [*3*]rotaxane formation has been explored using axles having internal and external alkyl chains of different lengths. Finally, the isomeric selectivity leading to the desired upper-to-upper orientation of these rather complex interlocked structures has been obtained thanks to the axle unidirectional threading process that, in low polarity solvents, always occurs through the largest access of the calix[6]arene cavity, i.e. that bearing the phenylurea groups. The high functional group tolerance of the templating approach used for the [*3*]rotaxane synthesis has allowed the employment of calix[6]arene macrocycles decorated onto their phenylureas with different functional groups, such as carboxyl, ester, and hydroxyl groups. Such functionalities were designed to be used as grafting points for inserting bridging units, eventually leading to the synthesis of calix[6]arene-based molecular capsules.

Experimental Section

General Methods

All solvents were dried using standard procedures; all other reagents were of reagent-grade quality obtained from commercial suppliers and used without further purification. Melting points are uncorrected. NMR spectra were recorded at 400 MHz for ^{1}H and 100 MHz for ^{13}C. Chemical shifts are expressed in ppm (δ) using the residual solvent signal as an internal reference (7.26 ppm for $CHCl_3$, 7.16 ppm for C_6D_5H, 5.32 for $CHDCl_2$ and 3.31 ppm for CD_2HOD). The terms m, s, d, t and q represent multiplet, singlet, doublet, triplet and quadruplet, respectively; the term “br. s” means a broad signal. Other abbreviations used in the text are DPA = diphenylacetyl, TPS = triphenylsilyl, and TsO = tosylate. Mass spectra were recorded in the ESI mode. Compounds **1**,[40] **TPU**,[28] **TA**[28], $\mathbf{3}_6$,[41] $\mathbf{3}_{12}$,[42] $\mathbf{6}_{12}$ and $\mathbf{7}_{12}$,[43] **12** and **14**[44] were synthesized according to published procedures.

Synthetic Procedure and Analytical Data

General procedure for the synthesis of the bis-viologen axles $\mathbf{4_{12}}$ and $\mathbf{5_{6\text{-}12}}$. In a sealed 100 mL glass autoclave, a solution of the appropriate pyridyl pyridinium tosylate (**1-2**, 0.6 mmol) and ditosylate ($\mathbf{3_m}$, 0.3 mmol) in dry acetonitrile (40 mL) was refluxed under vigorous stirring for 7 days. Afterwards, the solution was evaporated to dryness under reduced pressure.

$\mathbf{4}_{12}$: the solid residue of the evaporation was triturated with CH_3CN to afford 0.3 g of product $\mathbf{4}_{12}$ as a solid white powder (63%). **M. p.** = 156-158 °C. **^{1}H NMR** (CD_3OD, 400 MHz): δ = 9.22 (d, 8H, *J* = 6.9 Hz, $H_{\#}$ and $H_{¥}$), 8.63 (d, 8H, *J* = 6.4 Hz, $H_{\$}$ and $H_{§}$), 7.67 (d, 8H, *J* = 8.4 Hz, TsO), 7.22 (d, 8H, *J* = 8.0 Hz, TsO), 4.7-4.6 (m, 8H, H_α and H_6), 3.55 (t, 4H, *J* = 5.6 Hz, H_1), 2.36 (s, 12H, C*H*$_3$, TsO), 2.1-2.0 (m, 8H, H_β and H_5), 1.5-1.3 (m, 28H, $H_{2\text{-}4}$ and $H_{\gamma\text{-}\zeta}$) ppm; **^{13}C NMR** (CD_3OD, 100 MHz): δ = 151.2, 147.0, 143.7, 141.7, 129.9, 128.3, 126.9, 63.3, 63.2, 62.6, 33.2, 32.5 (2 res.), 30.6, 30.5, 30.2, 27.2, 26.9, 26.4, 21.3; **ESI-MS** (+): = m/z 1195.9 $[M\text{-}TsO]^+$.

$\mathbf{5}_6$: the solid residue of the evaporation was triturated with CH_3CN to afford 0.3 g of $\mathbf{5_6}$ as a solid white powder (65%). **M. p.** = 155-157 °C. **^{1}H NMR** (CD_3OD, 400 MHz): δ = 9.25 (d, 4H, *J* = 6.9 Hz, $H_{¥}$), 9.22 (d, 4H, *J* = 6.9 Hz, $H_{\#}$), 8.59 (d, 8H, *J* = 6.4 Hz, $H_{\$}$ and $H_{§}$), 7.66 (d, 8H, *J* = 8.0 Hz, TsO), 7.21 (d, 8H, *J* = 8.0 Hz, TsO), 4.76 (t, 4H, *J* = 7.0 Hz, H_α), 4.71 (t, 4H, *J* = 8.0 Hz, H_{12}), 3.53 (t, 4H, *J* = 6.8 Hz, H_1), 2.34 (s, 12H, TsO), 2.1-2.0 (m, 8H, H_β, H_{11}), 1.6-1.3 (m, 42H, $H_{2\text{-}10}$, $H_{\gamma\text{-}\delta}$) ppm; **^{13}C NMR** (CD_3OD, 100 MHz): δ = 151.1, 151.0, 147.1, 146.9, 143.7, 141.7, 129.9, 128.2 (2 res.), 126.9, 63.2, 62.9 (2 res.), 33.6, 32.5, 31.9, 30.7, 30.6 (3 res.), 30.5, 30.1, 27.2, 26.9, 26.2, 21.3; **ESI-MS** (+): m/z = 1279.1 $[M\text{-}TsO]^+$.

$\mathbf{5}_{12}$: the solid residue of the evaporation was recrystallised from CH_3OH/CH_3CN to afford 0.3 g of $\mathbf{5_{12}}$ as a solid white powder (62%). **M. p.** = 196-198 °C; **^{1}H NMR** (CD_3OD, 400 MHz): δ = 9.22 (d, 8H, *J* = 6.8 Hz, $H_{\#}$ and $H_{¥}$), 8.63 (d, 8H, *J* = 6.4 Hz, $H_{\$}$ and $H_{§}$), 7.67 (d, 8H, *J* = 8.0 Hz, TsO), 7.22 (d, 8H, *J* = 8.0 Hz, TsO), 4.70 (t, 8H, *J*

= 7.6 Hz, H_α and H_{12}), 3.53 (t, 4H, *J* = 7.0 Hz, H_1), 2.36 (s, 12H, TsO), 2.1 (br. s, 8H, H_β and H_{11}), 1.5-1.3 (m, 52H, $H_{2\text{-}10}$, $H_{\gamma\text{-}\zeta}$) ppm; **^{13}C NMR** (CD_3OD, 100 MHz): δ = 151.2, 147.0, 143.6, 141.7, 129.9, 128.3, 126.9, 63.3, 62.9, 33.6, 32.5, 30.7 (2 res.), 30.6 (2 res.), 30.5, 30.2, 30.1, 27.2 (2 res.), 26.9, 21.3; **ESI-MS** (+): m/z = 341.6 $[M\text{-}3TsO]^{3+}$.

Synthesis of *tert*-butyl 2-(4-nitrophenyl)acetate (**11**): 2-(4-nitrophenyl)acetic acid (2.5 g, 13.8 mmol) was dissolved in anhydrous dichloromethane (25 mL), then *tert*-butanol (3.1 g, 41.8 mmol) and DMAP (1.4 g, 11.0 mmol) were added. The mixture was cooled down to 0 °C, and DCC (4.1 g, 19.8 mmol) was slowly added. The solution was stirred at room temperature for 3 hours, after which the formation of a white precipitate (DCU) was observed. The solid was filtered off through a Buchner filtration, and the organic phase was washed with water (50 mL) and evaporated to dryness under reduced pressure. The crude product **11** was purified by column chromatography (SiO_2, hexane: ethyl acetate = 70:30) as a colourless oil in 70% yield. **^{1}H NMR** ($CDCl_3$, 400 MHz): δ = 8.18 (d, 2H, *J* = 8.7 Hz, $H_§$) ppm, 7.44 (d, 2H, *J* = 8.7 Hz, $H_¥$), 3.64 (s, 2H, H_2), 1.44 (s, 9H, H_1) ppm; **^{13}C NMR** ($CDCl_3$, 100 MHz): δ = 28.1, 42.5, 81.9, 123.8, 130.3, 142.2, 147.1, 169.5; **ESI-MS** (+): m/z= 238.2 $[M+H]^+$.

Synthesis of *tert*-butyl 2-(4-aminophenyl)acetate (**13**): to a solution of **11** (1.8 g, 7.6 mmol) in methanol (20 mL) kept under a hydrogen atmosphere, a tip of a spatula of Pd/C was added. After stirring at room temperature for 12 hours, the solution was vacuum filtered over celite under an inert atmosphere. The solvent was evaporated under reduced pressure, and the residue was portioned between dichloromethane and water. The separated organic phase was dried over $CaCl_2$, filtered, and evaporated to dryness to quantitatively afford **13** as a colourless oil. **^{1}H NMR** ($CDCl_3$, 400 MHz): δ = 7.05 (d, 2H, *J* = 8.4 Hz, $H_¥$), 6.64 (d, 2H, *J* = 8.4 Hz, $H_§$), 3.59 (bs, 2 H, ArNH_2), 3.40 (s, 2H, H_2), 1.43 (s, 9H, H_1) ppm; **^{13}C NMR** ($CDCl_3$,

100 MHz): δ = 28.2, 41.9, 80.6, 115.4, 124.8, 130.2, 145.3, 171.7; **ESI-MS** (+): m/z= 208.1 $[M+H]^+$.

General procedure for the synthesis of calix[*6*]arenes **TPU-ES** and **TPU-OTBS**: under a nitrogen atmosphere, a solution of triphosgene (103.1 mg, 347.3 µmol, mg, 1.1eq.) in toluene (10 mL) was poured into a 250 mL two-necked flask. A freshly prepared solution of triamino calix[*6*]arene **TA** (350 mg, 315.7 µmol, 1 eq.) and triethylamine (154 µL, 1.1051 mmol, 3.5 eq.) in toluene (20 mL) was added to the reactor. The mixture was stirred at 80 °C for 3 hours. After cooling the reactor at room temperature, compound **12** or **14** was added, and the reaction was stirred at room temperature for 12 hours. After completion of the reaction, the solvent was evaporated under reduced pressure. The crude product was purified by column chromatography (SiO_2, hexane: ethyl acetate = 70:30).

TPU-ES: the product was recovered in 72 % yield as a white solid. **M. p.** = 183-185 °C; **^{1}H NMR** ($CDCl_3$, 400 MHz): δ = 7.4-7.2, 7.1-7.0, 6.8 and 6.3 (6 br. s, 24H, N*H* and Ar*H*), 4.4 (br. s, 6H, H_{ax}), 4.1 (br. s, 6H, H_d), 3.84 (m, 6H, H_e), 3.7-3.3 (m, 18H, H_f, H_c and H_{eq}), 3.1-2.5 (br. s, 9H, -OC*H*$_3$), 1.42 (s, 27H, H_j), 1.4-1.1 (m, 36H, H_i, H_g); **^{13}C NMR** ($CDCl_3$, 100 MHz): δ = 129.7, 72.5, 69.9, 67.0, 42.2, 42.0, 34.4, 31.7, 31.6, 29.8, 28.2, 15.4; **HR-MS** (ESI, Orbitrap LQ) calculated for $C_{108}H_{139}N_6O_{18}$: m/z (z = 1): 1808.01404, 1809.01739, 1810.02075, 1811.02410, 1812.02746; found: 1808.01286, 1809.01598, 1810.01902, 1811.02156, 1812.02503.

TPU-OTBS: the product was recovered in 64 % yield as an orange solid. **M. p.** = 158-160 °C; **^{1}H NMR** ($CDCl_3$, 400 MHz): δ = 7.2, 7.1, 6.2 (3 br. s, 24H, Ar*H* and N*H*), 4.4 (br. s, 6H, H_c), 4.1 (br. s, 6 H, H_{ax}), 3.8 (br. s, 6H, H_d), 3.4 (br. s, 6H, H_e), 3.7-3.6 (m, 12H, H_f, H_{eq}), 2.8 (br. s, 9H, -OC*H*$_3$), 1,4-1.0 (m, 36H, H_i, H_g), 0.91 (s, 27H, H_j), 0.05 (s, 18H, H_k); **^{13}C NMR** ($CDCl_3$, 100 MHz): δ = 155.0, 152.2, 146.9, 137.2, 136.8, 135.9, 133.1, 127.8, 127.0, 123.3, 120.7, 72.5, 69.9, 67.0, 64.8, 60.4, 34.3, 31.7, 26.1, 18.4, 15.43, 5.06; **HR-MS** (ESI, Orbitrap LQ) calculated for $C_{111}H_{157}N_6O_{15}Si_3$:

m/z (z = 1): 1898.10092, 1899.10428, 1900.10763, 1901.11099, 1902.11434; found: 1898.10054, 1899.10317, 1900.10381, 1901.10644, 1902.11069.

General procedure for the synthesis of [*3*]rotaxanes *R*[(**TPU**)$_2$ ⊃ **6$_{12}$**], *R*[(**TPU**)$_2$ ⊃ **7$_{12}$**] and *R*[(**TPU-ES**)$_2$ ⊃ **7$_{12}$**]: a suspension of bis-viologen axle (**4$_{12}$** or **5$_{12}$**, 0.03 mmol) and wheel (**TPU** or **TPU-ES**, 0.06 mmol) in toluene (10 mL) was stirred at room temperature until it turned homogeneous and deeply red-coloured (24 hrs). Triethylamine (0.03 g, 0.12 mmol) and diphenylacetyl chloride (0.03 g, 0.12 mmol) were added. After stirring at room temperature for 16 hours, the solvent was evaporated to dryness under reduced pressure. The resulting red solid residue was purified by column chromatography (SiO_2, CH_2Cl_2:CH_3OH = 95:5). The isolated [*3*]rotaxane was then dissolved in dichloromethane, washed twice with an aqueous solution of NaOTs and twice with distilled water.

R[(**TPU**)$_2$ ⊃ **6$_{12}$**] was obtained as a red sticky solid in 15% yield (0.05 g). **^{1}H NMR** (benzene-d$_6$, 400 MHz): δ = 9.4 (br. s, 12H, -NH-), 8.2 (br. d, 12H, *J* = 7.7 Hz, TsO), 8.0, 7.9, 7.8 (3 br. s, 20H, H$_¥$, H$_a$, H$_§$), 7.58 (s, 12H, H$_h$), 7.43 (d, 12H, DPA), 7.2-7.0, 7.03, 6.91, 6.8, 6.7 (m, t, d, br. t, br. d, 42H, *J* = 8 Hz, *J* = 8 hz, (DPA), H$_{h'}$, H$_b$, H$_\#$, TsO, H$_c$, H$_\$$), 5.11 (s, 2H, H$_\theta$), 4.56 (d, 12H, *J* = 14.8 Hz, H$_{ax}$), 4.3 (br. t, 4H, *J* = 12.8 Hz, H$_1$), 3.89, 3.8 and 3.7 (s, br. d, 34H, O*CH*$_3$, H$_d$, H$_\alpha$), 3.6, 3.5, 3.5-3.3 (br. s, br. s, m, 40H, H$_6$, H$_e$, H$_f$, H$_{eq}$,), 1.97 (s, 12H, TsO), 1.8, 1.69, 1.6, 1.3, 1.2, 1.11, 1-0.9 (br. s, s, br. s, br. s, br. s, br. s, t, br. s, br. t, 100H, H$_i$, H$_{2\text{-}5}$, H$_{\beta\text{-}\zeta}$ and H$_g$)ppm; **^{13}C NMR** (benzene-d$_6$, 100 MHz): δ = 172.4, 153.9, 153.2, 148.3, 144.7, 143.7, 143.3, 141.6, 139.7, 139.4, 137.9, 134.2, 132.5, 129.7, 129.1, 128.9, 126.9, 125.9, 125.3, 121.5, 118.5, 117.0, 72.8, 70.3, 66.7, 65.4, 61.3, 61.1, 60.0, 57.7, 38.6, 34.9, 32.4, 31.9, 31.7, 30.2, 30.1, 30.0, 29.8, 29.7, 29.6, 29.4, 28.1, 26.6, 26.4, 23.1, 21.2, 15.6, 14.4; **HR-MS** (ESI, Orbitrap LQ) calculated for $C_{266}H_{316}N_{16}O_{34}S_2$: m/z (z = 2): 2171.14602 (24 %), 2171.64769 (70 %), 2172.14937 (100 %), 2172.65105 (95 %), 2173.15273 (68 %), 2173.65440 (39 %), 2174.15608 (18 %), 2174.65776 (7 %); Found: 271.14348 (21 %), 2171.64532 (64 %), 2172.14235 (99 %), 2172.664861

(100 %), 2173.15003 (80 %), 2173.65187 (53 %), 2174.15217 (30 %), 2174.65623 (13 %).

R[(**TPU**)$_2$ ⊃ **7$_{12}$**]: was obtained as a red sticky solid in 21% yield (0.07 g) 0.07 g (21%) as a red sticky compound. **^{1}H NMR** (benzene-d$_6$, 400 MHz): δ = 9.3-9.2 (br. s, 12H, -NH), 8.14 (d, 8H, *J* = 8 Hz, TsO), 8.0, 7.9, 7.8 (br. s, br. s, br. s, 20H, H$_¥$, H$_a$, H$_§$), 7.6 (br. s, 12H, H$_h$), 7.4 (d, 12H, H$_b$), 7.31 (d, 12H, *J* = 7.6 Hz, DPA), 7.1-7.0 (m, 20H, H$_{h'}$, DPA,), 6.91 (d, 8H, *J* = 16 Hz, TsO, H$_\#$), 6.8 (br. t, 6H, H$_c$), 6.7 (br. S, 4H, H$_\$$), 5.08 (s, 2H, H$_\theta$), 4.59 (d, 12H, *J* = 14.7 Hz, H$_{ax}$), 4.06 (t, 4H, *J* = 6.7 Hz, H$_1$), 3.95 (s, 9H, O*CH*$_3$), 3.86 (br. s, 34H, H$_d$ and H$_\alpha$), 3.7 (br. s, 4H, H$_{12}$), 3.6 (br. s, 12H, H$_e$), 3.5-3.2 (m, 18H, H$_{eq}$ and H$_f$), 2.1 (br. s, 4H, H$_{11}$), 1.96 (s, 12 H, TsO), 1.9, 1.68, 1.6, 1.6-0.9, and 1.14 (br. s, br. s, br. s, m, br. t, 110H, H$_{2\text{-}10}$, H$_{\beta\text{-}\zeta}$, Hi, and H$_g$) ppm; **^{13}C NMR** (benzene-d$_6$, 100 MHz): δ = 177.2, 172.4, 153.9, 153.2, 148.5, 148.4, 144.8, 143.4, 143.3, 141.5, 140.5, 139.9, 139.5, 139.1, 137.8, 134.2, 132.6, 129.9, 129.7, 129.2, 129.1, 129.0, 128.9, 128.8, 127.5, 127.4, 126.9, 125.9, 125.3, 121.5, 118.5, 117.1, 72.8, 70.4, 66.7, 65.1, 61.9, 61.3, 57.7, 57.5, 34.9, 32.3, 31.9, 31.2, 30.6, 30.4, 30.3, 30.2, 30.1, 30.0, 29.8, 29.6, 29.4, 28.9, 26.6, 26.2, 23.1, 21.1,21.0, 15.6, 14.4; **HR-MS** (ESI, Orbitrap LQ) calculated for $C_{278}H_{340}N_{16}O_{34}S_2$: m/z (z = 2): 2255.23992 (22 %), 2255.74160 (67 %), 2256.24327 (100 %), 2256.74495 (99 %), 2257.246632 (74 %), 2257.74830 (44 %), 2258.24998 (22 %), 2258.75166 (9 %); Found: 2255.23668 (18 %), 2255.74953 (58 %), 2256.24190 (93 %), 2256.74351 (100 %), 2257.246381 (83 %), 2257.74418 (59 %), 2258.24485 (34 %), 2258.74509 (17 %).

R[(**TPU-ES**)$_2$⊃ **7$_{12}$**] was obtained as a red sticky solid in 24% yield (0.04 g). **^{1}H NMR** (benzene-d$_6$, 400 MHz): δ = 9.3 (2 br. s, 12H, -NH), 8.14 (d, 8H, *J* = 8 Hz, TsO), 7.9, 7.8, 7.7 (3 br. s, 20H, H$_¥$, H$_a$, H$_§$), 7.58 (br. s, 12H, H$_h$), 7.40 (d, 10H, *J* = 7.5 Hz, DPA), 7.32 (d, 10H, *J* = 7.6 Hz, DPA), 7.2-7.0 (m, 28H, H$_b$, H$_\#$ and H$_{h'}$), 6.91 (d, 8H, *J* = 16 Hz, TsO), 6.7 (br. S, 4H, H$_\$$), 5.08 (s, 2H, H$_\theta$), 4.63 (d, 12H, *J* = 15 Hz, H$_{ax}$), 4.06 (t, 4H, *J* = 7 Hz, H$_1$), 3.95 (s, 9H, O*CH*$_3$), 3.9, 3.8, 3.6, (3 br. s, 32H, H$_d$, H$_\alpha$, H$_{12}$ and H$_e$),

3.5-3.4 (m, 40H, H_f, H_{eq} and H_c), 1.98 (s, 12H, TsO), 1.73 (s, 27H, H_j), 1.6-1.0, 1.44, 1.15 (m, s, t, 165H, H_2-11, Hi, $H_{\beta\text{-}\zeta}$, and H_g) ppm; **^{13}C NMR** (benzene-d_6, 100 MHz): δ = 129.9, 129.4, 128.8, 128.8, 128.7, 128.6, 128.5, 127.8, 127.5, 127.2, 127.2, 126.6, 118.1, 70.1, 66.6, 66.5, 64.8, 61.0, 57.4, 31.7, 28.7, 28.0, 27.8, 25.9, 20.9, 15.3; **HR-MS** (ESI, Orbitrap LQ) calculated for $C_{300}H_{386}N_{16}O_{40}$ [M-4OTs]: m/z (z = 4): 1213.21601, 1213.46685, 1213.71769, 1213.96853, 1214.21936, 1214.47020, 1214.72104, 1214.97188, 1215.22272; found: 1213.21960, 1213.47004, 1213.72126, 1213.97215, 1214.22240, 1214.47295, 1214.72394, 1214.97433, 1215.22577.

General procedure for the synthesis of [*3*]rotaxanes *R*[(**TPU**)$_2$ ⊃ **8$_{12}$**] and *R*[(**TPU-ES**)$_2$ ⊃ **8$_{12}$**]: a suspension of bis-viologen axle **5$_{12}$** (0.03 mmol) and wheel (**TPU** or **TPU-ES**, 0.06 mmol) in toluene (10 mL) was stirred at room temperature until it turned homogeneous and deeply red-coloured (24 hrs). Imidazole (0.009 g, 0.12 mmol) and chlorotriphenylsilane (0.035 g, 0.12 mmol) were then added in this order. After stirring at room temperature for 48 hours, the solvent was evaporated to dryness under reduced pressure. The resulting red solid residue was purified by column chromatography (SiO_2, CH_2Cl_2:CH_3OH = 95:5). The isolated [*3*]rotaxane was then dissolved in dichloromethane, washed twice with an aqueous solution of NaOTs and twice with distilled water.

R[(**TPU**)$_2$ ⊃ **8$_{12}$**] was obtained as a red sticky solid in 14% yield (0.015 g). **^{1}H NMR** (benzene-d_6, 400 MHz, 25 °C): δ = 9.3 (br. s, 12H, -NH), 8.17 (d, 8H, *J* = 8 Hz, TsO), 8.1-7.7 (2 m, 38H, TPS, H_a, $H_§$ and $H_¥$), 7.58 (s, 12H, H_h) 7.3-7.2 (m, 20H, TPS and H_b), 7.1 (br. s, 10H, $H_{h'}$), 6.92 (d, 8H, *J* = 8 Hz, TsO), 6.8-6.7 (m, 16H, $H_\#$ and $H_\$$), 4.57 (d, 12H, *J* = 14 Hz, H_{ax}), 3.94 (s, 9H, OC*H*3) 3.9 (br. s, 16H, H_1, H_d), 3.7 (br. s, 4H, H_α), 3.6 (br. s, 16H, H_{12} and H_e), 3.5-3.2 (m, 24H, H_f and H_{eq}), 2.1 (br. s, 4H, H_{11}), 1.98 (s, 12H, TsO), 1.9-0.8 (br. s, s, 5 br. s, t, br. s, 128H, H_2-10, Hi, H_g, and $H_{\beta\text{-}\zeta}$) ppm; **^{13}C NMR** (benzene-d_6, 100 MHz): δ = 144.3, 143.1, 135.6, 135.2, 130.1, 129.4, 129.0, 128.7, 128.0, 126.6, 125.6, 124.8, 121.3, 118.1, 72.5, 70.1, 66.4,

63.9, 61.0, 60.9, 32.9, 31.6, 30.2, 30.0, 29.7, 29.3, 29.0, 26.3, 26.1, 20.9, 15.3; **HR-MS** (ESI, Orbitrap LQ) calculated for $C_{272}H_{334}N_{16}O_{26}Si_2$ [M-4OTs]: m/z (z = 4): 1074.12055, 1074.37133, 1074.62209, 1074.87281, 1075.12351, 1075.37418, 1075.62485, 1075.87550, 1076.12614; found: 1074.12160, 1074.37233, 1074.62274, 1074.87341, 1075.12404, 1075.37483, 1075.62526, 1075.87554, 1076.12609. Calculated for $C_{279}H_{341}N_{16}O_{29}SSi_2$ [M-3OTs]: m/z (z = 3): 1489.16477, 1489.49916, 1489.83346, 1490.16771, 1490.50191, 1490.83607, 1491.17020, 1491.50432, 1491.83841; found 1489.16582, 1489.50006, 1489.83480, 1490.16818, 1490.50235, 1490.83659, 1491.17000, 1491.50462, 1491.83886. Calculated for $C_{286}H_{348}N_{16}O_{32}S_2Si_2$ [M-2OTs]: m/z (z = 2): 2319.25323, 2319.75480, 2320.25623, 2320.75754, 2321.25876, 2321.75991, 2322.26100, 2322.76211; found: 2319.25395, 2319.75584, 2320.25763, 2023.75902, 2321.26003, 2321.76056, 2322.26079, 2322.76104.

R[(**TPU-ES**)$_2$ ⊃ **8$_{12}$**] was obtained as a red sticky solid in 17% yield (0.029 g**). ^{1}H NMR** (benzene-d_6, 400 MHz): δ = 9.3 (2 br. s, 12H, -NH), 8.12 (d, 8H, *J* = 8 Hz, TsO), 7.9, 7.8, 7.8-7.7 (2 br. s, m, br. s, 58H, H¥, H_a, TPS and H§), 7.59 (s, 12H, H_h), 7.2 (m, 16H, TPS and H_b), 7 (br. s, 16H, $H_{h'}$ and H#), 6.91 (d, 8H, *J* = 8 Hz, TsO), 6.7 (br. d, 4H, H$_Ş$), 4.62 (d, 12H, *J* = 14, H_{ax}), 3.94 (s, 9H, OCH_3) 3.9-3.8 (m, 20H, H_α, H_1 and H_d), 3.63 (s, 12H, H_e), 3.5-3.2 (m, 40H, H_f, H_c, and H_{eq}, H_{12}), 1.99 (s, 12H, TsO), 1.9-1.2 (m, 168H, H_i, $H_{\beta\text{-}\zeta}$, $H_{2\text{-}11}$, and H_j), 1.15 (t, 18H, *J* = 7 Hz, H_g) ppm; **^{13}C NMR** (benzene-d_6, 100 MHz, 25 °C): δ = 144.6, 143.3, 135.6, 135.2, 130.1, 129.9, 129.4, 128.7, 128.0, 127.9, 126.6, 125.6, 125.2, 118.1, 72.5, 70.1, 66.5, 63.9, 61.7, 61.0, 41.5, 31.7, 31.2, 30.2, 30.0, 29.8, 29.6, 28.0, 26.1, 20.9, 15.3; **HR-MS** (ESI, Orbitrap LQ) calculated for $C_{308}H_{394}N_{16}O_{38}Si_2$ [M-4OTs]: m/z (z = 4): 1245.22267, 1245.47350, 1245.72434, 1245.97518, 1246.22602, 1246.47686, 1246.72770, 1247.22937; found: 1245.21594, 1245.46924, 1245.72095, 1245.97229, 1246.22278, 1246.72473, 1247.22192. Calculated for $C_{315}H_{401}N_{16}O_{41}SSi_2$ [M-3OTs]: m/z (z = 3): 1717.30093, 1717.63538, 1717.96984, 1718.30429, 1718.63874, 1718.97319, 1719.30764, 1719.64209, 1719.97655; found:

1717.29626, 171763025, 171796521, 1718.29895, 1718.96716, 1719.30078, 1719.63586, 1719.96838. Calculated for $C_{322}H_{408}N_{16}O_{44}S_2Si_2$ [M-2OTs]: m/z (z = 2): 2661.45747, 2661.95915, 2662.46082, 2662.96250, 2663.46418, 2663.96586, 2664.46753, 2664.96921, 2665.47089; found: 2661.44678, 2661.95190, 2662.45239, 2663.45532, 2663.95410, 2664.45728, 2664.95923, 2665.45752.

Synthesis of [3]rotaxane *R*[(**TPU-AC**)$_2$ ⊃ **7$_{12}$**]: to a solution of *R*[(**TPU-ES**)$_2$ ⊃ **7$_{12}$**] (0.02 g, 0.035 mmol) in 5 ml of dry dichloromethane, *p*-toluenesulfonic acid monohydrate (0.35 mmol) was added, and the resulting reaction mixture was refluxed for 1 hour. After this period, the crude product was purified by column chromatography (SiO_2, CH_2Cl_2:CH_3OH = 95:5). R[(**TPU-AC**)$_2$ ⊃ **7$_{12}$**] was obtained as a red sticky solid in 60% yield (0.011 g). **^{1}H NMR** (CD_2Cl_2, 400 MHz): δ = 8.28 (br. s, 16H, -NH and $H_¥$), 7.8-6.9 (m, H, TsO, $H_{h\text{-}h'}$, $H_{a\text{-}b}$ and $H_§$), 6.8 (br. s, 4H, $H_\#$), 5.7 (br. s, 4H, $H_\$$), 5.02 (s, 2H, H_θ), 4.47 (d, 12H, *J* = 14 Hz, $H_{\alpha x}$), 4.16 (t, 4H, *J* = 7 Hz, H_1), 4.1-3.7 (m, 44H, OC*H$_3$*, H_d, H_α, and H_e), 3.64 (q, 12H, *J* = 7 Hz, H_f), 3.6-3.3 (m, 24H, H_{eq}, and H_c), 3.0 (br. s, 4H, H_{12}), 2.38 (s, 12H, TsO), 2.2-0.5 (m, 132H, $H_{2\text{-}11}$, Hi, H_g and $H_{\beta\text{-}\zeta}$); **^{13}C NMR** (CD_2Cl_2, 100 MHz, 25 °C): δ = 143.3, 130.1, 129.3, 128.9, 128.8, 128.7, 127.4, 126.4, 118.2, 117.3, 73.0, 70.3, 66.9, 65.5, 61.7, 57.3, 31.3, 30.6, 30.0, 29.8, 29.5, 29.1, 28.8, 26.0, 21.4, 15.4; **HR-MS** (ESI, Orbitrap LQ) calculated for $C_{276}H_{338}N_{16}O_{40}$ [M-4OTs]: m/z (z = 4): 1129.12211, 1129.37293, 1129.62374, 1129.87454, 1130.12533, 1130.37611, 1130.62689, 1130.87766; found: 1129.12238, 1129.37272, 1129.62394, 1129.87418, 1130.12532, 1130.37554, 1130.62657, 1130.87690. Calculated for $C_{283}H_{345}N_{16}O_{43}S$ [M-3OTs]: m/z (z = 3): 1562.50019, 1562.83461, 1563.16899, 1563.50333, 1563.83764, 1564.17192, 1564.50618, 1564.84042; found: 1562.50044, 1562.83428, 1563.16907, 1563.50269, 1563.83620, 1564.17082, 1564.50493, 1564.83858. Calculated for $C_{290}H_{352}N_{16}O_{46}S_2$ [M-2OTs]: m/z (z = 2): 2429.25636, 2429.75799, 2430.25951, 2430.76094, 2431.26231, 2431.76362, 2432.26488, 2432.76611, 2433.26731; found: 2429.25649, 2429.75803, 2430.25933, 2430.76027, 2431.26130, 2431.76212, 2432.26331, 2432.76385, 2433.26532.

References

[1] G. Montà-González, F. Sancenón, R. Martínez-Máñez, V. Martí-Centelles, *Chem. Rev.* **2022**, *122*, 13636–13708.

[2] L. Tapia, I. Alfonso, J. Solà, *Organic & Biomolecular Chemistry* **2021**, *19*, 9527–9540.

[3] K. Acharyya, P. S. Mukherjee, *Angewandte Chemie* **2019**, *131*, 8732–8745.

[4] P. S. Bols, H. L. Anderson, *Acc. Chem. Res.* **2018**, *51*, 2083–2092.

[5] H.-T. Feng, Y.-X. Yuan, J.-B. Xiong, Y.-S. Zheng, B. Zhong Tang, *Chemical Society Reviews* **2018**, *47*, 7452–7476.

[6] D. Zhang, A. Martinez, J.-P. Dutasta, *Chem. Rev.* **2017**, *117*, 4900–4942.

[7] A. Díaz-Moscoso, P. Ballester, *Chemical Communications* **2017**, *53*, 4635–4652.

[8] T. Hasell, A. I. Cooper, *Nat Rev Mater* **2016**, *1*, 1–14.

[9] T. Lorenzetto, F. Fabris, A. Scarso, *Beilstein J. Org. Chem.* **2022**, *18*, 337–349.

[10] P. La Manna, C. Talotta, G. Floresta, M. De Rosa, A. Soriente, A. Rescifina, C. Gaeta, P. Neri, *Angewandte Chemie International Edition* **2018**, *57*, 5423–5428.

[11] M. Ziegler, J. L. Brumaghim, K. N. Raymond, *Angewandte Chemie* **2000**, *112*, 4285–4287.

[12] D. J. Cram, M. E. Tanner, R. Thomas, *Angewandte Chemie International Edition in English* **1991**, *30*, 1024–1027.

[13] P. Mal, B. Breiner, K. Rissanen, J. R. Nitschke, *Science* **2009**, *324*, 1697–1699.

[14] J. L. Bolliger, in *Effects of Nanoconfinement on Catalysis* (Ed.: R. Poli), Springer International Publishing, Cham, **2017**, pp. 17–48.

[15] Y. Voloshin, I. Belaya, R. Krämer, *The Encapsulation Phenomenon*, Springer International Publishing, Cham, **2016**.

[16] F. Hof, J. Rebek, *Proceedings of the National Academy of Sciences* **2002**, *99*, 4775–4777.

[17] F. Hof, S. L. Craig, C. Nuckolls, J. Rebek Jr., *Angewandte Chemie International Edition* **2002**, *41*, 1488–1508.

[18] K. D. Shimizu, J. Rebek, *Proceedings of the National Academy of Sciences* **1995**, *92*, 12403–12407.

[19] O. Mogck, M. Pons, V. Böhmer, W. Vogt, *J. Am. Chem. Soc.* **1997**, *119*, 5706–5712.

[20] M. Yamanaka, K. Kobayashi, *Asian Journal of Organic Chemistry* **2013**, *2*, 276–289.

[21] K. Puchnin, P. Zaikin, D. Cheshkov, I. Vatsouro, V. Kovalev, *Chemistry – A European Journal* **2012**, *18*, 10954–10968.

[22] A. M. Rincón, P. Prados, J. de Mendoza, *European Journal of Organic Chemistry* **2002**, *2002*, 640–644.

[23] S. Le Gac, X. Zeng, O. Reinaud, I. Jabin, *J. Org. Chem.* **2005**, *70*, 1204–1210.

[24] S. Moerkerke, M. Ménand, I. Jabin, *Chemistry – A European Journal* **2010**, *16*, 11712–11719.

[25] A. Arduini, R. Ferdani, A. Pochini, A. Secchi, F. Ugozzoli, G. M. Sheldrick, P. Prados, J. J. González, J. de Mendoza, *Journal of Supramolecular Chemistry* **2002**, *2*, 85–88.

[26] J. J. González, R. Ferdani, E. Albertini, J. M. Blasco, A. Arduini, A. Pochini, P. Prados, J. de Mendoza, *Chemistry – A European Journal* **2000**, *6*, 73–80.

[27] A. Arduini, R. Ferdani, A. Pochini, A. Secchi, *Tetrahedron* **2000**, *56*, 8573–8577.

[28] A. Arduini, A. Credi, G. Faimani, C. Massera, A. Pochini, A. Secchi, M. Semeraro, S. Silvi, F. Ugozzoli, *Chemistry – A European Journal* **2008**, *14*, 98–106.

[29] J. Scelle, H. Vervoitte, L. Bouteiller, L.-M. Chamoreau, M. Sollogoub, G. Vives, B. Hasenknopf, *Chemical Science* **2022**, *13*, 2218–2225.

[30] M. Yamashina, S. Kusaba, M. Akita, T. Kikuchi, M. Yoshizawa, *Nat Commun* **2018**, *9*, 4227.

[31] D. Tuncel, Ö. Ünal, M. Artar, *Israel Journal of Chemistry* **2011**, *51*, 525–532.

[32] G. Cera, A. Arduini, A. Secchi, A. Credi, S. Silvi, *The Chemical Record* **2021**, *21*, 1161–1181.

[33] G. Orlandini, L. Casimiro, M. Bazzoni, B. Cogliati, A. Credi, M. Lucarini, S. Silvi, A. Arduini, A. Secchi, *Org. Chem. Front.* **2020**, *7*, 648–659.

[34] M. Bazzoni, V. Zanichelli, L. Casimiro, C. Massera, A. Credi, A. Secchi, S. Silvi, A. Arduini, *European Journal of Organic Chemistry* **2019**, *2019*, 3513–3524.

[35] V. Zanichelli, L. Dallacasagrande, A. Arduini, A. Secchi, G. Ragazzon, S. Silvi, A. Credi, *Molecules* **2018**, *23*, 1156.

[36] V. Zanichelli, M. Bazzoni, A. Arduini, P. Franchi, M. Lucarini, G. Ragazzon, A. Secchi, S. Silvi, *Chemistry – A European Journal* **2018**, *24*, 12370–12382.

[37] R. L. E. Furlan, S. Otto, J. K. M. Sanders, *Proceedings of the National Academy of Sciences* **2002**, *99*, 4801–4804.

[38] M. Matache, E. Bogdan, N. D. Hădade, *Chemistry – A European Journal* **2014**, *20*, 2106–2131.

[39] A. Arduini, R. Bussolati, A. Credi, A. Secchi, S. Silvi, M. Semeraro, M. Venturi, *J. Am. Chem. Soc.* **2013**, *135*, 9924–9930.

[40] M. Bazzoni, L. Andreoni, S. Silvi, A. Credi, G. Cera, A. Secchi, A. Arduini, *Chemical Science* **2021**, *12*, 6419–6428.

[41] A. Arduini, R. Bussolati, A. Credi, G. Faimani, S. Garaudée, A. Pochini, A. Secchi, M. Semeraro, S. Silvi, M. Venturi, *Chemistry – A European Journal* **2009**, *15*, 3230–3242.

[42] R. M. Walczak, J. S. Cowart, J. R. Reynolds, *J. Mater. Chem.* **2007**, *17*, 254–260.

[43] D. H. Burns, H. Chan, J. D. Miller, C. L. Jayne, D. M. Eichhorn, *J. Org. Chem.* **2000**, *65*, 5185–5196.

[44] M. D. Hanwell, D. E. Curtis, D. C. Lonie, T. Vandermeersch, E. Zurek, G. R. Hutchison, *Journal of Cheminformatics* **2012**, *4*, 17.

Chapter 2. Template synthesis of calix[6]arene-based molecular cages

Introduction

Molecular cages offer tailored cavities for encapsulating guest molecules by multiple non-covalent interactions.[1] The ability to selectively encapsulate guests of suitable size, shape and physicochemical features is determined by the host container's respective size, shape, and functionalised cavity. The inclusion inside the 3D-host structure results in the isolation of the guest species from the external environment, and the constricted system confers novel physicochemical properties to the caged species. In this context, many supramolecular research groups focused on the feasibility of synthesising molecular cages endowed with specific cavities for different applications, such as recognition, separation,[2] stabilisation of species[3] and catalysis,[4,5] among others.[6,7] The first molecular cage example able to encapsulate neutral guests was reported by Cram in 1985, who described the synthesis of covalent-linked two hemisphere-shape cavitands *via* a lengthy and low-yield procedure.[8,9] During the years, different strategies have been used to prepare molecular cages. Between those, self-assembled molecular capsules held together by non-covalent interaction, such as hydrogen bonds or coordination bonds with metals, were developed.[10–14] The thermodynamic control and the reversibility of the self-assembled structures provide high yields and a good atom economy.[15] However, non-covalent capsular compounds do not often provide stable complexes with guests, as functional groups are involved in the framework of non-covalent interactions responsible for the formation of cage structure.[16] Covalently-linked molecular capsules are the stable alternative. The preparation of covalent cages employs the convergent linkage of the components to create a structure with a stable central cavity. The design of the building blocks is very important for the outcome

of the reaction. Molecular shape, spatial conformation, and the functional groups that will be interested in the linkage event are some of the key factors to take into consideration.

Synthetic strategies can be classified in relation to the type of bond used to assemble the covalent cage from building blocks: irreversible or reversible covalent bonds can be formed during the final liking reaction. Irreversible bonds have found limited application in the synthesis of molecular capsules, as the synthesis often gives the desired product in very low yield, affording oligomerisation by-products instead. Moreover, as no mistakes are permitted during the cage formation, the overall yield decreases with the number of reactive events needed for the cage formation. Nevertheless, the advantage compared to reversible bonds is the higher stability. The reversible bonds represent the basis of many cages' syntheses described in the literature. Indeed, they merge the advantages of covalent bonds and the reversibility of non-covalent interactions.[17–21] Thanks to the thermodynamic control of the process, the outcome will provide the most stable product in a few steps and generally with good yields.[22–24] The most dynamic covalent bond used for this purpose is the imine bond formed by the reaction of amine- and aldehyde-building blocks. The production of hemicarcerand octaimine from tetraaldehyde resorcin[4]arene derivative with *m*-phenylenediamine could be regarded as one of the first examples of reversible covalent cages.[25] More recently, Rebek and co-workers synthesised resorcin[4]arene-based imine capsules from the condensation of two tetraacetal cavitands with aromatic diamines.[26] The ability of these cylindrical hosts to complex neutral organic molecules was also studied. High yields observed in assembly through reversible bonds usually derive from self-correction mechanisms and thermodynamically controlled pathways. Nevertheless, in some cases, the kinetic product is the main outcome of the reaction, as Mastalerz and co-workers lately demonstrated.[27] Some parameters for the success of the imine cage synthesis can be attributed to the structural

conformation of the building blocks, their preorganisation, and the solubility of the products.

Despite the suitable geometry and the preorganisation of the building blocks, synthesising molecular capsules is sometimes impossible. To overcome this obstacle, various research groups found an appealing alternative to using template-assisted approaches. The template molecule has the role of spatially arranging the building blocks and stabilising the intermediates that lead to the formation of the cage. Following this method, Ballester and co-workers recently prepared chiral polyimine capsules **II** through a template-assisted assembly.[28] In this work, a bispyridyl-*N*-oxide was used as a template, which was demonstrated to form hydrogen interactions with two tetraaldehyde calix[4]pyrrole units simultaneously. In such a manner, two monomers were brought in proximity promoting the capsule formation through condensation with suitable diamines as linkers. When no template was added, the result was the formation of insoluble oligomerisation products.

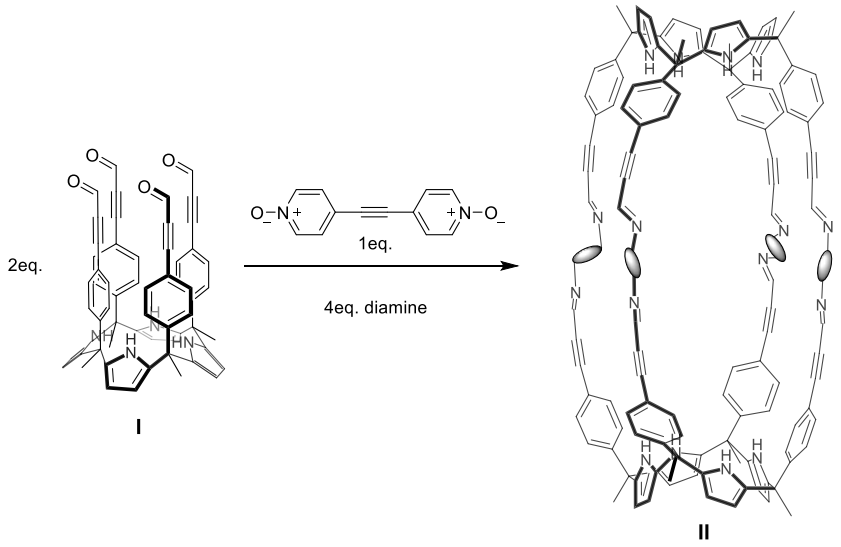

Scheme 2.1 Template assembly of polyimine capsule **II** from tetraaldehyde calix[4]pyrrole **I** in the presence of bispyridyl-*N*-oxide.

Very few examples can be found in the literature regarding the class of calix[6]arenes. For instance, the group of Jabin reported the synthesis of several tail-to-tail calix[6]arene tubes for the encapsulation of organic ions.[29,30] Calix[6]azatube **V** was formed in 34-42% yields by condensation of calix[6]arene **III**, functionalised with three tosylates moieties at its lower rim, with the *N*-protected triamino calix[6] derivative **IV**. The success and good yields of this reaction were attributed to the double role of caesium carbonate: used as the base in a mixture with K_2CO_3, the caesium cation was demonstrated to work as a template for this synthesis. The reaction between calix[6]tri-isocyanate **VI** and caxli[6]tri-amine **VII**, carried out under high dilution conditions, afforded calix[6]tube **VIII** in 26% yield mixed with the cross-linked by-product **IX**.

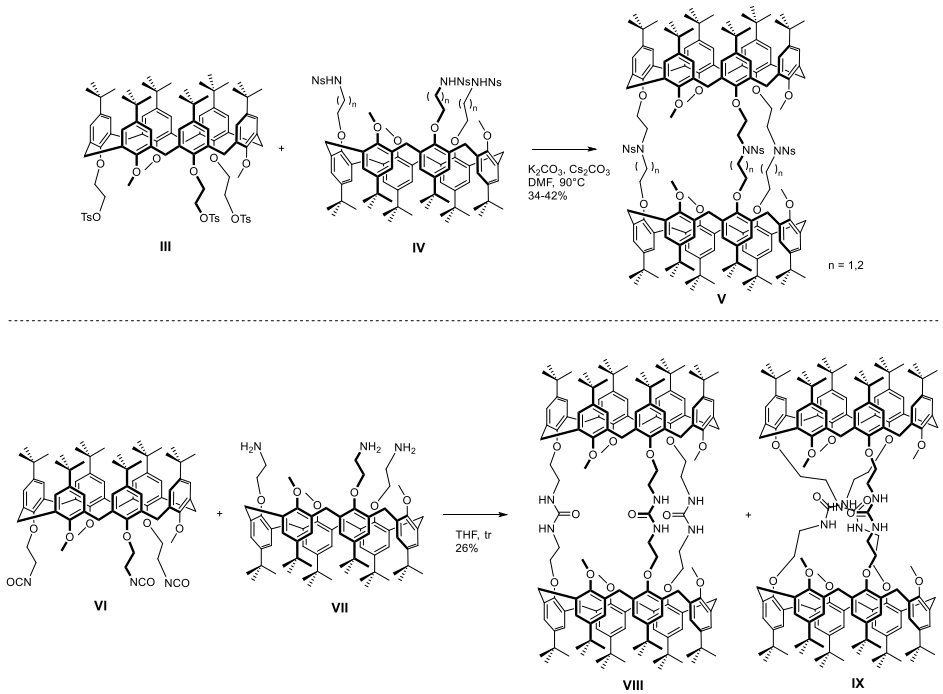

Scheme 2.2 Synthesis of tail-to-tail calix[6]arene tubes **V** and **VIII**.

In 2000, our group reported the formation and the study of complexation properties of covalently-linked double calix[6]arenes with imino and 1,4-phenylendiimino bridges[31] (Scheme 2.3). By reacting a trialdehyde calix[6]arene

derivative with a triamino calix[6]arene one, the three-point-grafted double calix[6]arene **X** was obtained in 26 % yield. Diversely, the bigger dimer **XI** was synthesised in 50 % yield from the condensation of two trialdheyde calix[6]arene monomers with 1,4-diaminobenzene as the linker. Unfortunately, these bis-calix[6]arenes showed poor complexation properties.

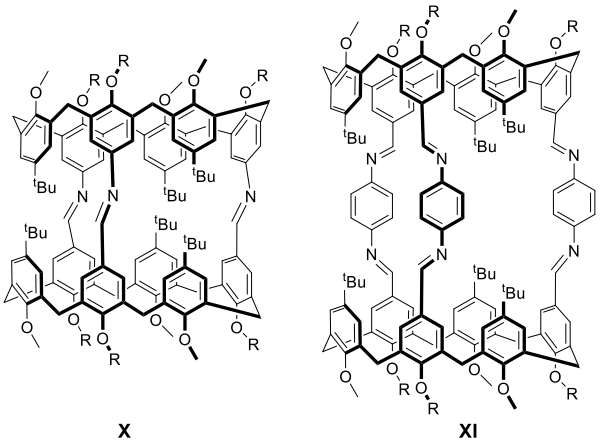

X **XI**

Scheme 2.3 Polyimino calix[6]arene dimers.

An example of an irreversibly-linked head-to-head calix[6]arene-based cage was delivered by our group (unpublished work) by reacting the triamino calix[6]arene derivative **XII** with the triisocyanate calix[6]arene **XIII**. Cage **XIV** was obtained in 10% yield. Also in this case, limited complexation properties were observed, probably due to the narrow size of the capsule portals, which were shielded by the bulky *tert*-butyl groups.

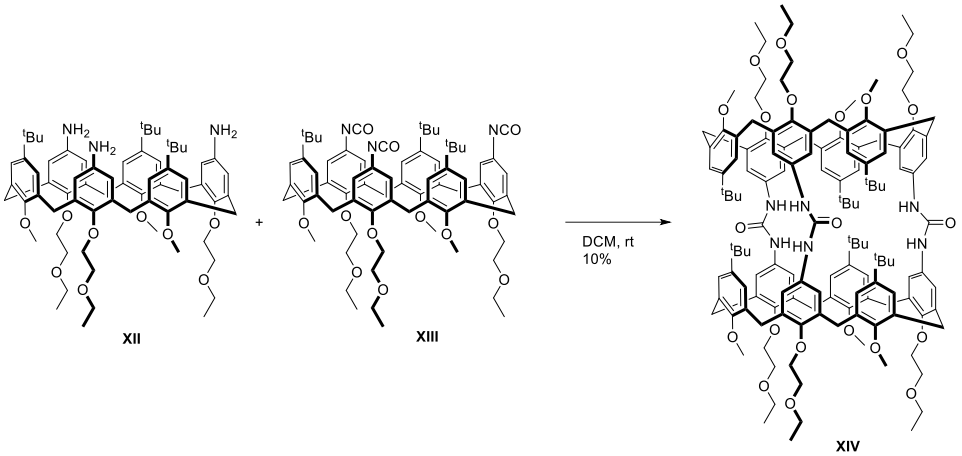

XII XIII XIV

Scheme 2.4 Synthesis of head-to-head bis-calix[6]arene **XIV**.

In this chapter, we present our results aimed at the design and synthesis of new oriented head-to-head bis-calix[6]arene containers, employing a template-assisted strategy. We devised to obtain a receptor in which both macrocycles' units are decorated with three *N*-phenylureido moieties at the upper rim. These latter functional groups have the role of interacting with the template through hydrogen bonds to promote cage formation. Furthermore, once the caged is formed, the ureas can also be used as a binding site for a potential guest molecule. As described in the previous chapter, we demonstrated the possibility to obtain head-to-head [3]rotaxanes with calix[6]arene derivatives bearing functional groups in the *para* position with respect to the phenylurea moieties.[32] We used the threading and capping approach exploiting the unidirectional threading process of bis-viologen salts in low polar solvents. In this case, instead of the formation of [3]rotaxane, we devised the template-assisted synthesis of cages by forming more versatile and conformationally adaptable [3]pseudorotaxane complexes, followed by a clipping reaction operating on the two complexed calix[6]arene monomers. As a result, the introduction of an appropriate linker could directly lead to the formation of a three-arm bridged calix[6]arene cage. The following decomplexation of the template should yield the empty capsule. To evaluate the method's feasibility, we aimed to use

different functionalised calix[6]arenes as monomers and employing various organic transformations for the formation of novel irreversible or reversible bonds. Moreover, the effect of the spacer between the two-station template on the efficiency of the cage assembly will also be accessed.

Results and Discussion

The first approach we envisioned for the synthesis of molecular cages involves the preparation of calix[6]arere derivatives functionalised at the upper rim with several functional groups, such as carboxylic acid, hydroxyl or aldehyde moieties (Figure 2.1).

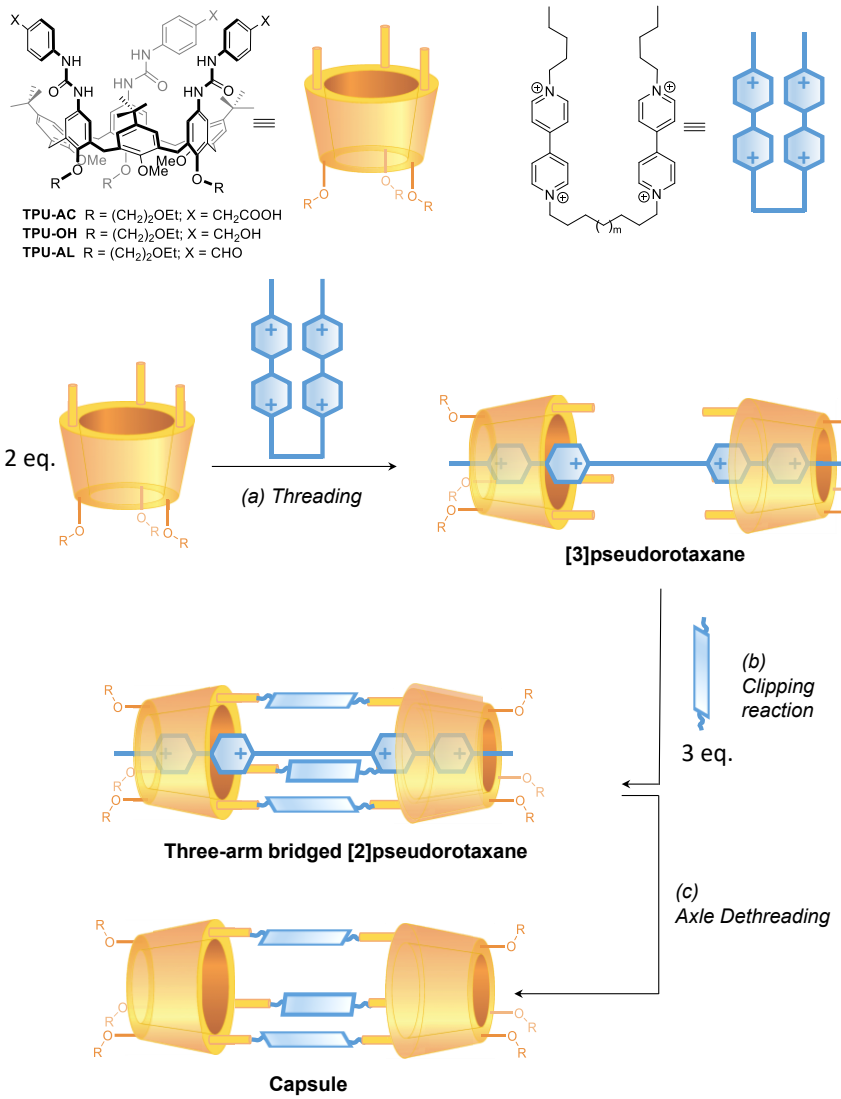

Figure 2.1 Synthetic approach for the preparation of calix[6]arene-based molecular capsules.

The formation of [3]pseudorotaxane would be accomplished by the unidirectional threading process (step *a*) of a two-station bis-viologen salt with 2 equivalents of functionalised calix[6]arene derivative. The addition of three equivalents of a proper linker molecule would afford the three-arm bridged calix[6]arene cage (*clipping reaction*). Finally, axle dethreading *via* chromatography purification should give the empty calix[6]arene-based capsule (step *c*).

For an effective templating effect, the distance between the two viologen stations of the axle should be adapted to permit the complexation of two calix[6]arene monomers without steric hindrance. In order to study this effect, three different axles were synthesised bearing different internal alkyl spacer between the two viologen units: C8, C12 and C16. Axles $\mathbf{3}_8$ (m = 8), $\mathbf{3}_{12}$ (m = 12) and $\mathbf{3}_{16}$ (m = 16), where m indicates the length of the alkyl spacer, were prepared in good yields by the reaction of pentylpyridylpiridinium tosylate **1** with the corresponding ditosylate $\mathbf{2}_m$ in acetonitrile at reflux conditions for four days (Scheme 2.5).

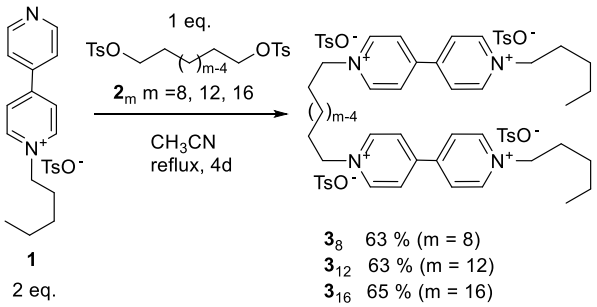

Scheme 2.5 Synthesis of axles $\mathbf{3}_m$.

The identity of the synthesised bis-viologen axles $\mathbf{3}_m$ was confirmed through NMR spectroscopy and ESI-MS measurements.

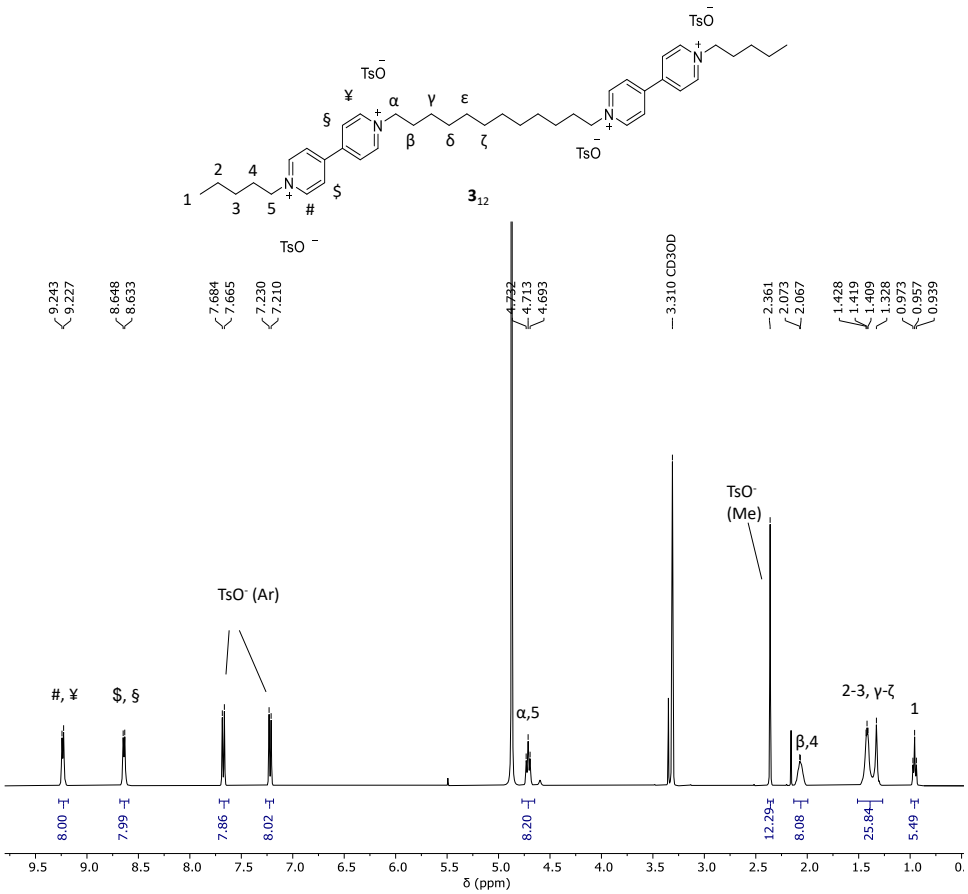

Figure 2.2 ^{1}H NMR spectrum (400 MHz, MeOD) of $\mathbf{3}_{12}$.

As an example, the ^{1}H NMR spectrum of $\mathbf{3}_{12}$, taken in CD_3OD (Figure 2.2), shows several diagnostic resonances, such as the multiplet centred at 4.71 ppm corresponding to the eight protons of the four methylene groups α and *5* linked to the pyridinium moieties, and a triplet at 0.96 ppm for the six protons of the two methyl groups *1*. The two bipyridinium units resonate as two doublets, each integrating for eight protons, at 9.24 (protons *¥*, *#*) and 8.63 ppm (*$*,*§*).

Once obtained the bis-viologen axles, the functionalisation of the calix[6]arene macrocycle was performed. First, we designed the calix[6]arene wheel decorated with three carboxylic groups onto the phenylureas (the same macrocycle in *R*[(**TPU-AC**)$_2$⊃**7**$_{12}$] in chapter 1, Scheme 1.8). The synthesis consists of the direct

insertion of 4-amino-phenylacetic acid on the scaffold of the known triamino calix[6]arene **TA**.[33] Thus, **TA** was activated with triphosgene in toluene at 80 °C for three hours to generate three isocyanate moieties at the upper rim. The resulting, not isolated, tricyano derivative was reacted with three equivalents of 4-aminophenylacetic acid, and the mixture was heated at 80 °C overnight. After chromatographic purification, **TPU-AC** was obtained in 82 % yield as a yellow solid.

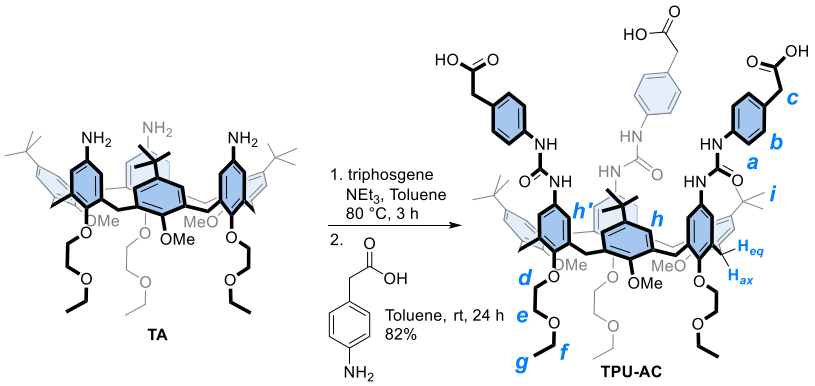

Scheme 2.6 Synthesis of **TPU-AC**.

The structure of **TPU-AC** was confirmed by NMR analysis and high-resolution mass spectroscopy (ORBITRAP LQ). The mass spectrum (Figure 2.3) shows a peak at m/z = 1638.81522 (z = -1), which was attributed to the mono negatively charged molecular ion, one at m/z = 1674.78950 (z = -1), due to the adduct of **TPU-AC** with one chloride anion. Finally, the peak at m/z = 818.90277 (z = -2) was assigned to the doubly negatively charged molecular ion of **TPU-AC**.

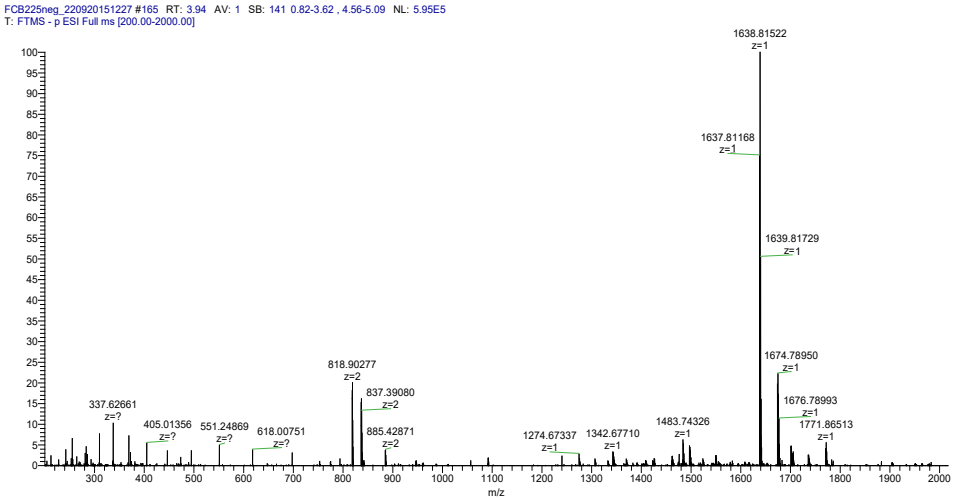

Figure 2.3 High-resolution mass spectrum of **TPU-AC**.

At first, an ^{1}H NMR experiment in deuterated dichloromethane revealed the formation of dimers of **TPU-AC** in solution (Figure 2.4 a). In fact, a splitting of the doublets corresponding to the axial and equatorial diastereotopic protons of the calix[6]arene methylene groups (H_{ax} and H_{eq}) was observed.

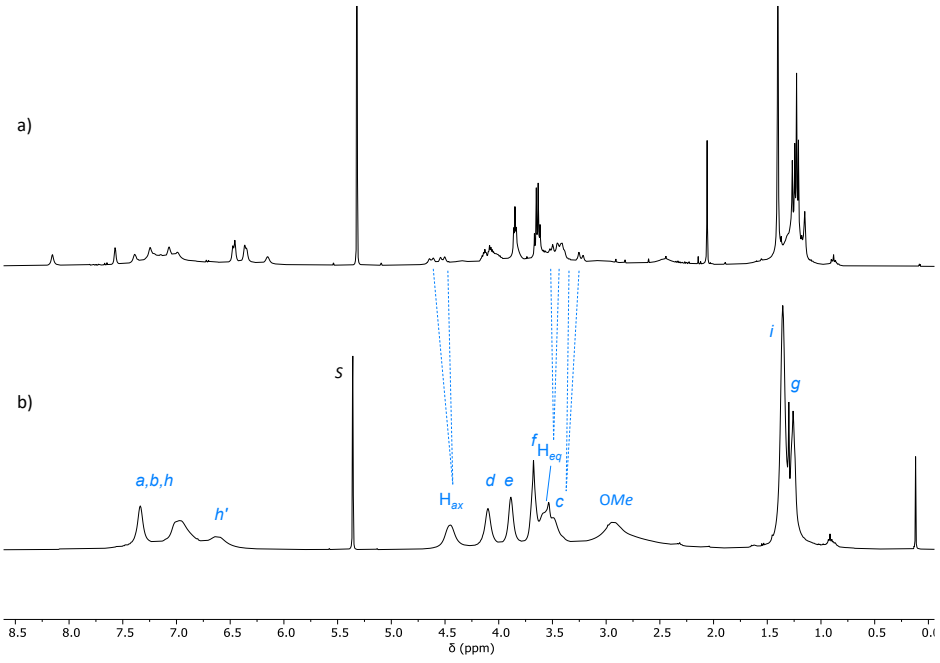

Figure 2.4 Stack plot of ^{1}H NMR spectra of **TPU-AC** a) recorded in DCM-d_2 and b) with the addition of two drops of methanol-d4.

Then, this hypothesis was confirmed when two drops of deuterated methanol were added to the NMR tube to break the hydrogen bonds network holding together the two macrocycles. The resulting ^{1}H NMR spectrum (Figure 2.4 b) no longer had the same characteristics, and it became very similar to the one of **TPU** (Figure 1.4 a) except for the peak corresponding to the methylene groups of the phenylacetyl moieties. The complete assignment was possible thanks to the 2D HSQC experiment (Figure 2.5).

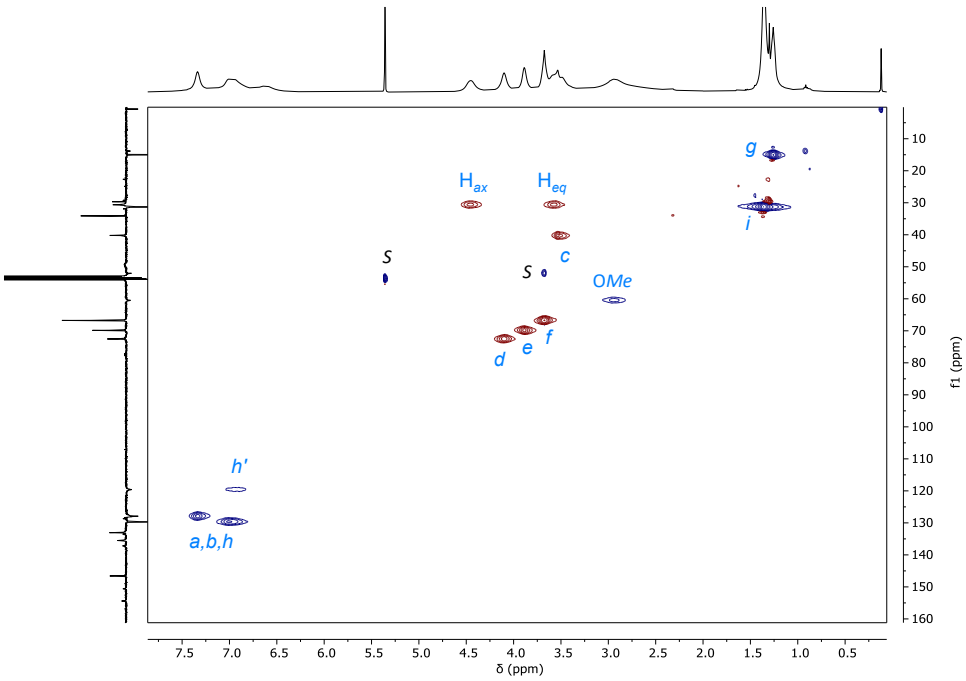

Figure 2.5 Edited HSQC 2D NMR spectrum (400 MHz, CD_2Cl_2+2 drops of CD_3OD) of compound **TPU-AC**.

With pure **TPU-AC** in hands, the ability of **TPU-AC** to form [3]pseudorotaxanes with axles $\mathbf{3}_m$ was tested. For this purpose, two equivalents of macrocycle **TPU-AC** were added to the solutions, each containing a suspension of insoluble axles $\mathbf{3}_m$ in dichloromethane. The mixtures were stirred at room temperature for 2 hours. During this time, axles $\mathbf{3}_m$ completely dissolved, and the solution turned homogeneous and red coloured as a result of the complexation. 1D and 2D NMR

experiments were performed in deuterated chloroform to evaluate the formation of [3]pseudorotaxanes and the orientation of the macrocycles.

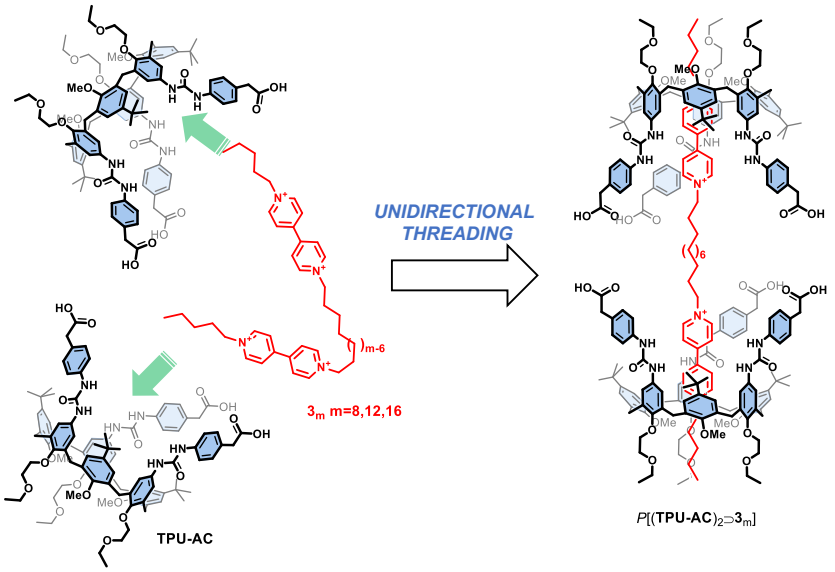

Scheme 2.7 Formation of [3]pseudorotaxanes *P*[(**TPU-AC**)$_2$⊃**3**$_m$].

Similar features were observed for each complex: two-station bis-viologen salts **3**$_m$ can be efficiently complexed by two macrocycles, and the system's symmetry suggests that the two **TPU-AC** units are facing each other. For instance, ^{1}H NMR spectrum of *P*[(**TPU-AC**)$_2$⊃**3**$_{12}$] shows every diagnostic signal of the formation of the oriented [3]pseudorotaxane complex (Figure 2.6): the peaks corresponding to NH protons, now involved in hydrogen bonds with tosylates, are downfield shifted at ~ 8.5 ppm; methoxy groups of **TPU-AC** experience a downfield shift from 2.9 to 4.0 ppm after the expulsion from the cavity; pyridinium protons of axle **3**$_{12}$ (labelled ¥, #, and $, §) split and upfield-shift at 7.7, 7.5, 6.9 and 6.8 ppm, respectively, when complexed in the asymmetric cavity of the calix[6]arene. Similarly, methylene groups linked to pyridinium rings (α and *5*) undergo splitting and upfield shift (red and purple lines).

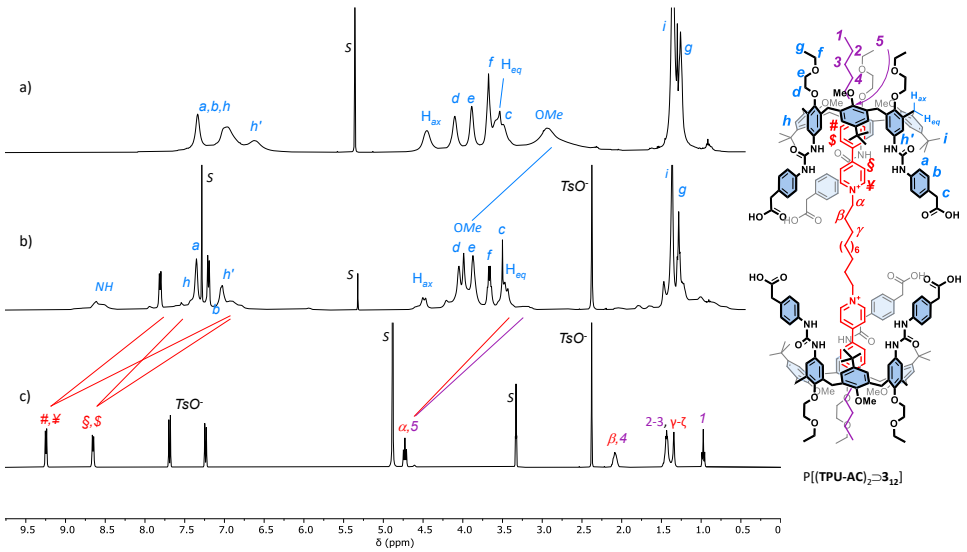

Figure 2.6 ^{1}H NMR stack plot (400 MHz) of a) **TPU-AC** (taken in CD_2Cl_2 for solubility reason); b) [3]pseudorotaxane *P*[(**TPU-AC**)$_2$⊃**3**$_{12}$] in $CDCl_3$; c) **3**$_{12}$ (taken in CD_3OD for solubility reasons).

Once verified the formation of [3]pseudorotaxanes with **TPU-AC**, the template-assisted dimerisation of this calix[6]arene derivative was tested in parallel with each of the axles **3**$_m$, in order to access the most suitable spacer for the reaction. First, the formation of [3]pseudorotaxanes was carried out *in situ*, suspending axle **3**$_m$ and **TPU-AC** (2 equiv.) in dichloromethane for 2 hours, as already described. Then, the next step was the carboxylic moieties activation. After several attempts with different activating agents (such as DCC and EDC), 2-chloro-1-methylpyridinium iodide was found to be the proper agent for this activation. Six equivalents of 2-chloro-1-methylpyridinium iodide were added to the reaction and the mixture was stirred at room temperature for one hour. Afterwards, a solution of three equivalents of the linker 1,4-benzenedimethanol in dichloromethane was added dropwise to the reaction for two hours. The reaction mixture was left stirring overnight, then the chromatographic purification led to the axle dethreading event, affording the empty calix[6]arene-based **Cage-1** as a white solid.

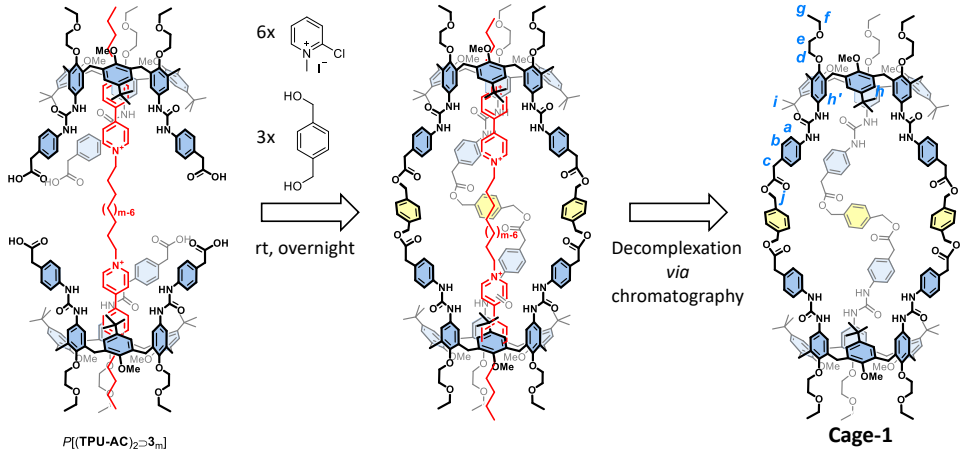

P[(**TPU-AC**)$_2$⊃**3**$_m$]

Entry	m	η
1	8	traces
2	12	11 %
3	16	-
4	no axle	-

Scheme 2.8 Synthesis of **Cage-1**.

The "short" axle **3**$_8$ provided **Cage-1** only in traces. Axle **3**$_{12}$ was found to be the most suitable template for this synthesis giving **Cage-1** in 11 % of yield, while with **3**$_{16}$ no product was detected. The reaction without the template was also tested: identical conditions were maintained except for the addition of the axle and the consequent [3]pseudorotaxane formation. In this case, no product was observed, demonstrating the potentiality of the template-assisted strategy.

The structure of **Cage-1** structure was confirmed with a series of NMR experiments. Compared to **TPU-AC**, a few new peaks appear at ca. 5 ppm in the ^{1}H NMR spectrum of the cage (Figure 2.7), which were assigned to linker methylene groups (*j*). The presence of several peaks in this region could be addressed by the coexistence of different conformations of the cage. The other signals are in agreement with those expected. It is possible to recognise the methoxy groups as broad peak at 2.9 ppm; the methylene protons of the ethoxy ethyl chains, labelled as *d*, *e*, and *f*, resonate at 4.1, 3.8 (two broad signals) and

3.6 ppm (quartet). Geminal methylene protons H_{ax} and H_{eq} give rise to two broad resonances at 4.4 ppm and 3.6 ppm, the latter hidden under the *f* peak. Between 1.4 and 1.1 ppm, we can find the singlet from *tert*-butyl moieties (*i*), and methyl groups *g*, as a triplet. The successful formation of **Cage-1** was thus devised by the latter evidence together with a matching integration of the signals. The complete spectrum assignment was accomplished through a 2D HSQC experiment.

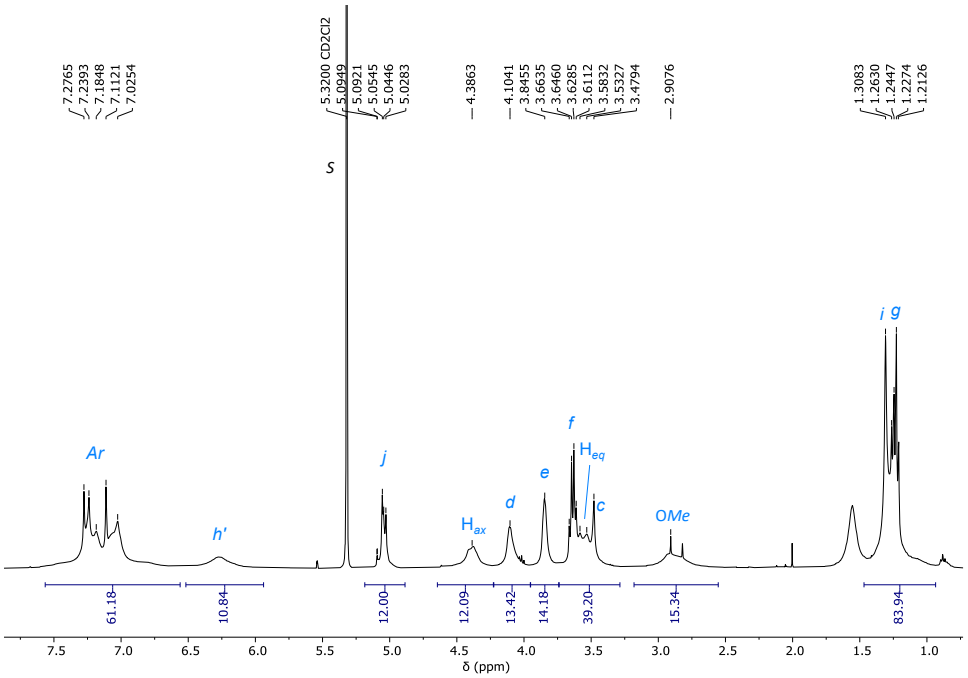

Figure 2.7 ^{1}H NMR spectrum (400 MHz, CD_2Cl_2) of **Cage-1**.

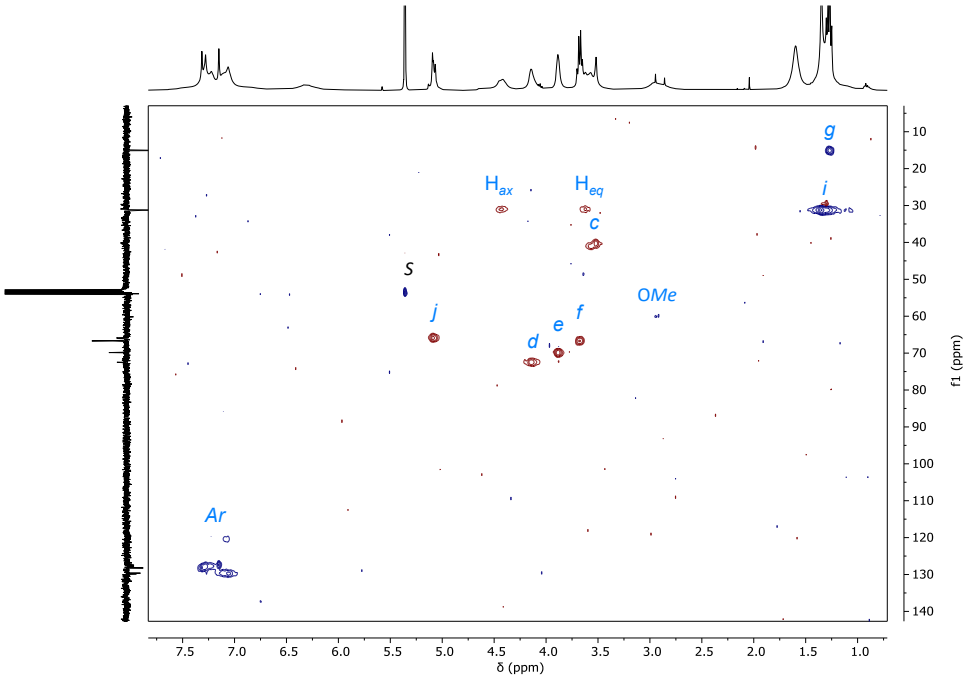

Figure 2.8 Edited HSQC 2D NMR spectrum (400 MHz, CD_2Cl_2) of compound **Cage-1**.

Finally, high-resolution mass spectrometry measurements (ORBITRAP LQ) confirmed once again the obtainment of **Cage-1**. The base peak at m/z = 1793.90439 (z = 2) is attributed to the doubly positively charged molecular ion, and the isotopic distribution of the cluster of peaks was in agreement with the calculated one (Figure 2.9).

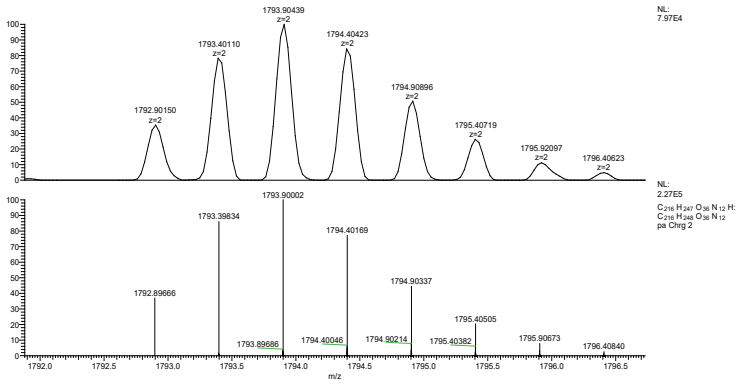

Figure 2.9 Inset of HR-MS (ESI, Orbitrap LQ) spectrum of compound **Cage-1**: experimental (top) and calculated (down) isotopic distribution for the doubly charged molecular ion.

To further expand the applicability of our template-based synthetic methodology, we devised the synthesis of a new calix[6]arene-based cage starting from a calix[6]arene derivative decorated on its phenylureas with hydroxymethyl groups. In principle, such functionalities can easily react with a difunctional acyl chloride molecule as the linker.

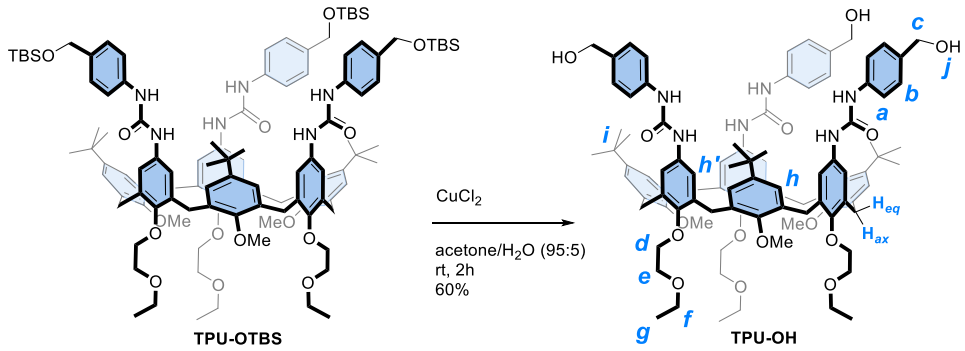

Scheme 2.9 Synthesis of **TPU-OH**.

To this aim, the hydroxymethyl groups of the already-prepared **TPU-OTBS** were deprotected by treating a solution of this host in 95:5 acetone/H_2O with copper(II) chloride. The reaction was stirred at room temperature for two hours. After chromatographic purification, **TPU-OH** was recovered in 60 % yield as a yellow solid. The use of $CuCl_2$ as an effective deprotecting agent for silyl ether PGs could appear odd if we consider that they are usually efficiently removed by fluoride ions sources (TBAF) or acidic or basic hydrolytic conditions. Nevertheless, when we tried the above conditions, we consistently observed the hydrolysis of the urea functions. **TPU-OH** was characterised through a series of NMR and high-resolution mass spectroscopy experiments. HR-MS (MALDI) confirmed its formation: a base peak at m/z = 1577.48420 (z = 1) was attributed to a molecular ion deriving by an adduct with Na^+, while the one at m/z = 1593.47028 to the adduct with K^+. ^1H NMR spectrum was recorded in deuterated acetonitrile (see Figure 2.11 a), and the signals assignment was confirmed by the corresponding 2D HSQC experiment (see Figure 2.10).

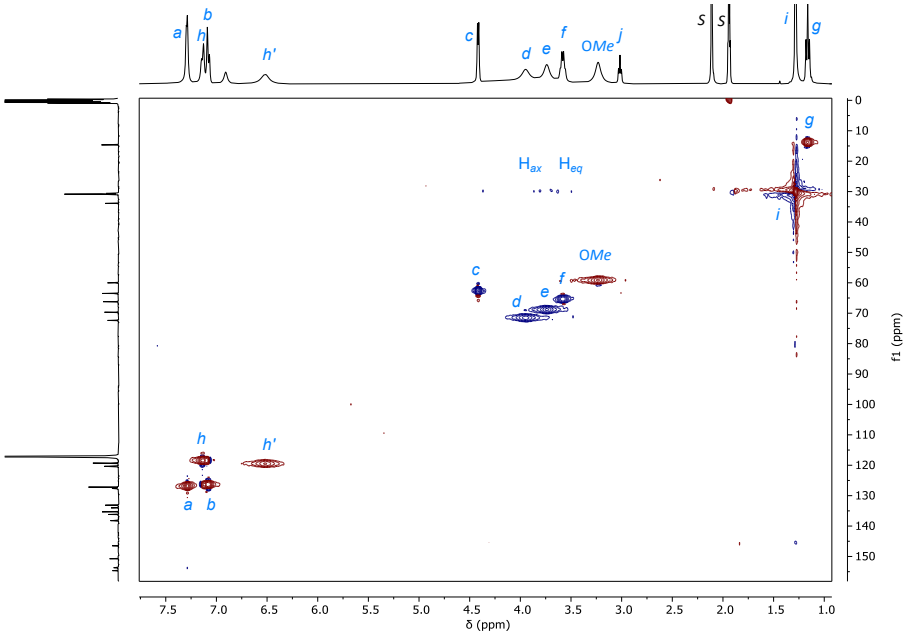

Figure 2.10 Edited HSQC 2D NMR spectrum (400 MHz, ACN-d) of compound **TPU-OH**.

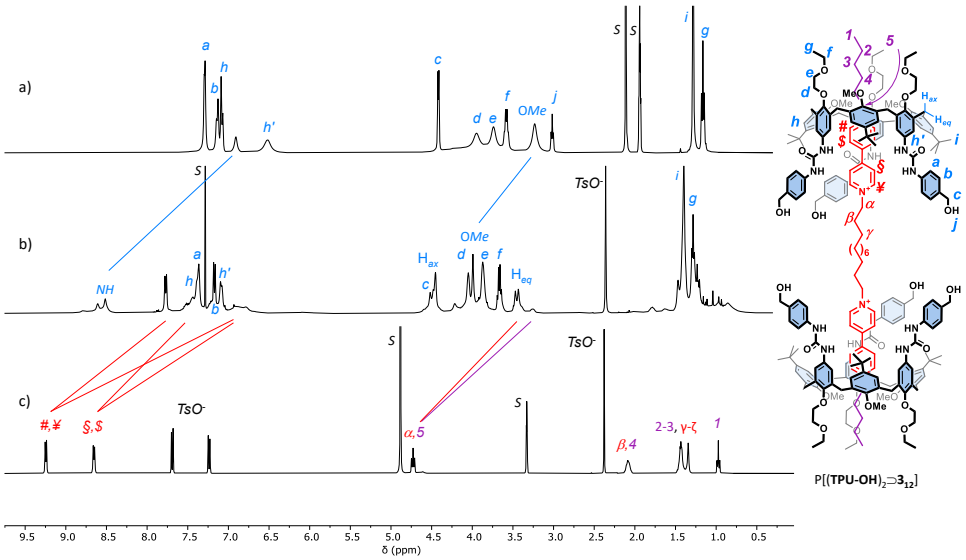

Figure 2.11 ^{1}H NMR stack plot (400 MHz) of a) **TPU-OH** (taken in CD_3CN-d for solubility reason); b) [3]pseudorotaxane *P*[(**TPU-OH**)$_2$⊃**3**$_{12}$] in $CDCl_3$; c) **3**$_{12}$ (taken in CD_3OD for solubility reasons).

The diagnostic signals witnessing the occurred deprotection are the doublet at 4.41 ppm, corresponding to the methylene protons (*c*) in the *para* position of the

phenylurea groups, and the triplet at 3.02 ppm assigned to the hydroxylic moieties (*j*). On the other hand, the signals of the bridging methylene groups of the calix[6]arene macrocycle (H_{eq} and H_{ax}) give rise to very broad and almost unrecognisable signals (see also HSQC). It thus seems like the PGs removal induces high fluxionality to the **TPU-OH** macrocycle.

Once the synthesis of **TPU-OH** was confirmed, our template-assisted strategy was applied to prepare the novel calix[6]arene-based dimer **Cage-2** (see Scheme 2.10). Like **Cage-1**, the method's effectiveness was tested by performing the "clipping reaction" in parallel using the three different axles $\mathbf{3}_m$. To this aim, two equivalents of **TPU-OH** were added to a suspension of $\mathbf{3}_m$ in dichloromethane. The resulting mixtures were stirred for about 2 hours until they became homogeneous and deeply red-coloured. The formation of the series of [3]pseudorotaxanes *P*[(**TPU-OH**)$_2$⊃$\mathbf{3}_m$], with m = 8, 12 and 16, was confirmed by 1D and 2D NMR analysis. As an example, in the ^{1}H NMR stack plot of **TPU-OH**, *P*[(**TPU-OH**)$_2$⊃$\mathbf{3}_{12}$] and $\mathbf{3}_{12}$ (Figure 2.11), the same complexation evidence found in the case of *P*[(**TPU-AC**)$_2$⊃$\mathbf{3}_{12}$] can be recognised.

A diluted solution of three equivalents of the linker in dichloromethane - we chose the terephthaloyl chloride - was added dropwise to that of each [3]pseudorotaxane *P*[(**TPU-OH**)$_2$⊃$\mathbf{3}_m$] for a period of two hours. After stirring overnight, each reaction mixture was submitted to chromatographic purification, which caused the axle's decomplexation, giving, in all the cases, the empty **Cage-2** as a white solid. Like **Cage-1**, the best result was obtained with axle $\mathbf{3}_{12}$, which led to the formation of **Cage-2** in 14 % yield. Only traces were observed with $\mathbf{3}_8$, and no product at all when $\mathbf{3}_{16}$ was used. Once again, the test reaction without the addition of the axle did not lead to **Cage-2**.

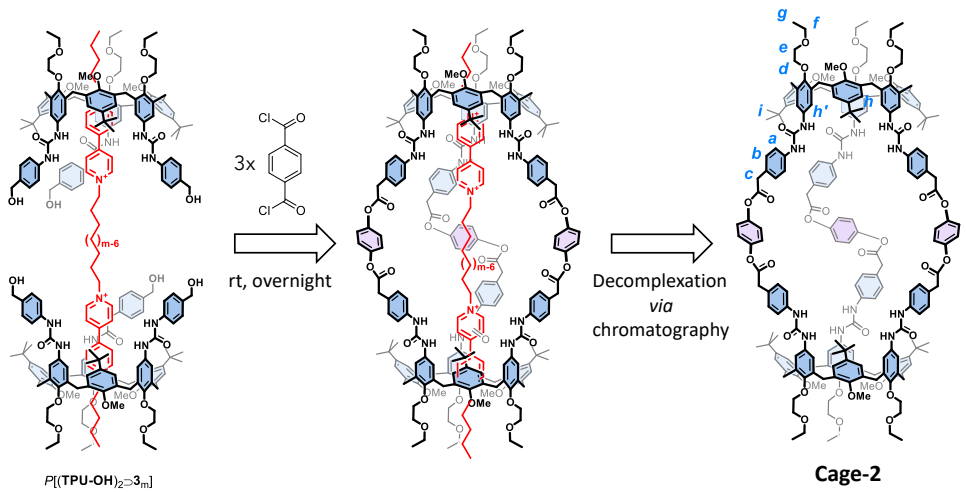

Entry	m	η
1	8	traces
2	12	14 %
3	16	-
4	no axle	-

Scheme 2.10 Synthesis of **Cage-2**.

Cage-2 was completely characterised through a series of NMR and high-resolution mass spectroscopy experiments. In the HR-MS spectrum (Figure 2.12), the monocharged molecular ion can be identified as a small peak with m/z = 3502.70596 (z = 1), while the base peak at m/z = 1751.85463 with z = 2 corresponds to the doubly charged molecular ion.

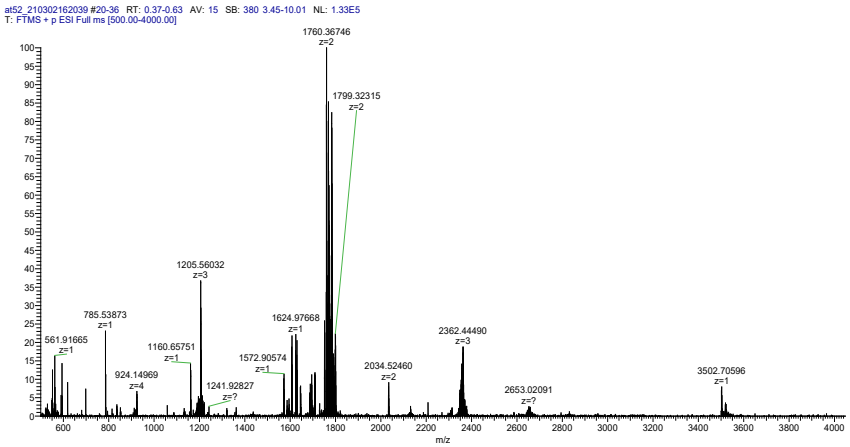

Figure 2.12 HR-MS (ESI, Orbitrap LQ) spectrum of **Cage-2**.

As usual, the ^{1}H NMR spectrum recorded in deuterated dichloromethane shows very broad resonances. However, an exhaustive signals assignment was accomplished through a 2D HSQC NMR experiment (see Figure 2.13). In the empty **Cage-2**, the methoxy groups resonate as a very broad signal at 3.1 ppm because they are found inside the calix[6]arene cavity, thus, highly shielded. Also, the peak corresponding to hydroxymethyl protons (*c*) is very broad, probably due to the fluxionality of the system. In this condition of fluxionality, it was very difficult to assess whether the two small signals visible over the broader one result from geminal coupling between protons that, upon the bridging event, have become diasterotopic.

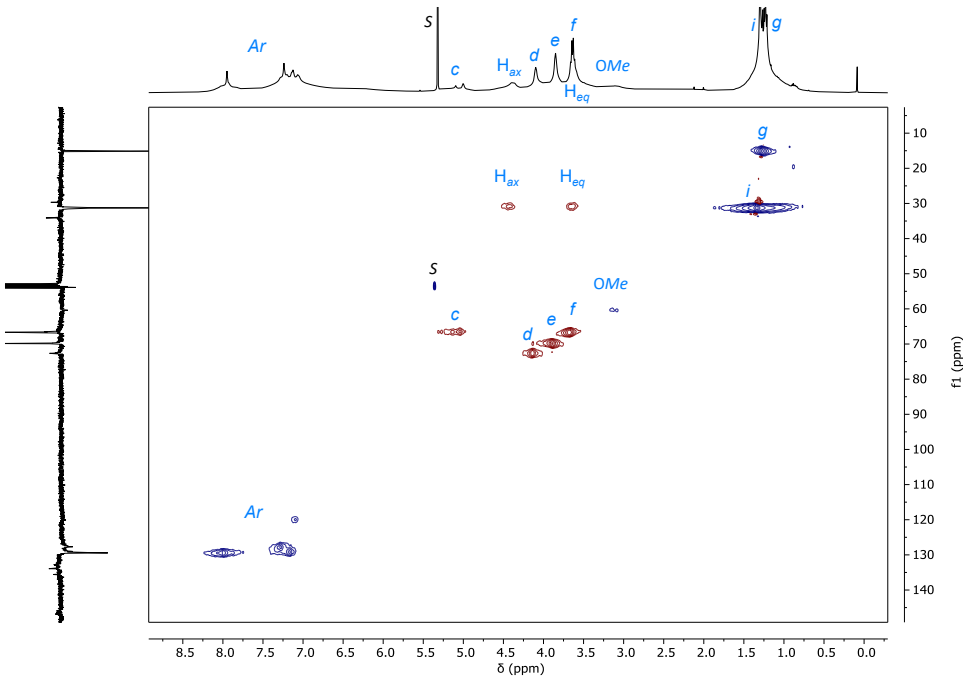

Figure 2.13 Edited HSQC 2D NMR spectrum (400 MHz, CD_2Cl_2) of compound **Cage-2**.

A further functionalised calix[6]arene monomer was accessed through the oxidation of **TPU-OH**. The resulting calix[6]arene decorated with three aldehyde moieties at the upper rim (**TPU-AL**) should be able, in principle, to react with three

diamine derivatives in order to generate six imine groups and thus form a molecular cage. The reaction between aldehydes and amines has been widely employed for the formation of molecular cages, as described in the introduction.[25,26]

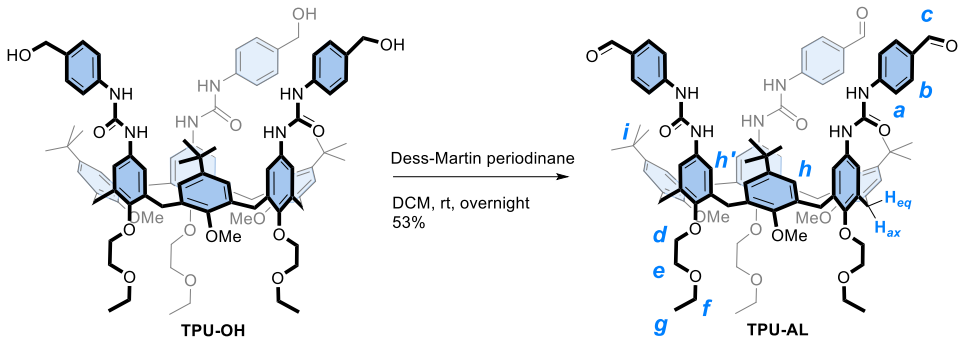

Scheme 2.11 Synthesis of **TPU-AL**.

Tri-aldehyde calix[6]arene **TPU-AL** was obtained in 53 % yield oxidising **TPU-OH** with the Dess-Martin periodinane (DMP) reactive in dichloromethane at room temperature. The achievement of **TPU-AL** was first demonstrated by high-resolution mass spectrometry (ORBITRAP LQ). The mass spectrum reveals three singly charged molecular ions: one with a base peak at m/z = 1550.79839 for the monocationic **TPU-AL**, one at m/z = 1567.82479, which was attributed to the adduct with NH_4^+, and finally one at 1572.77981 for the adduct with Na^+. The characterisation of **TPU-AL** was completed through NMR analysis. ^{1}H NMR spectrum shows very broad signals in deuterated chloroform; fortunately, it still evidences diagnostic signals for the formation of the aldehyde's groups, such as the broad peak at 9.77 ppm. As usual, the complete signals assignment was accomplished through a 2D HSQC experiment (see Figure 2.14).

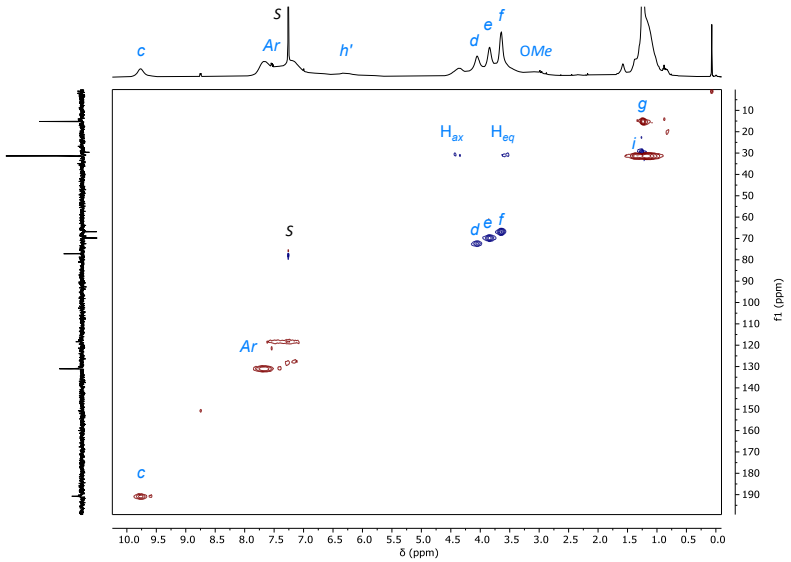

Figure 2.14 Edited HSQC 2D NMR spectrum (400 MHz, $CDCl_3$) of compound **TPU-AL**.

To determine whether this new macrocycle was able to efficiently complex the bis-viologen salt $\mathbf{3}_{12}$ and thus form [3]pseudorotaxane complex, axle $\mathbf{3}_{12}$ was equilibrated with two equivalents of **TPU-AL** in dichloromethane for two hours. Upon equilibration, the dissolution of the axle and the appearance of the expected red colour of the solutions were observed, suggesting the formation of the [3]pseudorotaxane complex. The formation of the latter species (*P*[(**TPU-AL**)$_2$⊃$\mathbf{3}_{12}$]) was confirmed as usual by NMR spectroscopy. The ^{1}H NMR spectra stack plot of **TPU-AL**, *P*[(**TPU-AL**)$_2$⊃$\mathbf{3}_{12}$] and the free axle $\mathbf{3}_{12}$ was reported in Figure 2.15. The most striking feature of the [3]pseudorotaxane spectrum (Figure 2.15 b) is the sharpening of the signals of the **TPU-AL** macrocycle when it is involved in the complexation. Clearly, such an improved signal resolution is due to the reduced fluxionality of the calix[6]arene macrocycles when entangled with the bis-viologen thread. The aldehydic protons (c) in the complex now resonate as a sharp signal at 9.70 ppm. The six methoxy groups (*OMe*) experience a downfield shift from 3.1 ppm (broad peak, in spectrum *a*) to 4.0 ppm (very sharp peak, in spectrum *b*). The presence of a unique singlet for the *OMe* protons and

two doublets for the geminal methylene protons H_{ax} and H_{eq} indicates a highly symmetric magnetic environment. This finding confirms the formation of a single head-to-head pseudorotaxane isomer.

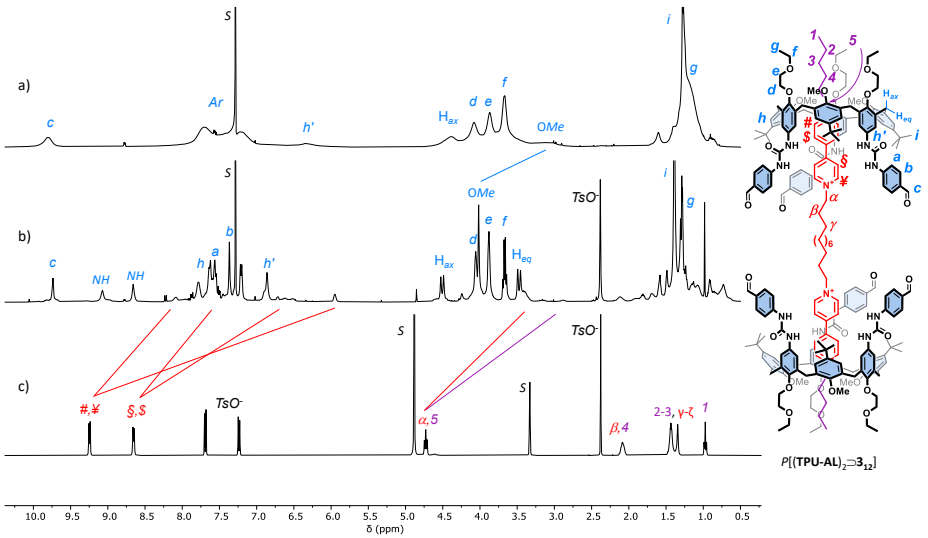

Figure 2.15 ^{1}H NMR stack plot (400 MHz, $CDCl_3$) of a) **TPU-AL**; b) [3]pseudorotaxane *P*[(**TPU-AL**)$_2$⊃**3**$_{12}$]; c) **3**$_{12}$ (taken in CD_3OD for solubility reasons).

Once the formation of the [3]pseudorotaxane complex was demonstrated, the **TPU-AL** dimerization was tested in the presence of axle **3**$_{12}$ by using diamino derivatives as the linkers. In principle, this reaction would promote the formation of a cage with six imine groups in the bridges. As usual, the reaction was carried out in dichloromethane at room temperature. After equilibrating two equivalents of **TPU-AL** with axle **3**$_{12}$, a diluted solution of three equivalents of *p*-phenylenediamine was added dropwise to the reaction mixture. It should be observed that this latter diamine derivative was chosen because it is rigid and aromatic. The rigidity should reduce the probability of intramolecular bridging reactions, while the aromaticity would generate highly delocalized bonds. After chromatographic separation, **Cage-3** was isolated in higher yields (51%) compared to the other previously synthesised cages. However, unlike the previous cases, this cage was isolated in yields comparable to the untemplated

reaction (48 vs 51%). This quite unexpected result can be accounted for if we consider the reversible nature of the imine bond, as already discussed in the introduction.

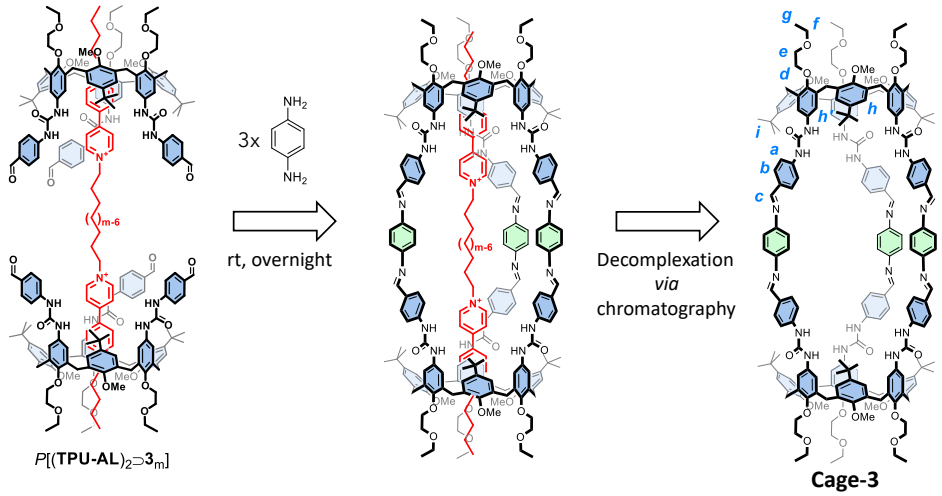

Entry	m	η
1	12	51
2	no axle	48

Scheme 2.12 Synthesis of **Cage-3**.

Confirmation of **Cage-3** formation was given by high-resolution mass spectrometry measurements (ORBITRAP LQ). The recorded MS spectrum displays a doubly charged molecular ion at m/z 1658.86598 (z = 2), whose isotopic pattern agrees with that of the doubly charged target molecule (Figure 2.16). A partial characterisation was also obtained through a series of NMR experiments. In fact, the empty cage gives rise to a ^{1}H NMR spectrum characterised by resonances even broader than those found in the spectra of **Cage-1** and **Cage-2** (cf. Figures 2.7 and 2.13 with 2.17). Fortunately, the typical features of the calix[6]arene scaffold can be detected in the corresponding 2D HSQC spectrum. In particular, a very weak but recognisable cross-peak at F_2,F_1 = 8.32,156 ppm was attributed to the coupling of the six protons (the broad signal labelled as *c* in Figure 2.17) of the imine groups with its attached ^{13}C nuclei.

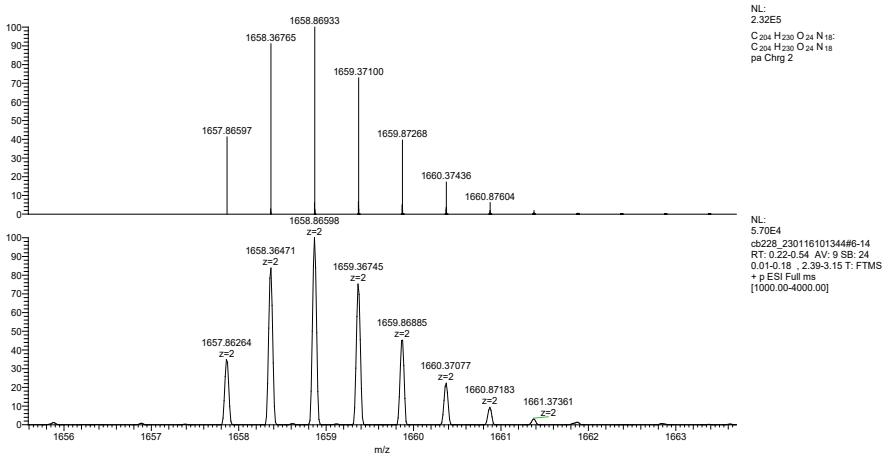

Figure 2.16 Inset of HR-MS (ESI, Orbitrap LQ) spectrum of compound **Cage-3**: calculated (top) and experimental (down) isotopic distribution for the doubly charged molecular ion.

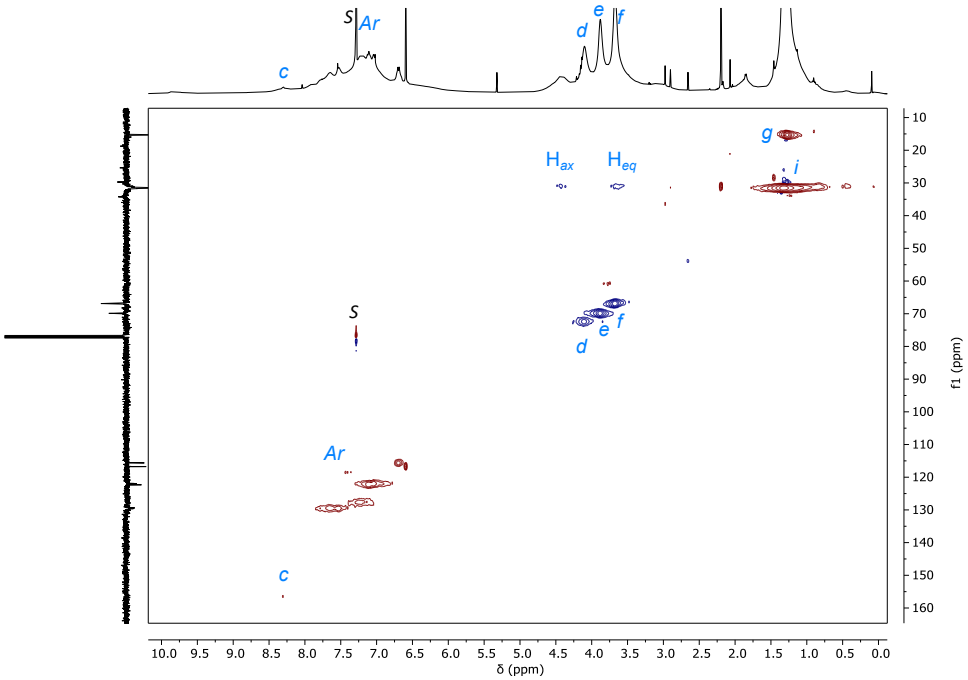

Figure 2.17 Edited HSQC 2D NMR spectrum (400 MHz, $CDCl_3$) of compound **Cage-3**.

A different strategy was then pursued to obtain molecular cages directly from the triamino calix[6]arene **TA**. For this purpose, we designed the reaction between **TA** and a diisocyanate molecule as the linker. As the linker, we chose to employ the commercial bis(4-isocyanatophenyl)methane (see Scheme 2.13), which has a methylene group between the phenylisocyanate moieties. In our opinion, this linker's high rotational freedom degree should facilitate the bridging reactions between the calix[6]arene monomers. The strategy adopted involved preparing a suspension of our axles and **TA** in dichloromethane. Differently from the previous examples, **TA** is not able to complex the bis-viologen salt because it lacks the phenylurea groups that, thanks to their H-bonding abilities, control the complexation event, as we mentioned before. As a result, no complexation was observed when **TA** was mixed in dichloromethane with each of the $\mathbf{3}_{m}$ salts. However, at this stage, a solution of the diisocyanate linker in dichloromethane was prepared and slowly dropwise added to the above heterogeneous and uncoloured reaction mixtures. After one eq. of diisocyanate was added, a pale red colour developed in the solution. We hypothesised that once the first reaction between the isocyanate and the calix[6]arene amino groups has occurred, the phenylurea of this intermediate began loosening the axle ion-pairing (see Scheme 2.13), favouring the bis-viologen threading. This process promotes the macrocycles' preorganisation, favouring the correct further clipping reactions leading to the final molecular cage. The reaction mixtures were stirred at room temperature overnight. The following chromatographic purification with DCM/MeOH led to the isolation of the empty **Cage-4**.

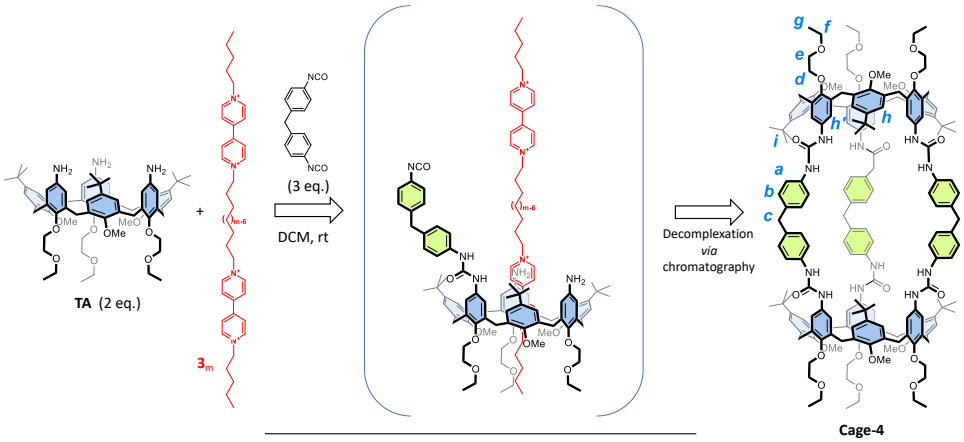

Entry	m	η
1	8	13 %
2	12	15 %
3	16	-
4	no axle	-

Scheme 2.13 Synthesis of **Cage-4**.

The reaction with axles $\mathbf{3}_8$ and $\mathbf{3}_{12}$ gave similar results. Indeed, **Cage-4** was isolated in 13% and 15% yield, respectively. $\mathbf{3}_{16}$ did not provide **Cage-4** as well as the reaction carried on without the template demonstrating, once again, the axle role for the success of the reaction. As usual, the identity of **Cage-4** was initially confirmed by high-resolution mass spectroscopy. The peak at m/z = 1484.81340 (z = 2) corresponds to the doubly charged molecular ion; that at m/z = 1495.30262 (z = 2) to its adduct with Na^+ and H^+; that at m/z = 1493.32762 (z = 2) to its adduct with NH_4^+ and H^+; and finally that at m/z = 1503.78962 (z = 2) to the adduct with K^+ and H^+.

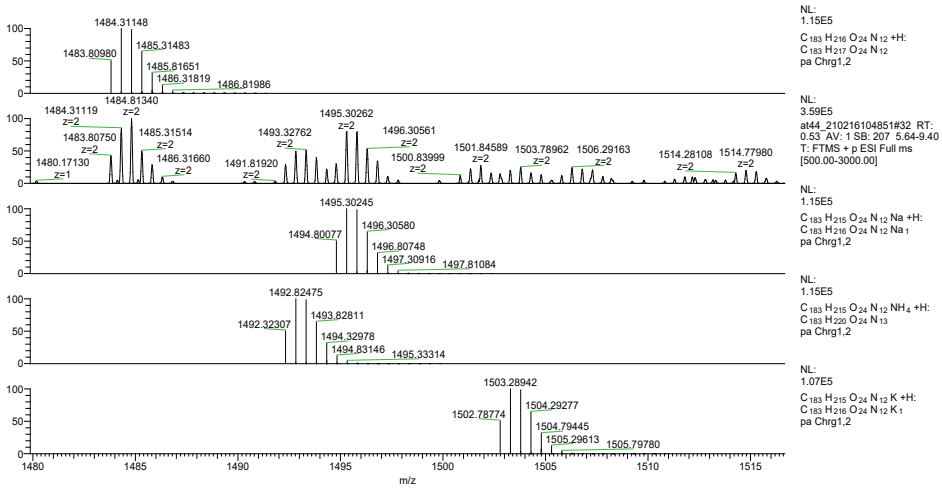

Figure 2.18 Inset of HR-MS (ESI, Orbitrap LQ) spectrum of compound **Cage-4**: experimental and calculated isotopic distribution for the double charged molecular ions.

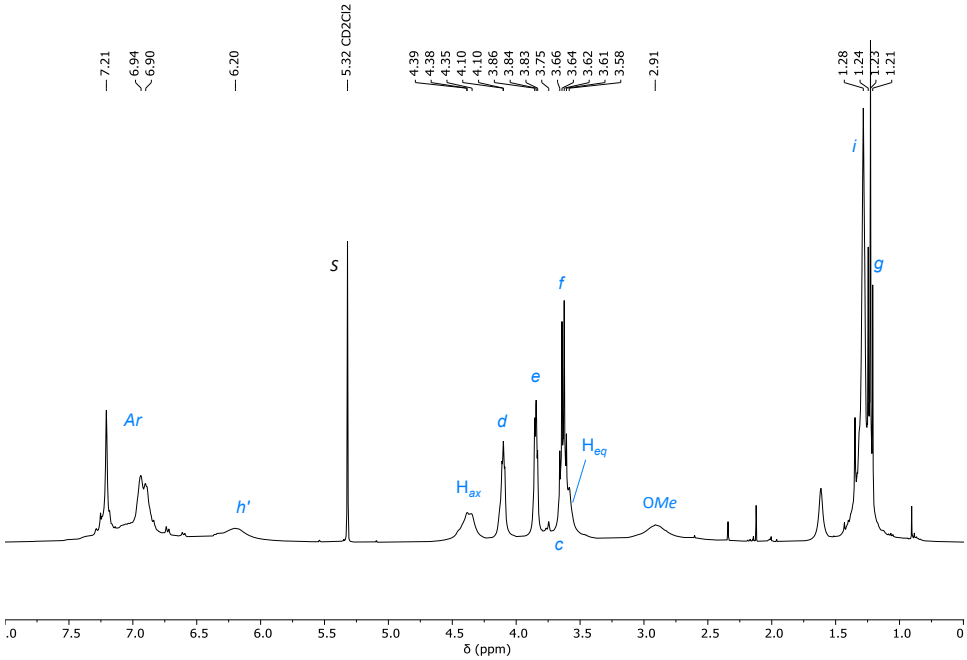

Figure 2.19 ^{1}H NMR spectrum (400 MHz, CD_2Cl_2) of **Cage-4**.

The ^{1}H NMR spectrum of **Cage-4** was recorded in deuterated dichloromethane (see Figure 2.19). The signal pattern agrees with those expected for this type of cage. It is possible to recognise the usual very broad peak at 2.9 ppm for the

methoxy groups; the methylene protons of the ethoxy ethyl chains at the calix[6]arene narrower rim, labelled as *d*, *e*, and *f*, resonate at 4.1, 3.8 (two broad signals) and 3.6 ppm (quartet). Geminal methylene protons H_{ax} and H_{eq} give rise to two broad resonances at 4.4 ppm and 3.6 ppm, the latter hidden under the *f* peak. Between 1.4 and 1.1 ppm, we can find the singlet from *tert*-butyl moieties (*i*), and methyl groups *g*, as a triplet. The diagnostic protons of the cage linkers, the methylene protons *c*, are hidden by the stronger resonances H_{eq} and *f*. Still, they are easily identified through the analysis of the HSQC spectrum (see Figure 2.20).

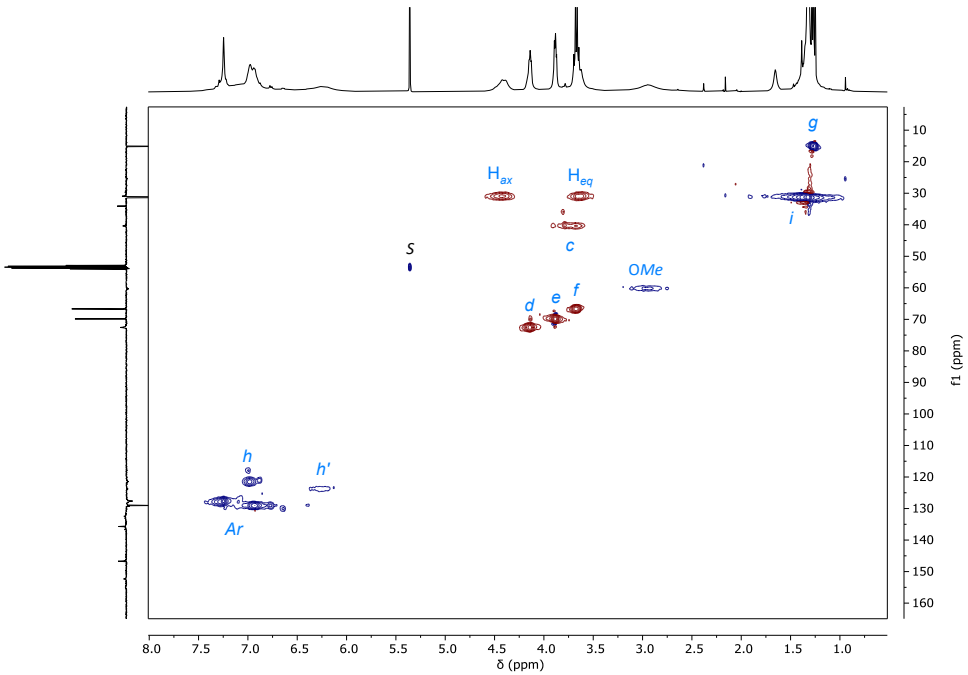

Figure 2.20 Edited HSQC 2D NMR spectrum (400 MHz, CD_2Cl_2) of **Cage-4**.

Cage-4 was also tested as a host for dioctylviologen salt (**DOV•**2TsO). The study wanted to disclose the ability of **Cage-4** to complex **DOV•**2TsO species for several reasons. First, we know that, in low polarity solvents, the complexation of viologen salts by *N*-phenylureido calix[6]arenes always occurs with axle threading from the macrocycle wider rim. Thus, it became mandatory for us to verify whether the cage portals were wide enough to allow the guest to enter the cavity.

Second, we were interested in investigating whether the aromatic cavity of **Cage-4** is able to host one or two **DOV•**2TsO molecules simultaneously, thus obtaining a 1:1 or 1:2 host-guest complex. The study was carried out using UV-Vis spectroscopy as the investigation tool. Figure 2.21 shows the absorption spectra of **DOV•**2TsO (blue line) and **Cage-4** (red line), characterised by an intense band with λ max = 257 nm and ε = 115'000 $M^{-1}cm^{-1}$.

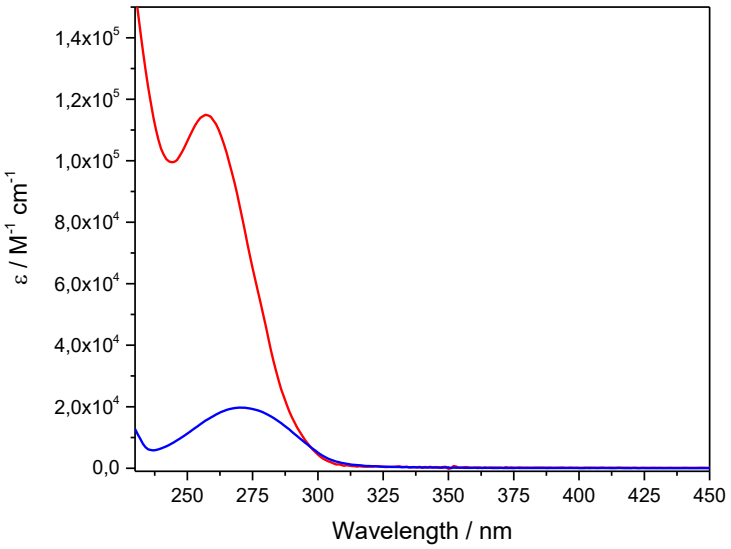

Figure 2.21 Absorption spectra (CH_2Cl_2, rt, λ = 225-450 nm region) of **DOV•**2TsO (blue line) and **Cage-4** (red line).

Then, the complexation was qualitatively evaluated by comparing the spectrum collected by recording, simultaneously, the spectra of the separated **Cage-4** and **DOV•**2TsO species, called the "sum" spectrum, with the spectrum of a mixture of both components, called the "mixture" spectrum. In this way, every difference between the two spectra is attributed to the formation of the complex. The "sum" spectrum was provided using a cuvette divided into two separate cells, each filled with equimolar solutions of **Cage-4** and **DOV•**2TsO (16 μM) in dichloromethane.

The "mixture" spectrum was obtained from the 1:1 mixture of the above solutions.

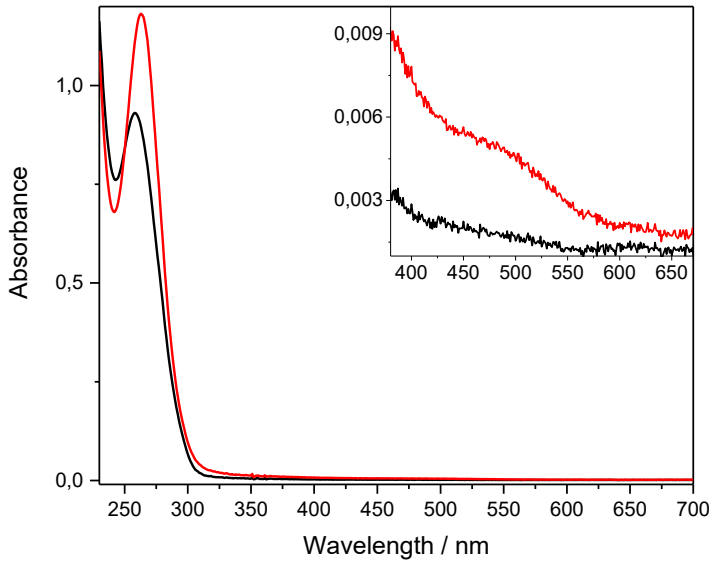

Figure 2.22 Sum of the absorption spectra of **Cage-4** and **DOV•**2TsO (black line) and the absorption spectrum of the mixture of **Cage-4** and **DOV•**2TsO (red line) (CH_2Cl_2, rt, λ = 225-700 nm region). Inset: zoom between 400-650 nm showing the CT band.

The spectra comparison was gathered in figure 2.22. It shows that the "mixture" spectrum (in red) experiences a hyperchromic variation together with a blueshift of the maximum (λ = 263 nm) with respect to the "sum" spectrum (in black). Moreover, the formation of a charge-transfer band is visible and centred at λ = 460 nm. These changes are compatible with previously complexation studies between calix[6]arenes and viologen salts,[34,35] thus suggesting that **DOV**$^{2+}$ is able to enter the cage. The association constant and the stoichiometry of the complexation were investigated through titration experiments. The first titration consisted of the addition of aliquots of a solution of **Cage-4** (110 µM, in DCM) to a solution of **DOV•**2TsO (10 µM, in DCM). By plotting the equivalents of **Cage-4** added versus the absorbance at 470 nm, we can detect a slope variation in correspondence of 0.5 equivalents. This finding is compatible with the complexation of two **DOV•**2TsO inside the cage.

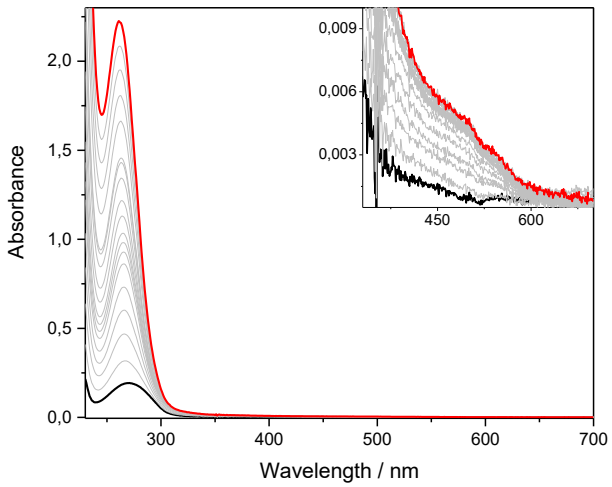

Figure 2.23 Titration absorption spectra of **DOV•**2TsO with **Cage-4** (CH_2Cl_2, rt, λ = 225-700 nm region). Inset: zoom between 400-650 nm showing the CT band.

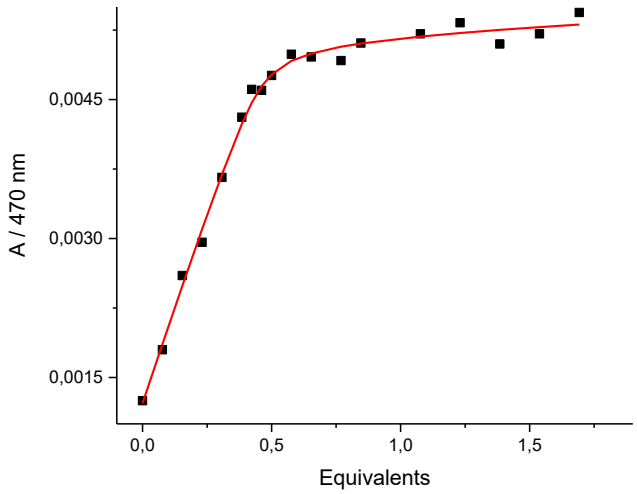

Figure 2.24 Binding isotherm (λ = 470 nm) for the complexation of **DOV•**2TsO with **Cage-4**. Black squares: experimental points; continuous red line: fitting.

Contrariwise, the second titration was carried out by adding aliquots of **DOV•**2TsO solution (80 μM, in DCM) to the cage solution (6 μM, in DCM). This

time, the slope variation is perceptible at 2 equivalents of the salt, again confirming the 1:2 host-guest stoichiometry of the complexation.

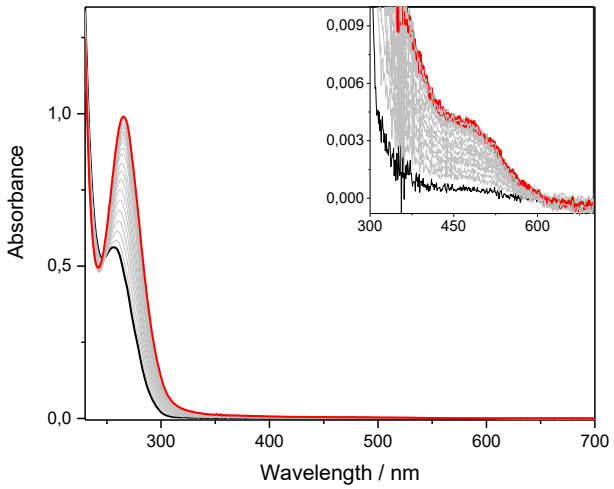

Figure 2.25 Titration absorption spectra of **Cage-4** with **DOV**•2TsO (CH_2Cl_2, rt, λ = 225-700 nm region). Inset: zoom between 400-650 nm showing the CT band.

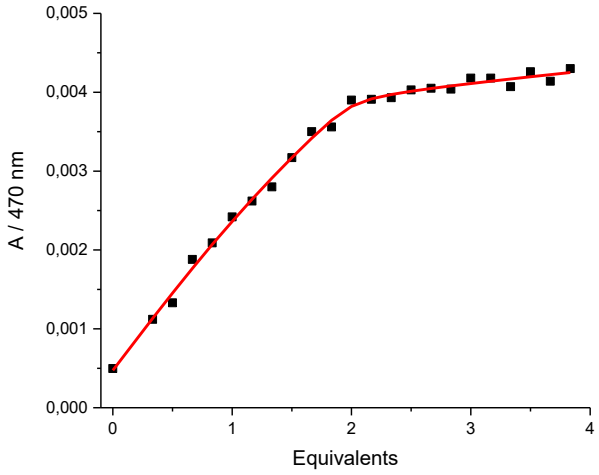

Figure 2.26 Binding isotherm (λ = 470 nm) for the complexation of **Cage-4** with **DOV**•2TsO. Black squares: experimental points; continuous red line: fitting.

From those results, it can be stated that both associations occur with a very high apparent binding constant ($\log\beta \geq 7$) in an indistinguishable way from each other. Finally, a kinetic experiment was performed using a stopped-flow apparatus to analyse the dynamics of the complexation process. **Cage-4** and **DOV•**2TsO were mixed in equimolar amounts in dichloromethane, and the consequent absorption changes were followed with time. The kinetic traces reached the plateau after 300 ms, suggesting that complexation is a fast process.

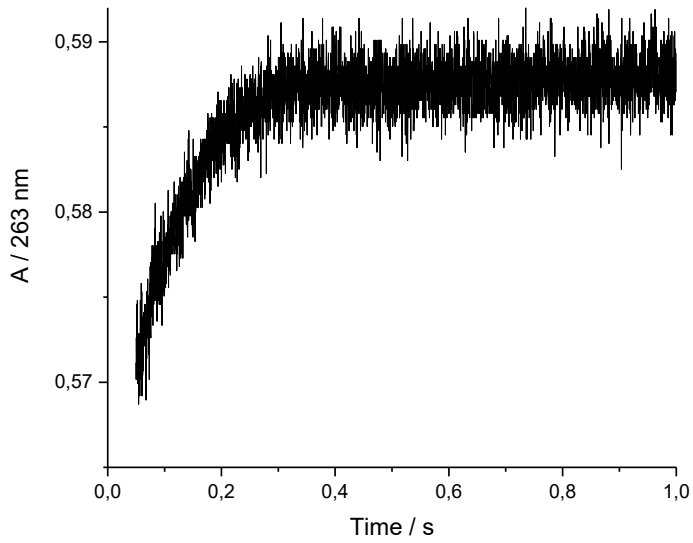

Figure 2.27 Absorption changes at 263 nm upon mixing equimolar amounts of **Cage-4** and **DOV•**2TsO.

Conclusions

In this chapter, the design, synthesis and characterisation of a series of head-to-head oriented bis-calix[6]arene cages have been reported. The synthetic strategy involved the template effect of a complexed bis viologen salt, which is able to preorganise the calix [6]arene macrocycles properly in the space before the

clipping reaction leading to the molecular cages. In the beginning, several calix[6]arene derivatives were afforded from the functionalisation of the upper rim with carboxylic acid, hydroxyl and aldehyde moieties. Then, the formation of [3]pseudorotaxanes deriving from the complexation of these calix[6]arenes and a series of bis-viologen salts bearing different spacer was demonstrated. In every case, only the head-to-head oriented [3]pseudorotaxane structure was obtained thanks to the unidirectional threading process of viologen salts in low-polarity solvents such as chloroform, dichloromethane, benzene or toluene. Successively, the reaction of these [3]pseudorotaxanes with proper difunctional linking units was tested. The best result was achieved in every case using axle $\mathbf{3}_{12}$, in which the two bis-viologen units are span by an alkyl chain spacer of 12 carbon atoms. Really noteworthy is the fact that the same reactions performed without the templating effect of the axle did not lead to the desired cage products. Only the synthesis of **Cage-3** was accomplished in comparable yields, either with or without the templating agent. This result can be accounted for by the reversible nature of the imine bonds assembled during the cage formation. In a second approach, **Cage-4** was synthesised from the direct reaction of triamino calix[6]arene derivative **TA** and a difunctional isocyanate linker. Also, this time, the effect of the templating axle was demonstrated. The proper length of the axle spacer was investigated as well. Moreover, complexation studies with dioctyl viologen salt demonstrated the ability of **Cage-4** to complex two molecules of DOV with high binding constants efficiently.

Acknowledgments

Thanks to Antonio Fiorentino (University of Bologna) for UV-Vis measurements.

Experimental Section

General Methods

All solvents were dried using standard procedures; all other reagents were of reagent-grade quality obtained from commercial suppliers and used without further purification. Melting points are uncorrected. NMR spectra were recorded at 400 MHz for ^{1}H and 100 MHz for ^{13}C. Chemical shifts are expressed in ppm (δ) using the residual solvent signal as an internal reference (7.26 ppm for $CHCl_3$, 7.16 ppm for C_6D_5H, 5.32 for $CHDCl_2$ and 3.31 ppm for CD_2HOD). The terms m, s, d, t and q represent multiplet, singlet, doublet, triplet and quadruplet, respectively; the term "br. s" means a broad signal. Mass spectra were recorded in the ESI mode. Compounds **1**,[36] **TA**,[33] $\mathbf{2}_8$,[37] $\mathbf{2}_{12}$,[38] $\mathbf{2}_{16}$ [39] and were synthesised according to published procedures.

Synthetic Procedure and Analytical Data

General procedure for the synthesis of the bis-viologen axles $\mathbf{3}_\mathbf{m}$. In a sealed 100 mL glass autoclave, a solution of pentylpyridyl pyridinium tosylate (**1**, 0.6 mmol) and ditosylate ($\mathbf{2}_\mathbf{m}$, 0.3 mmol) in dry acetonitrile (40 mL) was refluxed under vigorous stirring for 4 days. Afterwards, the solution was evaporated to dryness under reduced pressure.

$\mathbf{3}_8$: the solid residue of the evaporation was triturated with CH_3CN to afford 0.3 g of product $\mathbf{3}_6$ as a solid white powder (63%). **M. p.** = 161-163 °C; **^{1}H NMR** (CD_3OD, 400 MHz): δ = 9.25 (d, 8H, *J* = 6.8 Hz, $H_{\#}$ and $H_{¥}$), 8.65 (d, 8H, *J* = 6.6 Hz, $H_{\$}$ and $H_{§}$), 7.69 (d, 8H, *J* = 8.2 Hz, TsO), 7.24 (d, 8H, *J* = 7.9 Hz, TsO), 4.8-4.7 (m, 8H, H_α and H_5), 2.38 (s, 12H, C*H*$_3$, TsO), 2.1-2.0 (m, 8H, H_β and H_4), 1.5-1.4 (m, 16H, $H_{2\text{-}3}$ and $H_{\gamma\text{-}\delta}$), 0.98 (t, 6H, *J* = 6.8, H_1) ppm; **^{13}C NMR** (CD_3OD, 100 MHz): δ = 149.8, 145.6, 142.2, 140.3, 128.5, 126.9, 125.5, 61.9, 31.0, 30.9, 28.3, 27.9, 25.6, 21.8, 19.9, 12.7; **ESI-MS**(+): = m/z 1080.5 $[M\text{-}TsO]^+$.

3$_{12}$: the solid residue of the evaporation was triturated with CH_3CN to afford 0.32 g of product **3**$_{12}$ as a solid white powder (63%). **M. p.** = 164-166 °C; **^{1}H NMR** (CD_3OD, 400 MHz): δ = 9.25 (d, 8H, *J* = 6.6 Hz, $H_{\#}$ and $H_{¥}$), 8.65 (d, 8H, *J* = 6.5 Hz, $H_{\$}$ and $H_{§}$), 7.69 (d, 8H, *J* = 8.3 Hz, TsO), 7.24 (d, 8H, *J* = 8.0 Hz, TsO), 4.73 (t, 8H, *J* = 7.7 Hz, $H_α$ and H_5), 2.38 (s, 12H, C*H*$_3$, TsO), 2.1-2.0 (m, 8H, $H_β$ and H_4), 1.5-1.3 (m, 24H, $H_{2\text{-}3}$ and $H_{γ\text{-}ζ}$), 0.96 (t, 6H, *J* = 6.7 Hz, H_1) ppm; **^{13}C NMR** (CD_3OD, 100 MHz): δ = 149.8, 145.6, 142.2, 140.3, 128.5, 126.9, 125.5, 61.9, 31.2, 30.8, 29.2, 29.1, 28.8, 27.9, 25.9, 21.8, 19.9, 12.7; **ESI-MS**(+): = m/z 1136.5 $[M\text{-}TsO]^+$.

3$_{16}$: the solid residue of the evaporation was triturated with CH_3CN to afford 0.34 g of product **3**$_{16}$ as a solid white powder (65%). **M. p.** = 187-189 °C; **^{1}H NMR** (CD_3OD, 400 MHz): δ = 9.28 (d, 8H, *J* = 6.6 Hz, $H_{\#}$ and $H_{¥}$), 8.67 (d, 8H, *J* = 6.5 Hz, $H_{\$}$ and $H_{§}$), 7.71 (d, 8H, *J* = 8.3 Hz, TsO), 7.25 (d, 8H, *J* = 8.0 Hz, TsO), 4.75 (t, 8H, *J* = 7.7 Hz, $H_α$ and H_5), 2.39 (s, 12H, C*H*$_3$, TsO), 2.1-2.0 (m, 8H, $H_β$ and H_4), 1.5-1.3 (m, 32H, $H_{2\text{-}3}$ and $H_{γ\text{-}θ}$), 0.98 (t, 6H, *J* = 6.7 Hz, H_1) ppm; **^{13}C NMR** (CD_3OD, 100 MHz): δ = 149.8, 145.6, 142.2, 140.3, 128.5, 126.9, 125.5, 61.9, 31.2, 30.8, 29.7, 29.2, 29.1, 28.8, 28.3, 27.9, 25.9, 21.8, 19.9, 12.7; **ESI-MS**(+): = m/z 1192.5 $[M\text{-}TsO]^+$.

TPU-AC: under a nitrogen atmosphere, a solution of triphosgene (51.5 mg, 0.174 mmol, 1.1eq.) in toluene (30 mL) was poured into a 250 mL two-necked flask. A freshly prepared solution of triamino calix[6]arene **TA** (175 mg, 0.158 mmol, 1 eq.) and triethylamine (77 µL, 0.553 mmol, 3.5 eq.) in toluene (20 mL) was added to the reactor. The mixture was stirred at 80 °C for 3 hours. After cooling the reactor at room temperature, 4-aminophenylacetic acid (83.5 mg, 0.553 mmol, 3.5 eq.) was added, and the reaction was heated again at 80°C overnight. After completion of the reaction, the solvent was evaporated under reduced pressure. The crude product was purified by column chromatography (SiO_2, dichloromethane: methanol = 8:2 with 0.5% of acetic acid) to afford **TPU-AC** as yellow solid (0.212 g) in 82 % yield. **M. p.** = 197-199 °C; **^{1}H NMR** (CD_2Cl_2+CD_3OD (2 drops), 400 MHz): δ = 7.3, 6.9, 6.6 (3 br. s, 24H, Ar*H* and N*H*), 4.4 (br. s, 6H, H_{ax}),

4.1 (br. s, 6 H, H_d), 3.8 (br. s, 6H, H_e), 3.6 (br. s, 6H, H_f), 3.6-3.3 (m, 12H, H_c, H_{eq}), 2.9 (br. s, 9H, -OC*H*$_3$), 1,4-1.0 (m, 36H, H_i, H_g); **^{13}C NMR** (CD_2Cl_2+CD_3OD (2 drops), 100 MHz): δ = 154.4, 150.6, 146.6, 137.2, 135.5, 133.1, 129.7, 128.0, 119.6, 72.5, 68.9, 66.8, 60.5, 40.2, 34.1, 31.3, 30.6, 29.7, 15.0; **HR-MS** (ESI, Orbitrap LQ) calculated for $C_{96}H_{112}N_6O_{18}$: m/z (z = -2): 818.40220, 818.90388, 819.40556, 819.90724; found: 818.40125, 818.90277, 819.40424, 819.90594. Calculated for $C_{96}H_{113}N_6O_{18}$: m/z (z = -1): 1637.81168, 1638.81504, 1639.81839, 1640.82175; found: 1637.81168, 1638.81522, 1639.81729, 1640.81951. Calculated for $C_{96}H_{114}N_6O_{18}Cl$: m/z (z = -1): 1673.78726, 1674.79053, 1675.79046, 1676.79135, 1677.79319, 1678.79549; found: 1673.78503, 1674.78821, 1675.79053, 1676.78613, 1677.78882, 1678.78955.

TPU-OH: under a nitrogen atmosphere, **TPU-OTBS** (163 mg, 0.085 mmol, 1 eq.) was suspended in 10 mL of a mixture of acetone: H_2O 95:5, then $CuCl_2$ (40 mg, 0.3 mmol, 3.5 eq.) was added. The solution was stirred at room temperature for 2 hours. After completion of the reaction, the solvent was evaporated under reduced pressure. The crude product was purified by column chromatography (SiO_2, hexane: ethyl acetate = 50:50 + 10% MeOH), affording **TPU-OH** (80 mg) as a yellow solid in 60 % yield. **M. p.** = 146-148 °C; **^{1}H NMR** (CD_3CN, 400 MHz): δ = 7.3, 7.13, 7.08, 6.9, 6.5 (5 br. s, 30H, Ar*H* and N*H*), 4.4 (d, 6H, H_c, *J* = 5.2 Hz), 3.9 (br. s, 6 H, H_d), 3.7 (br. s, 6H, H_e), 3.6 (br. s, 6H, H_f), 3.2 (br. s, 9H, -OC*H*$_3$), 3.0 (t, 3H, H_j, *J* = 5.8 Hz), 1.3 (s, 27H, H_i), 1.2 (t, 9H, H_g, *J* = 7 Hz); **^{13}C NMR** (CD_3CN,100 MHz): δ = 155.8, 154.8, 151.8, 147.6, 139.3, 137.3, 136.4, 135.1, 134.2, 128.7, 128.3, 121.4, 120.4, 73.5, 70.8, 67.3, 64.6, 61.1, 35.0, 31.9, 31.7, 15.7; **HR-MS** (MALDI) calculated for $C_{93}H_{114}N_6O_{15}Na$: m/z (z = 1): 1577.48471; found: 1577.48420. Calculated for $C_{93}H_{114}N_6O_{15}K$: m/z (z = 1): 1593.471012; found: 1593.47028.

TPU-AL: under a nitrogen atmosphere, **TPU-OH** (50.5 mg, 0.032 mmol, 1 eq.) was suspended in 4 mL of dichloromethane, then Dess-Martin periodinane (41 mg,

0.097 mmol, 3 eq.) was added. The solution was stirred at room temperature overnight. After completion of the reaction, the solvent was evaporated under reduced pressure. The crude product was purified by column chromatography (SiO_2, hexane: ethyl acetate = 50:50 + 2% MeOH), affording **TPU-AL** (26.7 mg) as a white solid in 53 % yield. **M. p.** = 137-139 °C; **^{1}H NMR** ($CDCl_3$, 400 MHz): δ = 9.8 (br. S, 3H, H_c), 7.6, 7.2, 6.3 (3 br. s, 30H, Ar*H* and N*H*), 4.4 (br. s, 6H, H_{ax}), 4.1 (br. s, 6 H, H_d), 3.9 (br. s, 6H, H_e), 3.7 (br. s, 12H, H_{eq} and H_f), 3.1 (br. s, 9H, -OC*H*$_3$), 1.5-0.9 (m, 36H, H_i and H_g); **^{13}C NMR** ($CDCl_3$,100 MHz): δ =190.8, 131.1, 118.4, 69.8, 66.8, 31.4, 29.6, 15.2; **HR-MS** (ORBITRAP LQ) calculated for $C_{93}H_{109}N_6O_{15}$: m/z (z = 1): 1549.79454, 1550.79780, 1551.80094, 1552.80398, 1553.80696; found: 1549.79250, 1550.79839, 1551.80155, 1552.80374, 1553.80643. Calculated for $C_{93}H_{112}N_7O_{15}$: m/z (z = 1): 1566.82109, 1567.82433, 1568.82745, 1569.83048, 1570.83344; found: 1566.82178, 1567.82479, 1568.82838, 1569.83272.

Cage-1: a suspension of bis-viologen axle **3**$_m$ (20 mg, 0.015 mmol, 1 eq.) and **TPU-AC** (50 mg, 0.03 mmol, 2 eq.) in dichloromethane (10 mL) was stirred at room temperature until it turned homogeneous and deeply red-coloured (2 hrs). Triethylamine (21 µL, 0.15 mmol, 10 eq.) and 2-chloro-1-methylpyridinium iodide (23 mg, 0.09 mmol, 6 eq.) were then added in this order. After stirring at room temperature for 1 hour, a solution of 1,4-benzenedimethanol (6.3 mg, 0.045 mmol, 3 eq.) in dichloromethane (5 mL) was added dropwise to the reaction for two hours. The reaction mixture was stirred at room temperature overnight. After that, the solvent was evaporated to dryness under reduced pressure. The resulting red solid residue was purified by column chromatography (SiO_2, CH_2Cl_2:CH_3OH = 95:5), affording **Cage-1** (5.8 mg) as a white solid in 11 % yield. **M. p.** = 178-180 °C; **^{1}H NMR** (CD_2Cl_2, 400 MHz): δ = 7.3, 7.23, 7.18, 7.1, 7.0, 6.3 (6 br. s, 72H, N*H* and Ar*H*), 5.1 (m, 12H, H_j), 4.4 (br. s, 12H, H_{ax}), 4.1 (br. s, 12H, H_d), 3.84 (m, 12H, H_e), 3.7-3.3 (m, 36H, H_f, H_c and H_{eq}), 3.1-2.6 (br. s, 18H, -OC*H*$_3$), 1.3 (s, 54H, H_i), 1.3-1.1 (m, 18H, H_g); **^{13}C NMR** (CD_2Cl_2, 100 MHz): δ = 129.8, 129.6, 128.2, 72.5, 69.9, 66.7, 66.0, 65.8, 31.3, 15.1; **HR-MS** (ESI, Orbitrap LQ) calculated for

$C_{216}H_{248}N_{12}O_{36}$: m/z (z = 2):1792.89666, 1793.39834, 1793.90002, 1794.40169, 1794.90337, 1795.40505, 1795.90673; found: 1792.90150, 1793.40110, 1793.90439, 1794.40423, 1794.90896, 1795.40719, 1795.92097.

Cage-2: a suspension of bis-viologen axle $\mathbf{3}_m$ (40 mg, 0.03 mmol, 1 eq.) and **TPU-OH** (95 mg, 0.06 mmol, 2 eq.) in dichloromethane (20 mL) was stirred at room temperature until it turned homogeneous and deeply red-coloured (2 hrs). After stirring at room temperature for 2 hours, a solution of terephthaloyl chloride (18.5 mg, 0.09 mmol, 3 eq.) in dichloromethane (10 mL) was added dropwise to the reaction in two hours. The reaction mixture was stirred at room temperature overnight. After that, the solvent was evaporated to dryness under reduced pressure. The resulting red solid residue was purified by column chromatography (SiO_2, CH_2Cl_2:CH_3OH = 95:5), affording **Cage-2** (15 mg) as a white solid in 14 % yield. **M. p.** = 175-177 °C; **^{1}H NMR** (CD_2Cl_2, 400 MHz): δ = 8.0, 7.3, 7.2, 7.1, 6.4 (5 br. s, 72H, N*H* and Ar*H*), 5.1 (m, 12H, H_c), 4.4 (br. s, 12H, H_{ax}), 4.1 (br. s, 12H, H_d), 3.9 (m, 12H, H_e), 3.7 (m, 24H, H_f and H_{eq}), 3.1 (br. s, 18H, -OCH_3), 1.6-1.0 (m, 72H, H_i and H_g); **^{13}C NMR** (CD_2Cl_2, 100 MHz): δ =165.2, 133.9, 129.4, 127.7, 72.6, 69.8, 66.7, 34.1, 31.3, 29.7, 15.1; **HR-MS** (ESI, Orbitrap LQ) calculated for $C_{210}H_{235}N_{12}O_{36}$: m/z (z = 1): 3500.69215, 3501.69550, 3502.69886, 3503.70221, 3504.70557, 3505.70892; found: 3500.69150, 3501.70405, 3502.70589, 3503.71202, 3504.70312, 3505.73003. Calculated for $C_{210}H_{236}N_{12}O_{36}$: m/z (z = 2): 1750.84971, 1751.35139, 1751.85307, 1752.35474, 1752.85642; found: 1751.35289, 1751.85463, 1752.85700.

Cage-3: a suspension of bis-viologen axle $\mathbf{3}_m$ (40 mg, 0.03 mmol, 1 eq.) and **TPU-AL** (95 mg, 0.06 mmol, 2 eq.) in dichloromethane (20 mL) was stirred at room temperature until it turned homogeneous and deeply red-coloured (2 hrs). After stirring at room temperature for 2 hours, a solution of *p*-phenylenediamine (9.7 mg, 0.09 mmol, 3 eq.) in dichloromethane (10 mL) was added dropwise to the reaction in two hours. The reaction mixture was stirred at room temperature

overnight. After that, the solvent was evaporated to dryness under reduced pressure. The resulting red solid residue was purified by column chromatography (SiO_2, CH_2Cl_2:CH_3OH = 95:5), affording **Cage-3** (47 mg) as a brown solid in 51 % yield. **M. p.** = 145-147 °C; **^{1}H NMR** (CD_2Cl_2, 400 MHz): δ = 8.3 (br. s, 6H, H_c), 87.9, 7.5, 7.2, 7.1, 6.6 (5 br. s, 72H, N*H* and Ar*H*), 4.4 (br. s, 12H, H_{ax}), 4.1 (br. s, 12H, H_d), 3.9 (m, 12H, H_e), 3.7 (m, 24H, H_f and H_{eq}), 3.1 (br. s, 18H, -OCH_3), 1.6-1.0 (m, 72H, H_i and H_g); **^{13}C NMR** (CD_2Cl_2, 100 MHz): δ = 156.3, 129.5, 127.5, 122.3, 122.0, 115.6, 72.5, 69.9, 66.9, 31.5, 31.0, 15.3; **HR-MS** (ESI, Orbitrap LQ) calculated for $C_{204}H_{230}N_{18}O_{24}$: m/z (z = 2): 1657.86597, 1658.36765, 1658.86933, 1659.37100, 1659.87268, 1660.37436, 1660.87604; found: 1657.86264, 1658.36471, 1658.86598, 1659.36745, 1659.86885, 1660.37077, 1660.87183.

Cage-4: under a nitrogen atmosphere, a suspension of bis-viologen axle **3**$_m$ (72 mg, 0.055 mmol, 1 eq.) and **TA** (122 mg, 0.11 mmol, 2 eq.) in dichloromethane (40 mL) was stirred at room temperature. Then, a solution of 4,4'-methylene diphenyl diisocyanate (41.5 mg, 0.165 mmol, 3 eq.) in dichloromethane (15 mL) was added dropwise to the reaction in two hours. The reaction mixture was stirred at room temperature overnight. After that, the solvent was evaporated to dryness under reduced pressure. The resulting red solid residue was purified by column chromatography (SiO_2, CH_2Cl_2:CH_3OH = 95:5), affording **Cage-4** (25 mg) as a white solid in 15 % yield. **M. p.** = decomposition at 300 °C; **^{1}H NMR** (CD_2Cl_2, 400 MHz): δ = 7.3, 7.0, 6.9, 6.2 (4 br. s, 60H, N*H* and Ar*H*), 4.4 (br. s, 12H, H_{ax}), 4.1 (br. s, 12H, H_d), 3.9 (m, 12H, H_e), 3.7 (m, 30H, H_c, H_f and H_{eq}), 2.9 (br. s, 18H, -OCH_3), 1.5-1.1 (m, 72H, H_i and H_g); **^{13}C NMR** (CD_2Cl_2, 100 MHz): δ = 152.7, 147.1, 136.1, 132.9, 129.0, 128.0, 121.9, 73.0, 70.3, 67.1, 40.7, 34.5, 31.7, 31.4, 15.5; **HR-MS** (ESI, Orbitrap LQ) calculated for $C_{183}H_{217}N_{12}O_{24}$: m/z (z = 2): 1483.80980, 1484.31148, 1485.31483, 1485.81651, 1486.31819, 1486.81986; found: 1483.80750, 1484.31119, 1484.81340, 1485.31514, 1486.31660. Calculated for $C_{183}H_{216}N_{12}O_{24}Na$: m/z (z = 2): 1494.80077, 1495.30245, 1496.30580, 1496.80748, 1497.30916; found: 1495.30262, 1496.30561.

References

[1] J. W. Steed, J. L. Atwood, *Supramolecular Chemistry*, John Wiley & Sons, **2022**.

[2] M. A. Little, A. I. Cooper, *Advanced Functional Materials* **2020**, *30*, 1909842.

[3] A. Galan, P. Ballester, *Chemical Society Reviews* **2016**, *45*, 1720–1737.

[4] Y. Yu, J.-M. Yang, J. Rebek, *Chem* **2020**, *6*, 1265–1274.

[5] A. Pappalardo, R. Puglisi, G. Trusso Sfrazzetto, *Catalysts* **2019**, *9*, 630.

[6] G. Zhang, M. Mastalerz, *Chemical Society Reviews* **2014**, *43*, 1934–1947.

[7] W. Liu, J. F. Stoddart, *Chem* **2021**, *7*, 919–947.

[8] D. J. Cram, S. Karbach, Y. H. Kim, L. Baczynskyj, G. W. Kallemeyn, *J. Am. Chem. Soc.* **1985**, *107*, 2575–2576.

[9] J. C. Sherman, D. J. Cram, *J. Am. Chem. Soc.* **1989**, *111*, 4527–4528.

[10] M. M. Conn, J. Rebek, *Chem. Rev.* **1997**, *97*, 1647–1668.

[11] F. Hof, J. Rebek, *Proceedings of the National Academy of Sciences* **2002**, *99*, 4775–4777.

[12] J. Rebek Jr., *Angewandte Chemie International Edition* **2005**, *44*, 2068–2078.

[13] B. H. Northrop, F. Aricó, N. Tangchiavang, J. D. Badjić, J. F. Stoddart, *Org. Lett.* **2006**, *8*, 3899–3902.

[14] D. Beaudoin, F. Rominger, M. Mastalerz, *Angewandte Chemie International Edition* **2016**, *55*, 15599–15603.

[15] N. Nishimura, K. Kobayashi, *Angewandte Chemie International Edition* **2008**, *47*, 6255–6258.

[16] L. C. Palmer, J. Julius Rebek, *Org. Biomol. Chem.* **2004**, *2*, 3051–3059.

[17] K. Kobayashi, M. Yamanaka, *Chemical Society Reviews* **2015**, *44*, 449–466.

[18] C. D. Meyer, C. S. Joiner, J. F. Stoddart, *Chem. Soc. Rev.* **2007**, *36*, 1705–1723.

[19] M. Matache, E. Bogdan, N. D. Hădade, *Chemistry – A European Journal* **2014**, *20*, 2106–2131.

[20] A. Pun, D. A. Hanifi, G. Kiel, E. O'Brien, Y. Liu, *Angewandte Chemie International Edition* **2012**, *51*, 13119–13122.

[21] K. G. Andrews, K. E. Christensen, *Chemistry – A European Journal* **n.d.**, *n/a*, DOI 10.1002/chem.202300063.

[22] D. Chakraborty, P. Sarathi Mukherjee, *Chemical Communications* **2022**, *58*, 5558–5573.

[23] V. Martí-Centelles, *Tetrahedron Letters* **2022**, *93*, 153676.

[24] M. Mastalerz, *Angewandte Chemie International Edition* **2010**, *49*, 5042–5053.

[25] M. E. Belowich, J. Fraser Stoddart, *Chemical Society Reviews* **2012**, *41*, 2003–2024.

[26] A. Asadi, D. Ajami, J. Rebek, *Chemical Communications* **2014**, *50*, 533–535.

[27] T. H. G. Schick, F. Rominger, M. Mastalerz, *J. Org. Chem.* **2020**, *85*, 13757–13771.

[28] A. Galán, E. C. Escudero-Adán, P. Ballester, *Chemical Science* **2017**, *8*, 7746–7750.

[29] S. Le Gac, X. Zeng, O. Reinaud, I. Jabin, *J. Org. Chem.* **2005**, *70*, 1204–1210.

[30] S. Moerkerke, M. Ménand, I. Jabin, *Chemistry – A European Journal* **2010**, *16*, 11712–11719.

[31] A. Arduini, R. Ferdani, A. Pochini, A. Secchi, *Tetrahedron* **2000**, *56*, 8573–8577.

[32] F. Cester Bonati, M. Bazzoni, C. Baccini, V. Zanichelli, G. Orlandini, A. Arduini, G. Cera, A. Secchi, *Molecules* **2023**, *28*, 595.

[33] A. Arduini, A. Credi, G. Faimani, C. Massera, A. Pochini, A. Secchi, M. Semeraro, S. Silvi, F. Ugozzoli, *Chemistry – A European Journal* **2008**, *14*, 98–106.

[34] G. Cera, A. Arduini, A. Secchi, A. Credi, S. Silvi, *The Chemical Record* **2021**, *21*, 1161–1181.

[35] A. Credi, S. Dumas, S. Silvi, M. Venturi, A. Arduini, A. Pochini, A. Secchi, *J. Org. Chem.* **2004**, *69*, 5881–5887.

[36] A. Boccia, V. Lanzilotto, R. Zanoni, L. Pescatori, A. Arduini, A. Secchi, *Physical Chemistry Chemical Physics* **2011**, *13*, 4444–4451.

[37] T. B. Nguyen, A.-S. Castanet, T.-H. Nguyen, K. P. P. Nguyen, J.-F. Bardeau, A. Gibaud, J. Mortier, *Tetrahedron* **2006**, *62*, 647–651.

[38] A. Arduini, R. Bussolati, A. Credi, G. Faimani, S. Garaudée, A. Pochini, A. Secchi, M. Semeraro, S. Silvi, M. Venturi, *Chemistry – A European Journal* **2009**, *15*, 3230–3242.

[39] I. Merino, J. D. Thompson, C. B. Millard, J. J. Schmidt, Y.-P. Pang, *Bioorganic & Medicinal Chemistry* **2006**, *14*, 3583–3591.

Chapter 3. Orientational Threading of Stilbazolium Axles in a Non-palindrome Calix[6]arene Wheel

Introduction

Organic semiconductor-based lasers have attracted considerable interest in the last decades since they allow the femtosecond pulse generation, the broadband optical amplification and tuning of the lasing frequency.[1,2] Their principal limitation is the so-called aggregation-caused quenching (ACQ) effect that reduces their effectiveness as a gain media. To overcome the ACQ effect, organic solid-state lasers are currently based on encapsulating the dye molecules into a solid matrix that can keep them spatially separated.[1,3] Macrocyclic hosts can play a crucial role in this field thanks to their ability to encapsulate complementary guest molecules.[3] The guest encapsulation prevents self-aggregation phenomena and drastically changes the environment of the dye molecules, thus inevitably affecting their optical properties. Organic dyes encapsulation has been documented for several macrocyclic hosts such as cyclodextrins, calix[n]arenes and cucurbiturils.[3–6] Yet, the possibility of tuning the optical properties of an organic dye as a function of its geometrical arrangement inside the host cavity has been relatively less explored. Indeed, this represents a somewhat difficult task since it requires hollow macrocycles endowed with different functionalities on their cavity accesses.[7] Stilbazolium salts are "push-pull" organic dyes belonging to the class of cation styryl cyanines.[8] Their structure is constituted by an electron-poor *N*-alkylated pyridinium ring conjugated *via* a double bond with an electron-rich *para*-substituted aromatic ring. They have been widely studied thanks to their two-photon absorption in the near IR range (NIR),[9] as fluorescent sensors[10] and non-linear optical materials.[11] They represent suitable candidates to expand micro/nano lasers' capabilities and performances.[12] However, their optical properties are influenced by the abovementioned ACQ effect and other

non-radiative relaxation pathways. Photoisomerization *E-Z* of the double bond[13,14] is one of them, together with the internal conversion (IC) of one aromatic ring. This latter event occurs from the twisted intramolecular charged transfer (TICT) state.[15] The grade of these states' population is related to the environmental features, such as polarity and viscosity, which thus highly influence the stilbazolium properties.

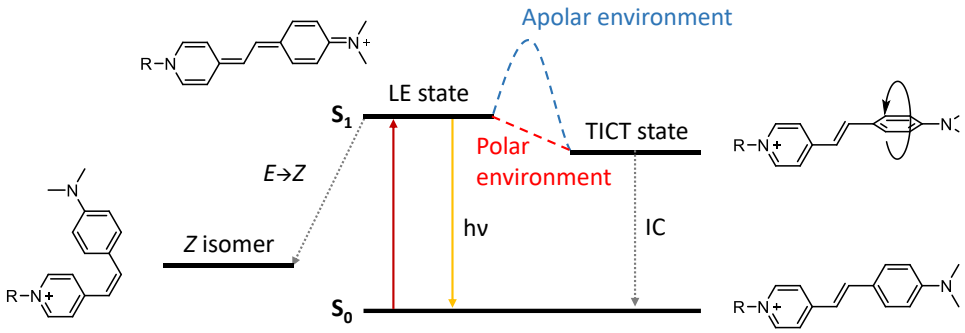

Figure 3.1 Deactivation pathways of excited stilbazolium structure (simplified energy diagram).

The peculiar non-symmetric structure of stilbazolium dyes fits particularly well with the hollow structure of the calix[6]arene host **TPU** depicted in Scheme 3.1. Host **TPU** is a non-palindrome heteroditopic receptor that can complex organic ion pairs in weakly polar solvents by interacting simultaneously with organic salts' cationic/anionic counterparts, as we have extensively verified with viologen-based guests.[16] In a recent communication,[17] we showed the ability of **TPU** to encapsulate a stilbazolium-based dye to give rise to a pair of orientational [2]pseudorotaxane isomers whose optical properties, notably the emission intensity and wavelength, were dependent on the relative orientation of the encapsulated dye inside the calix[6]arene cavity (Scheme 3.1).

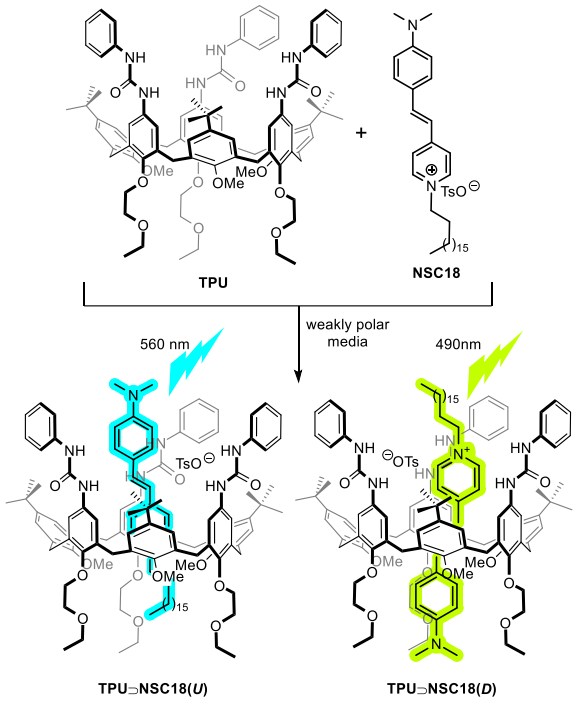

Scheme 3.1 [2]Pseudorotaxane orientational isomers **TPU⊃NSC18(*U*)** and **TPU⊃NSC18(*D*)** and orientational-dependent emission wavelength of the encapsulated stilbazolium dye **NSC18** inside the cavity of the non-palindrome heteroditopic calix[6]arene wheel **TPU**. The letter between brackets (***U*** and ***D***) defines the relative position of the dye dimethylamino group to the calix[6]arene phenylurea units.

Herein, we present our results to understand the critical factors affecting the formation of pseudorotaxane orientational isomers from **TPU** and a series of mono and bis-stilbazolium-based dyes. The results demonstrated that the orientation of stilbazolium dye inside the calix[6]arene cavity is affected by the length and bulkiness of the substituents present on the different chromophore aromatic moieties. In addition, the temperature also significantly affects the relative abundance of the orientational isomers in solution. Therefore, NMR spectroscopy was used to assess the relative abundance of the orientational isomers at different temperatures. Instead, UV-Vis titrations were used to investigate the apparent association constants of the encapsulated dye molecules.

Results and discussion

To study how the nature of the substituents present in the stilbazolium salts can affect the geometry of the dye encapsulation in the [2]pseudorotaxane complexes with **TPU**, a small library of stilbazolium salts differing for the length of the alkyl chain appended to the pyridinium ring (**NSCn**, with n = 1, 5 and 18), was initially synthesised by reacting the known styryl pyridine **NS** with the proper alkyl tosylates in refluxing acetonitrile (see Scheme 3.2).

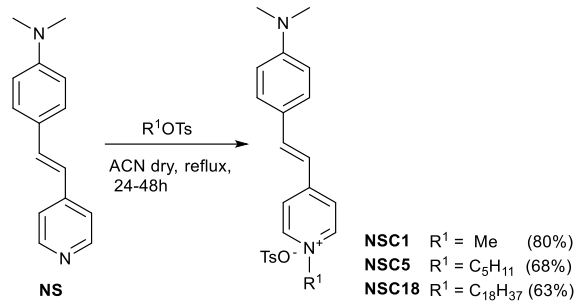

Scheme 3.2 Synthesis of axles **NSCn**.

NSC1, **NSC5** and **NSC18** were obtained as red solids compounds in 80%, 68% and 63% yield, respectively. They were characterised through NMR spectroscopy and ESI-MS measurements. ^{1}H NMR spectra of these compounds are characterised by the signals from the pyridinium part at 8.55 and 7.99 ppm (protons *6* and *5*); the double bond resonates at 7.86 and 7.10 ppm, while the electron-rich aromatic unit gives rise to two peaks at 7.62 and 7.23 ppm. A singlet, which integrates for six protons at 3.08 ppm, corresponds to the methyl groups of the dimethylamino moiety. Tosylate counterion resonates as two doublets at 7.72 and 6.80 ppm (aromatic protons) and as a singlet at 2.38 ppm, relative to the methyl group. Each stilbazolium salt is characterised by a different alkyl chain as assigned in Figure 3.2.

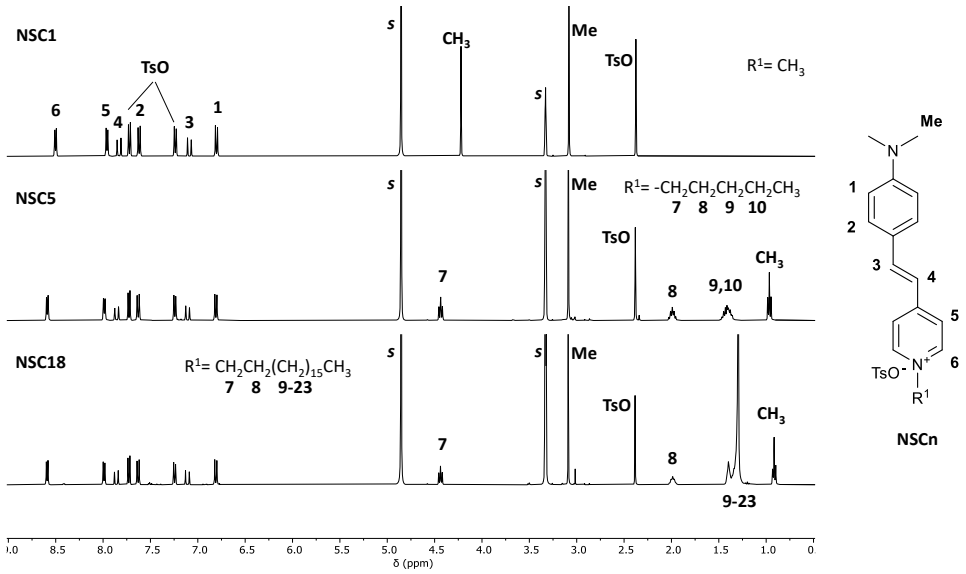

Figure 3.2 ^{1}H NMR spectra of stilbazolium **NSC1**, **NSC5** and **NSC18** (methanol-d4, 400MHz).

The choice to vary the length and bulkiness of the alkyl chain on the dye pyridinium ring was dictated by the observation that, because of their inherent asymmetry, and unlike the viologen salts,[16] stilbazolium salts can be encapsulated in the cavity of **TPU** by assuming two different geometrical arrangements. In the first one, the dye π-poor pyridinium ring is engulfed in the π-rich calix[6]arene cavity while the *p*-substituted aromatic ring is surrounded by the host phenylurea units (***U*** isomer, see Scheme 3.3). As a result, the pseudorotaxane is stabilised by a host/guest charge transfer interaction, as seen with viologen salts, whereas the H-bonding of the host phenylureas separates the dye ion-pairing.[18]

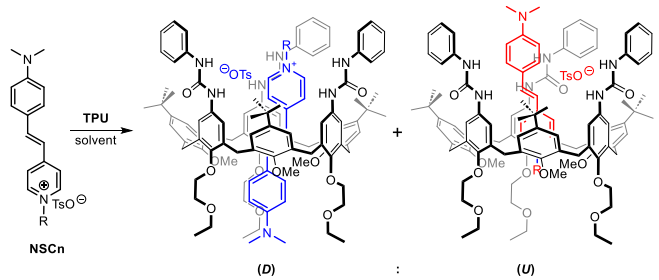

Scheme 3.3 Formation of orientational pseudorotaxane isomers ***D*** and ***U***.

In the reverse arrangement (***D*** isomer), the dye ion-pairing is only loosened by **TPU**. In fact, the pyridinium ring is kept faced to the phenylurea groups at the macrocycle wider rim. Most importantly, because of the different supramolecular interactions, the dye presents a peculiar charge distribution that accounts for the characteristic emission properties of each orientational isomer (see next chapter). Still, the interacting species' structural asymmetry also influences the pseudorotaxane formation mechanism. In principle, the two orientational isomers described in Scheme 3.3 can be formed through four different axle/wheel threading processes, i.e., with the dye alkyl chain through the calixarene wider (⇒ ***U***) and narrow rim (⇒ ***D***), respectively, or vice versa with the dye dimethylamino group through the macrocycle narrow (⇒ ***U***) and wider rim (⇒ ***D***), respectively. It is easily foreseen that whether a preferential threading mechanism can be forced by changing the nature of the dye substituents, then also the properties can be modulated at will.

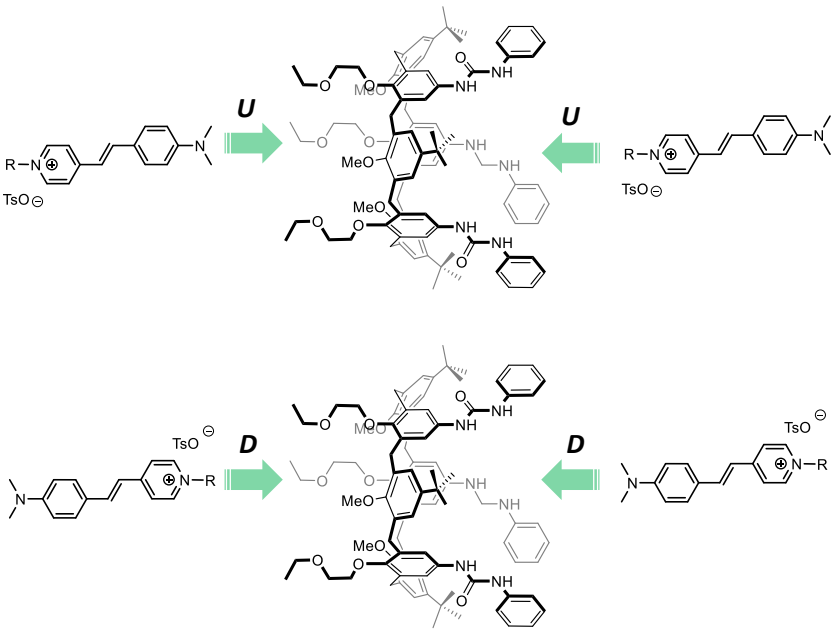

Figure 3.3 Pseudorotaxane threading processes of **NSCn** and **TPU**.

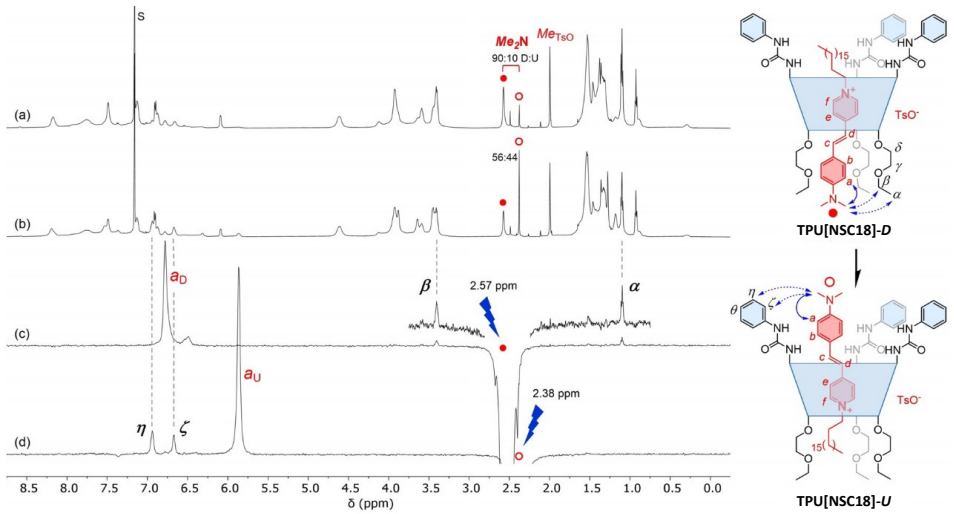

Figure 3.4 Stack plot of ^{1}H NMR spectra (C_6D_6,600 MHz) of a 1:1 mixture of **TPU** and **NSC18** recorded (a) upon sample preparation, (b) at the equilibrium; 1D ROESY spectra (mixing time 200 ms) recorded at equilibrium with selective irradiation of the Me_2N resonance at (c) 2.57 ppm and (d) 2.38 ppm. Adapted from ref. 17, copyright © 2020 Wiley-VCH Verlag GmbH & Co. KGaA, Weinheim.

The effect of the length of the alkyl chains was initially studied by recording ^{1}H NMR spectra of stilbazolium salt **NSC1**, **NSC5** and **NSC18** in their 1:1 mixtures with **TPU**. The spectra were taken in deuterated benzene at different temperatures (288, 298 and 333 K). Deuterated benzene was chosen for the following reasons: its relatively high boiling point allows us to explore the system at increasing temperatures than, i.e., chloroform. In addition, its low polarity prevents the dissolution of the stilbazolium axle when it is not complexed, thus leading to a more specific NMR outcome considering that only the 1:1 host–guest adduct should be present in the solution. Our previous studies[17] show that in this solvent, the dimethylamino group of **NSC18** resonates at 2.57 ppm in the ***D*** isomer and is upfield-shifted at 2.38 ppm in the ***U*** isomer (slow-exchange conditions). This was demonstrated by 1D ROESY measurements, in which the correlation between dimethylamino groups is visible with etoxhyethyl chains in the ***D*** isomer, and on the other hand, with phenylureas in the ***U*** isomer (see Figure 3.4). So, these peaks, whose chemical shift is not substantially affected by the

substituent R on the stilbazolium pyridinium ring, were used to investigate the isomer abundance in our systems.

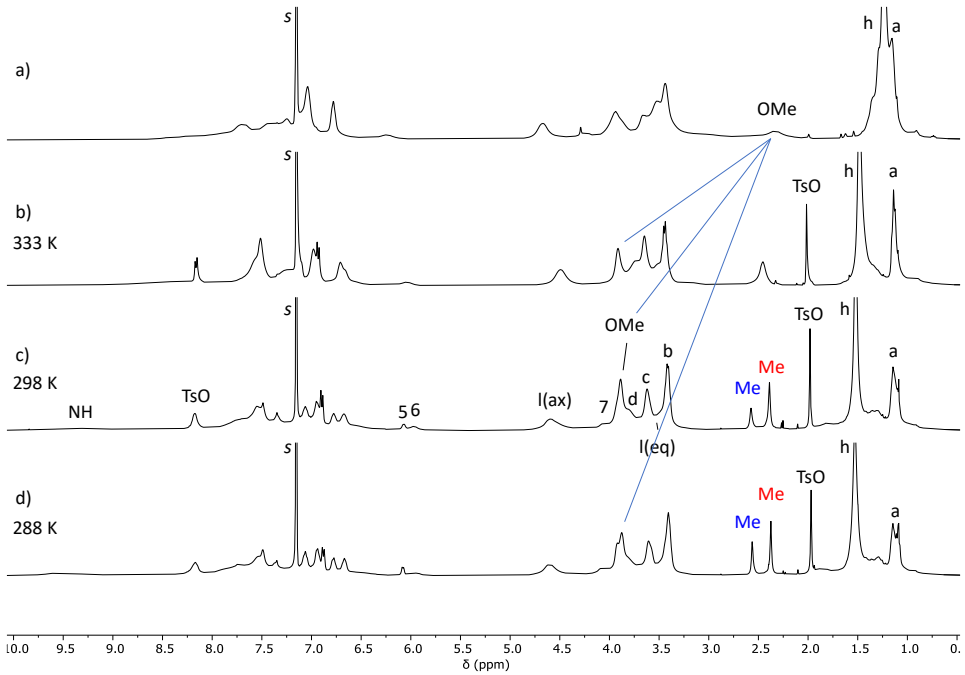

Figure 3.5 [1] H NMR stack plot of (a) **TPU**, (b) 1:1 mixture of **TPU** and **NSC5** recorded (b) at 333 K, (c) at 298 K and (d) at 288 K (C_6D_6, 400 MHz).

The first evidence of the salts' complexation upon mixing with **TPU** was their dissolution since, as stated before, they would be insoluble in this solvent at the 20 mmol concentration used in these experiments. However, the subsequent analysis of the NMR experiments gave us more insight into the complexes' formation. For example, the ^{1}H NMR spectra measured for the 1:1 mixture of **NSC5** with **TPU** at three different temperatures are gathered in Figure 3.5 and compared with the spectrum of the free **TPU**. Evidence of the complexation is diverse: the fluxionality of **TPU** in C_6D_6 appreciably decreases, and the peaks appear sharper when involved in the complexation; the methoxy protons (O*Me*) of the calix[6]arene are significantly downfield shifted from 2.3 ppm (in spectrum *a*) to 3.88 ppm (see continuous blue lines), witnessing the axle threading within the macrocycle cavity. Pyridinium protons resonate at very low ppm (proton *5* at

6.07 ppm and proton *6* at 5.96 ppm), as they are significantly shielded by the calix[6]arene scaffold. Two different peaks from the diagnostic dimethylamino moiety (labelled *Me* in Figure 3.5) were detected when the spectrum was recorded at 288 and 298 K (spectra *c* and *d*). The one that resonates at 2.37 ppm corresponds to the ***U*** isomer (in red), while the other at 2.56 ppm is relative to the ***D*** isomer (in blue). The integration of these two peaks reveals that the ratio of the two orientational isomers (***D***:***U***) does not change appreciably by lowering the temperature: 38:62 at 298 K (spectrum *c*) and 43:57 at 288 K (spectrum *d*), and the ***U*** isomer remains the more abundant in solution. At 333 K (spectrum *b*), coalescence is observed. From the above data (T_c = 333 K, $\delta\nu = |\delta_{Me}(\boldsymbol{D}) - \delta_{Me}(\boldsymbol{U})|$ = 77 Hz, and R = 8.31 J/K), it was possible to calculate, approximatively, the energy barrier for the ***U*** and ***D*** isomers interconversion from the Eyring equation.[19] The calculated $\Delta G^{\ddagger}$ was ca. 67 KJ/mol. From these results, it can be stated that **TPU** can efficiently complex **NSC5**. In addition, the "up" orientation is the favoured, and its relative amount increases with the temperature. An identical analysis was carried out for stilbazolium **NCS1**, endowed with the shorter alkyl chain ($R^1 = CH_3$), and **NSC18** bearing the longest alkyl chain of 18 carbon atoms. The ***D***/***U*** ratio was calculated by integrating the peaks corresponding to the dimethylamino group (*Me*), and the collected data were reposted in Table 3.1.

For **NSC1**, at room temperature, a singlet at 2.42 ppm for the diagnostic dimethylamino protons (*Me*) was the unique signal observed. This single signal may be due to a) the exclusive formation of one isomer or b) to fast-exchange conditions between the two orientational isomers (the free **NSC1** salt is not appreciably soluble in this solvent). The temperature range that can be exploited for NMR VT experiments is known to be narrow (ca. 280 to 343 K).

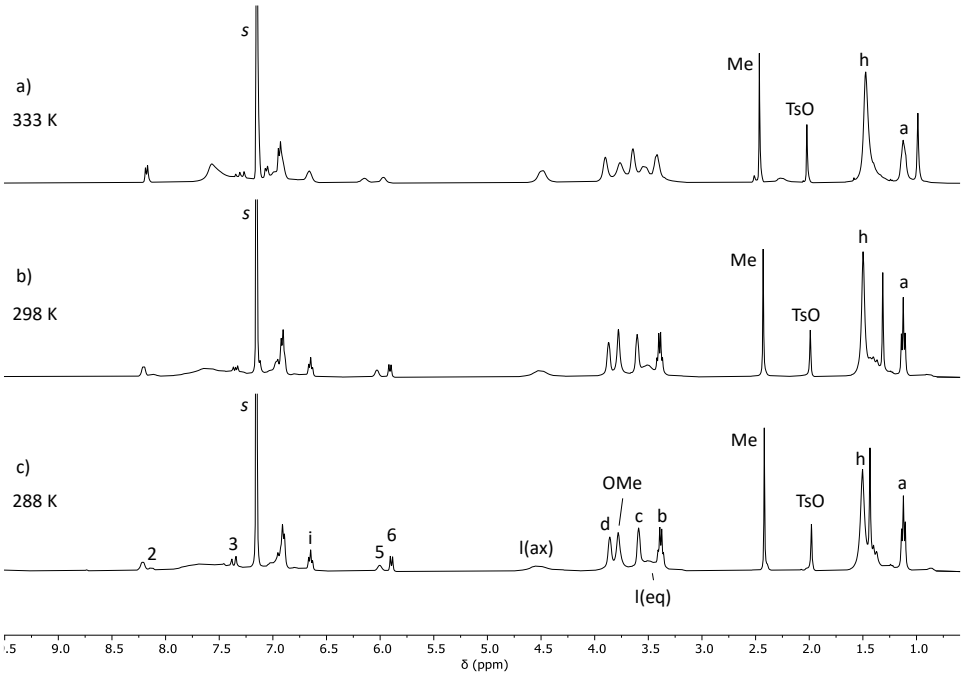

Figure 3.6 VT ^{1}H NMR stack plot of 1:1 mixture of **TPU** and **NSC1** recorded at (a) 333 K, (b) at 298 K and (c) at 288 K (C_6D_6, 400 MHz).

As a matter of fact, we neither observed a split of the signal by lowering the temperature down to 288 K nor a noticeable shift by increasing the temperature up to 333 K. This means that we never observed coalescence in this solvent (Figure 3.6). However, since this signal at RT has a chemical shift (2.42 ppm) very close to that of ***U*** in **NSC18** (2.38) and **NSC5** (2.37), we hypothesised the exclusive formation of this orientational isomer. A 1D ROESY experiment was thus carried out to identify which isomer was present in solution. A clear spatial correlation was detected between protons of the axle dimethylamino group (*Me*) and protons *i* and *j* of the phenylureas at the wheel's upper rim (pale blue dashed lines in Figure 3.7). This finding was a clear indication of the exclusive formation of orientational isomer ***U*** as previously hypothesised.

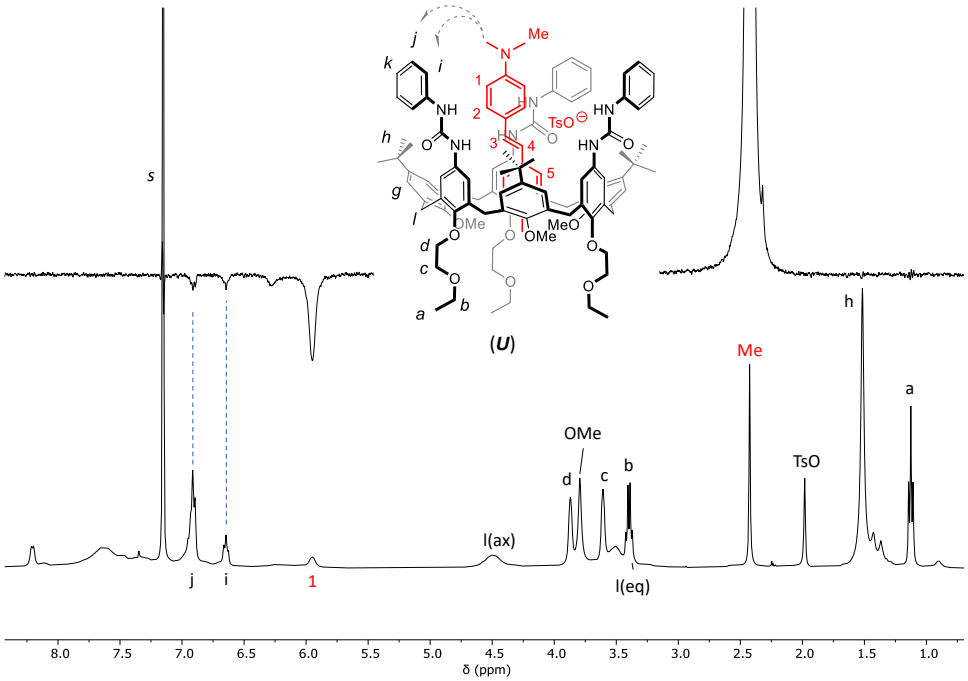

Figure 3.7 Stack plot of (top) 1D ROESY (Spin-lock = 200 ms) and (bottom) ^{1}H NMR of the 1:1 mixture of **TPU** and **NSC1** (C_6D_6, 400 MHz, 298 K). The blue dashed lines show the spatial proximity between protons *Me* of the **NSC1** axle and protons *I* and *j* of **TPU** (see sketch above the stack for the protons labelling).

The complexing behaviour of the stilbazolium salt with the longest alkyl chain, **NSC18**, displays a different outcome. At lower temperatures (288 K), the prevalent isomer is ***D*** with a ***D***/***U*** ratio of 60:40. At RT (298 K), the ratio changes to 56:44, and at higher temperatures (333K), the most abundant isomer becomes ***U*** with a ***D***/***U*** ratio of 42:58. Overall, these findings show us as the length of the alkyl chain appended to the pyridinium ring affects the relative stability of the orientational isomers.

Table 3.1 ***D*/*U*** ratio of orientational isomers in deuterated benzene at different temperatures; [a] only one peak detected; [b] see Ref. 17.

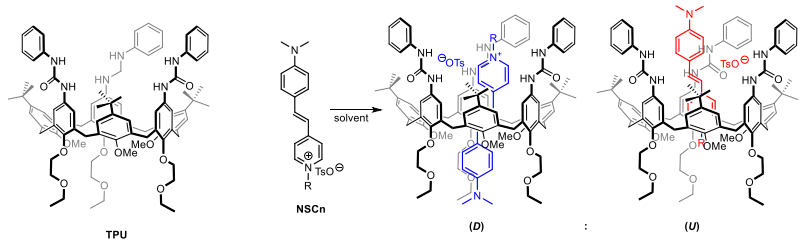

	D*/*U		
Compound	T = 288 K	T = 298 K	T = 333 K
NSC1	[a]	[a]	[a]
NSC5	43:57	38:62	[a]
NSC18	60:40[b]	56:44[b]	42:58[b]
NCS6(S)	81:19	80:20	78:22

To better understand the formation of these pseudorotaxane complexes, we devised the synthesis of a new stilbazolium axle, **NSC6(S)**, endowed with a bulky diphenylacetyl stoppering group at the end of its C6 alkyl chain (see Scheme 3.4). In principle, this axle can only thread the calix[6]arene cavity of **TPU** with its dimethylamino moiety because, as shown with several viologen-based threads (see Introduction chapter), the diphenylacetyl group present on the other side is too bulky. As a result, the threading of the axle Me_2N moiety from the calix[6]arene upper rim would generate the ***D*** isomer. In contrast, the threading from the lower rim would give rise to the ***U*** isomer, as depicted in Figure 3.8.

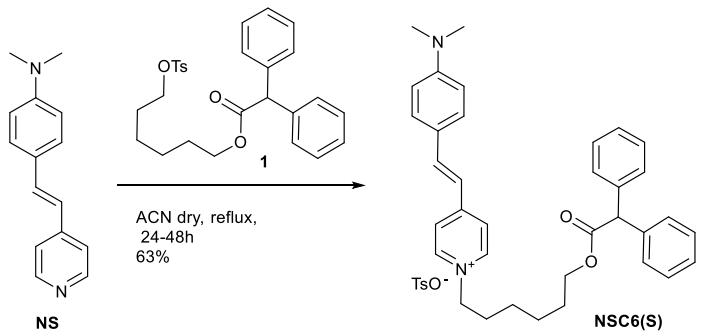

Scheme 3.4 Synthesis of **NSC6(S)**.

NSC6(S) was obtained in 63% yield by alkylating **NS** with tosylate **1**, in refluxing acetonitrile. As usual, **NSC6(S)** was fully characterised by NMR spectroscopy and ESI-MS measurements.

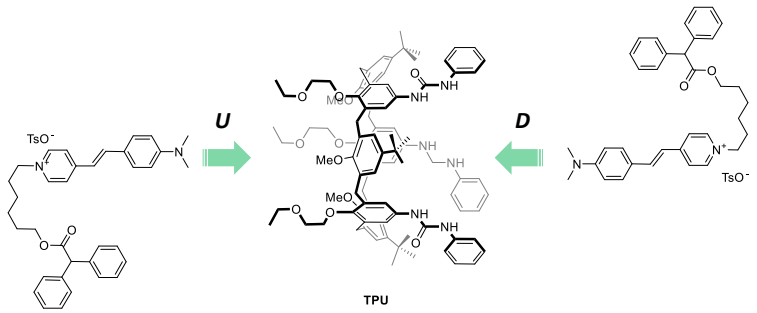

Figure 3.8 Possible threading process of **NSC6(S)** in calix[6]arene cavity.

Table 3.1 shows that the threading process is favoured from the upper rim of the calix[6]arene scaffold for mono-stopped **NSC6(S)**, and a ***D***/***U*** ratio of ca. 80:20 was observed for each temperature. However, the non-negligible amount of ***U*** isomer at diverse temperatures (20%) demonstrates that the axle threading process can occur from both calix[6]arene rims. This result looks pretty reasonable considering the small steric requirements of the dimethylamino group, which can overcome the energy barrier represented by the inward methoxy groups at the wheel's lower rim. On the other hand, threading from the upper rim is kinetically more favoured because this cavity access is more open and the phenylureas that can lose the axle ion pair.

The **NSC6(S)** result could help explain the previous outcomes obtained with the unstoppered **NSCn**. In fact, we can simplify the threading process by neglecting the lower rim thread, thus considering that the threading process occurs more easily from the upper rim (see Figure 3.9).

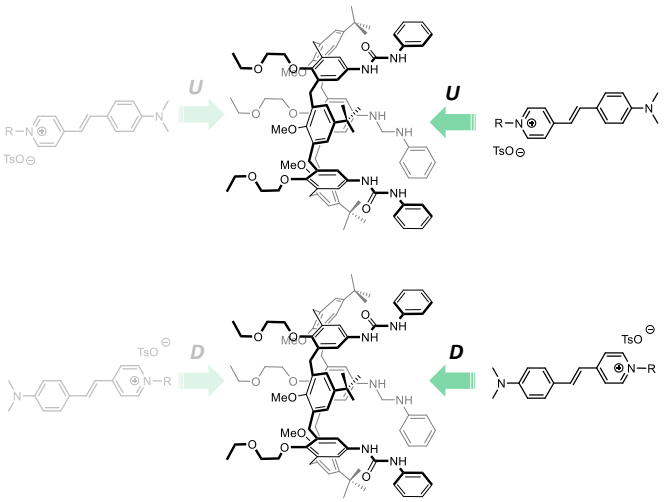

Figure 3.9 Simplification of the threading process.

In the case in which the pendant alkyl chain attached to the pyridinium moiety is "short" and with a modest steric hindrance, as in **NSC1** and **NSC5**, we observed a prevalence of ***U*** isomer (we previously hypothesised that for **NSC1** this is the only isomer present). The abundance of this isomer increases with the temperature. It is thus reasonable to conclude that the ***U*** isomer is slightly more stable than ***D***. With a "long" alkyl chain such as in **NSC18**, the bulkiness of the chain is such as to act as a kinetic stopper, considering that the alkyl chain would disentangle and organise itself before entering from the upper rim. Thus, in this case, the ***D*** isomer is prevalent at lower temperatures, but with increasing the temperature, the ratio shifts in favour of the ***U*** isomer, slightly most stable. In agreement with these results, the system with **NSC6(S)**, in which the stoppering group at the end of the alkyl chain avoids the threading process with this side of the molecule, prefers the formation of ***D*** isomer at each temperature, i.e., the product deriving from the fastest threading process.

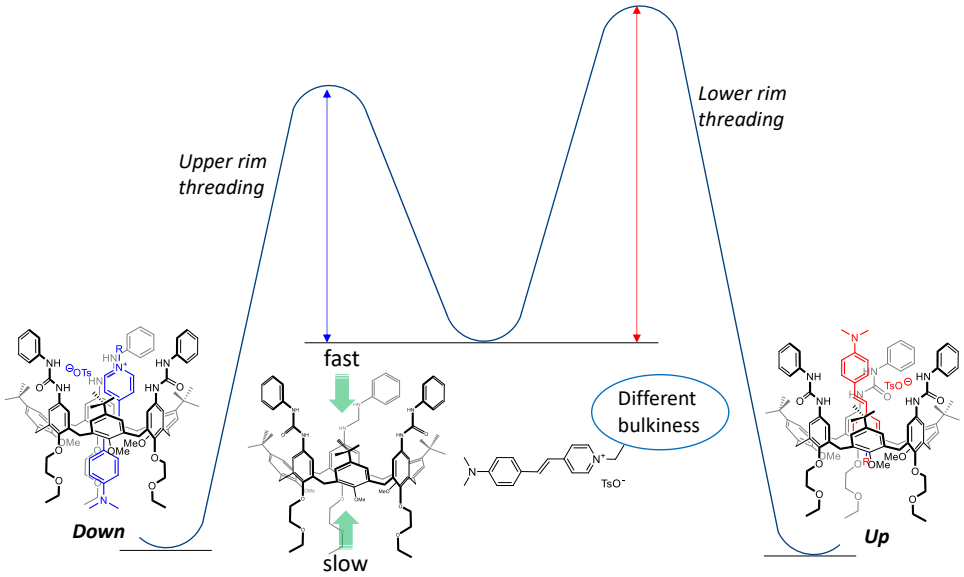

Figure 3.10 Schematic energy profile of the threading process in benzene of stilbazolium **NSCn** in **TPU** cavity.

To determine the relative stability of the pseudorotaxane isomers, the ***D*** and ***U*** structures were minimised using the "low-cost" density functional method B97-3c,[20] implemented in the ORCA computational software,[21] and the semi-empirical PM7 method,[22] implemented in MOPAC2016 software.[23] Solvent effects (benzene and dichloromethane) were simulated using the Conductor-like Polarizable Continuum Model (CPCM) method,[24] but the results were substantially identical to those carried out in vacuo and thus will not be presented. The energy difference in vacuo was 2.29 kcal/mol (estimated as *heat of formation* at 298 K) when calculated using the PM7 method and 57 kcal/mol when B97-3c hybrid functional was used (with this method, the complexes total energy is estimated at 0 K). The minimised geometries of the two isomers have been depicted in Figure 3.11, with their HOMO and LUMO MOs superimposed. As expected, the HOMO is always located on one of the wheel's aromatic units bearing a phenylurea group, whiles the LUMO is found on the axle's aromatic system faced to the HOMO. This arrangement of the MOs accounts for the charge

transfer interaction responsible for the red-orange coloured solutions of these complexes.

Moving to **SCN5**, the estimated energy difference between the two orientational isomers, calculated using the B97-3c functional, was almost null (ΔE = 0.7 kcal/mol, with ***U*** slightly more stable than ***D***).

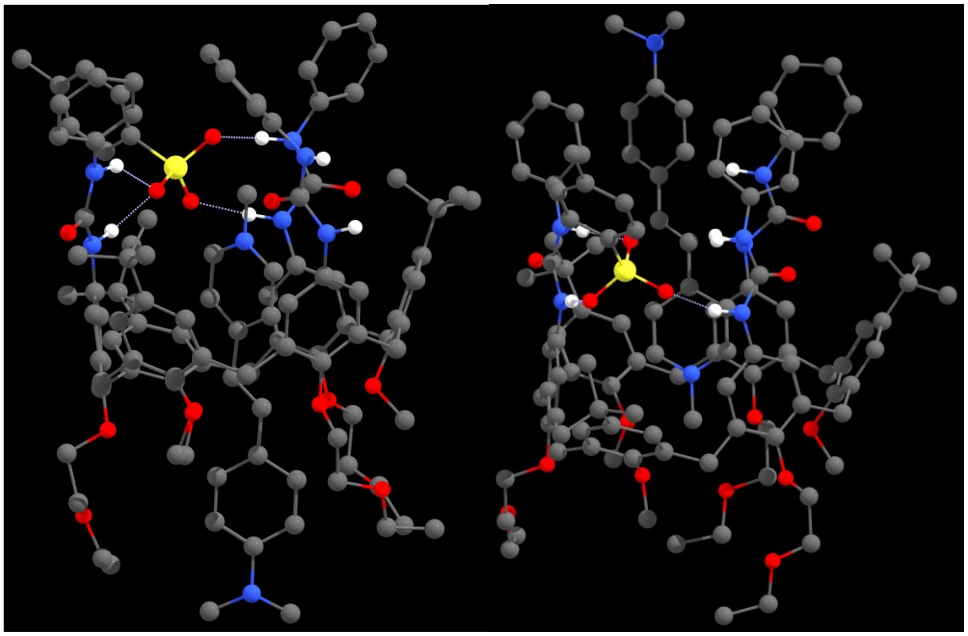

Figure 3.11 Minimised structures (B97-3c) for the [2]pseudorotaxane orientational isomers **TPU⊃NSC18(*D*)** (left) and **TPU⊃NSC18(*U*)** (right).

To get more insight into the threading process of this type of axle, a new series of stilbazolium salts was synthesised. In this case, the stilbazolium structure is endowed with a bulky group attached to the nitrogen atom in the electron-rich part of the molecule. In our opinion, this modification would alter the threading process's directionality, allowing the axle's entrance with its pyridinium head exclusively. This should enable us to determine the effect of the alkyl chain length on the threading process with more precision. 3,5-dimethylpiperidine moiety was chosen as it is bulky enough to prevent the transition inside the calix[6]arene cavity. At the same time, it should not appreciably affect the electronic properties

of the stilbazolium "push-pull" structure. These axles were synthesised by initially reacting 3,5-dimethylpyridine (mixture of isomers) and 4-fluorobenzaldehyde in refluxing dimethylformamide, using K_2CO_3 as the base.[25] The desired benzaldehyde **4** was obtained in 68% yield as a mixture of isomers, in which the prevalent isomer is the one bearing both methyl groups at the equatorial position. From now on, the other isomer with one methyl group at the equatorial position and the other at the axial position will not be taken into account, as a minority and for simplicity. Then, condensation of the benzaldehyde **4** with 4-methylpyridine in the presence of a base in DMF at 80 °C led to the pyridyl precursor **PS** in 85% yield. Afterwards, **PS** was alkylated with a proper alkyl chain to achieve stilbazolium salts **PSC1**, **PSC5** and **PSC18** as red solids in 92%, 68%, and 82% yield, respectively. They were all characterised by a series of NMR experiments and ESI-MS measurements.

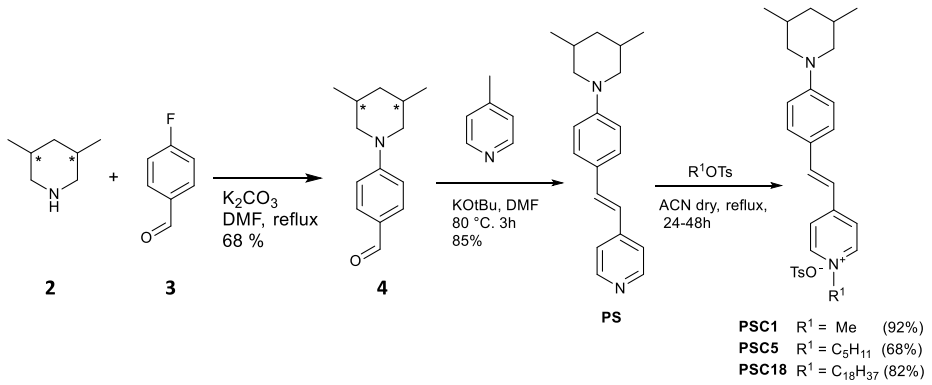

Scheme 3.5 Synthesis of axles **PSCn**.

^{1}H NMR spectra were recorded in $CDCl_3$ for **PSC5** and **PSC18**, and in CD_3OD for **PSC1** for solubility reasons. With respect to the **NSCn** series, the protonic spectra of these axles show a quasi-identical aromatic region. However, they differ for the dimethylpiperidine moiety. This latter group gives rise to several peaks: methyl groups, labelled β, resonate as a doublet at 0.98 ppm in CD_3OD and 0.94 ppm in $CDCl_3$, proton γ corresponds to the multiplet at 1.74 ppm (in both CD_3OD and $CDCl_3$). Diastereotopic protons α and δ generate two different signals each:

the doublet of doublets at 3.90 ppm (in CD_3OD, or at 3.78 ppm in $CDCl_3$) and the triplet at 2.38 ppm (in CD_3OD, or at 2.36 ppm in $CDCl_3$) are relative to protons α, while the multiplet at 1.87 ppm and the quadruplet at 0.83 ppm correspond to protons δ (1.84 and 0.78 ppm in $CDCl_3$).

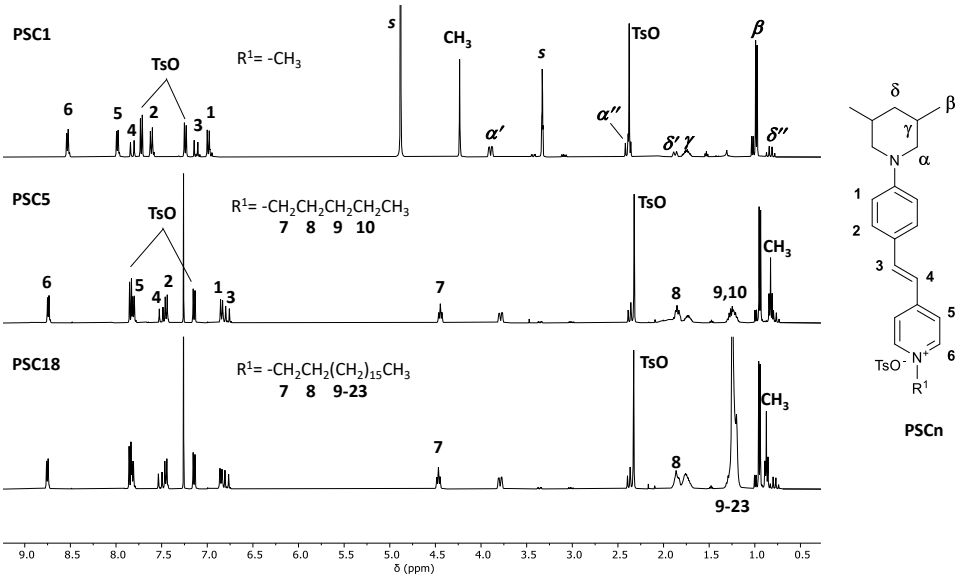

Figure 3.12 ^{1}H NMR spectra of stilbazolium **PSC1** (recorded in methanol-d4 for solubility reasons), **PSC5** and **PSC18** ($CDCl_3$, 400MHz).

As briefly stated before, since this type of axle cannot enter the calix[6]arene cavity with its dimethylpiperidine group, the threading process can only occur with the alkyl chain R^1, forming the ***U*** isomer from the upper rim, and the ***D*** isomer when the molecule enters from the lower rim (see Figure 3.13).

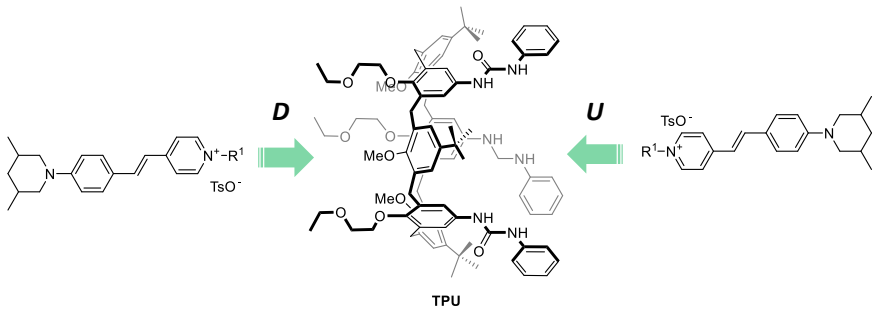

Figure 3.13 Possible threading process of **PSCn** in calix[6]arene cavity.

The [2]pseudorotaxane complexes were then obtained by mixing stoichiometric amounts of stilbazolium axles **PSCn** and **TPU** in deuterated benzene. Then, ^{1}H NMR spectra were recorded at increasing temperatures. The case of **PSC5** is reported as an example.

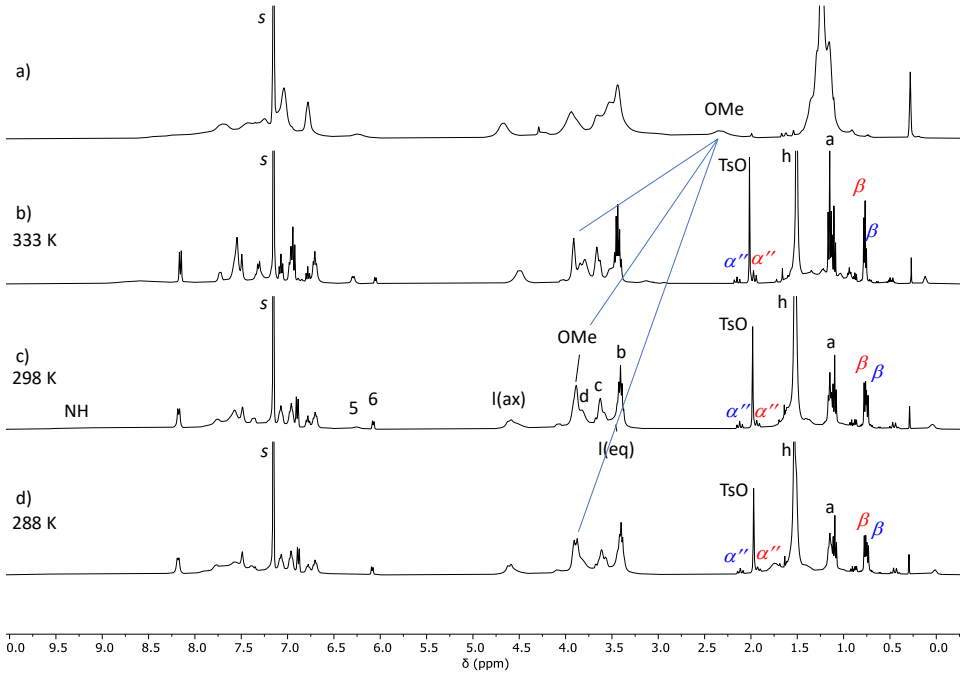

Figure 3.14 ^{1} H NMR stack plot of (a) **TPU**, (b) 1:1 mixture of **TPU** and **PSC5** recorded (b) at 333 K, (c) at 298 K and (d) at 288 K (C_6D_6, 400 MHz).

As usual, the same complexation evidence can be detected: so, the calix[6]arene signals result sharper as the complexation decreases the fluxionality; O*Me* groups experience a downfield shift from 2.3 ppm (in spectrum *a*) to 3.9 ppm with a sharpening of the peak (see continuous blue lines). In addition, the cavity highly shields the pyridinium protons, which resonate at very low ppm (proton *5* at 6.2 ppm and proton *6* at 6.0 ppm). The presence of each isomer was evaluated from the observation and integration of the peaks corresponding to *α* labelled protons of the dimethylpiperidine stopper unit. However, it was not so easy due to the crowd spectra. The orientation assignment was obtained afterwards, which will be discussed in the next chapter. The pair of signals at 3.7 and 2.1 ppm are relative

to the ***D*** isomer (α in blue), while the peaks at 3.4 and 1.9 ppm to the ***U*** isomer (α in red). The following HSQC spectrum shows the signal assignment of the system.

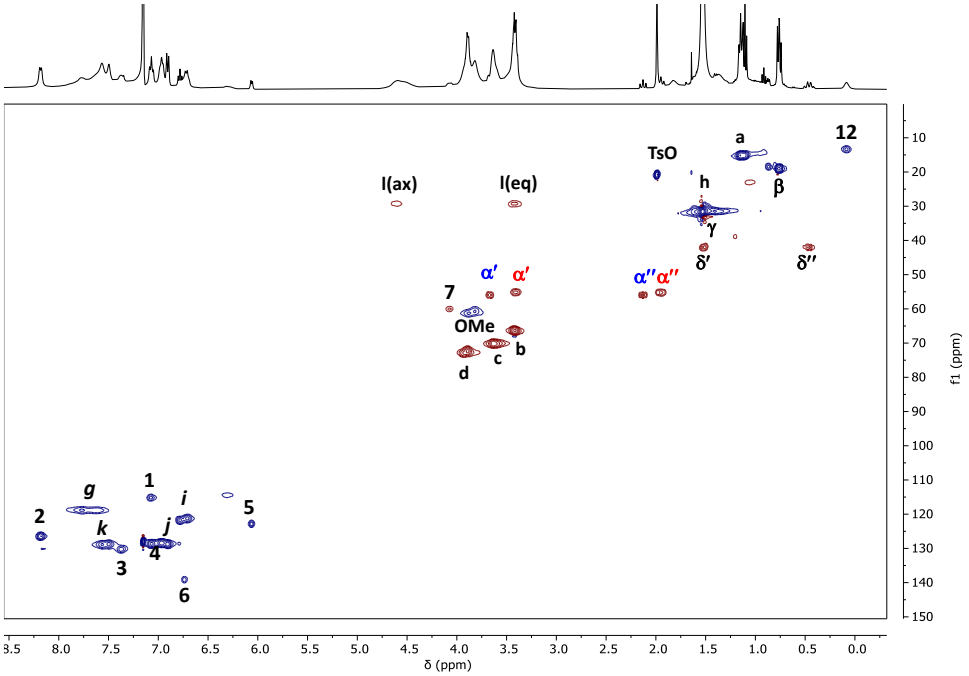

Figure 3.15 Edited HSQC NMR spectrum (400 MHz, benzene-d_6) of a 1:1 mixture of **TPU** and **PSC5** at 298 K.

From the stack plot reported in Figure 3.14, the ***D***/***U*** ratio was calculated by integrating the α" labelled peak. At lower temperatures (T = 288 K), a ***D***/***U*** ratio of 40:60 can be observed, while an increment in ***U*** isomer is visible with the increase of the temperature until a ***D***/***U*** ratio of 30:70 (T = 333 K). This is in agreement with the assumption that the stability of both isomers is very similar, the threading process is faster from the upper rim, but the "up" isomer is slightly more stable compared to ***D***. Complexes with **PSC1** as the axle displays a single peak relative to the α" proton. As in the case of **NSC1**, it is probably attributable to the formation of a single isomer (***U***). The results obtained with **PSC18** are in agreement with the described system. In the presence of a long alkyl chain, at lower temperatures, we observe the exclusive formation of isomer ***U***, and only 10% of ***D*** is detected at T = 333K.

Table 3.2 ***D*/*U*** ratio of isomers in deuterated benzene at different temperatures; [a] only one peak detected; [b] no complexation.

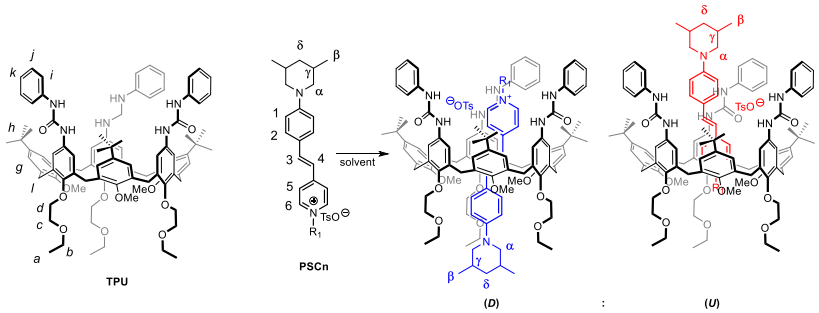

	D*/*U		
Compound	T = 288 K	T = 298 K	T = 333 K
PSC1	[a]	[a]	[a]
PSC5	40:60	35:65	30:70
PSC18	~0:100	5:95	10:90
PCS6(S)	[b]	[b]	[b]

Finally, **PSC6(S)**, endowed with both stoppering groups, was synthesised in 63% yield from the alkylation of its precursor **PS** with a tosylate C6 alkyl chain bearing a diphenyl acetyl stopper group. As expected, the ^{1}H NMR spectrum of the 1:1 mixture between this axle and **TPU** showed no complexation, confirming that 3,5-dimethylpiperidine and diphenyl acetate act as stopper groups.

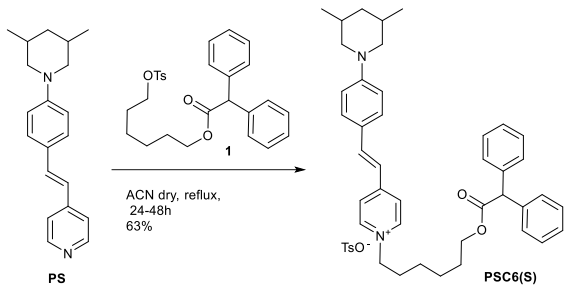

Scheme 3.6 Synthesis of **PSC6(S)**.

The apparent association constants of stilbazolium salt/**TPU** complexes were calculated by UV-Vis titrations in dichloromethane. It should be observed that the computed constants indicate the affinity of **TPU** for the axles, regardless of the percentage of each orientational isomer present in the solution. As will be more

evident in the next chapter, the two isomers present very different optical properties; therefore, any change in the stilbazolium optical spectra upon **TPU** addition must be seen as the result of the weighted average of the optical contribution of the two isomers.

Spectra of increasing concentration of **TPU** were recorded by adding incremental aliquots of a **TPU** solution in CH_2Cl_2 (2.25×10^{-4} M) to a solution of the appropriate stilbazolium salt (**NSCn** and **PSCn**) in the same solvent ($\sim 10^{-5}$ M). Dichloromethane was used instead of benzene for safety and solubility reasons. However, switching to the less dangerous toluene did not appreciably improve the solubility of **NSC1** and **PSC1**. Selected collections of absorption spectra recorded during the titration were gathered in Figure 3.16

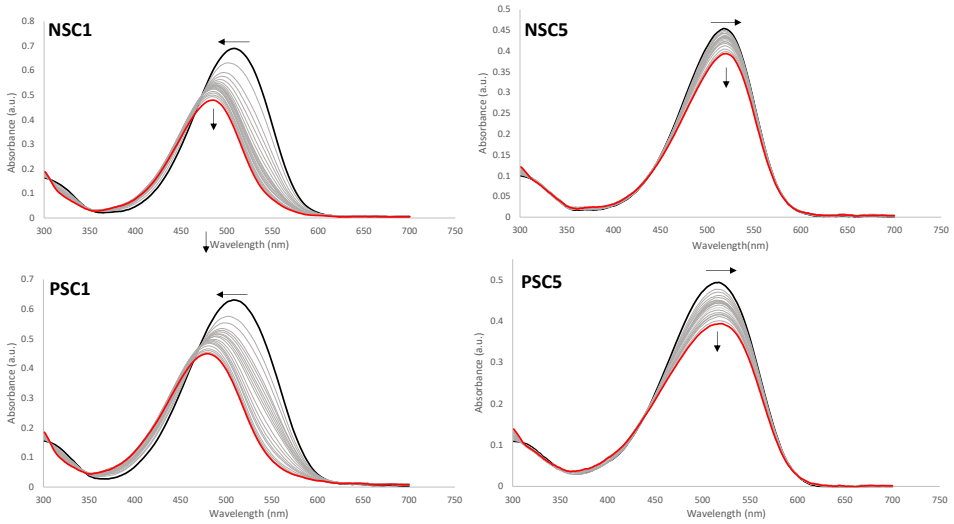

Figure 3.16 Collections of absorption spectra collected during the titrations of **NSC1** (top, left), **PSC1** (bottom, left), **NSC5** (top, right) and **PSC5** (bottom, right) with **TPU** in dichloromethane at 298 K ($C_{axle} = 10^{-5}$ M; $C_{TPU} = 2.25 \times 10^{-4}$ M). Black line: abs of the free axle; grey lines: abs after each wheel's aliquots added; red line: abs after addition of the last wheel addition.

From the analysis of the above collections of spectra, it is evident that the **TPU** addition causes a marked hypsochromic shift in the case of **NSC1** and **PSC1,** while a minor bathochromic shift is observed for **NSC5** and **PSC5**. To explain such an opposite behaviour, we considered that for **NSC5** and **PSC5**, both isomers are

simultaneously present in the solution, while for **NSC1** and **PSC1**, we know that only isomer ***U*** is dominant. For the latter salts, the observed hypsochromic shift could be thus the result of the stabilisation of the axle HOMO. Less clear is the behaviour observed when a longer alkyl chain is appended to the pyridinium ring. The absorption changes were fitted with a 1:1 model using the Specfit/32 software. The recorded data are reported in Table 3.3.

Table 3.3 Data from stilbazolium titration with **TPU**.

Entry	Compound	λ_{start} (nm)	λ_{end} (nm)	logK
1	**NSC1**	508	484	5.11±0.05
2	**NSC5**	518	523	4.38±0.13
3	**NSC18**	514	518	4.23±0.08
4	**NSC6(S)**	517	520	4.31±0.19
5	**PSC1**	508	479	5.15±0.06
6	**PSC5**	517	520	4.81±0.28
7	**PSC18**	520	524	4.44±0.12
8	**PSC6(S)**	520	527	

From Table 3.3, it is possible to observe that the apparent association constants relating to **NSC1** and **PSC1** are an order of magnitude larger than the others. Unfortunately, this study did not disclose the reason for this effect. Still, it is probably related to the outcome from the NMR experiments of **NSC1** and **PSC1**: a) one isomer (***U***) is dominating in solution with its π-poor pyridinium ring deeply engulfed in the π-rich aromatic pocket defined by the calixarene wheel; b) the alkyl chain of **NSCn** or **PSCn**, with n = 5, 18, have to lose their solvent molecules before to enter in the cavity, thus reducing the enthalpic gain upon inclusion into the calixarene cavity.

Further investigations are needed to understand the issue. Indeed, it is clear that the association constants decrease with increasing chain size. As expected, no complexation constant can be calculated with **PSC6(S)**.

Conclusions

In this chapter, we reported the study of the threading process of a series of stilbazolium salts within the calix[6]arene cavity in low-polarity solvents. Several stilbazolium salts endowed with different stoppering groups at their endings were synthesised and tested in the complexation with **TPU**. The isomer abundance was evaluated through NMR experiments at different temperatures and by 1D ROESY measurements. It was observed that the nature of the substituents present in the stilbazolium salts could affect the geometry of the dye encapsulation in the [2]pseudorotaxane complexes. In general, the threading process occurs preferentially from the upper rim of the calix[6]arene, as it is promoted by the urea groups able to loosen the stilbazolium ion-pair; moreover, the lower rim results more hindered due to the presence of the methoxy groups oriented inward the cavity. The stability of the isomer appears not much different from each other; however, the "up" orientation (***U***) appears slightly more stable, as also demonstrated with preliminary computational studies. Therefore, depending on the substituents and stoppering groups, the orientation of the complex can be controlled. Furthermore, the apparent association constants were calculated *via* spectroscopic (UV/Vis) titrations, and a dependence on the bulkiness of the substituent was once again evidenced. It is finally noteworthy that the complexation affects the absorption features, even though studying the spectroscopic properties is not straightforward as the system in solution is quite complicated. In fact, the synthesis, separation and study of the stilbazolium-base [2]rotaxane orientational isomers will be described in the next chapter.

Acknowledgments

Thanks to Caterina Baccini (University of Parma) for UV-Vis measurements.

Experimental Section

General Methods

All solvents were dried using standard procedures; all other reagents were of reagent-grade quality obtained from commercial suppliers and used without further purification. Melting points are uncorrected. NMR spectra were recorded at 400 MHz for ^{1}H and 100 MHz for ^{13}C. Chemical shifts are expressed in ppm (δ) using the residual solvent signal as an internal reference (7.26 ppm for $CHCl_3$, 7.16 ppm for C_6D_5H, 5.32 for $CHDCl_2$ and 3.31 ppm for CD_2HOD). The terms m, s, d, t and q represent multiplet, singlet, doublet, triplet and quadruplet, respectively; the term "br. s" means a broad signal. Mass spectra were recorded in the ESI mode. Compounds **NS**,[26] **1**[27] and **4**[25] were synthesised according to published procedures.

Synthetic Procedure and Analytical Data

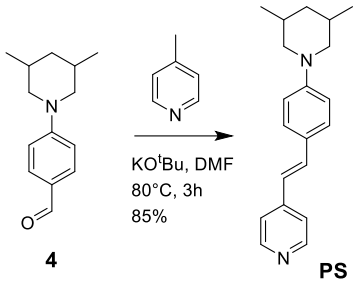

PS: under a nitrogen atmosphere, in a 100 mL ground bottom flask, **4** (2.0 g, 9.2 mmol) and *N*-methyl pyridine (857 mg, 9.2 mmol) were dissolved in dimethylformamide (40 mL). Potassium *tert*-butoxide (1.24 g, 11 mmol) was added. The reaction mixture was heated at 80 °C for 3 hours. After being cooled at room temperature, 200 mL of dichloromethane were added. The solution was washed with 200 mL of ice water and then three time with 200 mL of aqueous potassium hydroxide (1M). The organic phase was dried on sodium sulphate and then evaporated. The crude product was recrystallised from toluene/hexane to

give **PS** (2.3 g) as an orange solid in 85% yield. M.p. = 219-221 °C; ^{1}H NMR ($CDCl_3$, 400 MHz): δ = 8.52 (d, 2H, *J* = 6.2 Hz), 7.42 (d, 2H, *J* = 8.8 Hz), 7.32 (d, 2H, *J* = 6.2Hz), 7.23 (d, 1H, *J* = 16.3 Hz), 6.91 (d, 2H, *J* = 8.8 Hz), 6.82 (d, 1H, *J* = 16.3 Hz), 3.70 (m, 2H), 2.28 (t, 2H, *J* = 11.8 Hz), 1.81 (m, 3H), 0.94 (d, 6H, *J* = 6.5 Hz), 0.74 (q, 1H, *J* = 12.0 Hz) ppm; ^{13}C NMR ($CDCl_3$, 100 MHz): δ = 151.8, 149.1, 146.6, 134.2, 128.6, 126.0, 121.7, 120.7, 115.5, 56.3, 42.3, 30.8, 19.5. ESI-MS (+): m/z= 293.4 $[M+H]^+$.

General procedure for the synthesis of the stilbazolium salts. In a 100 mL ground bottom flask, **NS** or **PS** (1.3 mmol) and the opportune alkylating agent (1.7 mmol) were dissolved in dry acetonitrile (40 mL). The reaction mixture was refluxed under vigorous stirring overnight. Afterwards, the solution was evaporated to dryness under reduced pressure.

NSC1: alkylation of **NS** with methyltosylate. The purification through column chromatography on silica gel (eluent: CH_2Cl_2/CH_3OH = 65/35) yields **NSC1** as a red solid in 80% yield. M.p. = 239-241 °C; ^{1}H NMR (CD_3OD, 400 MHz): δ = 8.50 (d, 2H, *J* = 6.8 Hz), 7.96 (d, 2H, *J* = 6.8 Hz), 7.83 (d, 1H, *J* = 16 Hz), 7.72 (d, 2H, *J* = 8.1 Hz), 7.62 (d, 2H, *J* = 8.9 Hz), 7.24 (d, 2H, *J* = 8.0 Hz), 7.09 (d, 1H, *J* = 16.0 Hz), 6.80 (d, 2H, *J* = 8.9 Hz), 4.22 (s, 3H), 3.08 (s, 6H), 2.37 (s, 3H) ppm; ^{13}C NMR (CD_3OD, 100 MHz): δ = 154.7, 125.6, 143.8, 142.9, 142.2, 140.2, 130.1, 128.4, 125.6, 122.7, 122.1, 116.3, 111.7, 45.7, 38.8, 19.9. ESI-MS (+): m/z= 239.2 $[M-TsO]^+$.

NSC5: alkylation of **NS** with 1-pentyltosylate. Precipitation of the crude mixture from ethyl acetate yield **NSC5** as a red solid in 68%. M.p. = 209-211 °C; ^{1}H NMR (CD_3OD, 400 MHz): δ = 8.59 (d, 2H, *J* = 6.7 Hz), 7.99 (d, 2H, *J* = 6.6 Hz), 7.86 (d, 1H, *J* = 16.0 Hz), 7.73 (d, 2H, *J* = 8.1 Hz), 7.63 (d, 2H, *J* = 8.9 Hz), 7.24 (d, 2H, *J* = 8.0 Hz), 7.11 (d, 1H, *J* = 16.0 Hz), 6.81 (d, 2H, *J* = 8.9 Hz), 4.44 (t, 2H, *J* = 7.5 Hz), 3.09 (s, 6H), 2.38 (s, 3H), 1.99 (m, 2H), 1.42 (m, 4H), 0.97 (t, 3H, *J* = 7.0 Hz) ppm; ^{13}C NMR (CD_3OD, 100 MHz): δ = 155.0, 152.6, 143.1, 142.9, 142.3, 140.2, 130.2, 128.4,

125.9, 122.7, 122.3, 116.3, 111.7, 59.9, 38.8, 30.5, 27.9, 21.8, 19.9, 12.7. ESI-MS (+): m/z= 295.3 $[M\text{-}TsO]^+$.

NSC18: alkylation of **NS** with 1-octadecyltosylate. Precipitation of the crude mixture from ethyl acetate yield **NSC18** as a red solid in 63%. M.p. = 161 - 163 °C; ^{1}H NMR (CD_3OD, 400 MHz): δ = 8.59 (d, 2H, *J* = 7.0 Hz), 7.99 (d, 2H, *J* = 6.6 Hz), 7.86 (d, 1H, *J* = 16.0 Hz), 7.73 (d, 2H, *J* = 8.2 Hz), 7.63 (d, 2H, *J* = 8.9 Hz), 7.24 (d, 2H, *J* = 7.9 Hz), 7.11 (d, 1H, *J* = 16.0 Hz), 6.81 (d, 2H, *J* = 9.0 Hz), 4.44 (t, 2H, *J* = 7.4 Hz), 3.09 (s, 6H), 2.38 (s, 3H), 1.99 (m, 2H), 1.42-1.25 (m, 32H), 0.91 (t, 3H, *J* = 7.0 Hz) ppm; ^{13}C NMR (CD_3OD, 100 MHz): δ = 155.0, 152.6, 143.1, 142.9, 142.3, 140.2, 130.2, 128.4, 125.6, 122.7, 122.3, 116.3, 111.7, 59.9, 38.8, 31.7, 30.8, 29.4, 29.3, 29.2, 29.1, 28.7, 25.8, 22.3, 19.9, 13.0. ESI-MS (+): m/z= 477.4 $[M\text{-}TsO]^+$.

NSC6(S): alkylation of **NS** with **1**. The purification through column chromatography on silica gel (eluent: CH_2Cl_2/CH_3OH = 90/10) yields **NSC6(S)** as a red solid in 63% yield. M.p. = 144-146 °C; ^{1}H NMR ($CDCl_3$, 300 MHz): δ = 8.67 (d, 2H, *J* = 6.9 Hz), 7.84 (d, 2H, *J* = 8.1 Hz), 7.75 (d, 2H, *J* = 6.6 Hz), 7.46 (d, 1H, *J* = 15.9 Hz), 7.31 (d, 2H, *J* = 9.0 Hz), 7.29 (m, 10H), 7.12 (d, 2H, *J* = 8.1 Hz), 6.74 (d, 1H, *J* = 15.9 Hz), 6.63 (d, 2H, *J* = 9.0 Hz), 5.01 (s, 1H), 4.35 (t, 2H, *J* = 5.4 Hz), 4.06 (t, 2H, *J* = 5.1 Hz), 3.02 (s, 6H), 2.29 (s, 3H), 1.75 (m, 2H), 1.51 (m, 2H), 1.18 (m, 4H) ppm; ^{13}C NMR ($CDCl_3$, 100 MHz): δ = 172.5, 153.9, 152.1, 144.2, 143.5, 142.5, 139.1, 138.7, 130.5, 128.7, 128.6, 127.2, 126.0, 122.8, 122.5, 116.6, 111.9, 65.0, 59.8, 57.1, 40.1, 31.4, 28.4, 25.5, 25.2, 21.3; ESI-MS(+): m/z = 519.2 $[M\text{-}TsO]^+$.

PSC1: alkylation of **PS** with methyltosylate. Precipitation of the crude mixture from ethyl acetate yield **PSC1** as a yellow solid in 92%. M.p. = 233-235 °C; ^{1}H NMR (CD_3OD, 400 MHz): δ = 8.53 (d, 2H, *J* = 6.9 Hz), 7.99 (d, 2H, *J* = 7.0 Hz), 7.82 (d, 1H, *J* = 16.1 Hz), 7.72 (d, 2H, *J* = 8.2 Hz), 7.61 (d, 2H, *J* = 8.9 Hz), 7.24 (d, 2H, *J* = 8.0 Hz), 7.12 (d, 1H, *J* = 16.0 Hz), 6.99 (d, 2H, *J* = 8.9 Hz), 4.23 (s, 3H), 3.90 (m, 2H), 2.39 (t, 2H, *J* = 12.0 Hz), 2.38 (s, 3H), 1.87 (m, 1H), 1.75 (m, 2H), 0.98 (d, 6H, *J* = 6.6 Hz), 0.83 (q, 1H, J = 12.1 Hz) ppm; ^{13}C NMR (CD_3OD, 100 MHz): δ = 154.6, 152.9, 143.9,

142.4, 142.2, 140.3, 130.1, 128.4, 125.6, 122.3, 117.2, 114.3, 55.0, 45.8, 42.1, 30.4, 19.9, 18.1. ESI-MS (+): m/z= 307.3 $[M\text{-}TsO]^+$.

PSC5: alkylation of **PS** with 1-pentyltosylate. Precipitation of the crude mixture from ethyl acetate yield **NSC5** as a red solid in 68%. M.p. = 190-192 °C; ^{1}H NMR ($CDCl_3$, 400 MHz): δ = 8.74 (d, 2H, *J* = 6.8 Hz), 7.84 (d, 2H, *J* = 8.2 Hz), 7.81 (d, 2H, *J* = 6.7 Hz), 7.50 (d, 1H, *J* = 16.0 Hz), 7.45 (d, 2H, *J* = 9.0 Hz), 7.15 (d, 2H, *J* = 8.1 Hz), 6.84 (d, 2H, *J* = 8.9 Hz), 6.78 (d, 1H, *J* = 16.1 Hz), 4.45 (t, 2H, *J* = 7.4 Hz), 3.78 (m, 2H), 2.36 (t, 2H, J = 12.0 Hz), 2.32 (s, 3H), 1.85 (m, 3H), 1.74 (m, 2H), 1.25 (m, 4H), 0.94 (d, 6H, *J* = 6.6 Hz) 0.83 (t, 3H, *J* = 7.0 Hz), 0.78 (q, 1H, *J* = 12.0 Hz) ppm; ^{13}C NMR ($CDCl_3$, 100 MHz): δ = 153.8, 152.6, 144.0, 143.7, 142.2, 139.1, 130.5, 128.6, 126.1, 123.0, 117.3, 114.4, 60.4, 55.2, 42.2, 31.2, 30.6, 28.1, 22.1, 21.3, 19.3, 13.8; ESI-MS(+): m/z = 363.4 $[M\text{-}TsO]^+$.

PSC18: alkylation of **PS** with 1-octadecyltosylate. Precipitation of the crude mixture from ethyl acetate yield **PSC18** as a red solid in 82%. M.p. = 158-160 °C; ^{1}H NMR ($CDCl_3$, 400 MHz): δ = 8.75 (d, 2H, *J* = 6.7 Hz), 7.85 (d, 2H, *J* = 8.2 Hz), 7.82 (d, 2H, *J* = 6.9 Hz), 7.52 (d, 1H, *J* = 16.0 Hz), 7.45 (d, 2H, *J* = 8.9 Hz), 7.15 (d, 2H, *J* = 7.9 Hz), 6.85 (d, 2H, *J* = 8.7 Hz), 6.79 (d, 1H, *J* = 16.1 Hz), 4.47 (t, 2H, *J* = 7.4 Hz), 3.78 (m, 2H), 2.36 (t, 2H, J = 12.0 Hz), 2.33 (s, 3H), 1.85 (m, 3H), 1.76 (m, 2H), 1.25 (m, 30H), 0.95 (d, 6H, *J* = 6.6 Hz) 0.87 (t, 3H, *J* = 6.8 Hz), 0.79 (q, 1H, *J* = 12.1 Hz) ppm; ^{13}C NMR ($CDCl_3$, 100 MHz): δ = 154.0, 152.8, 144.3, 143.8, 142.4, 139.1, 130.7, 128.7, 126.2, 123.2, 117.4, 114.6, 60.6, 55.4, 42.4, 32.1, 31.7, 30.8, 29.9, 29.8, 29.8, 29.7, 29.5, 29.5, 29.2, 26.3, 22.8, 21.5, 19.4, 14.3; ESI-MS(+): m/z = 545.7 $[M\text{-}TsO]^+$.

PSC6(S): alkylation of **PS** with **1**. The purification through column chromatography on silica gel (eluent: CH_2Cl_2/CH_3OH = 90/10) yields **PSC6(S)** as a red solid in 55% yield. M.p. = 149-151 °C; ^{1}H NMR (CD_3OD, 400 MHz): δ = 8.54 (d, 2H, *J* = 6.6 Hz), 7.96 (d, 2H, *J* = 6.7 Hz), 7.81 (d, 1H, *J* = 16.0 Hz), 7.71 (d, 2H, *J* = 8.2 Hz), 7.60 (d, 2H, *J* = 9.0 Hz), 7.33-7.22 (m, 10H), 7.20 (d, 2H, *J* = 8.0 Hz), 7.10 (d, 1H, *J* = 16.0

Hz), 6.97 (d, 2H, *J* = 8.9 Hz), 5.06, (s, 1H), 4.35 (t, 2H, *J* = 7.4 Hz), 4.15 (t, 2H, *J* = 6.4 Hz), 3.88 (m, 2H), 2.37 (t, 2H, *J* = 12.0 Hz), 2.33 (s, 3H), 1.86 (m, 3H), 1.71 (m, 2H), 1.62 (m, 2H), 1.25 (m, 4H), 0.96 (d, 6H, *J* = 6.6 Hz) 0.80 (q, 1H, *J* = 12.1 Hz) ppm; ^{13}C NMR ($CDCl_3$, 100 MHz): δ = 174.2, 156.2, 154.3, 144.0,141.6, 140.3, 131.6, 129.8, 129.7, 129.6, 128.3, 127.0, 125.5, 124.0, 118.6, 115.7, 65.9, 61.1, 58.3, 56.3, 43.5, 32.0, 31.8, 29.3, 26.5, 26.2, 21.3, 19.5; ESI-MS(+): m/z = 587.6 [M-TsO]$^+$.

Eyring equation[19]

$$\Delta G^{+}_{+} = RT_c[22.96 + ln(T_c/\delta v)](Jmol^{-1})$$

UV-vis titration

The bindings affinity of **TPU** for stilbazolium salts were determined by UV-Vis titration at 298K in dichloromethane. A solution of the appropriate stilbazolium salt (~10^{-5} M) was titrated with incremental aliquots of a 2.25 × 10^{-4} M solution of **TPU** in the same solvent. The fitting of the absorbance in the 300 – 750 nm range for the different [**TPU**]/[SB salt] with the SPECFIT/32 software yielded for all the stilbazolium salts an apparent 1:1 binding constant.

References

[1] A. J. C. Kuehne, M. C. Gather, *Chem. Rev.* **2016**, *116*, 12823–12864.

[2] I. D. W. Samuel, G. A. Turnbull, *Chem. Rev.* **2007**, *107*, 1272–1295.

[3] H. Dong, C. Zhang, Y. S. Zhao, *J. Mater. Chem. C* **2017**, *5*, 5600–5609.

[4] M. Sayed, H. Pal, *J. Mater. Chem. C* **2016**, *4*, 2685–2706.

[5] R. N. Dsouza, U. Pischel, W. M. Nau, *Chem. Rev.* **2011**, *111*, 7941–7980.

[6] N. K. Petrov, D. A. Ivanov, M. V. Alfimov, *ACS Omega* **2019**, *4*, 11500–11507.

[7] N. Mourtzis, K. Eliadou, K. Yannakopoulou, *Supramolecular Chemistry* **2004**, *16*, 587–593.

[8] L. Strekowski, in *Top. Heterocycl. Chem.* (Ed.: L. Strekowski), Springer Berlin Heidelberg, Berlin, Heidelberg, **2008**, pp. 1–241.

[9] M. Pawlicki, H. A. Collins, R. G. Denning, H. L. Anderson, *Angewandte Chemie International Edition* **2009**, *48*, 3244–3266.

[10] J. N. Wilson, A. S. Brown, W. Michael Babinchak, C. D. Ridge, J. D. Walls, *Organic & Biomolecular Chemistry* **2012**, *10*, 8710–8719.

[11] H. Dong, Y. Wei, W. Zhang, C. Wei, C. Zhang, J. Yao, Y. S. Zhao, *J. Am. Chem. Soc.* **2016**, *138*, 1118–1121.

[12] S. W. Eaton, A. Fu, A. B. Wong, C.-Z. Ning, P. Yang, *Nat Rev Mater* **2016**, *1*, 16028–16039.

[13] U. Steiner, M. H. Abdel-Kader, P. Fischer, H. E. A. Kramer, *J. Am. Chem. Soc.* **1978**, *100*, 3190–3197.

[14] H. Görner, H. Gruen, *Journal of Photochemistry* **1985**, *28*, 329–350.

[15] B. Carlotti, G. Consiglio, F. Elisei, C. G. Fortuna, U. Mazzucato, A. Spalletti, *J. Phys. Chem. A* **2014**, *118*, 3580–3592.

[16] G. Cera, A. Arduini, A. Secchi, A. Credi, S. Silvi, *The Chemical Record* **2021**, *21*, 1161–1181.

[17] M. Bazzoni, F. Terenziani, A. Secchi, G. Cera, I. Jabin, G. De Leener, M. Luhmer, A. Arduini, *Chemistry – A European Journal* **2020**, *26*, 3022–3025.

[18] F. Ugozzoli, C. Massera, A. Arduini, A. Pochini, A. Secchi, *CrystEngComm* **2004**, *6*, 227–232.

[19] H. Günther, *NMR Spectroscopy: Basic Principles, Concepts and Applications in Chemistry*, John Wiley & Sons, **2013**.

[20] J. G. Brandenburg, C. Bannwarth, A. Hansen, S. Grimme, *J. Chem. Phys.* **2018**, *148*, 064104.

[21] F. Neese, *WIREs Computational Molecular Science* **2012**, *2*, 73–78.

[22] J. J. P. Stewart, *J Mol Model* **2013**, *19*, 1–32.

[23] "MOPAC2016 Home Page," can be found under http://openmopac.net/MOPAC2016.html, **n.d.**

[24] M. Garcia-Ratés, F. Neese, *Journal of Computational Chemistry* **2020**, *41*, 922–939.

[25] D. Osmaniye, B. Kaya Cavusoglu, B. N. Saglik, S. Levent, U. Acar Cevik, O. Atli, Y. Ozkay, Z. A. Kaplancikli, *Molecules* **2018**, *23*, 831.

[26] S. Brasselet, F. Cherioux, P. Audebert, J. Zyss, *Chem. Mater.* **1999**, *11*, 1915–1920.

[27] A. Arduini, F. Ciesa, M. Fragassi, A. Pochini, A. Secchi, *Angewandte Chemie* **2005**, *117*, 282–285.

Chapter 4. Stilbazolium-based oriented [2]rotaxane

Introduction

Photoactive materials, such as fluorophore and photoswitches, have great importance in developing new technologies. Fluorophore molecules are widely employed in sensors,[1,2] bioimaging applications[3,4] and optoelectronic devices.[5,6] Photoswitching systems are instead of particular interest in developing smart materials,[7,8] photopharmacology,[9] and molecular machines.[10,11] As presented in the previous chapter, stilbazolium dyes are a class of styryl cyanines characterised by a conjugated "push-pull" structure between an electron-poor *N*-alkylated pyridinium ring and an electron-rich *para*-substituted aromatic ring.[12] They express very interesting spectroscopic properties, which have been employed in fluorescent sensors[13] and non-linear optical materials.[14–16] Furthermore, their central double bond can experience *E*-*Z* photoisomerisation.[17] In the previous chapter, we demonstrated the ability of phenylureido calix[6]arene derivative **TPU** to efficiently complex stilbazolium dyes. Indeed, the non-palindrome nature of the calix[6]arene receptor cavity allows the formation of two orientational pseudorotaxane isomers with this asymmetric guest. We also observed that the orientation adopted by the encapsulated guest inside the host cavity affects the optical properties of the former. The isomers' interconversion can be modulated by changing the solvent polarity and the solution temperature. Still, their continuous interconversion avoids their separation, thus the thorough study of the properties of the isolated isomers.

In this chapter, the synthesis of orientational stilazolium-calix[6]arene [2]rotaxanes is presented. Thanks to their mechanically interlocked structures,

the isomers' interconversion result prevented allowing their separation. Furthermore, the investigation of the photophysical and photochemical properties of these [2]rotaxane isomers showed that the encapsulation of the stilbazolium salt inside the calix[6]arene cavity might enhance either its emission or photoisomerisation properties in relation to its geometrical orientation. Several examples of rotaxanes orientational isomers are reported in the literature,[18–21] but none of them displays different photophysical properties with regard to the orientation, as in this case.

Results and Discussion

To evaluate the properties of stilbazolium-based [2]rotaxanes, we designed a nonsymmetric axle endowed with 3,5-dimethylpiperidine and diphenylacetyl as stoppers. Such groups have enough bulkiness to prevent axle slippage from the calix[6]arene cavity different accesses. Moreover, they do not substantially affect the optical properties of the stilbazolium push-pull system compared to the *N*,*N*-dimethyl derivative studied in the previous chapter. Towards this end, the synthetic strategy started from the synthesis of mono-stopped stilbazolium salt **7**, as depicted in Scheme 4.1: the 3,5-dimethylpyridine (mixture of isomers) was initially reacted with 4-fluorobenzaldehyde in the presence of K_2CO_3 in dimethylformamide under reflux conditions.[22] The desired benzaldehyde **3** was obtained in 68% yield as a mixture of isomers, in which the prevalent isomer is the one bearing both methyl groups at the equatorial position. From now on, the other isomer with one methyl group at the equatorial position and the other at the axial position will not be taken into account, as a minority and for simplicity. Parallelly, alkylation in acetonitrile of 4-methylpyridine with 12-hydroxydocecyl 4-methylbenzenesulfonate **5** led to hydroxyl-terminated tosylate picolinium salt **6** in 81% yield. Subsequently, condensation in methanol of benzaldehyde **3** with picolinium salt **6** finally afforded the red-coloured stilbazolium salt **7** in 86% yield.

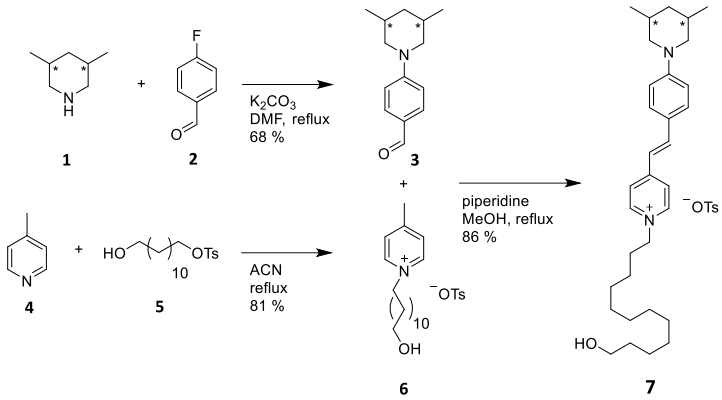

Scheme 4.1 Synthesis of stilbazolium salt **7**.

With stilbazolium salt **7** in hand, the formation of [2]pseudorotaxanes between triphenylureido triethoxyethyl calix[6]arene derivative **TPU** and stilbazolium **7** was tested. Since both components are asymmetric, two orientational pseudorotaxane isomers can be obtained. NMR studies were carried out by mixing stoichiometric amounts of wheel **TPU** and stilbazolium **7** in deuterated benzene, and ^{1}H experiments were recorded at room temperature upon mixing the components and then at the equilibrium (after 2 hours).

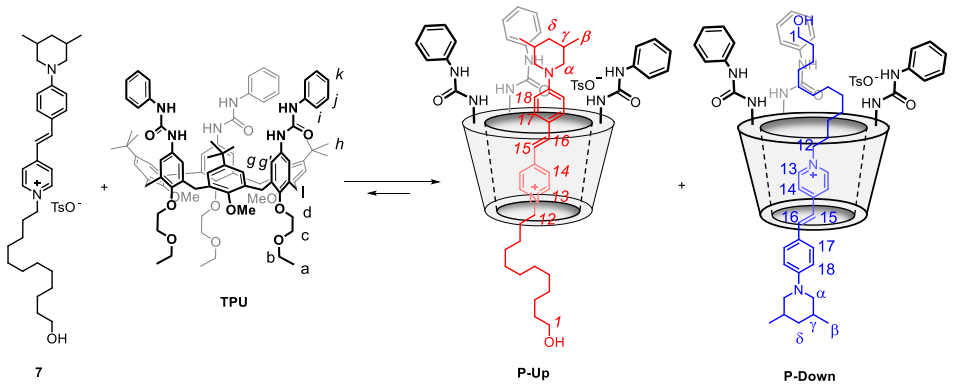

Scheme 4.2 Formation of [2]pseudorotaxanes **P-Up** and **P-Down**.

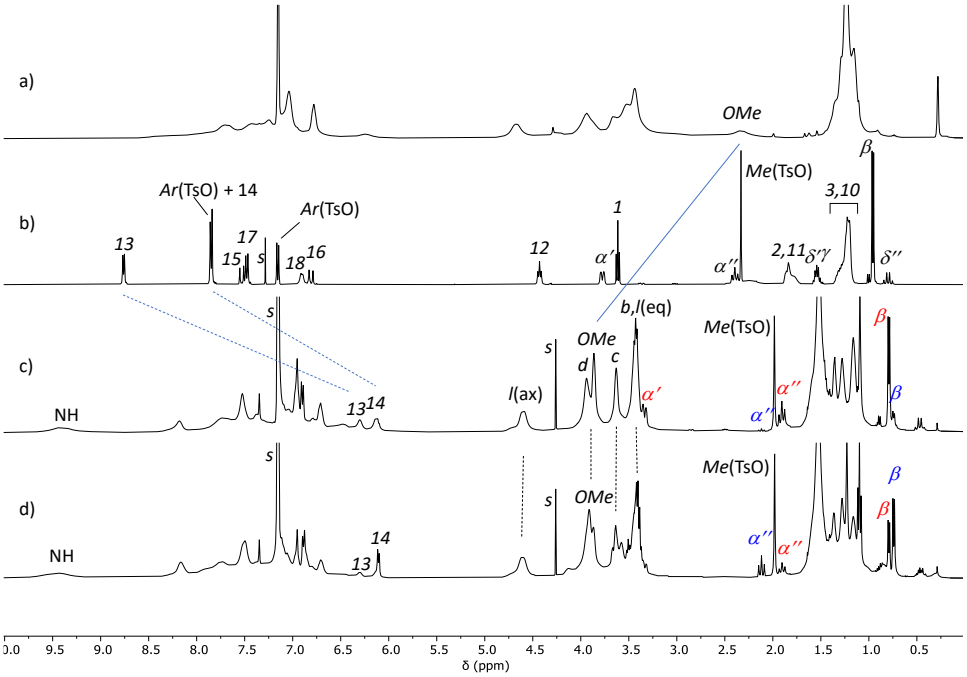

Figure 4.1 ^{1}H NMR spectra of (a) **TPU** (C_6D_6, 400 MHz) and (b) stilbazolium salt **7** (recorded in CD_3Cl for solubility reasons), and 1:1 mixture of **TPU** and **7** recorded (c) upon sample preparation, (d) at the equilibrium (C_6D_6, 400 MHz).

The stack plot gathered in Figure 4.1 compares the spectra of the separated compounds, i.e. **TPU** in (a) and stilbazolium **7** in (b), and the spectra of the mixture upon sample preparation (c) and after 2 hours of mixing (d). Some evidence of the complexation can be detected: the fluxionality of **TPU** in C_6D_6 is considerably reduced when involved in the complexation; NH signals, now engaged in hydrogen bonding with the tosylate, are downfield shifted at 9.4 ppm as a broad peak; the methoxy protons (O*Me*) of the calix[6]arene are significantly downfield shifted from 2.3 ppm to 3.85 ppm in spectra c and d (continuous blue line) with a sharpening of the peak. The latter shift indicates they are no longer oriented inward to the cavity because of the guest threading. Aromatic protons of **7** are upfield shifted due to the shielding effect of the cavity (dashed blue lines): pyridinium protons *13* and *14* resonate at 6.3 and 6.1 ppm, respectively. Moreover, it can be noticed that the guest signals are generally upfield shifted

thanks to the complexation inside the calix[6]arene. Still, most significant is the presence of two series/patterns of guest dimethylpiperidine signals, corresponding to different orientational pseudorotaxanes (in red for **P-Up** and blue for **P-Down**): two easily detectable doublets at 0.74 and 0.79 ppm correspond to methyl groups β in **P-Up** and **P-Down** pseudorotaxanes, respectively; the axial proton in α position is at 2.12 ppm in the **P-Down** isomer and 1.91 ppm in the **P-Up** isomer. Upon mixing the components (spectrum c), isomer **P-Up** is clearly prevalent over **P-Down** isomer (ratio at time ca. 0 of 82:18 Up/Down). Thus, **P-Up** is kinetically favoured. The most evident diagnostic signals are the methyl groups (*β*) and the CH_2 (*α*) of the dimethylpiperidine group, from which the signals can be integrated. The system reached equilibrium after ca. 2 hours, as the ratio of the two pseudorotaxanes did not change after this time. At the equilibrium (spectrum d), the kinetically less favoured isomer is the most favoured thermodynamically (ratio of 42:58 Up/Down). The assignment of the isomer orientation was achieved through subsequent NMR studies of separated rotaxanes (*vide infra*). As soon as the formation of the pseudorotaxanes was confirmed, the synthesis of rotaxanes was pursued (Scheme 4.3). So, axle **7** was equilibrated at room temperature in toluene with the wheel for two hours. After two hours, diphenylacetyl chloride and triethylamine were added to the reaction mixture, and the solution was stirred at room temperature overnight.

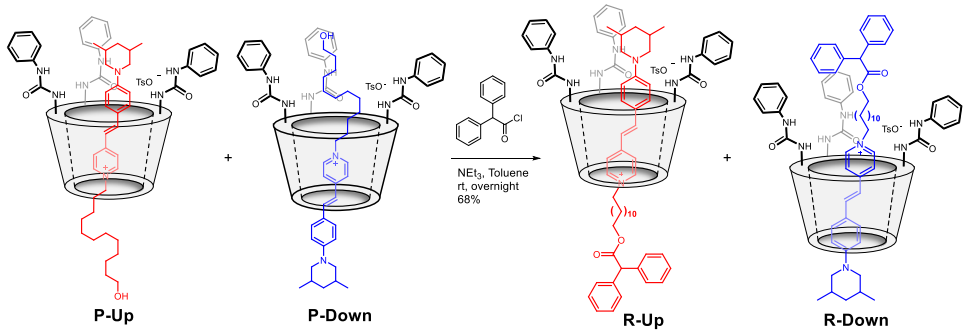

Scheme 4.3 Synthesis of stilbazolium-based [2]rotaxanes **R-Up** and **R-Down**.

Chromatographic purification led to the mixture of the two rotaxane orientational isomers, with an overall yield of 68%. The mixture was then separated by TLC using dichloromethane/methanol 9:5 mixture as the eluent, affording a bright orange solid (31% yield, Rf = 0.42) and a bright yellow one (37% yield, Rf = 0.50) in a 45:55 ratio. The success of the reaction was first demonstrated with high-resolution mass spectrometry. Considering the error of this technique, both isomers display identical mass spectra: the "orange" isomer gives rise to a singly-charged molecular ion at m/z = 2137.26416 (z = 1), which corresponds to the rotaxane having lost its tosylate anion and to a doubly charged one at m/z = 1069.13538 (z = 2). Similarly, in the spectrum obtained from the "yellow" isomer, the singly charged peak can be observed at m/z = 2137.26392 (z = 1), while the doubly charged one at m/z = 1069.13489 (z = 2).

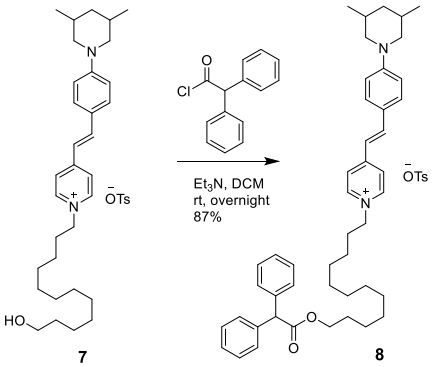

Scheme 4.4 Synthesis of **8**.

The formation of the rotaxanes was further confirmed through a series of 1D and 2D NMR experiments (see Experimental Section for the complete signal assignment, Figure 4.13 for **R-Up** and 4.14 for **R-Down**). These measurements, as usual, were also used to establish the orientation of the axle in the respective isolated isomers. The ^{1}H NMR spectra of the "orange" and "yellow" isomers, Figures 4.2c and 4.2d, respectively, were compared with the spectra of the pristine pseudorotaxanes mixture (Figure 4.2b) and the free dumbbell **8** (Figure

4.2a). This latter is a stilbazolium salt (**8**) endowed with a diphenylacetyl stopper on its alkyl chain. It was prepared in 87% yield by reacting the stilbazolium salt **7** with diphenylacetyl chloride in the presence of triethylamine in dichloromethane (see Scheme 4.4).

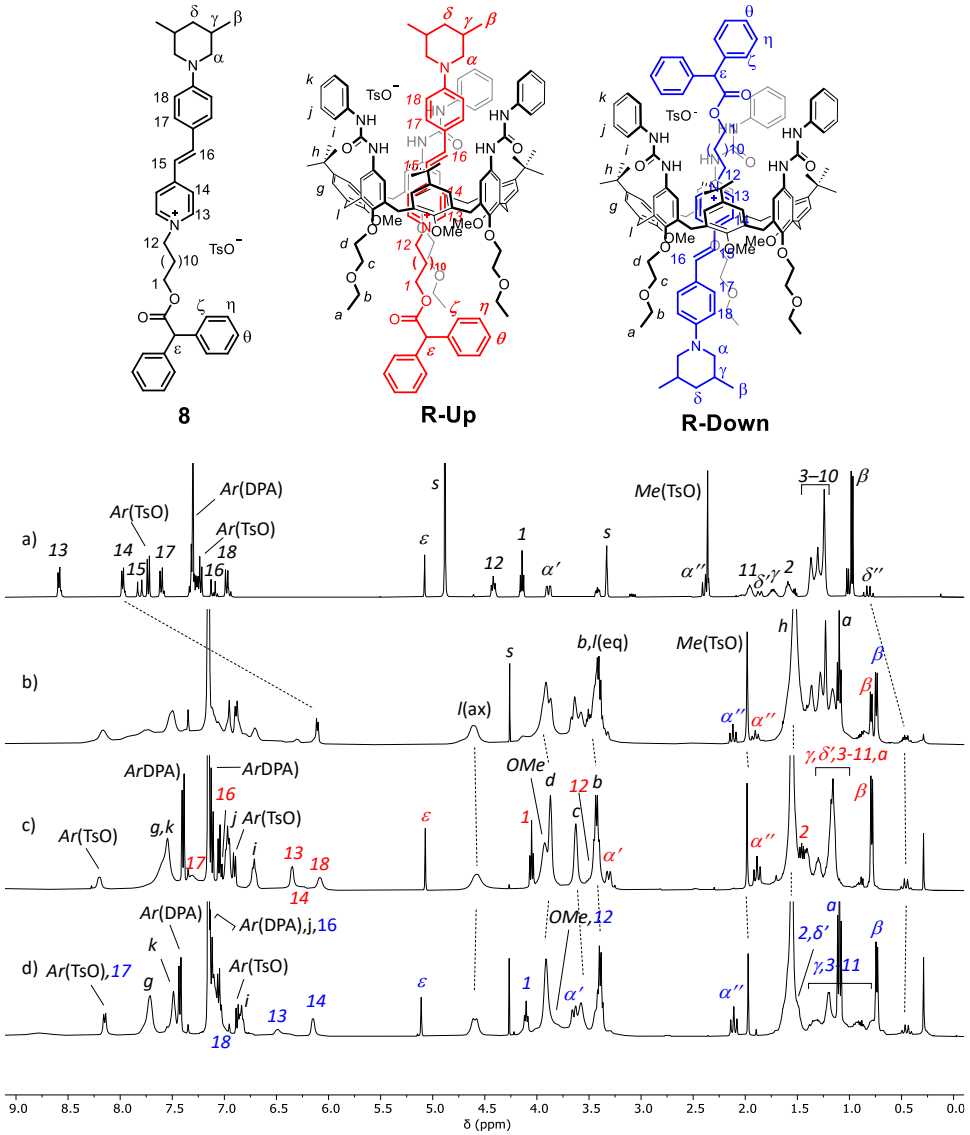

Figure 4.2 ^{1}H NMR stack plot (400 MHz) of (a) dumbbell **8**, (b) ca. 1:1 mixture of orientational pseudorotaxane isomers **P-Up** and **P-Down**, (c) rotaxane **R-Up**, and (d) rotaxane **R-Down**. All the spectra were taken in C_6D_6 except **8,** which was recorded in $CDCl_3$ for solubility reasons.

At first glance, the ^{1}H NMR spectra in C_6D_6 of the two rotaxane isomers showed similar features to those found in the pseudorotaxanes' mixture (cf. spectra *c* and *d* with *b* in Figure 4.2). However, the better signal resolution in *c* and *d* than in *b* indicates a calix[6]arene scaffold rigidification deriving by the axle blocking. The most important evidence of the occurred stoppering reaction can be attributed to the sharp signal at 5.1 ppm, labelled as *ε*, in spectra *c* and *d*, which is assigned to the methine proton of diphenylacetate stopper. The presence of a more crowded aromatic region sustains this hypothesis.

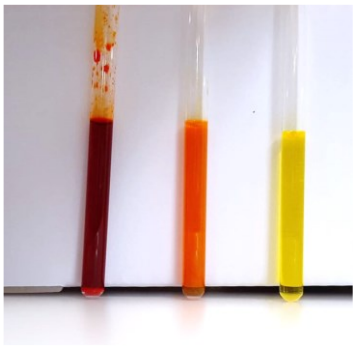

Figure 4.3 Picture of NMR tubes of dumbbell **8** (red), **R-Up** (orange) and **R-Down** (yellow).

To understand the axle orientation, in the beginning, we focused our attention on the dimethylpiperidine unit since it has characteristic signals in the aliphatic region which shift noticeably when the group is located near the three phenylureido moieties as in the isomer **R-Up**, or near the ethoxyethyl chains at the **TPU** lower rim as in the isomer **R-Down** (see Figure 4.2). As a result, the most visible difference between spectra *c* and *d* can be noticed in the signal of the CH_2 protons labelled *α*: in spectrum *c*, the equatorial proton *α*' resonates at 3.3 ppm, and the axial proton *α*'' at 1.9 ppm, whereas in spectrum *d* we can find the equatorial proton *α*' at 3.6 ppm and the axial *α*'' at 2.1 ppm. Considering that the phenylureas exert a shielding effect while the ethoxyethyl chains no, we presumed that spectrum *c* (orange isomer) corresponded to the **R-Up** isomer, as

the *α*' and *α*'' signals are more upfield-shifted. On the other hand, the spectrum *d* (yellow isomer) was assigned to the **R-Down** isomer since the above signals are more deshielded. The same behaviour can be noticed in the stilbazolium alkyl chain: if we assume that spectrum *c* corresponds to the **R-Up** isomer, the alkyl chain resonates between 1.5 and 1.15 ppm, while in spectrum *d* it is upfield shifted and found between 1.5 and 0.7 ppm, as these protons are less shielded in comparison with the **R-Up** isomer. It should be remarked that all the above assignments were made with the help of several 2D NMR experiments, especially TOCSY.

Finally, two tests were performed to verify the capability of the dimethyl piperidine group to act as a stopper and ensure that the stilbazolium cation cannot slip away from the **TPU** cavity. First, a stoichiometric amount of dumbbell **8** and **TPU** was dissolved in toluene and stirred at 70°C for 2 days. After this time, a ^{1}H NMR measurement and a thin layer chromatography were carried out, revealing only the presence of the two original components with no formation of any new compound. This result evidences that the dimethyl piperidine group is too bulky to permit the threading of the stilbazolium "dumbbell" into the cavity of **TPU**. In a second experiment, the rotaxanes' stability was probed by stirring them in methanol. In fact, it is known that polar solvents like methanol can disrupt the complexation by separating the interacting components if they are not interlocked together, as in the case of pseudorotaxanes. As expected, after stirring the rotaxanes' solutions in methanol for three hours, **R-Up** and **R-Down** did not dissociate, as verified by ^{1}H NMR and thin-layer chromatography. These outcomes confirm that dimethylpiperidine acts as a stoppering group; thus, **R-Up** and **R-Down** really behave as rotaxane structures.

Our hypothesis was confirmed by X-ray diffraction analysis. The slow evaporation of toluene/hexane solution of **R-Down** afforded yellow prismatic crystals, suitable

for X-ray diffraction measurement. The structural resolution confirmed unambiguously the down orientation of the stilbazolium axle (Figure 4.4), in accordance to previously reported NMR studies. The asymmetric unit includes one **TPU** molecule, one disordered stilbazolium axle **8** and one disordered tosylate. An accurate modelling of the crystallization solvent was not possible, and the residual electron density was consequently removed by the program MASK. Two penylureido arms of **TPU** are engaged in hydrogen bond interactions with tosylate counterion, with the donor-acceptor distances NH···$O_{tosylate}$ ranging from 2.74 to 2.98Å (Figure 4.4).

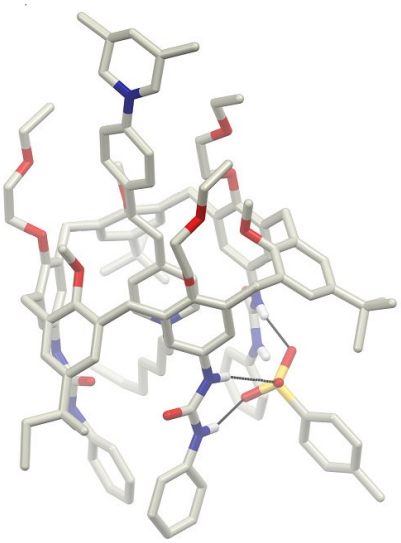

Figure 4.4 X-ray molecular structure of rotaxane **R-Down** with a partial labelling scheme, showing the hydrogen bond interactions between the N–H groups of phenylureido moieties and the oxygens of tosylate anion.

The remaining phenylureido arm is involved in hydrogen bond intermolecular interactions with neighbouring host molecules: N14···O32, 2.94 Å and N24···O32, 3.01 Å, giving rise to the crystal packing arrangement (Figure 4.5).

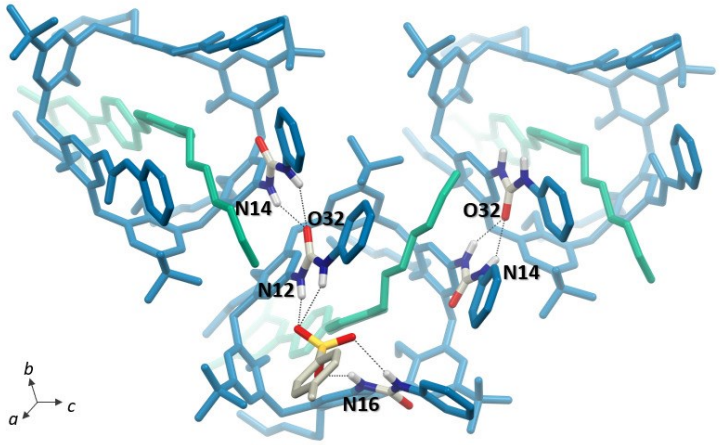

Figure 4.5 Packing and intermolecular hydrogen bond interactions between neighbouring rotaxanes (green colour for stilbazolium guest, light blue colour for **TPU**).

The supramolecular structure is also stabilized by means of several weak interactions. Two methoxy groups participate in weak CH---O interactions with hydrogen atoms attached to the pyridine, with distances ranging from 3.03 to 3.46 Å. Moreover, the ureido oxygen O34 displays a short contact with one of the CH2 hydrogens belonging to the dodecyl chain (Figure 4.6b), with a CH···O_{ureido} distance of 3.26 Å. The pyridine ring of the stilbazolium axle interacts with the macrocycle walls both through C-H···π interactions, (C2A···C04, 3.60 Å and C1A···*centroid 1*, 3.66 Å) and π···π stacking with one phenyl ring of the host wheel ($C_{pyridine}$···*centroid 2*, 3.30 Å and C_{phenyl}···*centroid 3*, 3.42 Å), as highlighted in Figure 4.6a,c.

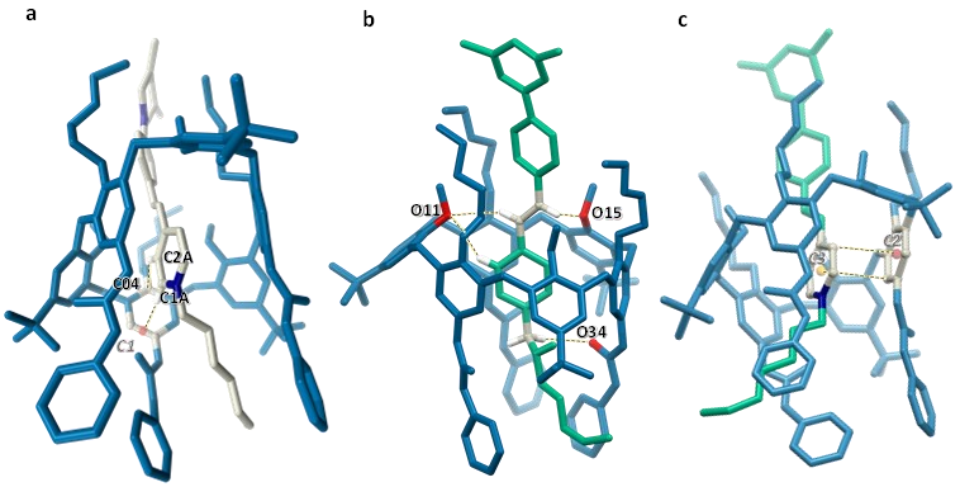

Figure 4.6 Weak host-guest interactions for rotaxane **R-Down**: a) CH---π, b) CH---O, c) π---π stacking interactions (tosylate anion is omitted for clarity).

Photophysical characterisation

The optical properties in solution of **8**, **R-Up** and **R-Down** were evaluated in toluene. The absorption spectrum of dumbbell **8** was demonstrated to be affected by the concentration of **8** itself. The peak maximum was observed around 470 nm at micromolar concentrations, gradually shifting towards shorter wavelengths when more concentrated. This influence is reasonably due to the equilibrium between the stilbazolium cation and the counterion, as already observed in similar stilbazolium salt systems.[23] In fact, upon the addition of an excess of tetrabutylammonium tosylate, the band experienced a blueshift of the maximum. The ion-pair constant was evaluated to be 2.0×10^5 M^{-1}.

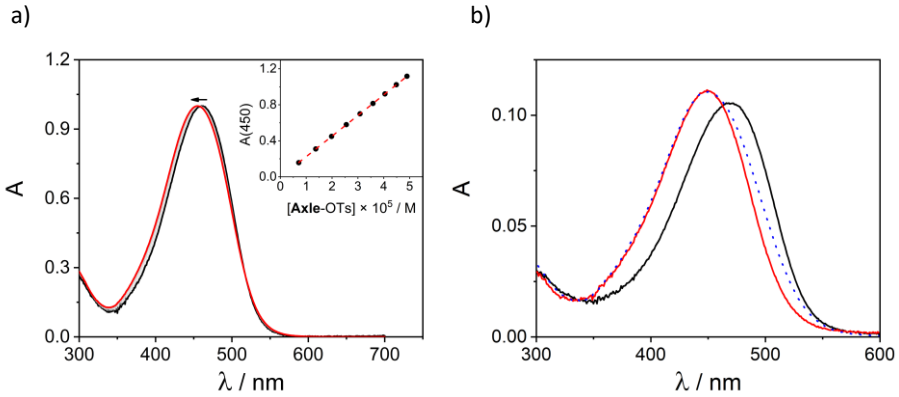

Figure 4.7 normalised absorption spectra of dumbbell **8** from 7 µM (black line) to 49 µM (red line) recorded in toluene; inset: absorption at different concentrations of **8** at 450 nm (a); absorption spectra of **8** (5 µM, black line), and after the addition of an excess of TBAOTs (red line) (b).

The ion pair influences the emission properties of dumbbell **8**, as well. The emission band undergoes redshift with the formation of the ion-pair, and simultaneously an increment of the emission quantum yield is detected. For this reason, emission properties of **8** were recorded with an excess of the tosylate in order to have only the ion-pair species in solution. In these conditions, the absorption band of **8** displays the maximum at 450 nm and its emission band is at 618 nm with a fluorescence quantum yield of ϕ_f= 18 %.

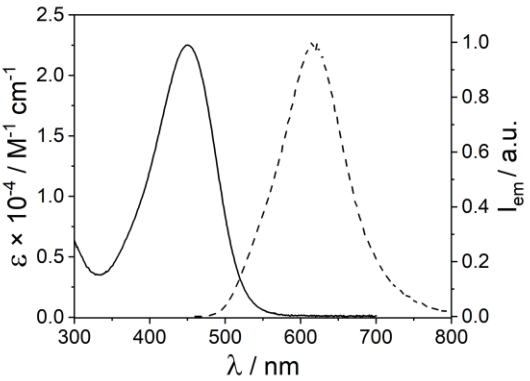

Figure 4.8 Absorption (continuous line) and emission spectra (dashed line) of **8** recorded in toluene.

Differently from dumbbell **8**, the optical properties of interlocked [2]rotaxanes are not influenced by the concentration, thanks to the encapsulation of the stilbazolium unit inside the macrocycle cavity. In the absorption spectra, they exhibit only the band corresponding to the stilbazolium unit, and it depends on the presence of the calix[6]arene and its relative orientation in relation to the stilbazolium element.

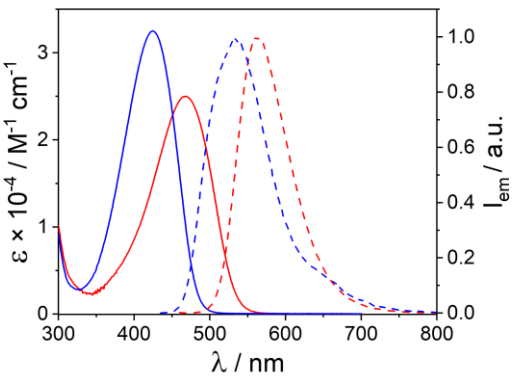

Figure 4.9 Absorption (continuous line) and emission spectra (dashed line) of **R-Up** (red lines) and **R-Down** (blue lines) recorded in toluene.

The absorption band of **R-Up** is centred at 468 nm, while the band of **R-Down** at 425 nm. The effect of the encapsulation is even more marked in the emission features. In comparison with dumbbell **8**, both [2]rotaxanes present a blue shifted emission band and smaller Stokes shifts. Also in emission, the band of **R-Up** (centred at 561 nm) is more redshifted than the one of **R-Down**, at 533 nm. Furthermore, the fluorescent emission quantum yield remarkably increases from 18% for **8** and 20% for **R-Down** to a very intense emission of ϕ_f= 83% for **R-Up**.

Table 4.1 Optical properties of the investigated compound in toluene. [a]Data recorded with an excess of tosylate counterion.

Compound	λ_{abs} (nm)	λ_{em} (nm)	ϕ_f
8	450[a]	618[a]	18%[a]
R-Up	469	561	83%
R-Down	425	533	20%

The qualitative interpretation of the encapsulation effects on the stilbazolium spectroscopic properties is not straightforward; however, we suggest the following explanation: it is already known that the push-pull structure of the stilbazolium ions is very sensitive to the environment and displays negative solvatochromism,[24] as a blue-shifted absorption is observed when the polarity of the solvent increases. In this regard, the non-palindromic calix[6]arene host is characterised by different groups at the rims, which render the upper rim the most polar part, and the lower rim the less-polar side. The orientation of the nonsymmetric calix[6]arene with respect to the stilbazolium push-pull structure produces a different environment. Therefore, in **R-Down** the calix[6]arene induces a more polar environment to the stilbazolium unit than in **R-Up**. In addition, stilbazolium fluorescence is favoured when the molecular rotations are limited by a rigid environment, which avoids non-radiative relaxations.[25,26] Thus, the exceptional enhancement of the emission in **R-Up** can be accounted for a deeper encapsulation of the stilbazolium and/or more rigid conditions.

The effect of the orientation on the spectroscopic properties of the stilbazolium salt was also examined in the solid state. Indeed, it is well known that the encapsulation of fluorophores into a rigid matrix, such as macrocycles[14,15] or organic molecular frameworks,[16,27] enhances the fluorescent properties in the solid state by avoiding the aggregation-caused quenching effect (ACQ).[28] As in

solution, also in the solid state, absorption and emission properties are influenced by the encapsulation and by the orientation of the calix[6]arene host (Table 4.2). The solid films were prepared by dropcasting the dichloromethane solutions of dumbbell **8** and the two rotaxane isomers (10^{-4} to 10^{-3} M) on quartz slides. After solvent evaporation and drying, the resulting films were analysed by transmission UV-Vis spectroscopy. The solid samples meant to be analysed by luminescence spectroscopy were instead prepared by placing the solid compounds between two glass slips.

The most remarkable feature is the emission quantum yield: **8** displays a very weak quantum yield of 1% due to the ACQ effect; the inclusion of the stilbazolium within the calix[6]arene cavity enhances the fluorescence up to 11% in **R-Up** and 32% in **R-Down**. The higher emission quantum yield of **R-Down** with respect to **R-Up** is probably related to the rotaxane structure in solid state.

Table 4.2 Optical properties of the investigated compound in solid state.

Compound	λ_{abs} (nm)	λ_{em} (nm)	ϕ_f
8	459	613	1%
R-Up	463	587	11%
R-Down	440	576	32%

Photochemical characterisation

As previously mentioned, the photoisomerisation process is one of the non-radiative relaxation pathways that strongly affect the spectroscopic properties of stilbazolium dyes.[17] To get more insight into our system, this process was evaluated for dumbbell **8** and both [*2*]rotaxanes using UV-Vis spectroscopy. *E-Z* photoisomerisation of **8** was investigated by irradiating at 436 nm a solution of **8** in toluene in the presence of an excess of tosylate counterion in order to have

only the ion-paired species in solution (the same condition used for the photophysical characterisation). Upon irradiation, the absorption band experiences a moderate decrease in intensity. This outcome was attributed to the photoisomerisation *E-Z* reaction. The starting situation' restoration was observed within a few hours after maintaining the solution in the dark (thermal back isomerisation).

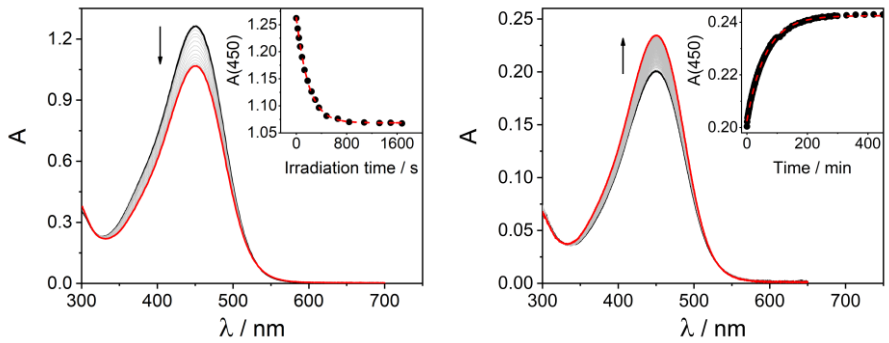

Figure 4.10 Time-dependent absorption spectra of a solution of *E*-**8** in toluene (5.5 × 10-5 M, black to red lines) upon irradiation at 436 nm. Inset: Absorption changes at 450 nm (right). Time-dependent absorption spectra of a solution of **8** in toluene (1.0 × 10-5 M, black to red lines) during thermal back isomerisation process. Inset: Absorption changes at 450 nm (black dots) (left).

The photoisomerisation quantum yields of *E to Z* and *Z to E* processes were calculated fitting the photokinetic profile: **8** showed $\phi_{E\rightarrow Z}$ of 14% and $\phi_{Z\rightarrow E}$ of 42%. The encapsulation and the orientation of **8** within the calix[6]arene macrocycle are responsible once again for the modification of the outcome. Upon irradiation of a toluene solution, **R-Up** displayed lower photoisomerisation conversion, with a quantum yield of the process $\phi_{E\rightarrow Z}$ = 7%. This is consistent with the photophysical results, in which **R-Up** has a very high fluorescence quantum yield, thus the other relaxation pathways must be less pronounced. The complete thermal back isomerisation was observed in a few hours.

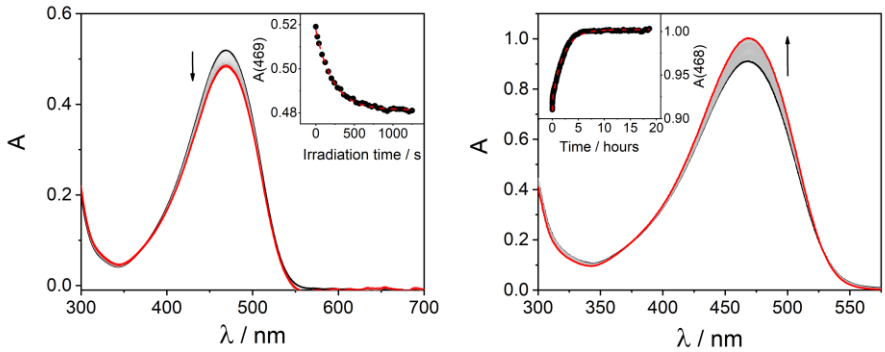

Figure 4.11 Time-dependent absorption spectra of a solution of *E*-**R-Up** in toluene (2.1 × 10-5 M, black to red lines), upon irradiation at 436 nm. Inset: Absorption changes at 469 nm (right). Time-dependent absorption spectra of a solution of **R-Up** in toluene (4.0 × 10-5 M, black to red lines), during thermal back isomerisation process. Inset: Absorption changes at 468 nm (black dots) (left).

Surprisingly, the irradiation of the solution of **R-Down** in toluene led to a remarkably higher photoisomerisation quantum yield, $\phi_{E\rightarrow Z}$ = 36%. Moreover, it was observed that the **R-Down** thermal back isomerisation is intensely slower than **8** and **R-Up**.

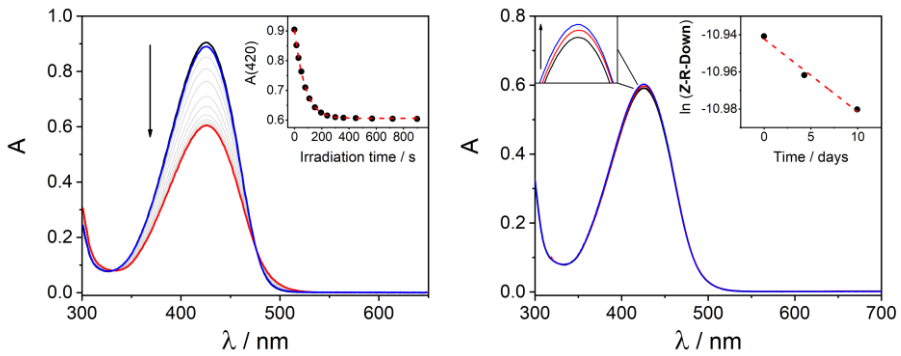

Figure 4.12 Time-dependent absorption spectra of a solution of *E*-**R-Down** in toluene (2.8 × 10-5 M, black to red lines) upon irradiation at 436 nm. Inset: Absorption changes at 425 nm (right). Time-dependent absorption spectra of a solution of **R-Down** in toluene (2.8 × 10-5 M, black to red lines) during thermal back isomerisation process. Inset: concentration changes over time of *Z* isomer (black dots) (left).

The exhaustive conversion from *Z* to *E* isomers was achieved by irradiating the solution rich in *Z* isomer at 546 nm, where the absorption of *E* isomer is approximately not present. In such a manner, a controlled switching from *E* to *Z* isomers, and the backward process from *Z* to *E*, was accomplished by irradiating **R-Down** solution first at 436 nm and then at 546 nm.

Table 4.3 Photochemical properties of the investigated compound in toluene. [a]Data recorded with an excess of tosylate counterion.

Compound	ϕ_{E-Z}	ϕ_{Z-E}	$K_{thermal}$ (s^{-1})
8[a]	14%	42%	3×10^{-4}
R-Up	7%	71%	1×10^{-4}
R-Down	36%	41%	$\sim 10^{-7}$

Once again, the orientation of the calix[*6*]arene macrocycle strongly influences the stilbazolium properties. To summarise, an exceptional enhancement of the photophysical properties was observed for **R-Up**, while the other orientation of **R-Down** promoted the photoisomerisation conversion, as in this case the *Z* isomer is more kinetically favoured. These outcomes seem to further justify the hypothesis of a different polar and/or rigid environment created by the calix[6]arene cavity in the two isomers.

Conclusions

In this chapter, the synthesis of stilbazolium-based [2]rotaxanes has been reported. The ability of stilbazolium salts to thread calix[6]are **TPU** from both rims led to the formation of two orientational [2]pseudorotaxane isomers, which were then blocked to form mechanically interlocked [3]rotaxanes. The orientation was assigned *via* NMR analysis and X-ray diffraction, which confirmed the rotaxanes structures. In addition, the separation of the two orientational isomers **R-Up** and

R-Down allowed the study of their photophysical and photochemical properties both in solution and in the solid state. Remarkably, the orientation deeply affects the stilbazolium properties, as the isomers exhibit different and complementary features. Indeed, **R-Up** is characterised by a strong emission quantum yield (ϕ_f = 83%) and a very low photoisomerisation, as the radiative decay of the excited state is prevalent. On the other hand, **R-Down** has opposite features, showing moderate fluorescence (ϕ_f = 20%) and considerable photoisomerisation properties. This orientation-depending system allows to select the suitable property (fluorescence or photoisomerisation) in function of the desired application.

Acknowledgments

Thanks to Leonardo Andreoni and Prof. Serena Silvi (University of Bologna) for the spectroscopical measurements. Thanks to Dr. Davide Balestri (University of Parma) for X-ray diffraction measurements.

Experimental Section

General Methods

All solvents were dried using standard procedures; all other reagents were of reagent-grade quality obtained from commercial suppliers and used without further purification. Melting points are uncorrected. NMR spectra were recorded at 400 MHz for ^{1}H and 100 MHz for ^{13}C. Chemical shifts are expressed in ppm (d) using the residual solvent signal as an internal reference (7.26 ppm for $CHCl_3$, 7.16 ppm for C_6D_5H, 5.32 for $CHDCl_2$ and 3.31 ppm for CD_2HOD). The terms m, s, d, t and q represent multiplet, singlet, doublet, triplet and quadruplet, respectively;

the term "br. s" means a broad signal. Mass spectra were recorded in the ESI mode. Compounds **3**[22] and **5**[29] were synthesised according to published procedures.

Synthetic Procedure and Analytical Data

6: In a two necks round-bottomed flask, picoline (1.018 mmol, 1.0 equiv), and 1,12-dodecanediol mono(4-methylbenzenesulfonate) **5** (1.12 mmol, 1.1 equiv) were dissolved in about 20 ml of dry acetonitrile under inert atmosphere. The reaction mixture was refluxed for two days. Afterwards, the solution was evaporated to dryness under reduced pressure. The solid residue was recrystallised from ethyl acetate to afford **6** (0.37 g) in 81 % yield as a white solid. **M. p.**= 100 − 102 °C. **^{1}H NMR** (CD_3OD, 400 MHz): δ = 8.78 (d, 2H, *J* = 6.3 Hz), 7.90 (d, 2H, *J* = 6.3 Hz), 7.70 (d, 2H, *J* = 6 Hz), 7.23 (d, 2H, *J* = 6 Hz), 4.53 (t, 2H, *J* = 6.6 Hz), 3.54 (t, 2H, *J* = 6.64 Hz), 2.66 (s, 3H), 2.37 (s, 3H), 1.99 (m, 2H), 1.53 (m, 2H), 1.40-1.26 (m, 16H) ppm. **^{13}C NMR** (CD_3OD, 100 MHz): δ = 159.78, 143.43, 142.30, 140.24, 128.48, 128.44, 125.57, 61.59, 60.79, 32.27, 30.97, 29.34, 29.26, 29.21, 29.10, 28.71, 25.76, 25.56, 20.55, 19.94. **ESI-MS**: *m/z* $[M\text{-}OTs]^+$ calcd. for $C_{18}H_{32}NO$: 278.25; found: 278.4.

7: in a two necks round-bottomed flask, **3** (0.534 mmol, 1.2 equiv) and **6** (0.455 mmol, 1.0 equiv) were dissolved in about 10 ml of methanol under an inert atmosphere. Then, piperidine (0.667 mmol, 1.5 equiv) was added, and the reaction mixture was refluxed overnight. Afterwards, the solution was evaporated to dryness under reduced pressure, and the solid residue was recrystallised from ethyl acetate to afford 0.25 g of **7** as a red solid (86%). **M. p.** = 151 - 153°C. **^{1}H NMR** ($CDCl_3$, 400 MHz): δ = 8.74 (d, 2H, *J* = 6.5 Hz), 7.83 (d, 4H, *J* = 8.2 Hz), 77.51 (d, 1H, *J* = 16 Hz), 7.45 (d, 2H, *J* = 8.7 Hz), 7.13 (d, 2H, *J* = 8 Hz), 6.88 (d, 2H, *J* = 8.3 Hz), 6.78 (d, 1H, *J* = 16 Hz), 4.40 (t, 2H, *J* = 7.4 Hz), 3.75 (d, 2H, *J* = 11.0), 3.59 (t, 2H, *J* = 6.7), 2.37 (t, 2H, *J* = 12 Hz), 2.31 (s, 3H), 1.90 - 1.70 (m,

3H), 1.52 (m, 2H), 1.36 – 1.12 (m, 18H), 0.93 (d, 6H, *J* = 6.5 Hz), 0.78 (q, 1H, *J* = 12 Hz) ppm. **^{13}C NMR** ($CDCl_3$, 100 MHz): δ = 153.82, 144.07, 143.81, 142.27, 139.27, 130.59, 128.75, 126.15, 123.28, 117.76, 114.94, 62.82, 60.47, 55.64, 42.16, 32.88, 31.57, 30.63, 29.48, 29.39, 29.34, 29.28, 29.00, 26.09, 25.81, 21.45, 19.37. **ESI-MS**: *m/z* $[M\text{-}OTs]^+$ calcd. for $C_{32}H_{49}N_2O$: 477.38; found: 477.5.

8: triethylamine (9.5 µL, 68 µmol, 1.1 equiv) was added to a mixture of **4** (40 mg, 62 µmol, 1.0 equiv) and diphenylacetyl chloride (16 mg, 68 µmol, 1.1 equiv) in dry dichloromethane (2 mL, 0.03 M) under nitrogen at room temperature. The mixture was stirred at room temperature overnight. The mixture was concentrated under vacuum, and the crude was purified by flash column chromatography on silica gel (dichloromethane/methanol 90:10) to afford **8** (45 mg, 53 µmol, 87%) as a red waxy solid. **^{1}H NMR** (CD_3OD, 400 MHz): δ = 8.57 (d, 2H, *J* = 6.8 Hz), 7.96 (d, 2H, *J* = 7.0 Hz), 7.97 (d, 1H, *J* = 6 Hz), 7.71 (d, 2H, *J* = 8.2 Hz), 7.59 (d, 2H, *J* = 9.0 Hz), 7.32-7.22 (m, 10H), 7.21 (d, 2H, *J* = 7.9 Hz), 7.09 (d, 1H, *J* = 16.0 Hz), 6.96 (d, 2H, *J* = 9.0 Hz), 5.06 (s, 1H), 4.40 (t, 2H, *J* = 7.4 Hz), 4.12 (t, 2H, *J* = 6.5 Hz), 3.87 (m, 2H), 2.36 (t, 2H, *J* = 7.9 Hz), 2.34 (s, 3H),1.94 (m, 2H), 1.84 (m, 1H), 1.72 (m, 2H), 1.57 (m, 3H), 1.39-1.18 (m, 16H), 0.96 (d, 6H, *J* = 6.6 Hz), 0.80 (q, 1H, *J* = 12.1 Hz) ppm. **^{13}C NMR** (CD_3OD, 100 MHz): δ = 174.3, 156.2, 155.3, 154.3, 144.4, 143.9, 143.7, 141.6, 140.3, 131.6, 129.8, 129.7, 129.5, 128.2, 126.9, 125.5, 123.9, 118.6, 115.7, 71.9, 66.2, 61.3, 58.3, 56.3, 55.4, 43.5, 32.2, 31.8, 30.7, 30.6, 30.5, 30.5, 30.4, 30.1, 30.1, 29.6, 28.7, 27.3, 27.1, 26.9, 21.3, 19.5, 19.0. **ESI-MS**: *m/z* $[M\text{-}OTs]^+$ calcd. for $C_{46}H_{59}N_2O_2$: 671.45; found: 671.3.

Rotaxanes: In a two necks round-bottomed flask, **7** (0.123 mmol, 1.0 equiv), and **TPU** (0.185 mmol, 1.5 equiv) were dissolved in about 1.5 ml of dry toluene and left equilibrating under magnetic stirring for 2 hours at room temperature. Afterwards, diphenyl acetyl chloride (0.136 mmol, 1.1 equiv) and triethylamine (0.136 mmol, 1.1 equiv) were added to the solution, and the reaction mixture was

stirred at room temperature overnight. After this period, the solvent was evaporated under reduced pressure, and the solid residue was purified by column chromatography on silica gel (*n*-hexane/ethyl acetate = 70:30), obtaining a mixture of two orientational isomers, with an overall yield of 68%. Next, the two orientational isomers were separated through thin plate chromatography (dichloromethane/methanol= 96:4) to afford 0.132 g of **R-Up** isomer as an orange solid (31%) and 0.163 g of **R-Down** isomer as a yellow solid (37%).

R-Up: **M. p.** = 134 – 136 °C. **^{1}H NMR** (C_6D_6, 400 MHz): δ = 8.20 (d, 2H, *J* = 7.6 Hz), 7.66 – 7.48 (bs, 4H), 7.40 (d, 2H, *J* = 7.2 Hz), 7.31 (bs, 1H), 7.12 (d, 2H, *J* = 7.64 Hz), 7.05 (d, 2H, *J* = 7.26 Hz), 7.02 (bs, 1H), 6.97 (bs, 2H), 6.35 (d, 2H, *J* = 5.90 Hz), 6.08 (bs, 2H), 5.07 (s, 1H), 4.58 (bs, 6H), 4.05 (t, 2H, *J* = 6.75 Hz), 3.92 (bs, 9H), 3.87 (bs, 6H), 3.63 (bs, 6H), 3.43 (q, 6H, *J* = 7 Hz), 3.32 (m, 2H), 1.98 (s, 3H), 1.89 (t, 2H, *J* = 11.8 Hz), 1.55 (bs, 30H), 1.46 (m, 2H), 1.41 (m, 2H), 1.16 (bs, 13H), 0.79 (d. 6H, *J* = 6.40 Hz), 0.46 (q, 1H, *J* = 12.4 HZ) ppm. **^{13}C NMR** (C_6D_6, 100 MHz): δ = 172.29, 154.43, 153.17, 151.90, 149.09, 147.72, 143.72, 140.60, 139.55, 136.89, 133.84, 132.78, 130.40, 129.33, 129.08, 128.87, 128.74, 127.49, 126.89, 124.86, 121.99, 121.48, 119.14, 118.65, 114.70, 72.70, 70.48, 66.70, 65.09, 61.16, 57.70, 55.47, 42.48, 34.73, 31.92, 31.24, 30.94, 30.56, 30.41, 30.11, 29.73, 29.64, 28.95, 26.18, 21.17, 19.49, 15.59. **HR-MS** (ESI, Orbitrap LQ) calculated for $C_{136}H_{167}N_8O_{14}$ [M-OTs]: m/z (z = 1): 2136.25963, 2137.26298, 2138.26634, 2139.26969, 2140.27305; found: 2136.26099, 2137.26416, 2138.26733, 2139.27026, 2140.27271; calculated for $C_{136}H_{168}N_8O_{14}$ [M-OTs+H]: m/z (z = 2): 1068.63345, 1069.13513, 1069.63681, 1070.13848, 1070.64016; found: 1068.63391, 1069.13538, 1069.63672, 1070.13831, 1070.64014.

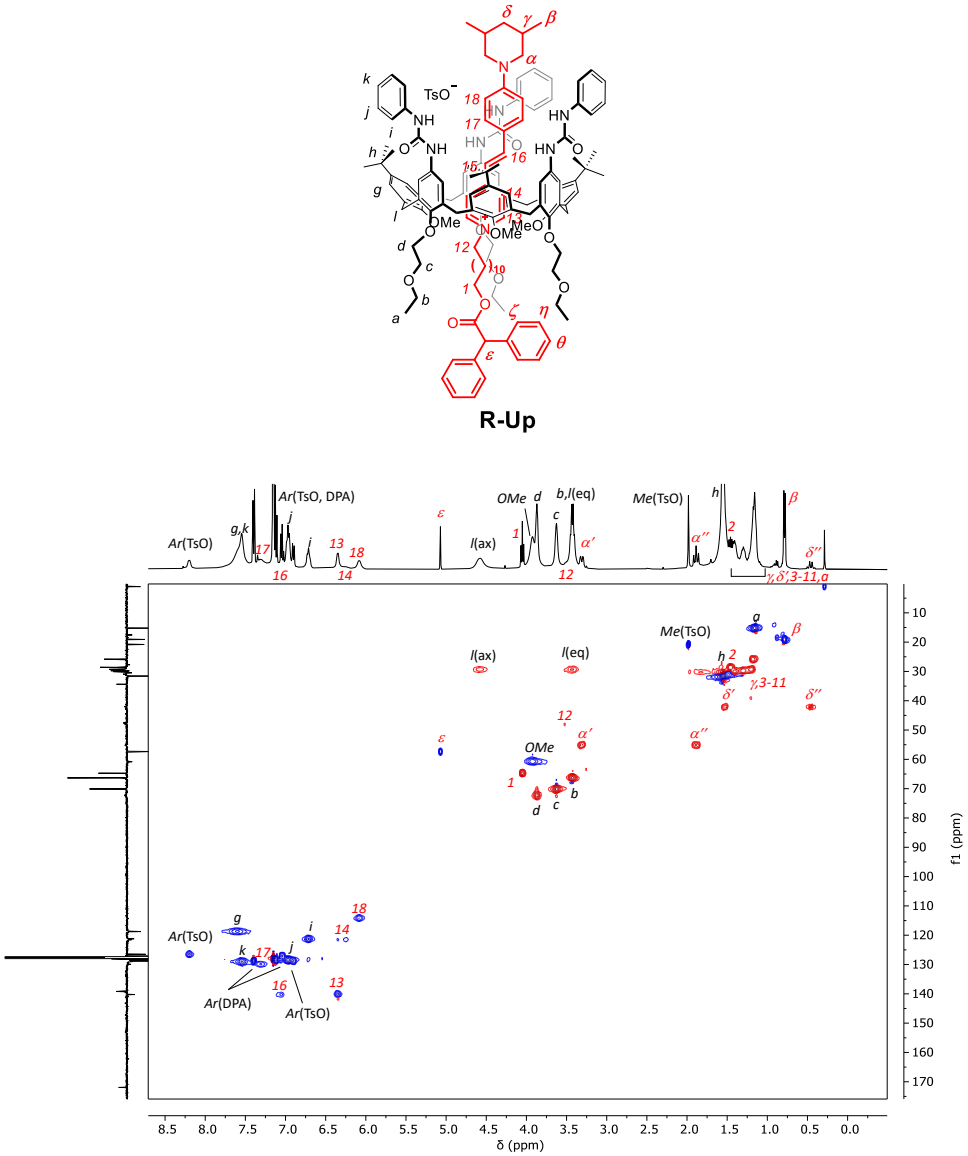

Figure 4.13 Edited HSQC NMR spectrum (400 MHz, benzene-d_6) of **R-Up**.

R-Down: **M. p.** = 143 – 145 °C. **^{1}H NMR** (C_6D_6, 400 MHz): δ = 8.15 (d, 2H, *J* = 7.9 Hz), 8.07 (bs, 2H), 7.82 – 7.6 (bs, 6H), 7.58 (bs, 4H), 7.43 (d, 2H, *J* = 7.6 Hz), 7.19 – 6.93 (bs, 10H), 6.90 – 6.74 (bs, 6H), 6.49 (bs, 2H), 6.14 (bs, 2H), 5.11 (s, 1H), 4.59 (bs, 6H), 4.10 (t, 2H, *J* = 6.75 Hz), 3.91 (bs, 9H), 3.63 (bs, 12H), 3.40 (bs, 8H), 2.11 (t, 2H, *J* = 12 Hz), 1.97 (s, 3H), 1.72 - 1.34 (bs, 30H), 1.38 – 1.15 (bs, 6H), 1.10 (t, 2H, *J* = 6.96), 1.05 – 0.78 (bs, 10H), 0.74 (d, 6H, *J* = 6.40 Hz), 0.44 (q, 1H, *J* = 12.4 HZ) ppm. **^{13}C NMR** (C_6D_6, 100 MHz): δ = 172.37, 154.90, 153.48, 152.34, 149.87, 147.32, 143.23, 140.51, 140.07, 139.69, 139.27, 136.32, 134.47, 132.84, 130.34, 129.15, 129.09, 128.86, 127.43, 126.80, 123.34, 122.25, 119.15, 118.27, 155.55, 73.41, 70.56, 66.74, 65.44, 61.86, 57.75, 56.26, 42.24, 34.68, 31.99, 30.89, 30.40, 30.22, 29.90, 29.64, 29.08, 26.34, 23.17, 21.16, 19.32, 15.56, 14.38. **HR-MS** (ESI, Orbitrap LQ) calculated for $C_{136}H_{167}N_8O_{14}$ [M-OTs]: m/z (z = 1): 2136.25963, 2137.26298, 2138.26634, 2139.26969, 2140.27305; found: 2136.26074, 2137.26392, 2138.26733, 2139.27026, 2140.27319; calculated for $C_{136}H_{168}N_8O_{14}$ [M-OTs+H]: m/z (z = 2): 1068.63345, 1069.13513, 1069.63681, 1070.13848, 1070.64016; found: 1068.63345, 1069.13513, 1069.63681, 1070.13848, 1070.64016.

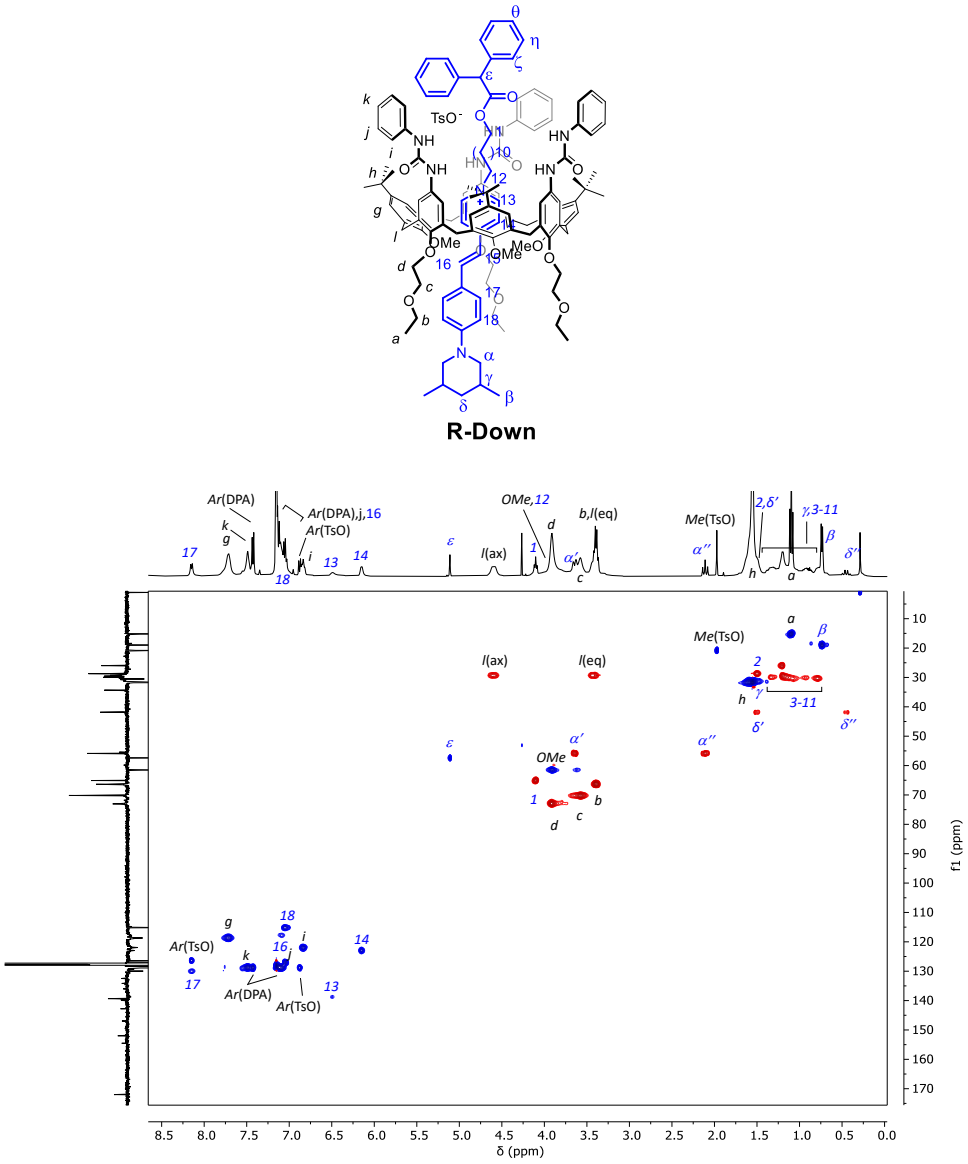

Figure 4.14 Edited HSQC NMR spectrum (400 MHz, benzene-d_6) of **R-Down**.

XRD measurements

Good quality crystals of rotaxane **R-Down** suitable for structural determination were obtained from the slow evaporation of a toluene/hexane solvent mixture. Single crystal XRD measurement was performed at low temperature (200K) with a Bruker Venture D8 diffractometer equipped with Photon II area detector, using a CuKα microfocus radiation source (λ = 1.54184). The data collection strategy was composed of a series of phi and omega scans in order to cover the sphere of reciprocal space. Data were indexed, integrated, and scaled using CrysAlis Pro software.[30] The structures were solved by the dual space algorithm implemented in the SHELXT code[31] in Olex2.[32] Fourier analysis and refinement were performed by the full-matrix least-squares methods based on F^2 implemented in SHELXL-2014.[33]

Table 4.4 Crystal data and structure refinement for **R-Down**.

Identification code	cu_FCB127_DOWN_LONG_DC
Empirical formula	$C_{126.11}H_{144.49}N_8O_{15}S$
Formula weight	2044.38
Temperature/K	200.00(10)
Crystal system	monoclinic
Space group	$P2_1/c$
a/Å	23.6388(8)
b/Å	40.7432(7)
c/Å	18.7852(5)
α/°	90
β/°	111.780(3)
γ/°	90
Volume/Å^3	16800.9(8)
Z	4
ρ_{calc}g/cm^3	0.808
μ/mm^{-1}	0.532

F(000) 4373.0
Crystal size/mm^3 0.15 × 0.07 × 0.05
Radiation Cu Kα (λ = 1.54184)
2Θ range for data collection/° 4.338 to 133.194
Index ranges -27 ≤ h ≤ 28, -48 ≤ k ≤ 48, -22 ≤ l ≤ 22
Reflections collected 127786
Independent reflections 29449 [R_{int} = 0.0845, R_{sigma} = 0.0504]
Data/restraints/parameters 29449/721/1339
Goodness-of-fit on F^2 1.368
Final R indexes [I>=2σ (I)] R_1 = 0.1490, wR_2 = 0.3957
Final R indexes [all data] R_1 = 0.1963, wR_2 = 0.4404
Largest diff. peak/hole / e Å^{-3} 0.82/-0.55

Absorption and Luminescence Spectra

UV-vis absorption and luminescence spectra were recorded with a Cary 300 (Agilent) spectrophotometer and a FS5 (Edinburgh) spectrofluorometer, respectively. Measurements were performed on air-equilibrated toluene (Sigma-Aldrich) solutions at room temperature. All the solutions were prepared and examined in a dark room only illuminated by red light in order to avoid undesired photoisomerisation of the investigated compounds. Luminescence quantum yields were determined using $[Ru(bpy)_3]Cl_2$ in water (ϕ_f=0.04) as standard. The quantum yields were determined at least on two different samples of the same compound and the values were averaged. Luminescence lifetimes were measured with a FLS920 (Edinburgh) time-correlated single-photon counting spectrofluorometer, exciting the sample at 405 nm with a pulsed laser.

Characterisation of solid compounds

Solid films of the investigated compounds were prepared by dropcasting dichloromethane solutions (10^{-4} to 10^{-3} M) on quartz slides. The dropcasted solutions were left drying and then put under vacuum for 16 h. The obtained films

were analysed by transmission UV-Vis spectroscopy. The solid samples meant to be analysed by luminescence spectroscopy were prepared by putting the solid compound between two glass slips.

References

[1] D. Wu, A. C. Sedgwick, T. Gunnlaugsson, E. U. Akkaya, J. Yoon, T. D. James, *Chemical Society Reviews* **2017**, *46*, 7105–7123.

[2] T. L. Mako, J. M. Racicot, M. Levine, *Chem. Rev.* **2019**, *119*, 322–477.

[3] J. Chan, S. C. Dodani, C. J. Chang, *Nature Chem* **2012**, *4*, 973–984.

[4] Z. Guo, S. Park, J. Yoon, I. Shin, *Chemical Society Reviews* **2014**, *43*, 16–29.

[5] S.-J. Zou, Y. Shen, F.-M. Xie, J.-D. Chen, Y.-Q. Li, J.-X. Tang, *Materials Chemistry Frontiers* **2020**, *4*, 788–820.

[6] O. Ostroverkhova, *Chem. Rev.* **2016**, *116*, 13279–13412.

[7] Z. L. Pianowski, *Chemistry – A European Journal* **2019**, *25*, 5128–5144.

[8] A. Goulet-Hanssens, F. Eisenreich, S. Hecht, *Advanced Materials* **2020**, *32*, 1905966.

[9] M. J. Fuchter, *J. Med. Chem.* **2020**, *63*, 11436–11447.

[10] S. Corra, M. Curcio, M. Baroncini, S. Silvi, A. Credi, *Advanced Materials* **2020**, *32*, 1906064.

[11] F. Lancia, A. Ryabchun, N. Katsonis, *Nat Rev Chem* **2019**, *3*, 536–551.

[12] L. Strekowski, *Heterocyclic Polymethine Dyes: Synthesis, Properties and Applications*, Springer, **2008**.

[13] J. N. Wilson, A. S. Brown, W. Michael Babinchak, C. D. Ridge, J. D. Walls, *Organic & Biomolecular Chemistry* **2012**, *10*, 8710–8719.

[14] H. Dong, Y. Wei, W. Zhang, C. Wei, C. Zhang, J. Yao, Y. S. Zhao, *J. Am. Chem. Soc.* **2016**, *138*, 1118–1121.

[15] B. Hua, C. Zhang, W. Zhou, L. Shao, Z. Wang, L. Wang, H. Zhu, F. Huang, *J. Am. Chem. Soc.* **2020**, *142*, 16557–16561.

[16] Y. Wei, H. Dong, C. Wei, W. Zhang, Y. Yan, Y. S. Zhao, *Advanced Materials* **2016**, *28*, 7424–7429.

[17] U. Steiner, M. H. Abdel-Kader, P. Fischer, H. E. A. Kramer, *J. Am. Chem. Soc.* **1978**, *100*, 3190–3197.

[18] J. E. H. Buston, J. R. Young, H. L. Anderson, *Chem. Commun.* **2000**, 905–906.

[19] A. J. Baer, D. H. Macartney, *Org. Biomol. Chem.* **2005**, *3*, 1448–1452.

[20] V. Zanichelli, M. Bazzoni, A. Arduini, P. Franchi, M. Lucarini, G. Ragazzon, A. Secchi, S. Silvi, *Chemistry – A European Journal* **2018**, *24*, 12370–12382.

[21] M. Bazzoni, L. Andreoni, S. Silvi, A. Credi, G. Cera, A. Secchi, A. Arduini, *Chemical Science* **2021**, *12*, 6419–6428.

[22] U. A. Çevik, D. Osmaniye, B. N. Sağlik, B. K. Çavuşoğlu, S. Levent, A. B. Karaduman, S. Ilgin, A. Ç. Karaburun, Y. Özkay, Z. A. Kaplancikli, G. Turan, *Med Chem Res* **2020**, *29*, 1000–1011.

[23] H. Görner, *Journal of Photochemistry and Photobiology A: Chemistry* **2011**, *218*, 199–203.

[24] B. Carlotti, G. Consiglio, F. Elisei, C. G. Fortuna, U. Mazzucato, A. Spalletti, *J. Phys. Chem. A* **2014**, *118*, 3580–3592.

[25] W. Yang, Y. Li, H. Liu, L. Chi, Y. Li, *Small* **2012**, *8*, 504–516.

[26] A. Paudics, D. Hessz, M. Bojtár, B. Gyarmati, A. Szilágyi, M. Kállay, I. Bitter, M. Kubinyi, *Molecules* **2020**, *25*, 5111.

[27] H. He, E. Ma, Y. Cui, J. Yu, Y. Yang, T. Song, C.-D. Wu, X. Chen, B. Chen, G. Qian, *Nat Commun* **2016**, *7*, 11087.

[28] M. Kumar Bera, P. Pal, S. Malik, *Journal of Materials Chemistry C* **2020**, *8*, 788–802.

[29] S. Ballot, N. Noiret, *Tetrahedron Letters* **2003**, *44*, 8811–8814.

[30] P. R. O. CrysAlis, *Yarnton, Oxfordshire, England* **2014**.

[31] G. M. Sheldrick, *Acta Cryst A* **2015**, *71*, 3–8.

[32] O. V. Dolomanov, L. J. Bourhis, R. J. Gildea, J. a. K. Howard, H. Puschmann, *J Appl Cryst* **2009**, *42*, 339–341.

[33] G. M. Sheldrick, *Acta Cryst C* **2015**, *71*, 3–8.

Chapter 5. Synthesis and Characterization of new Gold(I) cavitand complexes for asymmetric transformations

Introduction

Gold[1] is a precious and inert metal used since prehistoric times as ornamental metal thanks to its ductility and malleability. The potentiality of gold(I) in organic chemistry was discovered only in the late nineties by Tales[2] and Tanaka,[3] who reported the first gold(I)-catalysed addition, in homogeneous fashion, of alcohols to alkynes and the hydration of alkynes, respectively. Nowadays, gold(I) catalysis has become the most effective strategy for the selective activation of alkynes and thus a resourceful approach for the formation of new carbon-carbon and carbon-heteroatom bonds.[4–7]

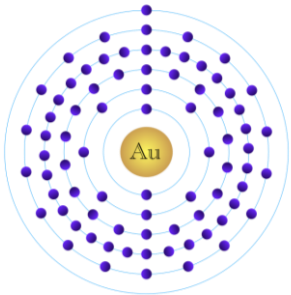

Figure 5.1 Gold atom.

Gold properties strongly relies on the relativistic effects observed for every heavy metal.[8–11] These effects correlate the atomic number of the heavy metal and lean on the acceleration of electrons that orbit around the nucleus: the higher the atomic number, the more the electrons closest to the nucleus are attracted and accelerate. Consequently, the *s* and *p* orbitals are stabilized and contracted, whereas the *d* and *f* orbitals are expanded and destabilized, as their electrons

experience a weaker nuclear attraction. The effect is more prominent when the metal has the *4f* and *5d* orbitals filled, as in the case of gold. It experiences the contraction of the *6s* orbital and the expansion of the *5d* orbitals. Therefore, the repulsion of electrons in the filled *5d* orbital is deeply reduced.

Relativistic effects grant gold numerous properties. Marked Lewis acidity, highest electronegativity among transition metals (χ 2.4), resistance to oxidation, and linear dicoordination geometry of gold(I) are among them.[12] Reasonably, gold(I) linear complexes experience a contacted and notable strong bond between the gold atom and the ligand.[13,14] As a result, steric and electronic properties of the ligand can intensely influence the reactivity of the gold complexes.

The ability of gold(I) complexes to selectively activate π-bonds towards nucleophilic addition can be explained by the Dewar-Chatt-Duncanson model. Three different interactions of *p* orbitals of the alkyne with the *d* orbitals of the gold are involved: first, a σ-donation from the fully occupied orbitals of the alkyne to an empty *d* orbital of the metal (Figure 5.2, a); second, a π-backdonation from the orbital *d* of the metal to an empty π* orbital of the alkyne (Figure 5.2, b); third interaction derives from the other filled π orbital which is perpendicular to the equatorial plane (Figure 5.2, c). The consequence of these interactions is the movement of alkyne electron density towards antibonding π* orbital, that causes the elongation of the alkyne bond. Therefore, the triple bond enhances its electrophilicity becoming more susceptible of nucleophilic attack.

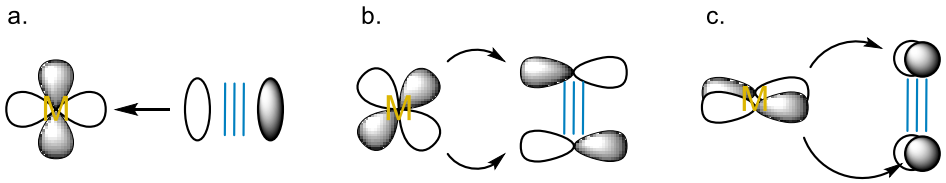

Figure 5.2 a) σ-donation L-> M; b) π-backdonation M -> L; c) perpendicular π-backdonation M-> L.

Gold(I) chloride complexes [LAuCl] are mainly generated from the exchange of (dimethylsulfide)gold(I) chloride with the desired ligand L (generally a phosphine or an N-heterocyclic carbene). However, the catalytically active gold(I) species is formed *in situ* from the precatalyst [LAuCl] *via* chloride abstraction using chloride scavengers such as silver salts bearing a weakly coordinating counterion.[15–19]

Homogeneous gold(I) catalysis has gained a remarkable importance in catalytic transformations thanks to the ability of gold(I) to yield complex molecules under very mild reaction condition.[4–6,20–22] Cycloisomerization of 1,*n*-enynes is admitted one of the most valuable reactions proceeding *via* homogeneous gold(I) catalysis as various carbon-carbon or carbon-heteroatoms bonds are formed in a single reaction step. Complex mechanisms though skeletal rearrangements are at the basis of the cyclization of 1,*n*-enynes (in details for 1,6-enynes, Scheme 5.1). Initially, gold(I) selectively activates the triple bond of the alkyne generating the (η^2-alkyne)gold(I) species **1**, which undergoes intramolecular nucleophilic attack by the alkene moiety through *5-exo*-dig or *6-endo*-dig cyclization, affording the corresponding cyclopropyl gold(I) carbene **2** or **3**.[23–27] Afterward, different skeletal rearrangements can occur depending on the substitution pattern of the substrate, the reaction conditions, and the gold(I) catalyst.

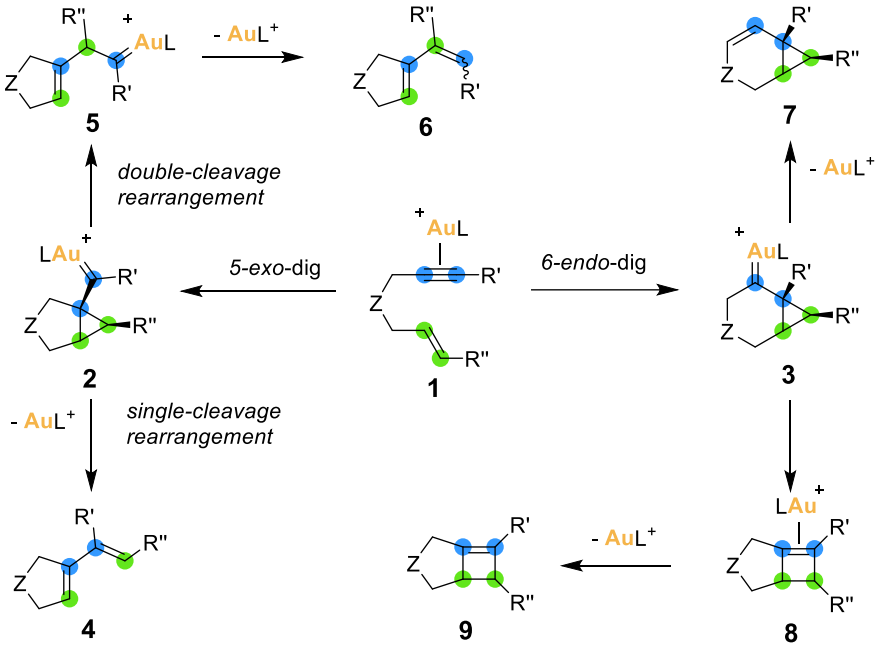

Scheme 5.1 Gold(I)-catalyzed cyclization of 1,6-enynes.

Intermediate **2** can be subjected to single-cleavage rearrangement which involves the 1,3-migration of the alkene terminal carbon to the alkyne terminal carbon to achieve 1,3-diene **4**;[28] alternatively, the insertion of the terminal carbon of the alkene between the two carbons of the alkyne leads to diene **6** through the double-cleavage rearrangement process and consequent demetallation. Intermediate **3** can suffer the demetallation to give cyclic alkene **7**. The other pathway suggests the ring expansion of **3** and the subsequent formation of (η^2-cyclobutene)gold(I) complex **8**, demetallation of which yields compound **9**.

Despite the advances of homogeneous gold catalysis, enantioselective gold(I)-catalysed transformations were found to be particularly challenging to implement.[29–35] At the basis of the challenging enantioinduction, there is the linear coordination displayed by gold(I) complexes, in which the crucial chiral part of the ligand is located far from the substate and the reactive site, resulting in an inefficient transfer of the chiral information. In addition, the transformations proceed through an outer sphere mechanism, and unlike allene or alkene, alkyne

fragment is not prochiral. Moreover, the free rotation of the ligand-gold(I) and gold(I)-substrate bonds does not propose a fixed conformation of the components in space (Figure 5.3). All these features suggest a substantial challenge for the achievement of high enantiocontrol in gold(I)-catalysed reactions.

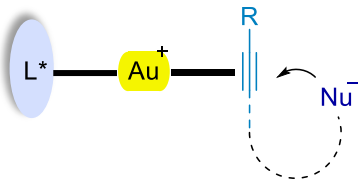

Limitation in enantioinduction transformations:
- Linear coordination geometry of gold(I)
- Outer-sphere mechanism
- Free rotation of L*-gold and gold-substrate bonds

Figure 5.3 Gold(I) coordination geometry.

Several strategies have been developed to to overcome the limitations caused by the above-mentioned reasons. The most common approaches exploit the use of chiral binuclear gold(I) complexes with bisphosphines, such as BINAP, BIPHEB and SEGPHOS, or diaminocarbene ligands (Figure 5.4, a).[36–38] Asymmetric transformations achieved by this method include intra- and intermolecular cyclopropanation,[39–41] cycloisomerization of 1,n-enynes[42–45] as well as other annulations.[46–50] Another system involves the use of mononuclear gold(I) complexes with phosphoramidite ligands based on BINOL, TADDOL or SPINOL derivatives (Figure 5.4, b).[51–55] Their efficiency was demonstrated in the enantioselective cyclization of allenes.[56–58] A further successful approach precludes the simultaneous use of chiral or non-chiral gold(I) complexes with chiral phosphate counteranions (Figure 5.4, c).[59–62] Thanks to the tight ion pairs between the cationic gold and the counterion, the chiral information of the counteranion is kept in proximity to the point where the reaction occurs. The limitation of this strategy consists in the use of terminal alkynes, since the

phosphate anion is basic enough to deprotonate alkyne, deactivating the catalytic system.[63,64]

a. Chiral binuclear gold(I) complexes

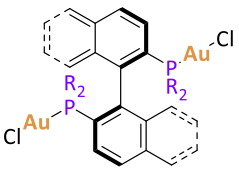

b. Monodentate phosphoramidite gold(I) complexes

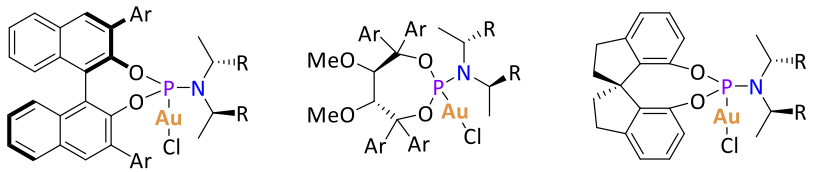

BINOL-derived TADDOL-derived SPINOL-derived

c. Chiral counterion

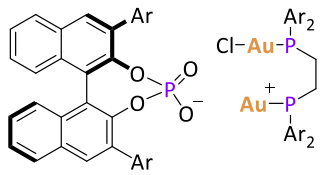

Figure 5.4. Chiral gold(I) complexes.

More recently, the group of Echavarren developed a new class of chiral gold(I) catalysts characterized by a C_2-chiral element.[65] The complexes are based on the modified JohnPhos ligand with a diarylpyrrolidine moiety at the *para* position of the biphenyl scaffold. This specific design permits the formation of a rigid "pocket": the rotation of the C_{aryl}-P bond is blocked by the bulky substituents of the phosphine, and the gold active site is faced directly to the chiral centre (**I**, Scheme 5.2). Chiral JohnPhos-type catalysts have been employed in the enantioselective cyclization of 1,6-dienynes, which allowed to reach impressive enantiomeric excess. π-π Interactions between the chiral cavity and the substrate are responsible for the enantioselective folding of the enynes.

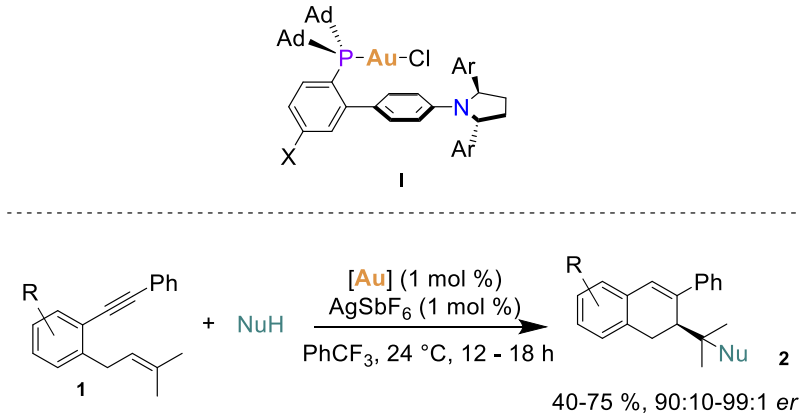

Scheme 5.2 Chiral JohnPhos-type catalyst for enantioselective cyclization of 1,6-dienynes.

Lately, excellent enantioselectivities and yields in the cycloaddition of 1,6-dienynes were obtained applying a new class of chiral 1,3-disubsituted ferrocene ligands (**II**, Scheme 5.3).[66] Also in this case, the gold(I) catalytic system forces the substrate to fold in a selective manner, given the chiral environment and π-π non-covalent interactions.

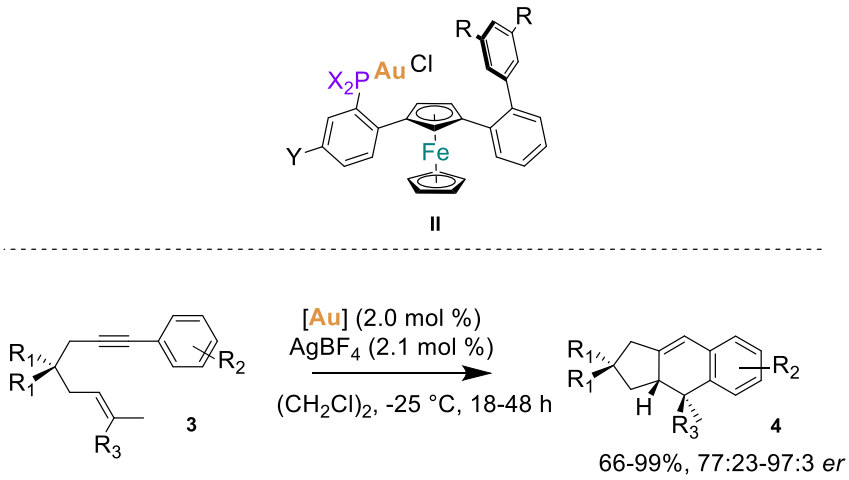

Scheme 5.3 Ferrocene-based gold(I) complexes for cycloaddition of 1,6-dienynes.

A different approach is based on the use of chiral counterions in a supramolecularly-directed catalysis strategy.[67] This system consists of gold(I) complex with JohnPhos-type ligand bearing an H-bond donor group (urea or thiourea) and a BINOL-derived chiral counterion responsible for the asymmetrical information (**III**, Scheme 5.4). The presence of an H-bond donor group allows the separation of the anion from the gold(I) coordination sphere, which permits the coordination of the substrate and, at the same time, the fixation of the chiral anion near to the substrate through hydrogen interactions. The cycloisomerization of 1,6-enynes, *via 5-exo-dig* or *6-endo-dig* cyclization, with or without the addition of a nucleophile, were accomplished enantioselectively with excellent product yields.

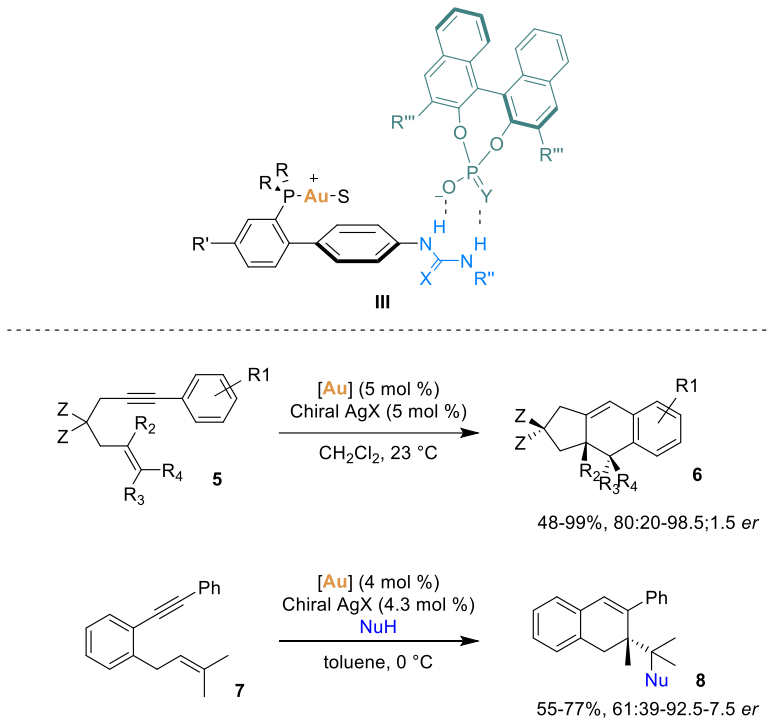

Scheme 5.4 Hydrogen bond-directed chiral counterion catalysts and their application on cycloaddition of 1,6-enynes.

Another intriguing supramolecular approach was explored by using of macrocycle structures as platforms to influence asymmetric reactivities. In enzymes, the cavity of the macrocycle can be seen as a pocket, which dictates the substrate size, stabilizes intermediates, and influences the result of the chemical transformation.[68] In addition, the complexation of the metal centre in the supramolecular pocket isolates the metal active site from the bulk phase, allowing therefore higher stability and reactivity.

Recently, several cavitand scaffolds were employed in the encapsulation of gold(I). For instance, Sollogoub and co-workers developed gold(I) complexes embedded into cyclodextrins by covalent interactions and demonstrated their functions and applications. NHC-capped *β*-cyclodextrin was used as a nanoreactor for the asymmetric alkoxycyclization reaction of 1,6-enynes (**IV**, Scheme 5.5).[69]

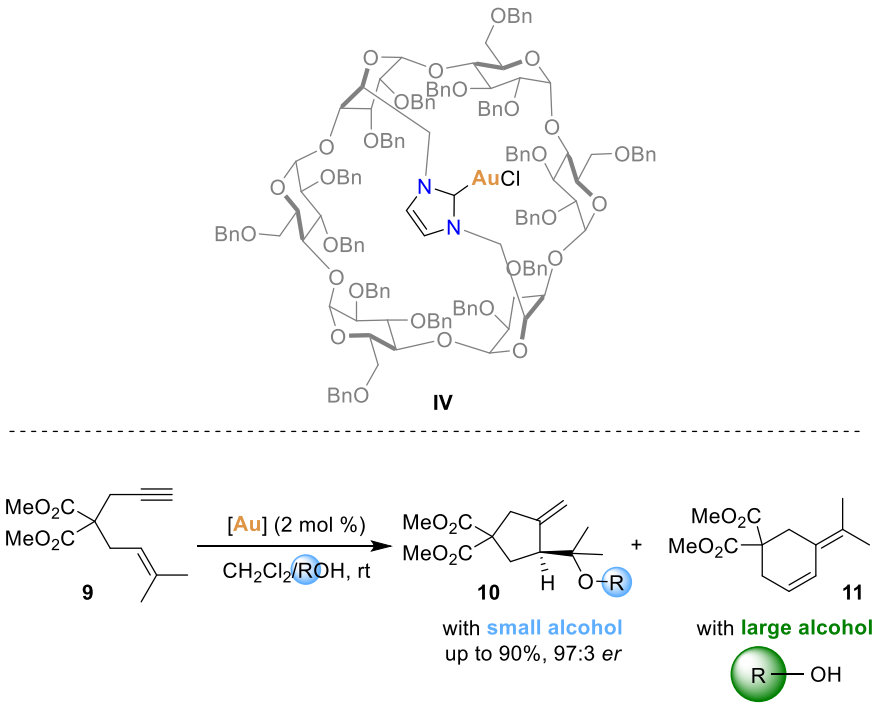

Scheme 5.5 Enantioselective alkoxycyclization of 1,6-enyne using NHC-capped *β*-cyclodextrin gold(I) catalyst.

Firstly, the constrained environment favours the formation of the six-membered ring when a nucleophile is not present. It was found that the introduction of small alcohols, used as nucleophiles, alters the cyclization route from *6-endo-dig* to *5-exo-dig* to give products **10**. In detail, the product obtained with methanol as nucleophile was achieved with excellent enantioselectivities (product **10**, 97:3 *er*). On the other hand, bulky alcohols turn out not to act as nucleophiles, and the formation the reaction outcome becomes the product of *6-endo-dig* cyclization **11**. So, the asymmetric shape of the cavity is responsible for the stereoselective and enantioselective transformation. Also, the confined structure is able to sterically discriminate the size of the nucleophile.

In 2021, calix[*6*]arenes were explored for the first time as ligands for gold(I) complexes. Our group synthesized a new class of triphosphine calix[*6*]arenes to complexate gold(I).

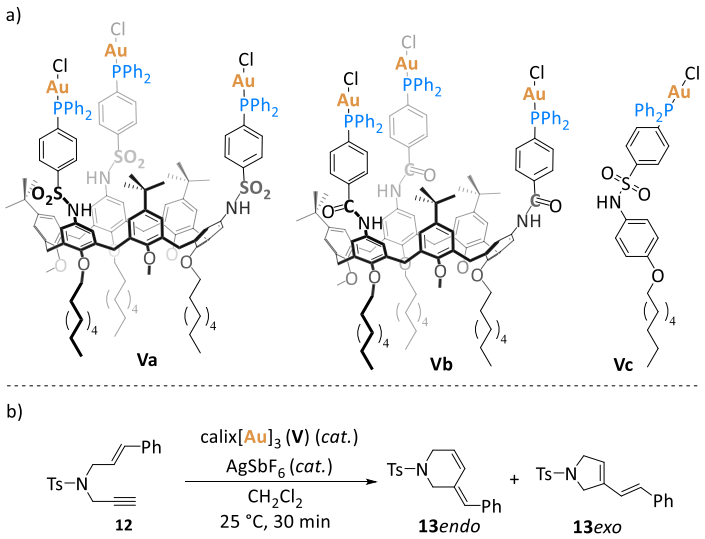

Entry	[Au]	*endo/exo*	yield *endo* (%)
1	**Va** (0.5 mol %)	14:1	91
2	**Vb** (0.5 mol %)	13:1	87
3	**Vc** (2 mol %)	11:1	93

Scheme 5.6 Triphosphine calix[*6*]arene Au(I) complexes (a); general scheme for cycloisomerizations of 1,6-enynes (b).

Differently from other macrocycles, these ligands able to bind three gold(I) nuclei could be employed both for molecular recognition and catalysis.[70] Trisulfonamide and triamide scaffolds bearing diphenylphosphino groups at the *para* position respect to the SO_2-NH or CO-NH moieties can thread dialkyl viologen salts inside the cavity leading to pseudorotaxane species, the conformation of which is influenced by the counterion of the bonded gust and H-bonding domain of the macrocycle.[71] Noteworthy, the catalytic activity of both gold(I) complexes was studied in the cycloisomerization of 1,6-enynes.[72] Both catalysts (**Va** and **Vb**) showed similar reactivity and selectivity: cycloisomerization products were obtained in high yields, and the formation of the *6-endo-dig* isomer was predominant to the *5-exo-dig* isomer (91% and 85% yield, 14:1 and 13:1 *endo*:*exo* ratio, respectively) (Scheme 5.6, b). Moreover, preliminary studies on the role of the cavity demonstrated that the selectivity is influenced by the cooperative character of the three gold(I) centres. With the aim to bring the gold active sites closer to the calix[*6*]arene cavity, the synthesis of diametric diphosphine gold(I) complexes was investigated.[73]

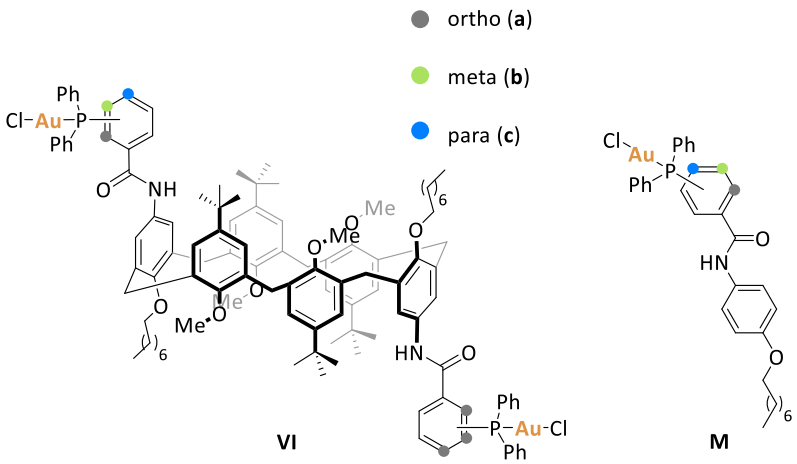

Scheme 5.7 Diametric diphosphine calix[*6*]arene Au(I) complexes.

The diametric scaffold is characterized by the *1,2,3-alternate* conformation with the two functional groups facing opposite sides of the macrocycle. Three different diphosphine calix[*6*]arene ligands bearing phosphine moieties at the *ortho* (**VIa**), *meta* (**VIb**) and *para* (**VIc**) position were developed (Scheme 5.7). The process of the 1,6-enyne cycloisomerization was used to explore the influence of the calixarene cavity and the position of the gold(I) atom respect to the macrocycle (Scheme 5.8). While no significant variation was observed using *para*- and *meta*-substituted catalysts (1.1:1 *endo:exo*), the *ortho*-substituted complex **VIa** provided an enhanced selectivity towards the formation of the 6-*endo-dig* cyclization product (1.8:1 *endo:exo*).

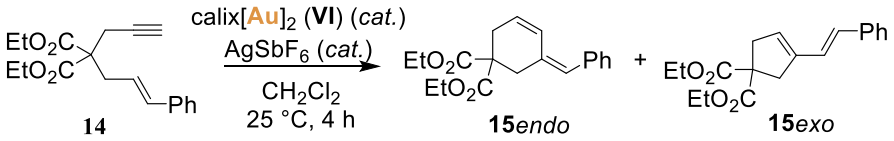

Entry	[Au]	*endo/exo*	conv (%)
1	**Mc** (2 mol %)	1.0:1.0	89
2	**VIc** (1 mol %)	1.1:1.0	88
3	**Mb** (2 mol %)	1.2:1.0	86
4	**VIb** (1 mol %)	1.1:1.0	91
5	**Ma** (2 mol %)	1.5:1.0	86
6	**VIa** (1 mol %)	1.8:1.0	89

Scheme 5.8 Cycloisomerization of 1,6-enynes catalysed by diametric diphosphine calix[*6*]arene Au(I) complexes.

The same family of catalysts was tested subsequently for the intramolecular cyclization of 1,6-dienynes (Scheme 5.9).[74] In this case, *para*-substituted catalyst **VIc** was found to be the most efficient towards the stereoselective formation of the tetracyclic skeleton, whereas larger amounts of 6-*endo-dig* stereoisomers were obtained by using the *ortho*-substituted catalyst. Steric effects could be responsible for such difference in the products distribution. A small library of 1,6-dienynes with several substituted *N*-tethered sulfonamide groups was reacted in the presence of the catalyst **VIc** to evaluate the applicability of this method.

Tetracyclic products were obtained with yields ranging from good to excellent (50-90%).

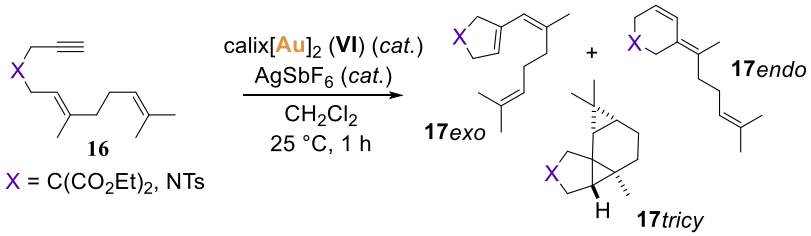

Entry	X	[Au]	*exo:endo:tricy*	conv (%)
1	$C(CO_2Et)_2$	**VIc**	1.0:0.1:7.2	100
2	$C(CO_2Et)_2$	**VIb**	1.0:0.1:5.4	100
3	$C(CO_2Et)_2$	**VIa**	1.0:0.16:4.7	100
4	NTs	**VIc**	0:1.0:7.1	100
5	NTs	**VIb**	0:1.0:5.0	100
6	NTs	**VIa**	0:1.0:4.7	100

Scheme 5.9 Intramolecular cyclopropanation of 1,6-dienynes catalyzed by diametric diphosphine calix[*6*]arene Au(I) complexes.

Resorcin[*4*]arene is the other supramolecular ligand for gold(I). The first example of resorcin[4]arene-based gold(I) complex for homogeneous gold catalysis was designed by Iwasawa and co-workers.[75] This resorcin[4]arene gold(I) cavitand bearing phosphoramidite, phosphite of phosphonite moieties was prepared as ligand for gold(I) nucleus. The metal centre is placed in the inner sphere of the cavity and surrounded by three quinoxaline wall units. These gold(I) catalysts were evaluated in the Conia-ene reaction of *β*-keto ester alkyne leading to the formation of products **19** and **20**. The best result was achieved by employing the catalyst **VIIa** (62% yield of **19**) (Scheme 5.10).

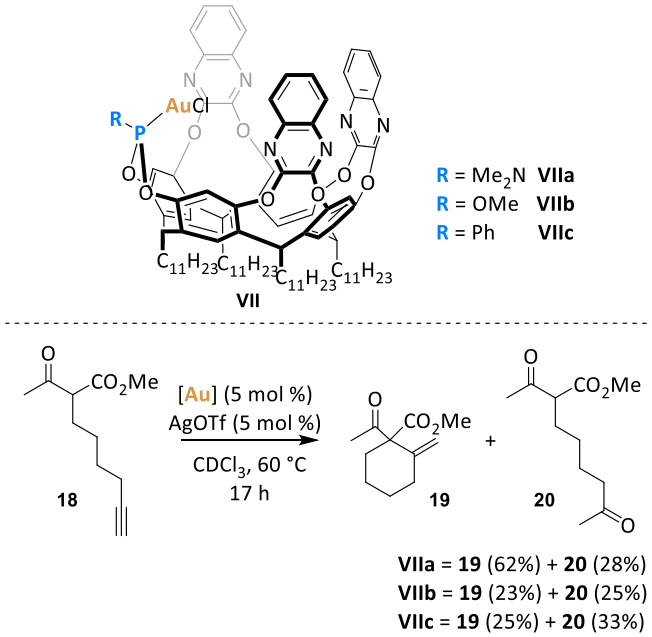

Scheme 5.10 First resorcin[4]arene-based gold(I) catalysts and their application in the Conia-ene reaction.

Moreover, the same research group also described the synthesis of an oriented binuclear-gold(I) resorcin[*4*]arene cavitand in which the phosphoramidite ligands point outside the cavity, and both chlorogold(I) fragments are placed inwardly (Scheme 5.11).[76] The catalytic activity of the complex was tested in Conia-ene reaction, but surprisingly the formation of product **19** was not detected, like in the case of mononuclear complexes **VIIa-VIIc**. Instead, the product of the intermolecular dimerization, the conjugated enyne **22**, was obtained in 45% yield. Therefore, the binuclear-gold(I) catalyst was employed for the homo- or hetero-dimerization of terminal alkynes, and the macrocyclization by intramolecular dimerization.

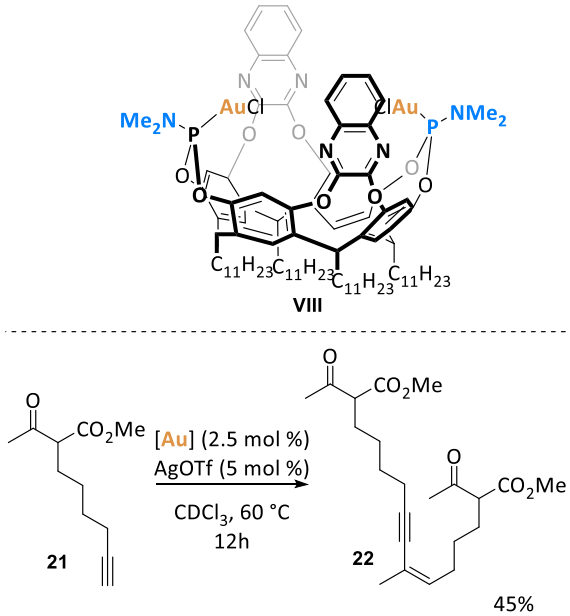

Scheme 5.11 Inwardly oriented-Au binuclear resorcin[4]arene complex and dimerization reaction of terminal alkynes.

The same reaction was used to study the effect of the "walls" in the catalytic event.[77] Different cavitands bearing different "walls" (quinoxaline, pyrazine, or methylene-bridged walls) which highly influence the shape/properties of the cavity were synthesized (Scheme 5.12). These results demonstrated the importance of the quinoxaline "walls", as they strongly promote the interaction between the two alkynes and stabilize the intermediates thanks to the expanded π-cloud environment.

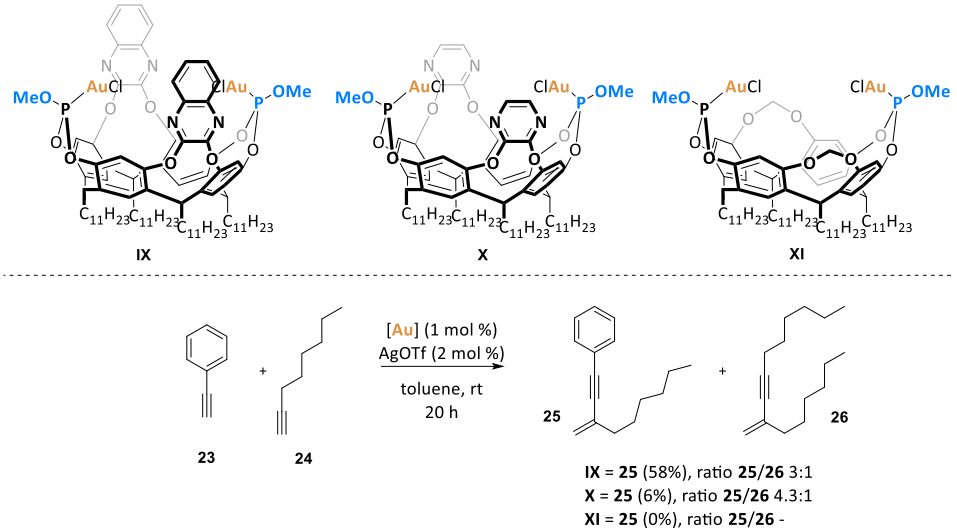

Scheme 5.12 Evaluation of the role of cavitand walls in the dimerization of terminal alkynes.

Other reactions were explored using resorcin[4]arene-based gold(I) cavitand complexes, such as the hydration of alkynes,[78,79] the lactonization of γ-alkynoic acids,[80] or the cycloisomerization of arylalkynes.[81]

Lately, the group of Echavarren explored the application of resorcin[4]arene-based gold(I) complexes for the selective cyclization of 1,6-dienynes and for the more challenging enantioselective alkoxycyclization of 1,6-enynes.[82] For this purpose, a new family of achiral gold(I) cavitands bearing different "walls" was synthesized and employed in the cycloisomerization of 1,6-dienynes, while chiral complexes were used in the asymmetric transformation. Starting from the first class of complexes, the group of Echavarren designed several achiral resorcin[4]arene cavitands with one or two phenyl phosphonite groups for the complexation of gold(I) (Scheme 5.13): mononuclear gold(I) cavitands bearing quinoxalines (complex **A**) or naphthoquinones (complex **B**) walls, and additionally complex **C**, with only two walls and two free phenol groups, and complex **D** with a bulky triptycene quinone wall, were synthesized. Cationic catalyst **G** was also obtained from the corresponding complex **A**, after the chloride abstraction with

$AgSbF_6$ in the presence of acetonitrile. Binuclear gold(I) complexes were achieved with both quinoxaline (**E**) and naphthoquinone (**F**) walls.

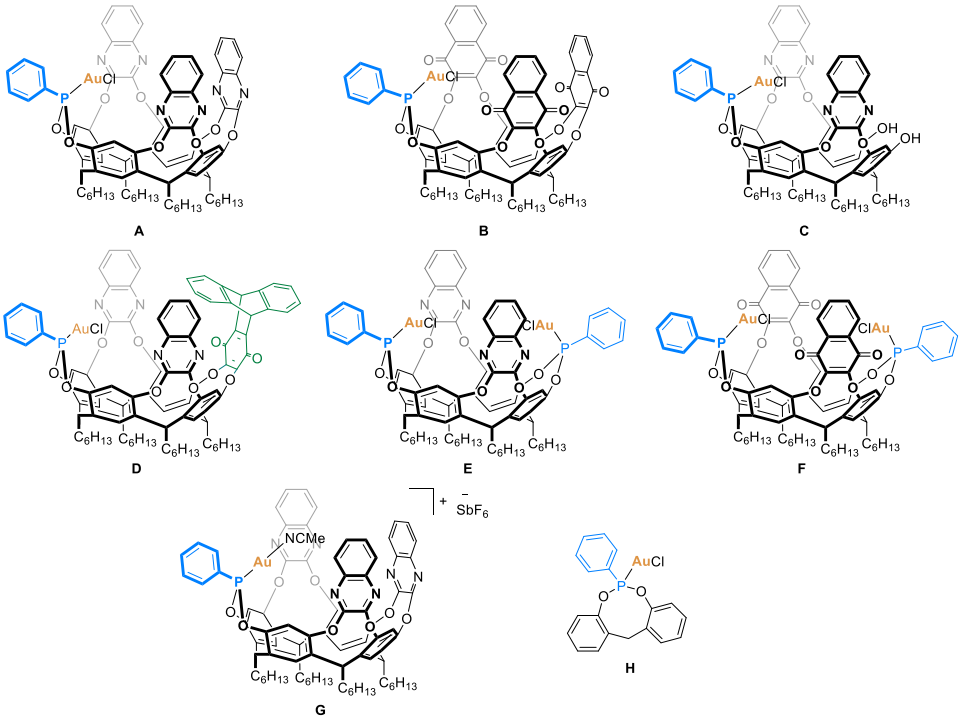

Scheme 5.13 Achiral mononuclear and dinuclear gold(I) cavitand complexes.

These gold(I)-cavitand complexes were then applied in the *exo*/*endo* selective cyclization of (*Z*)-1,6-dienyne **27** (Table 5.1). The reaction carried out with traditional gold(I) catalysts, such as $[Au(PPh_3)Cl]$ or $[Au(P(OMe)_3Cl]$, led to the exocyclic single-cleavage skeletal rearrangement product **28a**, as the main reaction outcome. Conversely, using gold(I)-cavitand complexes in the same transformation, the inversion of the selectivity was observed, as the endocyclic single-cleavage skeletal rearrangement product **28b** was principally formed. Mononuclear gold(I) cavitand **A**, as well as the equivalent cationic **G,** found to be the most suitable cavitand catalyst, gave products **a** and **b** forming in high yields and in 1:5 ratio.

Table 5.1 *Exo*/*endo* cycloisomerization of (*Z*)-1,6-dienyne **27**.

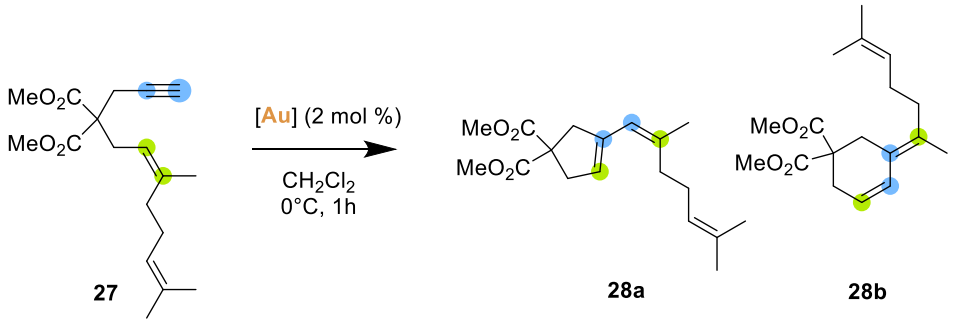

Entry	[Au]	$AgSbF_6$ [mol %]	Yield [%] (**28a**/**28b**)
1	$[Au(PPh_3)Cl]$	2	65 (11:1)
2	$[Au(P(OMe)_3)Cl]$	2	56 (>20:1)
3	**A**	2	95 (1:5)
4	**B**	2	89 (8:1)
5	**C**	2	79 (1:2)
6	**D**	2	83 (1:1)
7	**E**	4	92 (1:1)
8	**F**	4	87 (3:1)
9	**G**	-	97 (1:5)
10	**H**	2	77 (>20:1)

Finally, the non-cavitand gold(I) complex **H** with analogue active site and similar electronic properties was prepared and tested to evaluate the importance of the cavity. Also in this case, the *exo*-cyclized product **28a** was favoured, demonstrating the essential function of the cavitand cavity in the selective transformation.

A new family of chiral gold(I) cavitand containing the chiral information in the phosphoramidite site on the resorcin[4]arenes was prepared (Scheme 5.14). Mononuclear gold(I) cavitands were obtained with the metal active centre inside the cavity (complex **I**, **J**), or outside it (complex **K**), using 1,1-dicholo-*N,N*-bis((*S*)-1-phenylethyl)phosphanamine as a chiral precursor. Binuclear gold(I) complexes with both metal centres inside the cavity (**L**-**O**), or one inside and one outside the cavity (**P**-**S**) were synthesized using different *S,S*-bis(1-arylehtyl)amines. From complex **L**, cationic complex **T** was generated through chloride abstraction by $AgSbF_6$ and the addition of acetonitrile. Dicationic complex **U** was achieved *via*

abstraction of both chlorides with $AgSbF_6$ and the complexation of a bidentate phthalonitrile.

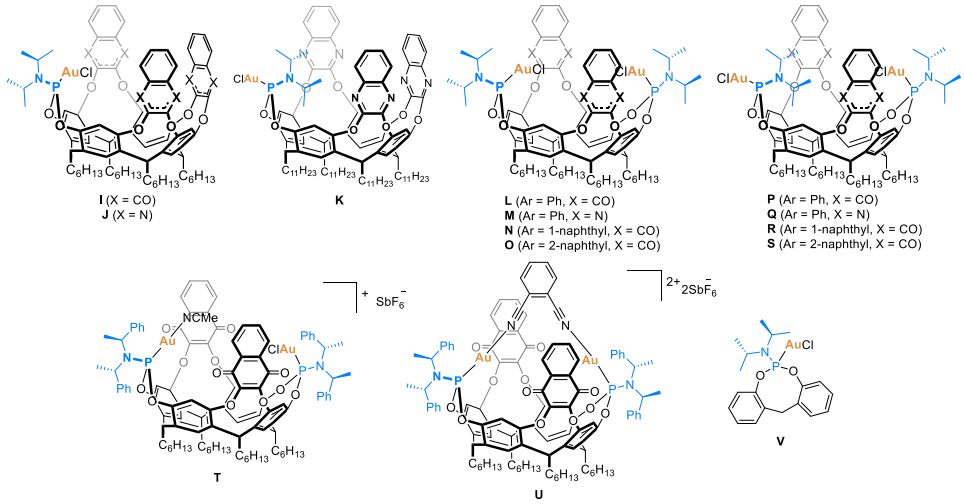

Scheme 5.14 Chiral gold(I)-cavitand complexes.

This family of chiral gold(I)-cavitand complexes was then tested in the enantioselective alkoxycyclization of *E*-1,6-dienyne **29** in the presence of ethanol as nucleophile (Table 5.2).

Table 5.2 Enantioselective alkoxycyclization of *E*-1,6-dienyne **29**.

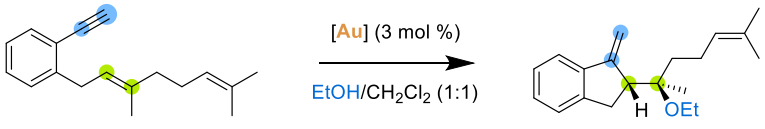

29 **30**

Entry	[Au]	$AgSbF_6$ [mol %]	T [°C]	t [h]	Yield [%]	*er*
1	**I**	3	23	1	83	51:49
2	**J**	3	23	1	74	59:41
3	**K**	3	23	1	36	45:55
4	**L**	6	23	1	90	89.11
5	**M**	6	23	1	80	86:14
6	**N**	6	23	1	84	74:26
7	**O**	6	23	1	83	88:12
8	**P**	6	23	1	86	55:45
9	**Q**	6	23	1	69	57:43
10	**R**	6	23	1	67	68:32
11	**S**	6	23	1	91	53:47
12	**V**	3	23	1	48	57:43
13	**L**	3	23	1	88	89:11
14	**T**	-	23	1	89	89:11
15	**U**	-	23	3	74	81:19
16	**T**	-	-50	18	90	96:4

Low enantioselectivities were observed when mononuclear gold(I) cavitands (**I**, **J** and **K**) or binuclear gold(I) cavitands with a single AuCl fragment outside the cavity (**P**, **Q**, **R** and **S**) were used. However, binuclear gold(I) complexes with both gold(I) chloride moieties inside the cavity gave product **30** forming in high yield and with good enantioselectivity. The best result was achieved with cationic catalyst **T** at low temperatures (down to -50 °C), here the product **30** was isolated in 90 % yield with 96:4 *er*. Dicationic complex **U** bearing the phthalonitrile as ligand provided a slight decrease in yield and *er* (74%, 81:19 *er*). Finally, non-cavitand catalyst **V** with equivalent active site, used to verify the role of the cavitand in the reaction, provided lower yield and poor enantioselectivity (entry 12, Table 5.2).

Considering these outcomes, the idea within this work was to increase the performance of gold(I)-cavitand complexes in asymmetric transformations. The addition of new bulky groups, eventually chiral, close to gold active sites, should induce an additional constrained environment able to promote higher performing, enantioselective reactions. To do so, we envisioned the design of new gold(I) complexes starting from previously synthesized gold(I) cavitands (Scheme 5.15). Achiral dinuclear cavitand **F** and chiral dinuclear cavitand **L** were selected as precursors. Organosulfur compounds, such as thioethers or thioureas, were chosen as ligands for the great affinity of S to bind gold metal. In dinuclear cavitands **F** or **L**, the complexation of one gold atom would place the new (chiral) ligand towards the cavity and the other gold(I) chloride fragment (**T1** and **T2**) able to become the active, catalytic site, upon chloride scavenger. The stability of Au-S bond is the key of the system: this new bond must be strong enough to resist to reaction conditions, as the *in situ* activation of the non-coordinated AuCl would be required *via* chloride abstraction with $AgSbF_6$. The proximity of the ligand to the gold active site should induce the asymmetric transformation.

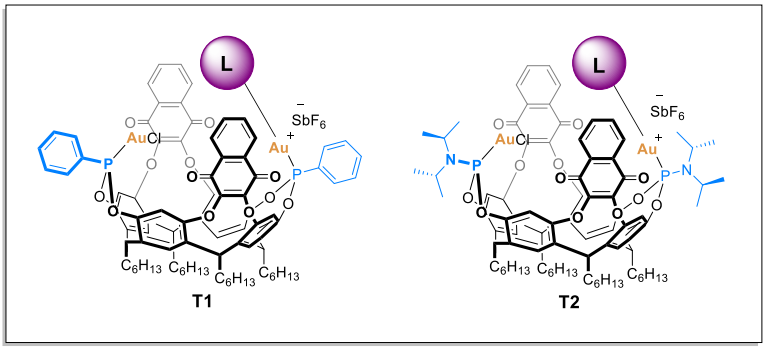

Scheme 5.15 Aim of this work: synthesis of new chiral macrocyclic gold(I) catalysts.

Results and Discussion

A new family of achiral and chiral resorcin[4]arene-based gold(I)-cavitand complexes was designed in order to improve the complexity and enhance their performance in catalysis. For this purpose, dinuclear gold(I) cavitands were used and the coordination of a new moiety was explored as a strategy to modify the cavitand cavity.

This project started from the preparation of cavitands **F** and **L** (Scheme 5.13 and 5.14) characterized by naphthoquinone walls, previously reported by Echavarren group.[82] The cavitand synthesis followed the procedure described by the group of Iwasawa.[75,76] First, the condensation of resorcinol and heptanal under acidic conditions was performed to achieve resorcin[4]arene **32** in 97% yield. Then, resorcin[4]arene **32** was reacted with 2,3-dichloronaphthoquinone in the presence of a base to obtain the tetranaphthoquinone resorcin[4]arene **33** (Scheme 5.16).

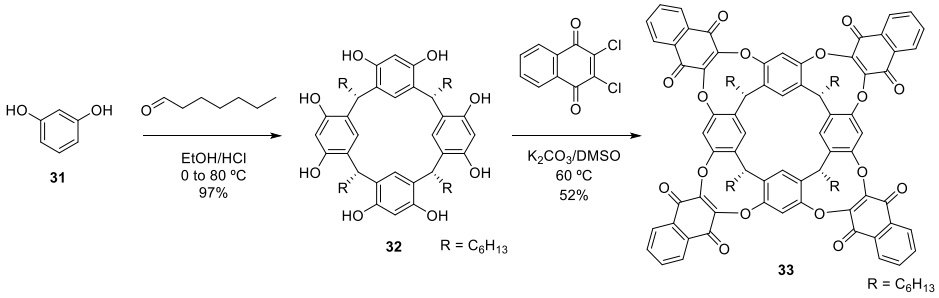

Scheme 5.16 Synthesis of resorcin[4]arene **33**.

Selective cleavage of two naphthoquinone walls from tetranaphthoquinone **33** was afforded using 2.4 equivalents of cathecol as nucleophile and an excess of CsF in DMF at 70 °C for 20 minutes (procedure reported by Gutierrez-Tunstad group,[83] Scheme 5.17).

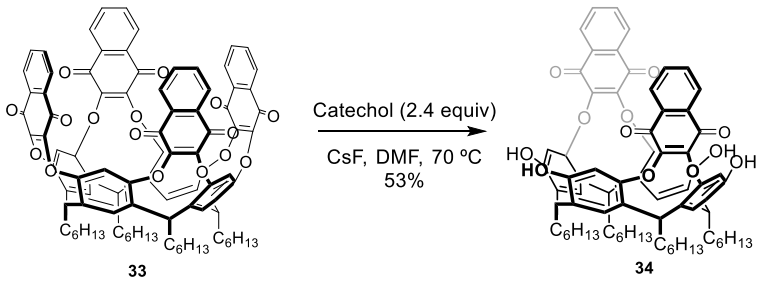

Scheme 5.17 Selective wall excision reaction.

Bis-phenylphosphonite cavitand **35** was then achieved by the reaction between tetraphenol **34** and dichlorophenylphosphine in toluene at room temperature. Finally, dinuclear gold(I) cavitand **F** was reached by the coordination of two gold atoms using chloro(dimethylsulfide)gold(I) (Scheme 5.18).

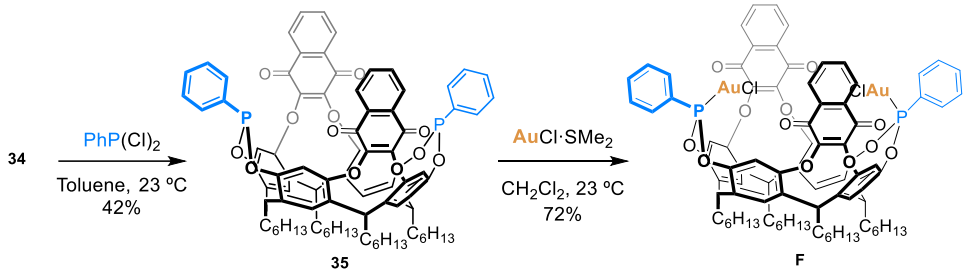

Scheme 5.18 Synthesis of achiral gold(I) complex **F**.

To obtain chiral gold(I) cavitand **L**, 1,1-dichloro-*N,N*-bis((*S*)-1-phenylethyl)phosphanamine **36** was prepared from bis((*S*)-1-phenylethyl)amine which was reacted with phosphorous dichloride in the presence of n-butyllithium (Scheme 5.19).

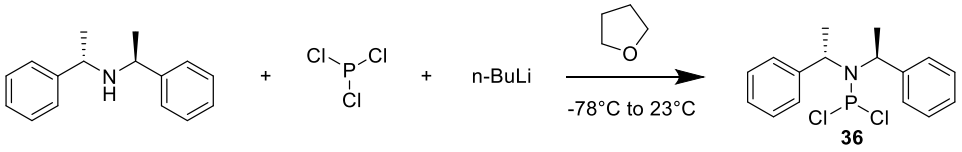

Scheme 5.19 Synthesis of chiral 1,1-dichloro-*N,N*-bis((*S*)-1-phenylethyl)phosphanamine **36**.

Then, tetraphenol **34** was reacted with **36** in toluene at room temperature. From this reaction, a mixture of out-out **37** and in-out **38** phosphoramidites was obtained in overall yield of 44% (Scheme 5.20).

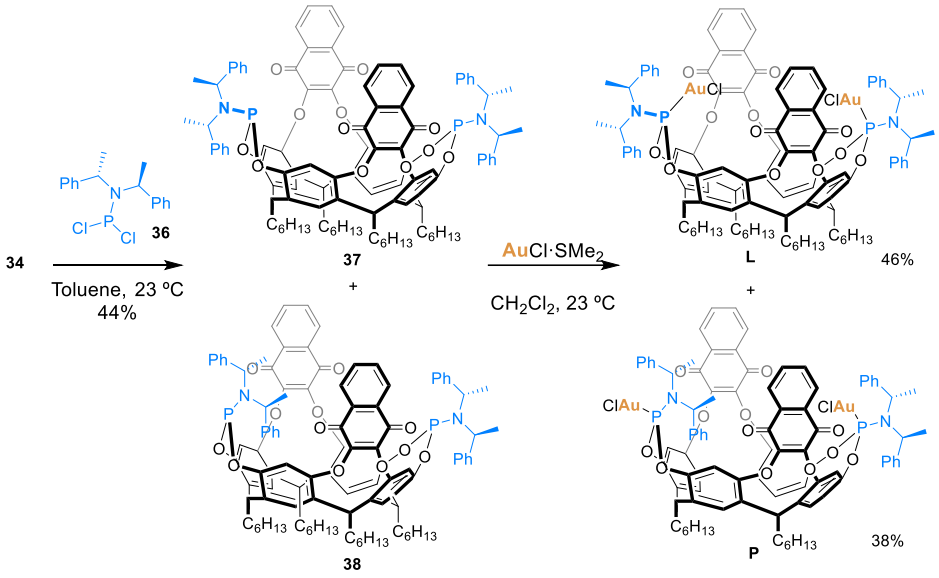

Scheme 5.20 Synthesis of chiral gold(I) complexes **L** and **P**.

Since the two compounds are not separable through chromatographic purification, they were used directly for the coordination of gold(I) with $AuCl{\cdot}SMe_2$. Only at this point, after the separation by column chromatography, complex **L** bearing both gold(I) chlorides inside the pocket was achieved in 46% yield, while complex **P** with a gold(I) chloride outside the cavity was obtained in 38% yield.

Once obtained dinucreal gold(I) cavitands **F** and **L**, the coordination of thioether compounds was attempted. As a preliminary study, a commercially available achiral thioether was tested as a ligand. Complex **F** was treated with one equivalent of $AgSbF_6$ and an excess of tetrahydrothiophene in dichloromethane (Scheme 5.21).

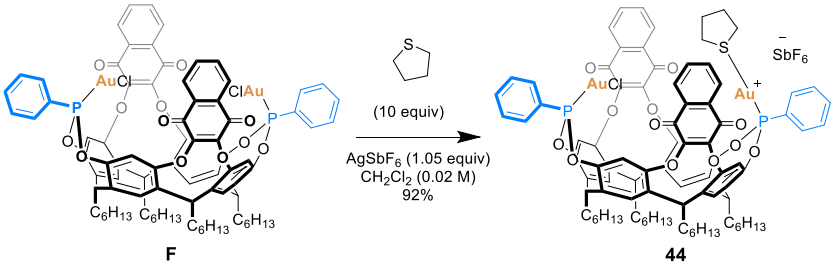

Scheme 5.21 Synthesis of achiral cavitand **44**.

Achiral monocationic digold(I) complex **44** was obtained in high yield using ten equivalents of tetrahydrothiophene.

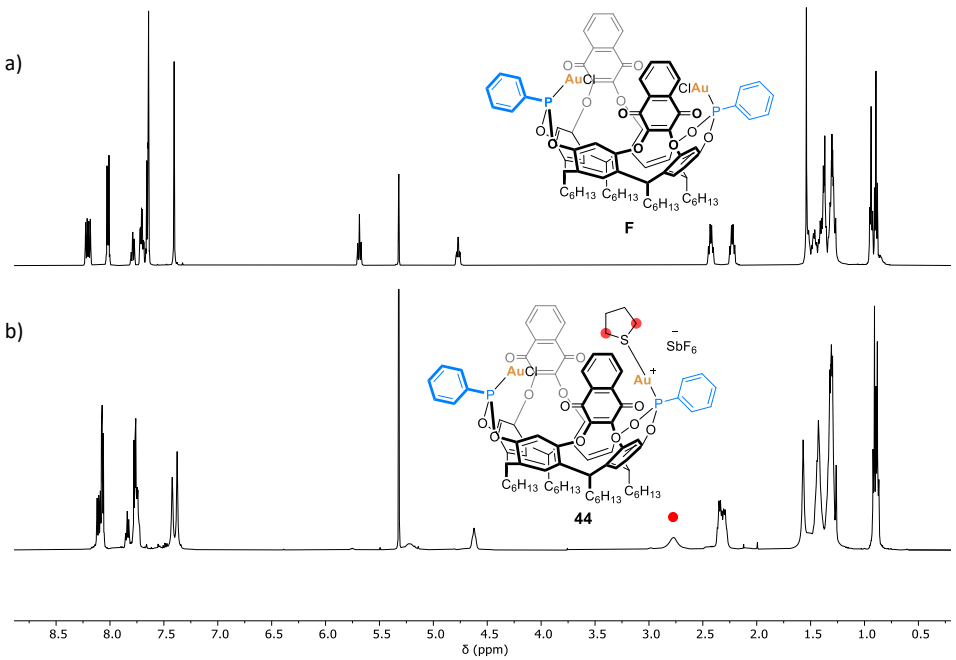

Figure 5.4 ^{1}H NMR spectra of **F** (a) and **44** (b) recorded in CH_2Cl_2 (400 MHz, T = 298 K).

Complexation of the achiral thioether was observed through NMR experiments. Comparing ^{1}H spectra of **F** and complex **44** (Figure 5.4), the presence of a new broad peak can be noticed at 2.77 ppm, corresponding to both CH_2 groups near the complexed sulfur atom in the ligand. In addition, crystals of **44** were obtained

by crystallization from a mixture of dichloroethane and pentane, and the structure was confirmed by X-ray diffraction (Figure 5.5).

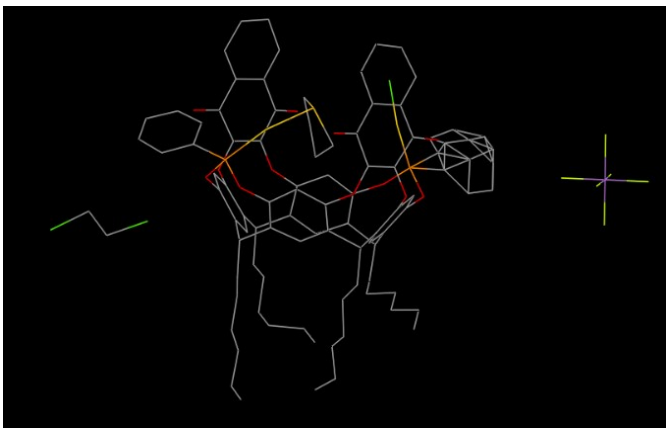

Figure 5.5 X-ray diffraction structure of complex **44**.

X-ray structure evidenced the presence of the achiral ligand pointing towards the centre of the cavity and towards the gold(I) chloride moiety.

Once obtained the achiral thioether-based cavitand **44**, the following step was the synthesis of a chiral thioether. (1*R*,4*R*,5*R*)-isothiocineole **46** was synthesized by the solvent-free reaction between elemental sulfur and limonene (**45**), following the literature procedure (Scheme 5.22).[84]

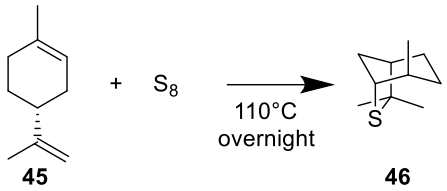

Scheme 5.22 Synthesis of (1*R*,4*R*,5*R*)-Isothiocineole.

Distillation of the crude mixture gave pure isothiocineole. Complexes **F** was then treated with $AgSbF_6$ and (1*R*,4*R*,5*R*)-isothiocineole in CH_2Cl_2 (Scheme 5.23).

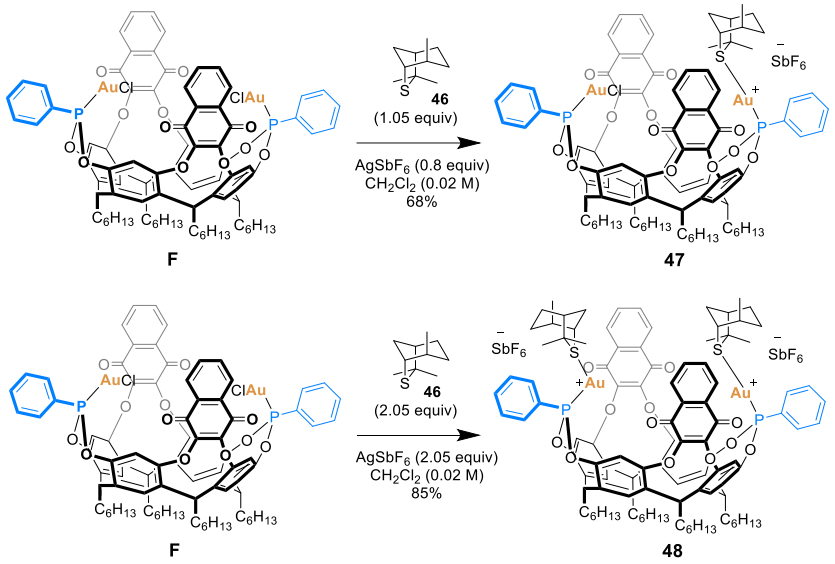

Scheme 5.23 Synthesis of chiral complexes **47** and **48**.

Preparing monocationic compound **47**, it was noticed that a very small excess of $AgSbF_6$ could abstract the second chloride and easily form the dicationic product **48**. As the mixture was not purifiable by precipitation, the coordination conditions were changed. Adding only 0.8 equivalent of $AgSbF_6$, a mixture of monocationic complex and starting compound **F** was obtained. Then, pure **47** was provided in 68% yield by precipitation from a mixture of dichloromethane and pentane. Dicationic complex **48**, obtained as a by-product, was also synthesized. As expected, complex **48** was obtained by chloride abstraction with 2.05 equivalents of $AgSbF_6$ following by the coordination of two chiral isothiocineoles, affording the dicationic complex in 85% yield. Both structures were confirmed by NMR experiments and HR-MS. The evidence of the complexation can be found in ^{1}H NMR spectra: (1*R*,4*R*,5*R*)-isothiocineole **46**, monocoordinated complex **47** and dicoordinated complex **48** spectra are compared below (Figure 5.6). The red-labelled signal, corresponding at the CH group directly attached to the sulfur in the thioether, is the most diagnostic peak. When the ligand is not complexed, it can be observed at 3.33 ppm, instead when complexed, it is downfield shifted at

3.76 and at 3.83 in **47** and **48** respectively. In addition, the integration of the peaks is in agreement with the structures: the integration of the signal in spectrum b corresponds to one proton, while in spectrum c it corresponds to two protons.

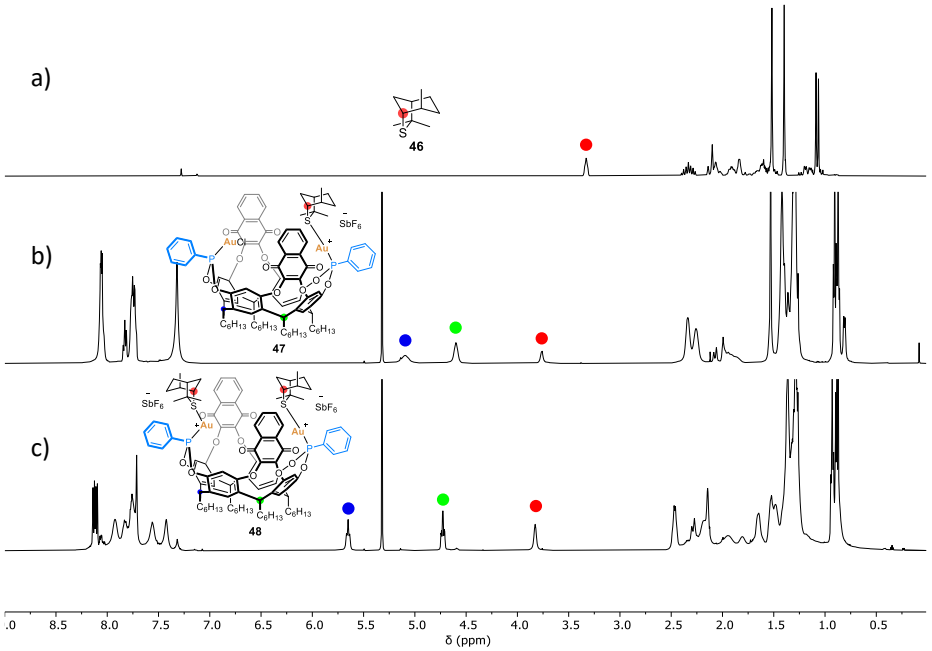

Figure 5.6 ^{1}H NMR spectra of **46** in $CDCl_3$ (a), monocomplexed cavitand **47** (b) and dicomplexed cavitand **48** (c) in CH_2Cl_2 (400 MHz, T = 298 K).

Moreover, crystals of **48** were obtained by crystallization from a mixture of dichloroethane and pentane. The preliminary X-ray structure confirmed the presence of two isothiocineole ligands complexed to the cavitand gold atoms (Figure 5.7).

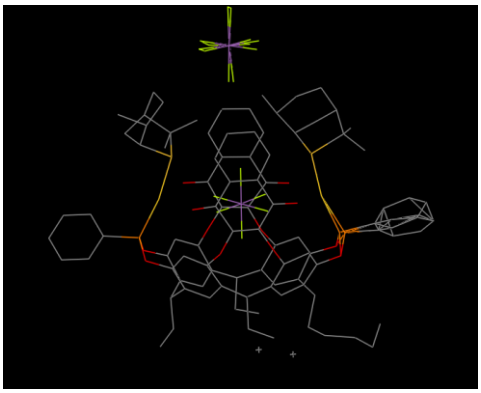

Figure 5.7 X-ray diffraction structure of complex **48**.

Then, complexation of thioether ligands was attempted on cavitand **L**. At the beginning, the synthesis of the new complexes was tried with the same condition used for complexes **44** and **47**. So, **L** was treated in dichloromethane with $AgSbF_6$ (0.8 equiv) and tetrahydrothiophene (10 equiv) to obtain **49**, and in the other case, with (1*R*,4*R*,5*R*)-isothiocineole (1.05 equiv) to obtain **50** (Scheme 5.24).

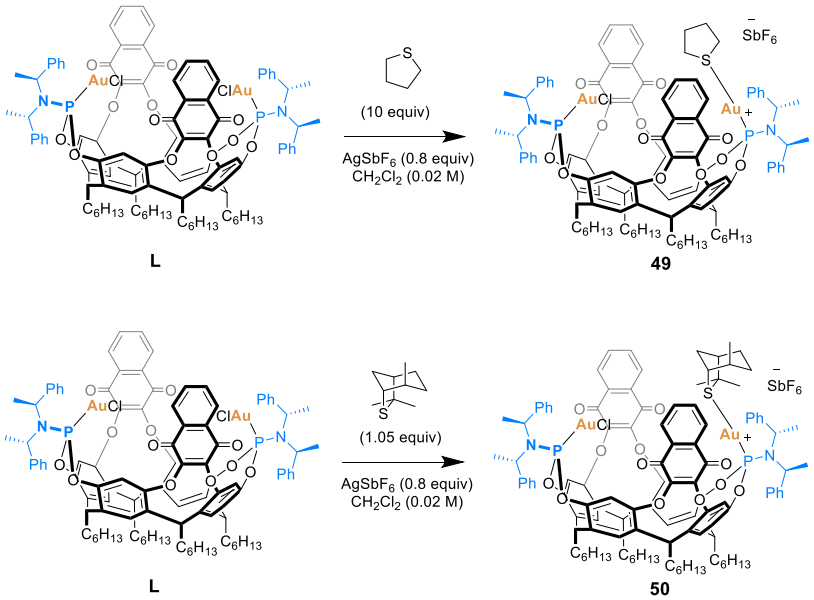

Scheme 5.24 Synthesis of chiral complexes **49** and **50**.

The stack plot of ^{1}H NMR spectra of **L** and **49** is the following:

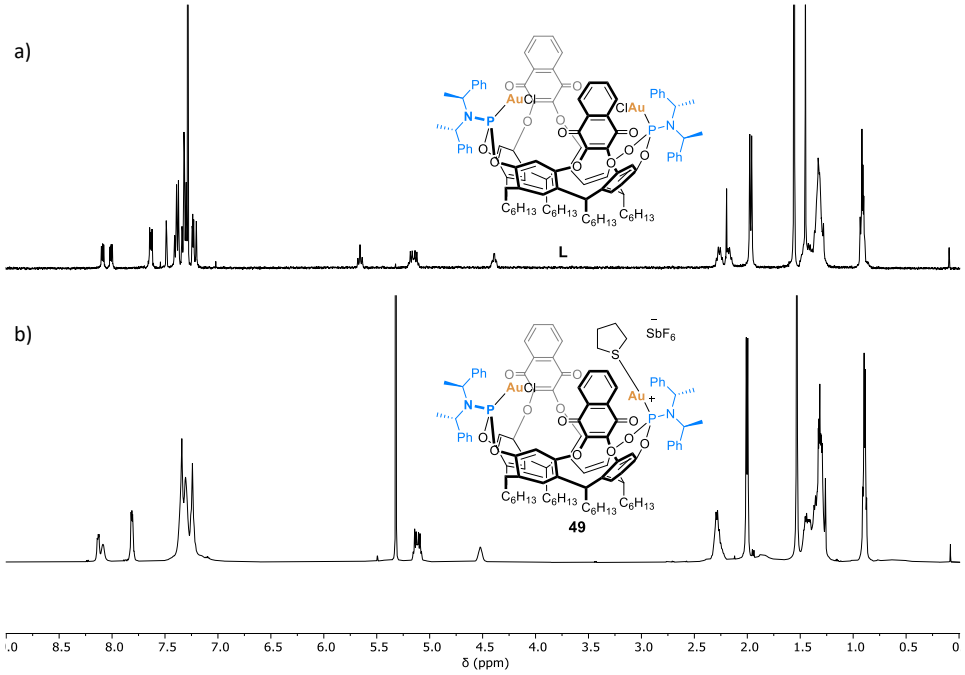

Figure 5.8 ^{1}H NMR spectra of **L** in $CDCl_3$ (a) and **49** in CH_2Cl_2 (b) (400 MHz, T = 298 K).

From these spectra it can be noticed a different pattern of signals between 6 and 4 ppm: only two signals from CH protons instead of three and their overall integration is 3 instead of 4. Moreover, thioether signals are not clear or present. At this stage, the possibility of cavitands to form clusters, independently by the presence of the thioether ligand, was considered, as it was previously observed in the synthesis of the cationic catalyst **T** under similar conditions (see supporting information of [82]). In that case, the formation of a trimeric gold(I) cavitand was observed, in which gold(I) of one monomer was linked to a nitrogen atom of the quinoxaline wall of another cavitand. One hypothesis is that cavitand **L** forms clusters when in presence of $AgSbF_6$: probably gold(I) is bonded to a nitrogen of phosphoramidites group of another cavitand instead of the complex with the thioether. To confirm this hypothesis, compound **49** was tried in catalysis to verify its reactivity in the alkoxycyclization reaction of (*E*)-1,6-enynes (Table 5.3).

Table 5.3 Alkoxycyclization of (*E*)-1,6-dyenine **29** with cavitand **49**.

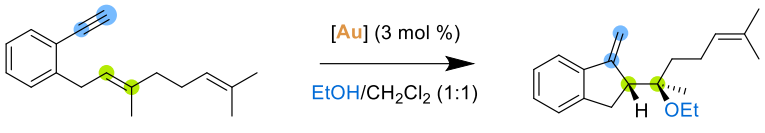

29 **30**

Entry[a]	[Au]	T [°C]	t [h]	Conversion [%]
1	**49**	23	overnight	0
2	**49**	23	7 days	0
3	**49**	40	7 days	0

[a] (0.06 mmol scale), 0.1 M.

As expected, using compound **49** as catalyst, no reactivity was detected and no conversion of starting material was observed, even increasing the reaction time or the temperature. This result seemed to confirm the cluster formation, as in this case no gold atoms were available for the coordination of the substrate. Furthermore, another test was performed: in one case, cavitand **L** was treated with 0.9 equivalents of $AgSbF_6$ and 1.05 equivalents of (1*R*,4*R*,5*R*)-isothiocineole; in the other case, the same experiment was carried out but without the addition of the thioether (test *a*). The ^1H NMR spectra of both experiments were found to be identical, and that confirmed the formation of clusters in which thioether ligands are not present (Figure 5.9).

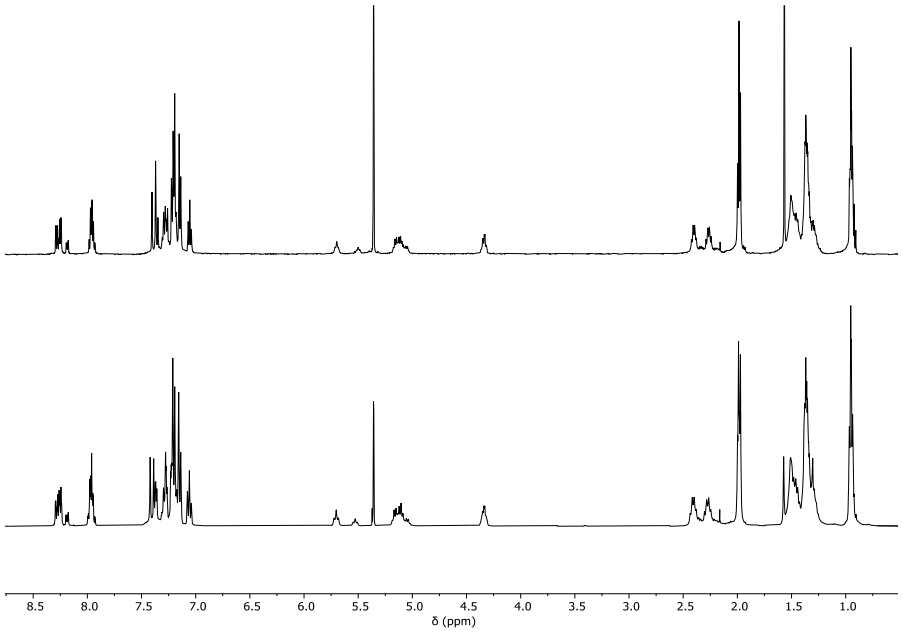

Figure 5.9 ^{1}H NMR spectrum of **50** (up) and test *a* (bottom) in CD_2Cl_2.

Afterwards, thioureas were also tested as ligands for dinuclear gold(I) cavitands. The idea was inspired by the "H-bonded counterion-directed catalysis" previously reported by the group of Echavarren:[67] in this work the chiral information is transported by the chiral counterion holding close to the active site by hydrogen bonds with ureas or thioureas group on the catalyst scaffold. With the purpose of merging gold(I) cavitands and chiral counterion effect to induce asymmetric transformations, a thiourea was evaluated as ligand for gold(I). The simultaneous use of the thiourea-cavitand gold(I) complex and chiral counteranions in the catalytic reaction should create a system in which, as previously reported, the chiral information is kept close to the reaction by hydrogen bonds with the thiourea moiety, as shown in Scheme 5.25.

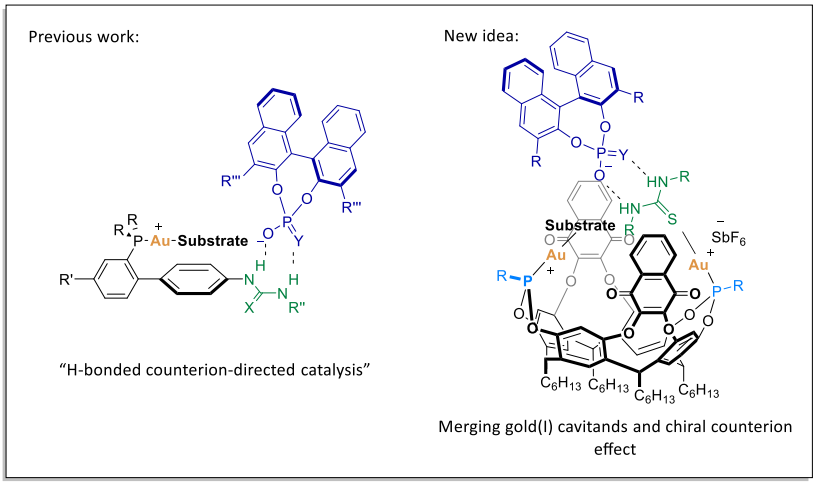

Scheme 5.25 Idea of merging gold(I) cavitands and chiral counterion effect.

With this aim, cavitand **F** was treated with 0.8 equivalents of $AgSbF_6$ and 1.05 equivalents of *N,N'*−bis[3,5−bis(trifluoromethyl)phenyl]thiourea (Scheme 5.26). Subsequent precipitation from a mixture of dichloromethane and pentane afforded complex **51** in 72% yield.

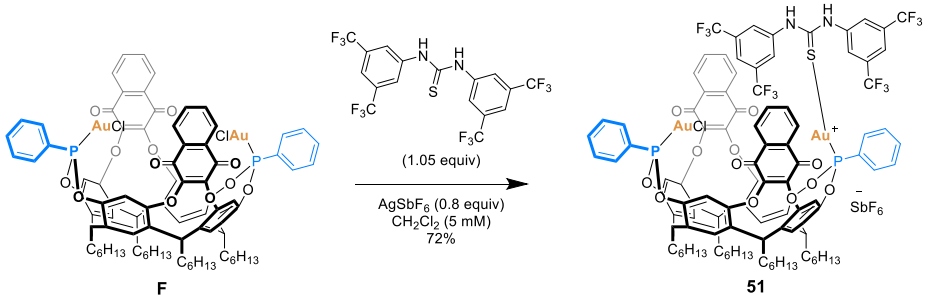

Scheme 5.26 Synthesis of achiral gold(I) cavitand **51**.

NMR experiments confirmed the mono-coordination of *N,N'*−bis[3,5−bis(trifluoromethyl)phenyl]thiourea.

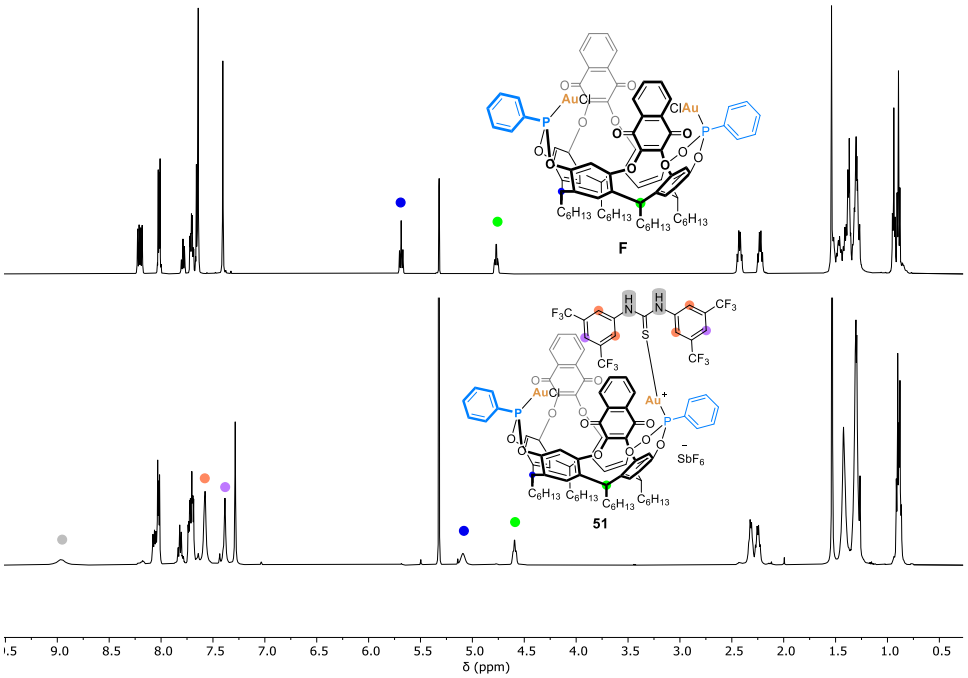

Figure 5.10 Comparison between ^{1}H NMR spectra of complexes **F** and **51**.

Comparing ^{1}H NMR spectra of complexes **F** and **51** (Figure 5.10), it can be noticed the change in the signal pattern between 6 and 4.5 ppm and the appearance of new signals from NH thiourea moiety at 9 ppm and two singlets corresponding to the aromatic protons of the ligand, at 7.6 and 7.4 ppm. Once demonstrated the formation of the thiourea complex **51**, only preliminary tests were carried out to merge the effect of cavitands and chiral ions in catalysis due to the lack of time. However, this hindered achiral cavitand was tried in the cycloisomerization of 1,6-dienynes.

This last part will treat the catalytic outcomes in the *exo*/*endo* selective cyclization of (*Z*) and (*E*)-1,6-dienynes and in the alxokycyclization of (*E*)-1,6-dienynes with newly synthesized cavitands. Recently, the group of Echavarren tested a series of gold(I) cavitand complexes in the cycloisomerization of (*Z*)-1,6-dyenune **27**. It was observed that this reaction, if performed with traditional gold(I) catalysts, as [Au(PPh$_3$)Cl] or [Au(P(OMe)$_3$Cl], generated product **28a** as the main product

through the exocyclic single-cleavage rearrangement pathway. Contrarily, gold(I)-cavitand catalysts provided the inversion of the selectivity, yielding principally product **28b** as a result of the endocyclic single-cleavage skeletal rearrangement mechanism.

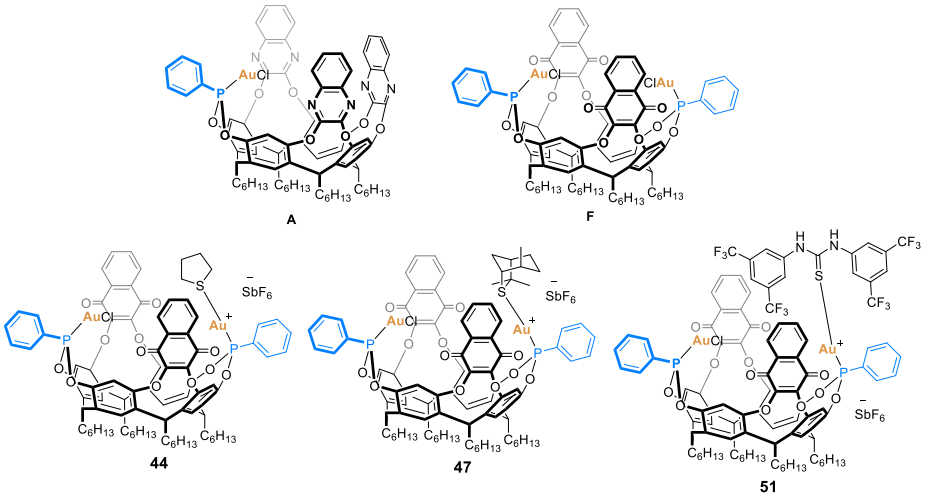

Scheme 5.27 Previously synthetized gold(I) cavitands **A** and **F**, and new cationic cavitands **44**, **47** and **51**.

The best result was obtained with mononuclear gold(I) cavitand **A** bearing three quinoxaline walls, which led to 1:5 ratio of **28a**/**28b**. As a comparison, precursor of this work, dinuclear cavitand **F**, afforded **28a**/**28b** in 3:1 ratio. Therefore, new cationic cavitands **44**, **47** and **51** were proved in the cyclization of (*Z*) and (*E*)-1,6-dienynes **27** and **52** in the same conditions (Table 5.4). The addition of $AgSbF_6$ should cleave the chloride from the non-coordinated gold atom, allowing the coordination of the substrate, while the S-based ligand should hinder the cavity forcing the substrate to fold in specific way.

Table 5.4 *Exo*/*endo* cyclization of (*Z*)-1,6-dienyne **27** (a) and (*E*)-1,6-dyenine **52** (b).

a)

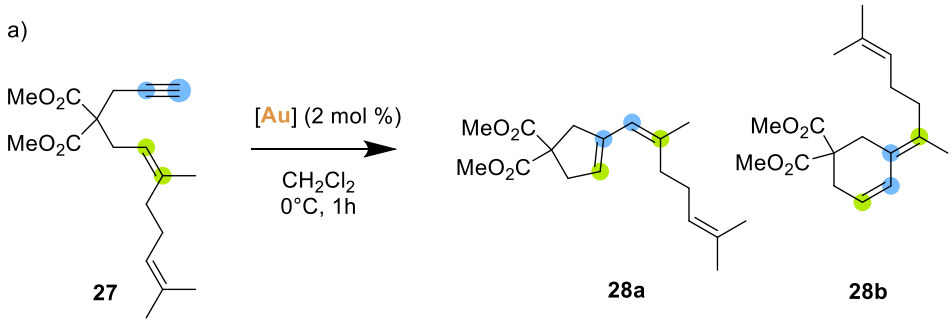

Entry[a]	[Au]	$AgSbF_6$ [mol %]	**53a/53b**
1	$[Au(PPh_3)Cl]$	2	11:1
2	$[Au(P(OMe)_3)Cl]$	2	>20:1
3	**A**	2	1:5
4	**F**	4	3:1
5	**44**	4	1.85:1
6	**47**	4	1.7:1
7	**51**	4	2.5:1
8	**44**	-	2.8:1
9	**51**	-	3:1

[a] (0.06 mmol scale), 0.1M.

b)

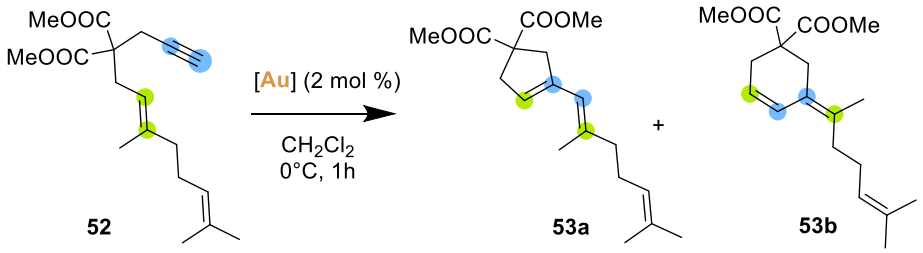

Entry[a]	[Au]	$AgSbF_6$ [mol %]	**28a/28b**
1	**44**	4	1.8:1
2	**47**	4	1.85:1
3	**51**	4	2:1
4	**44**	-	2.3:1
5	**51**	-	3:1

[a] (0.06 mmol scale), 0.1M.

The results with (*Z*) and (*E*)-1,6-dienynes were comparable. Cavitands with thioethers as ligand displayed a perceptible difference in the catalytic activity. In this case, ratio of about 1.8:1 of **a**/**b** was observed. With cavitand **51** bearing thiourea ligand, the catalytic transformation provided similar result to that with catalyst **F**. Unfortunately, these cavitands were reactive in the cyclization of 1,6-

dienyne even when $AgSbF_6$ was not added (entry 8 and 9 of Table 5.4 a, entry 4 and 5 of Table 5.4 b). This suggests that the bond between gold(I) and S of the ligand is quite labile and the substrate can displace easily the thioether/thiourea ligand. Especially in this case, the ratio **a**/**b** was found to be also comparable with the one obtained with cavitand **F**.

Finally, the use of the newly devised thioether-bonded chiral cavitands **47** and 48 was evaluated in the alkoxycyclization of (*E*)-1,6-dienyne **29** (Table 5.5).

Table 5.5 Alkoxycyclization of (*E*)-1,6-dyenine **29**.

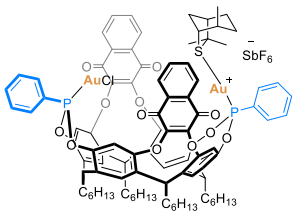

47

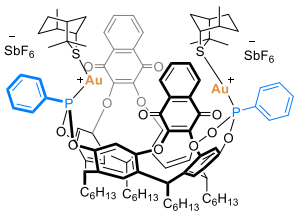

48

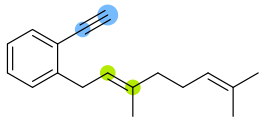

29

[Au] (3 mol %)

$EtOH/CH_2Cl_2$ (1:1)

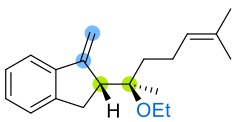

30

Entry[a]	[Au]	$AgSbF_6$	T [°C]	t [h]	*er*[b]
1	**47**	6 mol %	23	overnight	52:48
2	**47**	-	23	overnight	50:50
3	**48**	-	23	overnight	52:48

[a] (0.06 mmol scale), 0.1 M.
[b] Column OD-H, flow 1 mL/min, eluent Hexene:IPA 100:0, 254 nm, Rt 7.25/ 9.00 min.

The conversion of substrate **29** was monitored by GC and it has been noticed to be slower in comparison with the catalysis reported in the paper, in which the substrate completely converted in 1 hour (Table 5.5). With catalyst **47** and **48**, after 1 hour the conversion was very low and after 5 hours the prevalent compound was still the substrate. The reaction was left overnight and after that time the conversion was almost 100%. The crude products were purified by flash column chromatography (SiO_2, cyclohexane/ethyl acetate 98:2) and then, the *er*

of **34** was measured through chiral HPLC. Unfortunately, the result was a racemic product in every case. The same reactivity was observed for the mono-cationic cavitand **26**, cavitand **26** without the presence of $AgSbF_6$, and the di-cationic cavitand **27**. It is reasonable to think that in these conditions the substrate can displace the thioether complexed on gold(I), but presumably not so easily or quickly as the reaction rate is considerably slower.

Conclusions

A series of new achiral and chiral digold(I) resorcin[4]arene-based cavitand complexes were synthesized. Thioethers or thioureas were used as ligands for the coordination of one or both gold atoms, leading to a modification of the cavity in steric hindrance and chirality. Thus, these new gold(I) cavitand catalysts were tested in the cycloisomerization and alkoxycyclization of 1,6-dienynes. Even though the results were not remarkably positive, some differences in the reactivity were displayed, demonstrating the potential of the strategy. The successful coordination of thiourea could pave the way to the merged strategy between cavitand and chiral counterion effects.

Acknowledgments

Thanks to Prof. Antonio Echavarren to giving me the possibility to work in his group for six months at ICIQ, Tarragona, Spain. Thanks to Dr. Inmaculada Martín-Torres and Gala Ogalla for the support in the project.

Experimental Section

General Methods

The synthesis of the ligands and gold(I) complexes was carried out under argon in solvents dried by passing through an activated alumina column on a PureSolvTM Solvent Purification System (SPS, Innovative Technologies, Inc., MA). Yields refer to chromatographically and spectroscopically pure (^{1}H NMR) homogeneous material, unless otherwise stated. Thin layer chromatography was carried out using TLC aluminum sheets coated with 0.2 mm of silica gel (Merck Gf234) using short-wave UV light as visualizing agent and, $KMnO_4$ or acidic vanillin followed by heat as developing agents. Chromatographic purifications were carried out using flash grade silica gel (SDS Chromatogel 60 ACC, 40-60 µm) as the stationary phase manually, or using a CombiFlash®Rf instrument with normal phase disposable columns of different sizes (Teledyne Isco). Reactions were monitored by TLC and UHPLC (Agilent Technologies 1290 Infinity II, LC/MS with single-quad detector InfinityLab (APCI ionization source). Melting points were determined using a MP70 Melting Point System (Mettler Toledo). NMR spectra were recorded at 298 K on BrukerAvance Ultrashield NMR spectrometers (300 MHz, 400 MHz, 500 MHz and 500 MHz with CryoProbe). Chemical shifts (δ) are reported in parts per million (ppm) and referenced to residual solvent (For ^{1}H NMR: $CDCl_3$ at 7.26 ppm, CD_2Cl_2 at 5.31 ppm, for ^{13}C NMR: $CDCl_3$ at 77.16 ppm, CD_2Cl_2 at 54.00 ppm). The following abbreviations were used to explain multiplicities: s = singlet, d = doublet, t = triplet, q = quartet, p = “pentet” (quintet), m = multiplet, br s = broad singlet. Coupling constants (J) are reported in Hertz (Hz). Mass spectra were recorded on a Waters LCT Premier Spectrometer (ESI and APCI) or on an Autoflex Broker Daltonics (MALDI and LDI). Specific optical rotation measurements were carried out on a Jasco P-1030 model polarimeter equipped with a PMT detector using the sodium line at 589 nm. Chiral HPLC analyses were performed on an Agilent Technologies 1200 series. SFC analyses were performed on an Agilent

Technologies 1260 Infinity II, a Waters ACQUITY UPC2 System with diode array detector and by Chiral Technologies Europe analytical service. X-ray diffraction data were collected at 100 K on a Rigaku MicroMax-007HF, Mo *Kα* rotating anode, equipped with a Pilatus 200 K detector or on a Bruker APEX DUO, Mo *Kα* Microfocus source E025 IuS anode, equipped with an APEX DUO detector using omega scans.

Synthetic Procedure and Analytical Data

Phosphonite 35: $PhP(Cl)_2$ (904 µL, 1.23 mmol) was added to a mixture of tetraphenol **34** (205.0 g, 0.18 mmol) and pyridine (146 µL, 1.81 mmol) in dry toluene (3.6 mL, 0.05 M) under an argon at room temperature. After stirring for 23 h, the reaction mixture concentrated under vacuum and the crude was purified by flash column chromatography on silica gel (cyclohexane/EtOAc 1:0 to 7:3) to afford phosphonite **35** (102 mg, 0.076 mmol, 42% yield) as a yellow solid. The spectral data were fully consistent with those previously reported.[82] **M.p.** 309–311 °C; **^{1}H NMR** (500 MHz, CD_2Cl_2): δ = 8.00 (dd, *J* = 5.7, 3.2 Hz, 4H), 7.96 – 7.88 (m, 4H), 7.66 – 7.56 (m, 10H), 7.46 (s, 4H), 7.37 (s, 4H), 5.72 (t, *J* = 8.2 Hz, 2H), 4.73 (td, *J* = 8.3, 2.2 Hz, 2H), 2.34 (q, *J* = 7.9 Hz, 8H), 1.54 – 1.28 (m, 32H), 0.92 (h, *J* = 3.6 Hz, 12H) ppm; **^{31}P NMR** (203 MHz, CD_2Cl_2): δ = 170.8 ppm; **^{13}C NMR** (126 MHz, CD_2Cl_2): δ = 182.9, 153.9, 152.7 (d, *J* = 3.6 Hz), 152.5, 140.3 (d, *J* = 11.2 Hz), 138.0 (d, *J* = 3.1 Hz), 136.2, 134.8, 131.9, 130.9, 130.4, 130.2, 129.1 (d, *J* = 6.3 Hz), 127.2, 124.1, 117.6 (d, *J* = 3.0 Hz), 36.7, 34.0, 32.7, 32.6, 32.4, 29.9 (d, *J* = 5.3 Hz), 28.5 (d, *J* = 1.6 Hz), 23.2 (d, *J* = 1.8 Hz), 14.4 (d, *J* = 1.6 Hz) ppm.

Complex F: $(Me_2S)AuCl$ (184 mg, 0.62 mmol) was added to a solution of phosphonite **35** (400 mg, 0.30 mmol) in dry CH_2Cl_2 (0.05 M) under argon at 23 °C. The reaction mixture was stirred at 23 °C for 1 h and then concentrated under vacuum. The crude was purified by flash column chromatography on silica gel using cyclohexane to cyclohexane/EtOAc/CH_2Cl_2 8:1:1 as eluent. Complex **F** was obtained as a white solid in 72% yield. The spectral data were fully consistent with

those previously reported.[82] **M.p.** = 321–323 °C; **^{1}H NMR** (500 MHz, CD_2Cl_2): δ = 8.20 (ddd, *J* = 14.7, 8.3, 1.4 Hz, 4H), 8.02 (dd, *J* = 5.7, 3.3 Hz, 4H), 7.79 (td, *J* = 7.3, 1.5 Hz, 2H), 7.74 – 7.68 (m, 4H), 7.67 – 7.63 (m, 8H), 7.40 (s, 4H), 5.69 (t, *J* = 8.2 Hz, 2H), 4.77 (td, *J* = 8.0, 3.0 Hz, 2H), 2.43 (q, *J* = 7.7 Hz, 4H), 2.23 (q, *J* = 8.2 Hz, 4H), 1.49 – 1.24 (m, 32H), 0.99 – 0.92 (m, 6H), 0.93 – 0.86 (m, 6H) ppm; **^{31}P NMR** (203 MHz, CD_2Cl_2): δ = 138.0 ppm; **^{13}C NMR** (126 MHz, CD_2Cl_2): δ = 182.8, 154.4 (d, *J* = 2.2 Hz), 151.9, 148.3 (d, *J* = 8.0 Hz), 137.7 (d, *J* = 2.2 Hz), 136.9 (d, *J* = 2.9 Hz), 134.9 (d, *J* = 9.6 Hz), 132.9, 132.2, 131.9, 131.8, 130.8, 129.7 (d, *J* = 14.1 Hz), 127.8, 124.1, 118.4 (d, *J* = 4.2 Hz), 36.5, 33.9, 33.4, 32.4 (d, *J* = 8.1 Hz), 30.9, 29.8, 28.4 (d, *J* = 6.6 Hz), 23.2 (d, *J* = 7.5 Hz), 14.4 ppm.

1,1-dichloro-*N,N*-bis((*S*)-1-phenylethyl)phosphanamine (36): A reported procedure was followed.[85] A flame-dried Schlenk tube was charged with (1*S*,1'*S*)-bis(1-phenylethyl)amine (1 equiv) and anhydrous THF (0.44 M) under argon, the solution was then cooled to -78 °C and nBuLi (1.1 equiv) was added dropwise. The mixture was stirred at -78 °C for 30 min and then PCl_3 (1.3 equiv) was added dropwise to the solution of lithium amide at -78 °C under argon. The reaction mixture was warmed to 23 °C and stirred overnight. The mixture was concentrated in vacuo, and the residual PCl_3 was removed via repetitive THF dilution (x3) and vacuum evaporation to give 1,1-dichloro-*N,N*-bis((*S*)-1-phenylethyl)phosphanamine (**36**) that was used in the next step without further purification. **^{31}P NMR** (162 MHz, C_6D_6): δ = 168.7 ppm.

Phosphoramidites 37 and 38: Triethylamine (1.48 mL, 10.59 mmol) was added to a mixture of tetraphenol **34** (2.0 g, 1.76 mmol) in dry toluene (29.4 mL, 0.06 M) under argon at 23 °C. The mixture was stirred at 23 °C for 5 min. Then N,N-bis[(1S)-1-phenylethyl]phosphoramidous dichloride **36** (1.73 g, 5.29 mmol) in dry toluene (5.8 mL) was added to the mixture, which was stirred for 5 h. The mixture was filtered through a pad of Celite, washed with toluene and then the filtrate was concentrated under vacuum. The crude was purified by flash column

chromatography on silica gel (cyclohexane to cyclohexane/CH_2Cl_2/EtOAc 8:1:1) to afford a mixture of **37** and **38** (1.3 g, 0.77 mmol, 44% yield, **37**/**38** 1.2:1 ratio) as a yellow solid.

Complex L and complex P: (Me_2S)AuCl (460 mg, 1.56 mmol) was added to a solution of phosphonites **37** and **38** (1.22 g, 0.74 mmol) in dry CH_2Cl_2 (0.05 M) under argon at 23 °C. The reaction mixture was stirred at 23 °C for 1 h and then concentrated under vacuum. The crude was purified by flash column chromatography on silica gel using cyclohexane to cyclohexane/EtOAc/CH_2Cl_2 8:1:1 as eluent. Complex **L** was obtained as a yellow solid in 46% yield (726 mg, 0.35 mmol) and complex **P** in 38% yield (596 mg, 0.28 mmol), as a yellow solid.

Complex L: M. p. = 146–148 °C; **^{1}H NMR** (500 MHz, CD_2Cl_2): δ = 8.04 – 7.98 (m, 2H), 7.96 – 7.90 (m, 2H), 7.65 – 7.57 (m, 4H), 7.49 (d, *J* = 1.7 Hz, 2H), 7.44 – 7.32 (m, 20H), 7.25 (dd, *J* = 6.4, 2.9 Hz, 6H), 5.61 (t, *J* = 8.2 Hz, 2H), 5.18 (dq, *J* = 17.1, 6.8 Hz, 4H), 4.54 (td, *J* = 8.1, 3.1 Hz, 2H), 2.34 (q, *J* = 7.7 Hz, 4H), 2.28 – 2.11 (m, 4H), 2.01 (d, *J* = 7.1 Hz, 12H), 1.53 – 1.23 (m, 32H), 0.90 (q, *J* = 7.1 Hz, 12H) ppm; **^{31}P NMR** (203 MHz, CD_2Cl_2): δ = 120.3 ppm; **^{13}C NMR** (126 MHz, CD_2Cl_2): δ = 182.7, 182.5, 154.0 (t, *J* = 1.8 Hz), 151.9, 151.7, 146.9 (d, *J* = 4.3 Hz), 146.5 (d, *J* = 4.6 Hz), 141.4 (d, *J* = 3.7 Hz), 137.1, 136.9, 136.8 (dd, *J* = 6.8, 2.8 Hz), 134.6 (d, *J* = 10.4 Hz), 130.8 (d, *J* = 3.6 Hz), 128.9, 128.8, 128.4, 127.8, 127.6, 123.6, 118.9 (d, *J* = 4.1 Hz), 118.6 (d, *J* = 4.3 Hz), 54.7 (d, *J* = 8.8 Hz), 36.4, 33.8, 33.3, 32.4 (d, *J* = 8.7 Hz), 30.4, 29.8 (d, *J* = 17.4 Hz), 28.3 (d, *J* = 17.9 Hz), 23.2 (d, *J* = 2.7 Hz), 21.6 (d, *J* = 2.6 Hz), 14.4 (d, *J* = 5.0 Hz) ppm.

Complex P: M. p. = 292–294 °C; **^{1}H NMR** (500 MHz, CD_2Cl_2): δ = 8.12 – 8.04 (m, 1H), 7.96 (ddd, *J* = 12.1, 6.6, 1.9 Hz, 2H), 7.76 – 7.69 (m, 2H), 7.61 – 7.53 (m, 2H), 7.52 – 7.48 (m, 1H), 7.42 – 7.26 (m, 15H), 7.24 – 7.11 (m, 9H), 7.09 – 7.00 (m, 2H), 6.97 – 6.90 (m, 2H), 5.42 (br s, 1H), 5.17 (ddt, *J* = 18.0, 14.2, 5.9 Hz, 3H), 4.86 (t, *J* = 7.7 Hz, 1H), 4.75 (dq, *J* = 19.2, 7.0 Hz, 2H), 4.42 (td, *J* = 8.1, 3.2 Hz, 1H), 2.44 – 2.07 (m, 14H), 2.03 (d, *J* = 7.1 Hz, 6H), 1.54 – 1.20 (m, 32H), 1.03 – 0.80 (m, 12H)

ppm; **^{31}P NMR** (203 MHz, CD_2Cl_2): δ = 126.7, 117.7 ppm; **^{13}C NMR** (126 MHz, CD_2Cl_2): δ = 182.8, 182.4, 181.8, 180.9, 154.1, 153.7, 153.3 (d, *J* = 2.6 Hz), 151.9, 150.7 (d, *J* = 13.6 Hz), 150.5 (d, *J* = 6.2 Hz), 149.8, 148.5, 148.3, 141.5 (d, *J* = 3.5 Hz), 141.3, 137.1, 136.3 (d, *J* = 3.5 Hz), 136.1 (d, *J* = 3.9 Hz), 135.8, 134.9 (d, *J* = 12.3 Hz), 134.5 – 134.2 (m), 133.7, 131.1, 130.9 (d, *J* = 2.0 Hz), 130.8, 130.6, 129.3, 128.9, 128.6 (d, *J* = 6.6 Hz), 128.4 (d, *J* = 3.7 Hz), 127.2 (d, *J* = 2.2 Hz), 126.8, 126.3, 125.4, 125.2, 123.2, 121.6, 118.9, 117.5 (d, *J* = 6.6 Hz), 116.2, 115.9, 54.8 (d, *J* = 8.5 Hz), 40.2 (d, *J* = 7.1 Hz), 36.5, 35.3, 34.2, 33.5, 32.5 – 32.3 (m), 32.2, 31.6 (d, *J* = 16.0 Hz), 30.8, 29.9, 29.8 – 29.6 (m), 28.2 (d, *J* = 1.8 Hz), 27.9, 27.8, 23.4 – 22.8 (m), 21.9, 21.3 (d, *J* = 3.2 Hz), 14.9 – 13.9 (m) ppm.

Cavitand 44: Tetrahydrothiophene (24.3 µL, 275 µmol) was added to a solution of complex **F** (49.8 mg, 27.5 µmol) in CH_2Cl_2 (6 mL, 5 mM). $AgSbF_6$ (9.9 mg, 29 µmol) was added to the mixture, and it was stirred overnight under argon. The reaction crude was filtered through a pad of Celite and washed with CH_2Cl_2. The filtrate was concentrated under reduced pressure and the crude product was recrystallized from CH_2Cl_2/pentane to give **44** (53 mg, 92%) as a yellow solid. **M. p.** = 290-292 °C; **^{1}H NMR** (500 MHz, CD_2Cl_2): δ = 8.13 – 8.04 (m, 8H), 7.87 – 7.81 (m, 2H), 7.79 – 7.71 (m, 8H), 7.42 (s, 4H), 7.38 (s, 4H), 5.22 (s, 2H), 4.62 (t, *J* = 8.8 Hz, 2H), 2.77 (s, 4H), 2.42 – 2.23 (m, 8H), 1.52 – 1.18 (m, 36H), 0.95 – 0.82 (m, 12H); **^{31}P NMR** (203 MHz, CD_2Cl_2): δ = 144.0; **^{13}C NMR** (126 MHz, CD_2Cl_2): δ = 181.1, 152.8, 149.4, 136.1, 135.0, 134.6, 131.2, 131.0, 130.4, 129.5, 126.7, 123.7, 117.11, 39.6, 36.2 (d, J = 9.6 Hz), 34.6, 31.7, 31.1, 30.6, 29.7, 29.1, 27.6 (d, *J* = 15.6 Hz), 22.6 (d, *J* = 3.15), 13.8; **HR-MS** (ESI+) calculated for m/z [C84H82Au2ClO12P2]+, [M-C4H8S-SbF6]+: 1773.4296; found: 1773.4261.

Recrystallization method:

In a vial, the solid (ca. 30 mg) was dissolved in ca. 1.5 mL of dichloromethane. Pentane was added with a pipette until the solution turned cloudy. The vial was

left in the fridge for a couple of hours, then the precipitate was collected by filtration and washed with pentane.

(1R,4R,5R)-Isothiocineole (46): (R)-Limonene (8.4 ml, 0.064 mol), elemental sulfur (2.3 g, 0.09 mol) and γ-terpinene (8.7 ml, 0.06 mol) were added in a round bottom flask fitted with a reflux condenser. The reaction mixture was heated to 110 °C overnight. After that, the reaction mixture was allowed to cool down and a distillation apparatus was connected. After separation of various volatiles, (1R,4R,5R)-isothiocineole (1.1 g, 10%) was distilled at 115 °C/28 mm Hg. The spectral data were fully consistent with those previously reported.[84]

Cavitand 47: (1R,4R,5R)-Isothiocineole **46** (5.04 mg, 29.6 µmol) was added to a solution of complex **F** (51.0 mg, 28.2 µmol) in CH_2Cl_2 (6 mL, 5 mM). $AgSbF_6$ (7.7 mg, 22.5 µmol) was added to the mixture, and it was stirred overnight under argon. The reaction crude was filtered through a pad of Celite and washed with CH_2Cl_2. The filtrate was concentrated under reduced pressure and the crude product was recrystallized from CH_2Cl_2/pentane to give **47** (42 mg, 68%) as a yellow solid. **M. p.** = 167-169 °C; **^{1}H NMR** (500 MHz, CD_2Cl_2): δ = 8.11 – 8.01 (m, 8H), 7.86 – 7.80 (m, 2H), 7.79 – 7.70 (m, 8H), 7.31 (s, 8H), 5.09 (bs, 2H), 4.60 (bs, 2H), 3.76 (s, 1H), 2.40 – 2.18 (m, 8H), 2.10-1.80 (m, 4H), 1.46 – 1.22 (m, 42H), 0.93 – 0.84 (m, 12H), 0.81 (d, *J* = 6.9 Hz, 2H); **^{31}P NMR** (203 MHz, CD_2Cl_2): δ = 144.5; **^{13}C NMR** (126 MHz, CD_2Cl_2): δ = 181.3, 152.9, 149.9, 136.2, 135.3, 134.9, 131.3 (d, *J* = 18.5 Hz), 130.8, 129.9 (d, *J* = 14.1 HZ), 127.0, 123.9, 117.3, 66.5, 62.4, 48.7, 36.6, 36.3, 35.3, 35.2, 35.0, 32.2 (d, *J* = 1.8 HZ), 31.2, 30.1, 29.6, 29.5, 28.0, 27.9, 25.6, 24.4, 23.0 (d, *J* = 3.1), 18.6, 14.2 (d, *J* = 2.8). **HR-MS** (ESI+) calculated for m/z [C84H82Au2ClO12P2]+, [M-C10H18S-SbF6]+: 1773.4296; found: 1773.4249; **α_D^{589}** = –108.2 deg.cm^2.g^{-1} (CH_2Cl_2, c 1.00, 298.5 K).

Cavitand 48: (1R,4R,5R)-Isothiocineole **46** (7.9 mg, 46.4 µmol) was added to a solution of complex **F** (40.0 mg, 22.1 µmol) in CH_2Cl_2 (4.5 mL, 5 mM). $AgSbF_6$ (15.6 mg, 45.3 µmol) was added to the mixture, and it was stirred overnight under argon. The reaction crude was filtered through a pad of Celite and washed with CH_2Cl_2. The filtrate was concentrated under reduced pressure and the crude product was recrystallized from CH_2Cl_2/pentane to give **48** (48 mg, 85%) as a yellow solid. **M. p.** = 176-178 °C; **^{1}H NMR** (500 MHz, CD_2Cl_2): δ = 8.16 – 8.09 (m, 4H), 7.98 – 7.69 (m, 14H), 7.71 – 7.48 (m, 4H), 7.47 – 7.26 (m, 4H), 5.65 (t, *J* = 8.2, 2H), 4.73 (td, *J* = 8.0, 3.03 Hz, 2H), 3.83 (s, 2H), 2.53 – 2.41 (m, 4H), 3.31 – 1.20 (m, 64H), 0.96 – 0.83 (m, 18H); **^{31}P NMR** (203 MHz, CD_2Cl_2): δ = 137.4; **^{13}C NMR** (126 MHz, CD_2Cl_2): δ = 182.7, 154.3 (d, *J* = 2.3 HZ), 154.2, 151.8, 146.7, 137.5, 136.0, 134.9, 133.8, 133.8, 131.1, 130.9, 129.9, 127.2, 126.7, 123.9, 66.2, 61.3, 48.6, 36.3, 35.6, 34.5, 33.8, 32.2, 32.1, 30.5, 30.1, 29.6, 28.2, 27.9, 24.5, 23.1, 23.0, 18.8, 14.2; **HR-MS** (ESI+) calculated for m/z [C94H99Au2O12P2S]+, [M-HSbF6-SbF6-C10H18S]+: 1907.5658; found: 1907.45692; $\boldsymbol{\alpha_D^{589}}$ = –17.3 deg.cm^2.g^{-1} (CH_2Cl_2, c 0.182, 300 K).

Cavitand 51: *N,N*'−bis[3,5−bis(trifluoromethyl)phenyl]−thiourea (9.3 mg, 18.6 µmol) was added to a solution of complex **F** (32.0 mg, 17.7 µmol) in CH_2Cl_2 (3.5 mL, 5 mM). $AgSbF_6$ (4.9 mg, 14.1 µmol) was added to the mixture, and it was stirred overnight under argon. The reaction crude was filtered through a pad of Celite and washed with CH_2Cl_2. The filtrate was concentrated under reduced pressure and the crude product was recrystallized from CH_2Cl_2/pentane to give **51** (32 mg, 72%) as a yellow solid. **M. p.** = 296-298 °C; **^{1}H NMR** (500 MHz, CD_2Cl_2): δ = 8.96 (s, 2H), 8.1 – 8.0 (m, 8H), 7.85 – 7.78 (m, 2H), 7.75 – 7.67 (m, 8H), 7.58 (s, 6H), 7.38 (s, 4H), 7.29 (s, 4H) 5.09 (bs, 2H), 4.89 (m, 2H), 2.36 – 2.20 (m, 8H), 1.46 – 1.25 (m, 32H), 0.93 – 0.84 (m, 12H); **^{31}P NMR** (203 MHz, CD_2Cl_2): δ = 143.8; **^{13}C NMR** (126 MHz, CD_2Cl_2): δ = 181.5, 153.2, 149.7, 136.8, 136.3, 136.0, 135.3, 134.8, 133.5, 133.2, 131.3 (d, *J* = 18.5 Hz), 130.8, 130.1, 129.8 (d, *J* = 14.0 HZ), 127.0,

126.0, 123.9, 123.8, 122.6, 121.7, 119.5, 117.6, 36.6, 35.2, 32.2 (d, *J* = 3.3 HZ), 32.0, 31.4, 30.1, 29.6 (d, *J* = 3.7), 28.0, 27.9, 23.0 (d, *J* = 4.2), 14.2.

Cyclization of *Z*-1,6-dienyne (27): gold(I) cavitand (2 mol %) and $AgSbF_6$ (4 mol %) were added to a solution of *Z*-1,6-dienyne **27** (69 mg, 0.23 mmol) in 2.25 mL CH_2Cl_2 (0.1 M) at 0 °C. The mixture was stirred at 0 °C for 60 min. The reaction was quenched by addition of 3 drops of NEt_3 and concentrated. The crude was purified by flash column chromatography (cyclohexane/EtOAc 4:1) to afford a mixture of **28a**/**28b** as a colorless oil. **^{1}H NMR** (400 MHz, $CDCl_3$): δ = **28a**: 5.73 (s, 1H), 5.39 (s, 1H), 5.14 (ddq, *J* = 8.5, 5.8, 1.5 Hz, 1H), 3.73 (s, 6H), 3.17 (d, *J* = 2.2 Hz, 2H), 3.03 (s, 2H), 2.16 – 2.01 (m, 4H), 1.77 (m, 3H), 1.69 (m, 3H), 1.62 (m, 3H); **28b**: 6.42 (dt, *J* = 10.2, 2.1 Hz, 1H), 5.65 (dt, *J* = 10.2, 4.1 Hz, 1H), 5.14 (ddq, *J* = 8.5, 5.8, 1.5 Hz, 1H), 3.70 (s, 6H), 2.87 (q, *J* = 1.4 Hz, 2H), 2.66 (dd, *J* = 4.3, 2.0 Hz, 2H), 2.16 – 2.01 (m, 4H), 1.77 (m, 3H), 1.69 (m, 3H), 1.62 (m, 3H) ppm. NMR data are in agreement with the ones previously reported in the literature.[86]

Synthesis of *E*-(1,6)-dienyne 29:

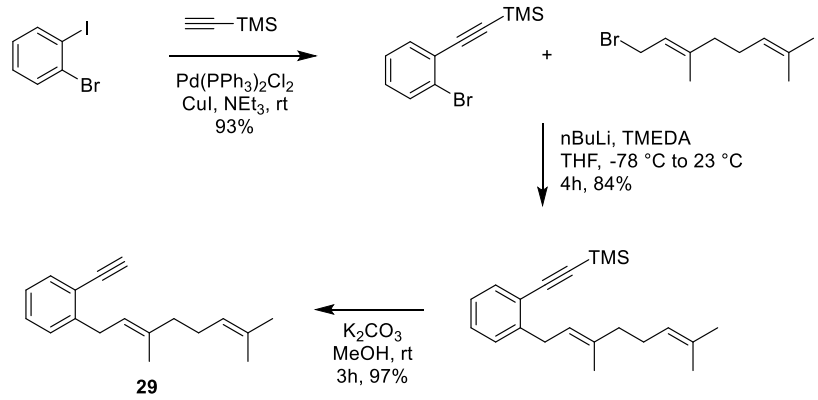

((2-Bromophenyl)ethynyl)trimethylsilane: to a solution of $Pd(PPh_3)_2Cl_2$ (2.5 mol %), copper(I) iodide (5 mol %) and 1-bromo-2-iodobenzene (1 equiv) in dry NEt_3 (0.25 M) was added ethynyltrimethylsilane (1.1 equiv) dropwise at 23 °C under argon. The reaction was stirred for 18 h at 23 °C. The reaction mixture was diluted

with EtOAc, filtered through a pad of celite, washed with EtOAc and concentrated under reduced pressure. The crude was purified by flash column chromatography (SiO2, cyclohexane) to afford ((2-Bromophenyl)ethynyl)trimethylsilane (8.3 g, 32.8 mmol, 93% yield) as a colorless oil. The spectral data were fully consistent with those previously reported.[87]

(E)-((2-(3,7-Dimethylocta-2,6-dien-1-yl)phenyl)ethynyl)trimethylsilane: A THF solution (12.3 mL, 0.8 M) of ((2-bromophenyl)ethynyl)trimethylsilane (2.5 g, 9.87 mmol, 1 equiv) was treated with nBuLi (2.5 M, 4.74 mL, 11.9 mmol, 1.2 equiv) at -78 °C for 20 min before the addition of tetramethylethylenediamine (1.48 mL, 9.87 mmol, 1 equiv); the mixture was stirred for an additional 20 min. Geranyl bromide (3.22 g, 14.81 mmol, 1.5 equiv) was added at -78 °C and the resulting mixture was allowed to react at 23 °C for 12 h. After addition of water, the aqueous phase was extracted with Et_2O (x3) and the combined organic layers were washed with brine, dried over $MgSO_4$, and concentrated under reduced pressure. The crude material was purified by column chromatography on silica using cyclohexane as eluent to give (E)-((2-(3,7-dimethylocta-2,6-dien-1-yl)phenyl)ethynyl)trimethylsilane (2.57 g, 8.28 mmol, 84% yield) as a colorless oil. **^{1}H NMR** (500 MHz, $CDCl_3$): δ = 7.42 (dd, *J* = 7.6, 1.4 Hz, 1H), 7.22 (td, *J* = 7.5, 1.5 Hz, 1H), 7.17 (ddd, *J* = 7.7, 1.5, 0.7 Hz, 1H), 7.10 (td, *J* = 7.4, 1.5 Hz, 1H), 5.34 (ddd, *J* = 7.3, 6.7, 1.3 Hz, 1H), 5.09 (tdd, *J* = 5.5, 2.8, 1.4 Hz, 1H), 3.52 (d, *J* = 7.3 Hz, 2H), 2.15 – 2.00 (m, 4H), 1.71 (s, 3H), 1.66 (s, 3H), 1.58 (s, 3H), 0.24 (s, 9H) ppm. The spectral data were fully consistent with those previously reported.[82]

29: K_2CO_3 (2.05 g, 14.8 mmol, 2 equiv) was added to a mixture of (E)-((2-(3,7-dimethylocta-2,6-dien-1-yl)phenyl)ethynyl)trimethylsilane (2.3 g, 7.41 mmol, 1 equiv) in MeOH (37 mL, 0.2 M). The mixture was stirred at 23 °C for 3 h. After addition of water, the aqueous phase was extracted with CH_2Cl_2 (x3) and the combined organic layers were washed with brine, dried over $MgSO_4$ and

concentrated under reduced pressure. The crude was purified by flash column chromatography (SiO_2, cyclohexane) to afford **29** (1.6 g, 6.8 mmol, 97% yield) as a colorless oil. **^{1}H NMR** (500 MHz, $CDCl_3$): δ = 7.46 (dd, *J* = 7.7, 1.4 Hz, 1H), 7.28 – 7.24 (m, 1H), 7.19 (dd, *J* = 7.8, 1.3 Hz, 1H), 7.13 (td, *J* = 7.5, 1.4 Hz, 1H), 5.32 (tt, *J* = 7.3, 1.2 Hz, 1H), 5.09 (tdd, *J* = 5.5, 2.7, 1.4 Hz, 1H), 3.53 (d, *J* = 7.3 Hz, 2H), 3.25 (s, 1H), 2.14 – 2.01 (m, 4H), 1.70 (s, 3H), 1.67 (s, 3H), 1.59 (s, 3H) ppm. The spectral data were fully consistent with those previously reported.[82]

Alkoxycyclization Reaction: gold(I) cavitand (3 mol %) was added to a mixture of **29** (1 equiv) in CH_2Cl_2/EtOH (1:1, 0.25 M) at room temperature. The mixture was stirred for 18h. The reaction was quenched with 3 drops of NEt_3 and concentrated under reduced pressure. Purification by flash column chromatography on SiO_2 (cyclohexane to cyclohexane/CH_2Cl_2 4:1) afforded **58** as a colorless oil. **^{1}H NMR** (400 MHz, CD_2Cl_2): δ = 7.47 – 7.41 (m, 1H), 7.25 – 7.22 (m, 1H), 7.20 (dd, *J* = 7.1, 1.5 Hz, 1H), 7.18 – 7.13 (m, 1H), 5.59 (d, *J* = 1.8 Hz, 1H), 5.13 (dddt, *J* = 7.2, 5.7, 2.8, 1.4 Hz, 1H), 5.09 (d, *J* = 1.6 Hz, 1H), 3.39 (qd, *J* = 7.0, 1.1 Hz, 2H), 3.26 (dt, *J* = 6.5, 2.6 Hz, 1H), 3.09 (dd, *J* = 17.1, 2.8 Hz, 1H), 2.99 (dd, *J* = 17.1, 8.4 Hz, 1H), 2.15 – 1.92 (m, 2H), 1.76 – 1.55 (m, 8H), 1.16 (t, *J* = 7.0 Hz, 3H), 0.79 (s, 3H) ppm. The spectral data were fully consistent with those previously reported.[82]

References

[1] A. Stephen, K. Hashmi, *Gold Bull* **2004**, *37*, 51–65.

[2] J. H. Teles, S. Brode, M. Chabanas, *Angew Chem Int Ed Engl* **1998**, *37*, 1415–1418.

[3] E. Mizushima, K. Sato, T. Hayashi, M. Tanaka, *Angewandte Chemie International Edition* **2002**, *41*, 4563–4565.

[4] A. Fürstner, *Chemical Society Reviews* **2009**, *38*, 3208–3221.

[5] C. Obradors, A. M. Echavarren, *Acc. Chem. Res.* **2014**, *47*, 902–912.

[6] L. Fensterbank, M. Malacria, *Acc. Chem. Res.* **2014**, *47*, 953–965.

[7] R. Dorel, A. M. Echavarren, *Chem. Rev.* **2015**, *115*, 9028–9072.

[8] P. Pyykkö, *Angewandte Chemie International Edition* **2002**, *41*, 3573–3578.

[9] P. Pyykkö, *Angewandte Chemie International Edition* **2004**, *43*, 4412–4456.

[10] H. Schwarz, *Angewandte Chemie International Edition* **2003**, *42*, 4442–4454.

[11] D. J. Gorin, F. D. Toste, *Nature* **2007**, *446*, 395–403.

[12] M. C. Gimeno, A. Laguna, *Chem. Rev.* **1997**, *97*, 511–522.

[13] D. J. Gorin, B. D. Sherry, F. D. Toste, *Chem. Rev.* **2008**, *108*, 3351–3378.

[14] W. Wang, G. B. Hammond, B. Xu, *J. Am. Chem. Soc.* **2012**, *134*, 5697–5705.

[15] D. V. Partyka, T. J. Robilotto, M. Zeller, A. D. Hunter, T. G. Gray, *Organometallics* **2008**, *27*, 28–32.

[16] P. Pérez-Galán, N. Delpont, E. Herrero-Gómez, F. Maseras, A. M. Echavarren, *Chemistry – A European Journal* **2010**, *16*, 5324–5332.

[17] A. S. K. Hashmi, T. Hengst, C. Lothschütz, F. Rominger, *Advanced Synthesis & Catalysis* **2010**, *352*, 1315–1337.

[18] G. C. Fortman, S. P. Nolan, *Organometallics* **2010**, *29*, 4579–4583.

[19] G. C. Fortman, S. P. Nolan, *Chemical Society Reviews* **2011**, *40*, 5151–5169.

[20] E. Jiménez-Núñez, A. M. Echavarren, *Chem. Rev.* **2008**, *108*, 3326–3350.

[21] C. Obradors, A. M. Echavarren, *Chemical Communications* **2014**, *50*, 16–28.

[22] R. Dorel, A. M. Echavarren, *J. Org. Chem.* **2015**, *80*, 7321–7332.

[23] C. Nieto-Oberhuber, M. P. Muñoz, E. Buñuel, C. Nevado, D. J. Cárdenas, A. M. Echavarren, *Angewandte Chemie* **2004**, *116*, 2456–2460.

[24] C. Nieto-Oberhuber, S. López, M. P. Muñoz, D. J. Cárdenas, E. Buñuel, C. Nevado, A. M. Echavarren, *Angewandte Chemie* **2005**, *117*, 6302–6304.

[25] C. Ferrer, M. Raducan, C. Nevado, C. K. Claverie, A. M. Echavarren, *Tetrahedron* **2007**, *63*, 6306–6316.

[26] E. Soriano, J. Marco-Contelles, *Acc. Chem. Res.* **2009**, *42*, 1026–1036.

[27] A. Escribano-Cuesta, P. Pérez-Galán, E. Herrero-Gómez, M. Sekine, A. A. C. Braga, F. Maseras, A. M. Echavarren, *Organic & Biomolecular Chemistry* **2012**, *10*, 6105–6111.

[28] N. Cabello, E. Jiménez-Núñez, E. Buñuel, D. J. Cárdenas, A. M. Echavarren, *European Journal of Organic Chemistry* **2007**, *2007*, 4217–4223.

[29] R. A. Widenhoefer, *Chemistry – A European Journal* **2008**, *14*, 5382–5391.

[30] S. Sengupta, X. Shi, *ChemCatChem* **2010**, *2*, 609–619.

[31] A. Pradal, P. Y. Toullec, V. Michelet, *Synthesis* **2011**, 1501–1514.

[32] Y.-M. Wang, A. D. Lackner, F. D. Toste, *Acc. Chem. Res.* **2014**, *47*, 889–901.

[33] W. Zi, F. D. Toste, *Chemical Society Reviews* **2016**, *45*, 4567–4589.

[34] Y. Li, W. Li, J. Zhang, *Chemistry – A European Journal* **2017**, *23*, 467–512.

[35] G. Zuccarello, I. Escofet, U. Caniparoli, A. M. Echavarren, *ChemPlusChem* **2021**, *86*, 1283–1296.

[36] C. Bartolomé, D. García-Cuadrado, Z. Ramiro, P. Espinet, *Inorg. Chem.* **2010**, *49*, 9758–9764.

[37] Y.-M. Wang, C. N. Kuzniewski, V. Rauniyar, C. Hoong, F. D. Toste, *J. Am. Chem. Soc.* **2011**, *133*, 12972–12975.

[38] Z. L. Niemeyer, S. Pindi, D. A. Khrakovsky, C. N. Kuzniewski, C. M. Hong, L. A. Joyce, M. S. Sigman, F. D. Toste, *J. Am. Chem. Soc.* **2017**, *139*, 12943–12946.

[39] M. J. Johansson, D. J. Gorin, S. T. Staben, F. D. Toste, *J. Am. Chem. Soc.* **2005**, *127*, 18002–18003.

[40] I. D. G. Watson, S. Ritter, F. D. Toste, *J. Am. Chem. Soc.* **2009**, *131*, 2056–2057.

[41] J. F. Briones, H. M. L. Davies, *J. Am. Chem. Soc.* **2012**, *134*, 11916–11919.

[42] M. P. Muñoz, J. Adrio, J. C. Carretero, A. M. Echavarren, *Organometallics* **2005**, *24*, 1293–1300.

[43] C.-M. Chao, D. Beltrami, P. Y. Toullec, V. Michelet, *Chemical Communications* **2009**, *0*, 6988–6990.

[44] C.-M. Chao, M. R. Vitale, P. Y. Toullec, J.-P. Genêt, V. Michelet, *Chemistry – A European Journal* **2009**, *15*, 1319–1323.

[45] S. A. Gawade, S. Bhunia, R.-S. Liu, *Angewandte Chemie International Edition* **2012**, *51*, 7835–7838.

[46] G. Zhou, F. Liu, J. Zhang, *Chemistry – A European Journal* **2011**, *17*, 3101–3104.

[47] L. Huang, H.-B. Yang, D.-H. Zhang, Z. Zhang, X.-Y. Tang, Q. Xu, M. Shi, *Angewandte Chemie* **2013**, *125*, 6899–6903.

[48] R. Guo, K.-N. Li, B. Liu, H.-J. Zhu, Y.-M. Fan, L.-Z. Gong, *Chemical Communications* **2014**, *50*, 5451–5454.

[49] Y. Sota, M. Yamamoto, M. Murai, J. Uenishi, M. Uemura, *Chemistry – A European Journal* **2015**, *21*, 4398–4404.

[50] W. Zi, H. Wu, F. D. Toste, *J. Am. Chem. Soc.* **2015**, *137*, 3225–3228.

[51] I. Alonso, B. Trillo, F. López, S. Montserrat, G. Ujaque, L. Castedo, A. Lledós, J. L. Mascareñas, *J. Am. Chem. Soc.* **2009**, *131*, 13020–13030.

[52] A. Z. González, F. D. Toste, *Org. Lett.* **2010**, *12*, 200–203.

[53] A. Z. González, D. Benitez, E. Tkatchouk, W. A. I. Goddard, F. D. Toste, *J. Am. Chem. Soc.* **2011**, *133*, 5500–5507.

[54] H. Teller, M. Corbet, L. Mantilli, G. Gopakumar, R. Goddard, W. Thiel, A. Fürstner, *J. Am. Chem. Soc.* **2012**, *134*, 15331–15342.

[55] G. Cera, M. Bandini, *Israel Journal of Chemistry* **2013**, *53*, 848–855.

[56] M. R. Luzung, P. Mauleón, F. D. Toste, *J. Am. Chem. Soc.* **2007**, *129*, 12402–12403.

[57] S. Suárez-Pantiga, C. Hernández-Díaz, E. Rubio, J. M. González, *Angewandte Chemie* **2012**, *124*, 11720–11723.

[58] Y. Wang, P. Zhang, Y. Liu, F. Xia, J. Zhang, *Chemical Science* **2015**, *6*, 5564–5570.

[59] G. L. Hamilton, E. J. Kang, M. Mba, F. D. Toste, *Science* **2007**, *317*, 496–499.

[60] K. Aikawa, M. Kojima, K. Mikami, *Angewandte Chemie* **2009**, *121*, 6189–6193.

[61] K. Aikawa, M. Kojima, K. Mikami, *Advanced Synthesis & Catalysis* **2010**, *352*, 3131–3135.

[62] X.-F. Tu, L.-Z. Gong, *Angewandte Chemie* **2012**, *124*, 11508–11511.

[63] M. Raducan, M. Moreno, C. Bour, A. M. Echavarren, *Chemical Communications* **2012**, *48*, 52–54.

[64] S. Ferrer, A. M. Echavarren, *Organometallics* **2018**, *37*, 781–786.

[65] G. Zuccarello, J. G. Mayans, I. Escofet, D. Scharnagel, M. S. Kirillova, A. H. Pérez-Jimeno, P. Calleja, J. R. Boothe, A. M. Echavarren, *J. Am. Chem. Soc.* **2019**, *141*, 11858–11863.

[66] U. Caniparoli, I. Escofet, A. M. Echavarren, *ACS Catal.* **2022**, *12*, 3317–3322.

[67] A. Franchino, À. Martí, A. M. Echavarren, *J. Am. Chem. Soc.* **2022**, *144*, 3497–3509.

[68] T. Iwasawa, R. J. Hooley, J. Rebek, *Science* **2007**, *317*, 493–496.

[69] C. Tugny, N. del Rio, M. Koohgard, N. Vanthuyne, D. Lesage, K. Bijouard, P. Zhang, J. Meijide Suárez, S. Roland, E. Derat, O. Bistri-Aslanoff, M. Sollogoub, L. Fensterbank, V. Mouriès-Mansuy, *ACS Catal.* **2020**, *10*, 5964–5972.

[70] G. Cera, G. Giovanardi, A. Secchi, A. Arduini, *Chemistry – A European Journal* **2021**, *27*, 10261–10266.

[71] G. Cera, M. Bazzoni, A. Arduini, A. Secchi, *Org. Lett.* **2020**, *22*, 3702–3705.

[72] D. Pflästerer, A. S. K. Hashmi, *Chemical Society Reviews* **2016**, *45*, 1331–1367.

[73] G. Giovanardi, A. Secchi, A. Arduini, G. Cera, *Beilstein J. Org. Chem.* **2022**, *18*, 190–196.

[74] G. Giovanardi, D. Balestri, A. Secchi, G. Cera, *Organic & Biomolecular Chemistry* **2022**, *20*, 6464–6472.

[75] M. P. Schramm, M. Kanaura, K. Ito, M. Ide, T. Iwasawa, *European Journal of Organic Chemistry* **2016**, *2016*, 813–820.

[76] N. Endo, M. Kanaura, M. P. Schramm, T. Iwasawa, *Tetrahedron Letters* **2016**, *57*, 4754–4757.

[77] M. Kanaura, N. Endo, M. P. Schramm, T. Iwasawa, *European Journal of Organic Chemistry* **2016**, *2016*, 4970–4975.

[78] N. Endo, M. Inoue, T. Iwasawa, *European Journal of Organic Chemistry* **2018**, *2018*, 1136–1140.

[79] M. Inoue, K. Ugawa, T. Maruyama, T. Iwasawa, *European Journal of Organic Chemistry* **2018**, *2018*, 5304–5311.

[80] T. D. Ho, M. P. Schramm, *European Journal of Organic Chemistry* **2019**, *2019*, 5678–5684.

[81] L. E. Rusali, M. P. Schramm, *Tetrahedron Letters* **2020**, *61*, 152333.

[82] I. Martín-Torres, G. Ogalla, J.-M. Yang, A. Rinaldi, A. M. Echavarren, *Angewandte Chemie International Edition* **2021**, *60*, 9339–9344.

[83] P. P. Castro, G. Zhao, G. A. Masangkay, C. Hernandez, L. M. Gutierrez-Tunstad, *Org. Lett.* **2004**, *6*, 333–336.

[84] O. Illa, M. Arshad, A. Ros, E. M. McGarrigle, V. K. Aggarwal, *J. Am. Chem. Soc.* **2010**, *132*, 1828–1830.

[85] Z. Zheng, Y. Cao, Q. Chong, Z. Han, J. Ding, C. Luo, Z. Wang, D. Zhu, Q.-L. Zhou, K. Ding, *J. Am. Chem. Soc.* **2018**, *140*, 10374–10381.

[86] C. Nieto-Oberhuber, M. P. Muñoz, S. López, E. Jiménez-Núñez, C. Nevado, E. Herrero-Gómez, M. Raducan, A. M. Echavarren, *Chemistry – A European Journal* **2006**, *12*, 1677–1693.

[87] T. Higashino, A. Ueda, J. Yoshida, H. Mori, *Chemical Communications* **2017**, *53*, 3426–3429.

General Conclusions

The research described in this Doctoral Thesis aimed to apply the principles and methods of supramolecular chemistry to the development of new calix[6]arene- and resorcin[4]arene-based materials for different applications.

First, a series of calix[6]arene upper-to-upper oriented [3]rotaxanes was prepared using a threading and capping approach. The isomeric selectivity leading to the desired upper-to-upper orientation was achieved thanks to the unidirectional threading process of viologen-based axles, which, in low polarity solvents, always threads the calix6]arene cavity through the upper rim. Furthermore, the correct axle length was evaluated, and the high functional group tolerance of the templating approach was demonstrated. Then, this latter study paved the way for the supramolecular-assisted synthesis of novel head-to-head bis-calix[6]arene cages as new containers for *host-guest* systems. The synthetic strategy involved the template effect of a bis-viologen salt, which is able to preorganised two functionalised calix[6]arene macrocycles properly in the space before the clipping reaction leading to the molecular cages. Preliminary studies on the complexation properties were also performed, demonstrating the promising features of these new *hosts*.

Successively, the non-palindrome cavity of the tris-(*N*-phenylureido)-calix[6]arene macrocycle was also exploited as a *host* for a series of stilbazolium salts. This class of dyes endowed with very interesting optical features can thread the calix[6]arene cavity from both sides, leading to the formation of two orientational isomers, but depending on the substituents and stoppering groups, the orientation of the complex can be controlled. The synthesis of the two orientational stilbazolium-based [2]rotaxane isomers allowed the straightforward study of the spectroscopic properties of the isomers both in solution and in the solid state. Furthermore, we demonstrated how encapsulation improves either the photophysical or photochemical properties

with respect to the free axle, with a remarkable dependence on the orientation of the calix[6]arene cavity.

Finally, a new series of achiral and chiral digold(I) resorcin[4]arene-based cavitand complexes were prepared using thioethers or thioureas as ligands for gold. These new gold(I) cavitand catalysts were then tested in the cycloisomerisation and alkoxycyclisation reactions of 1,6-dienynes.

Biography

Federica Cester Bonati was born in Parma in 1994. She obtained the bachelor's degree in chemistry (108/110) in 2016 under the supervision of Prof. Paolo Pelagatti at the University of Parma, working on Pd-catalysed amination and amidation reactions for the preparation of MOFs ligands. In 2018, she obtained the master's degree in industrial chemistry (110/110 *cum laude*), carrying out the research project *via* Overworld Scholarship at University of Michigan under the supervision of Prof. Vincent Pecoraro. Her master thesis deals with the synthesis and characterization of functional Metallacrowns for bioimaging applications. In the same hear, she started a research fellowship supported by Chiesi Farmaceutici S.p.A. in the group of Prof. Arturo Arduini and Prof. Andrea Secchi at the University of Parma with a project entitled "Synthesis of cyclic compounds with potential kinase inhibitor activity". Since 2019 she is carrying out her PhD in the same research group under the supervision of Prof. Andrea Secchi and Prof. Gianpiero Cera. Her research focuses on the design, synthesis and structural characterization of new materials based on calix[6]arenes. During the PhD (September 2021 – February 2022), she joined as visiting student the group of Prof. Antonio M. Echavarren at ICIQ, in Tarragona, Spain. The results achieved during the doctorate are described in this thesis.

List of publications

Cera G., **Cester Bonati F.**, Bazzoni M., Secchi A., Arduini A., Calix[6]arene-based Brønsted acids for molecular recognition and catalysis, *Organic & Biomolecular Chemistry*, **2021**, 19, 1546-1554.

Pilato S., Aschi M., Bazzoni M., **Cester Bonati F.**, Cera G., Moffa S., Canale V., Ciulla M., Secchi A., Arduini A., Fontana A., Siani G., Calixarene-based artificial ionophores for chloride transport across natural liposomal bilayer: Synthesis, structure-function relationships, and computational study, *BBA – Biomembranes*, **2021**, 1863, 183667.

Cera G., Bazzoni M., Andreoni L., **Cester Bonati F.**, Massera C., Silvi S., Credi A., Secchi A., Arduini A., Thioureidocalix[6]arenes Pseudorotaxanes, *European Journal of Organic Chemistry*, **2021**, 5788–5798.

Moffa S., Aschi M., Bazzoni M., **Cester Bonati F.**, Secchi A., Bruni P., Di Profio P., Fontana A., Pilato S., Siani G., Synthesis, characterization, and computational study of aggregates from amphiphilic calix[6]arenes. Effect of encapsulation on degradation kinetics of curcumin, *Journal of Molecular Liquids*, **2022**, 368, 120731.

Cester Bonati F., Secchi A. Cera G., Recent advances with calix[6]- and calix[8]arene organometallic catalysts, *Tetrahedron Letters*, **2022**, 112, 154221.

Cester Bonati F., Bazzoni M., Baccini C.; Zanichelli V., Orlandini G., Arduini A., Cera G., Secchi A., Calix[6]arene-Based [3]Rotaxanes as Prototypes for the Template Synthesis of Molecular Capsules, *Molecules*, **2023**, 28, 595.

Andreoni L.,[‡] **Cester Bonati F.**,[‡] Groppi J., Balestri D., Cera G., Credi A., Secchi A., Silvi S., Selective enhancement of organic dye properties through encapsulation in rotaxane orientational isomers, *Chemical Communications*, **2023**, Advance Article.